GROUNDWATER CONTAMINATION PREVENTION USING AN ELECTROKINETIC BARRIER– COBALT TRAPPING

By

Rimaz Abakar

This thesis is submitted in partial fulfillment of the requirements for the degree of

Master of Science in Engineering in Environmental Engineering (MSc Eng)

Faculty of Graduate Studies

Lakehead University

Thunder Bay, Ontario, Canada

February, 2015

Abstract

The quality of groundwater in many regions around the world has been compromised due to pollution from anthropogenic activities such as deposition of solid wastes containing heavy metals in landfills, industrial spills and leaching from mine tailings. Inorganic contaminants such as lead, cobalt, and cadmium have been a growing concern owing to their detrimental environmental and health effects. Several methods have been used to remediate contaminated soils and groundwater. These methods include phytoremedation, biosorption, neutralization, and chemical oxidation. These methods, however, have several limitations and disadvantages including quality control, lack of selectivity and generation of additional contamination and waste sludge.

Electrokinetic remediation is a growing technology used largely to remediate and restore soils and groundwater affected by organic and inorganic contamination. Electrokinetics is the application of a direct current to a wet soil to transport or remove water and/or ions via the soil pores. Two main phenomena are observed when a voltage gradient is applied to a wet and compacted soil. The first is the movement of the soil's pore fluid towards the cathode, known as electro–osmosis. The second is electro–migration which is the movement of ions towards the oppositely charged electrode.

Though much work reported in the literature has focused on the application of electrokinetic phenomena to remediate contaminated soils, this thesis focuses on utilizing electrokinetic phenomena to prevent groundwater contamination at an industrial mine site. The first objective of this work was to investigate the applicability of an electrokinetic barrier to prevent groundwater contamination downstream of a tailings management area at a Canadian mine site by trapping cobalt near the cathode. To meet the first objective, direct current was applied either continuously or intermittently. The second objective was to examine the fate of the cobalt accumulated in the soil after the termination of the electrokinetic barrier.

The experimental studies showed the effectiveness of the applied voltage gradient in reducing the net flow of water downstream of the barrier and diminishing cobalt concentration and mass in the effluent. Furthermore, the influences of electro–osmosis,

electro–migration, and the sharp pH gradient which favored cobalt adsorption/precipitation near the cathode resulted in trapping cobalt in the cathode region near the inlet of the cell.

Additionally, using intermittent current to power the electrokinetic barrier yielded results that were generally comparable to those obtained with continuous current. This finding offered important insights for future work on the use of solar powered electrokinetic barriers.

Wash out tests in which the potential gradient was stopped midway through the test were conducted to address the second objective. The concentration of cobalt in the effluent did not increase after the termination of the potential gradient, for the duration of the test. The accumulated cobalt was retained in the soil and was not washed out of the cells.

In summary, this study demonstrated that an electrokinetic barrier can be successfully used to prevent groundwater contamination due to cobalt by taking advantage of the coupled effects of electro–osmosis, electro–migration and water electrolysis at the electrodes.

Acknowledgements

First, I would like to express my limitless gratitude to Allah (SWT) for giving me the strength, the patience and guidance to complete this work.

I also would like to thank my dear mother, Soad Ahmed Adam, for her continuous support, positive energy and constant prayers.

A very special and sincere thank goes to Dr. Catalan for his encouragement and full support. Dr. Catalan provided me with his knowledge, his time and his resources. He also gave me direction, listened with respect to my ideas and guided my thoughts. I appreciate everything he has done; from having high expectations of me to financially supporting my research. I am very grateful for it all.

I must also thank Dr. Mohammedelhassan, my supervisor, for his support, easy going character, kindness, and for his patience with me. I appreciated the freedom I was granted and the responsibilities I was given.

The financial support for this project by Musselwhite Mine–Goldcorp Inc. and Ontario Centres of Excellence (OCE) must be acknowledged and is much appreciated. I must also acknowledge the staff at Musselwhite Mine for allowing me access to materials and data that were essential for the completion of this work.

Thanks are also due to the Civil Engineering lab technician, Mr. Conrad Hagstrom, for all his assistance and the knowledge he passed onto me with open heart.

Last but not least, I would like to thank my family and dear friends for allowing me to vent my frustration, for listening to me and for their small acts of kindness, love and care they never stopped showing me. The emotional support was essential for me to keep going especially in the dead of winter in Thunder Bay.

Table of Contents

List of Reactions

List of Equations

List of Tables

List of Figures

1.0 Introduction

An increase in mining activities in Canada between 2001 and 2008 led to approximately 55% increase in mine waste generation (Statistics Canada, 2013). In 2008 alone, the mining industry produced 1118 million tonnes of wastes from gold mining and processing which included waste rock and overburden, rejected mineral ores and mine tailings as compared to 720 million tonnes in 2001 (Statistics Canada, 2013).

More specifically, Musselwhite mine is a Canadian gold mine owned and operated by Goldcorp Canada Ltd. and is concerned about elevated cobalt concentrations in the groundwater between its tailings management area and a nearby lake. As of 2013, cobalt's concentration in some groundwater wells in the mine site exceeded the World Health Organization recommended limit for cobalt in fresh water to protect aquatic life against chronic toxicity and it is steadily approaching the acute toxicity limit. In order to prevent cobalt from reaching the nearby lake, an electrokinetic barrier was proposed to be installed perpendicular to the flow of the groundwater between the tailings management area and the lake.

The main objectives of this study are to assess the feasibility of groundwater contamination prevention using an electrokinetic barrier at the Musselwhite mine, to examine the effectiveness of using intermittent current to power the electrokinetic barrier as opposed to using continuous current, and to determine the long term fate of cobalt after the termination of the electrokinetic barrier and the elimination of the source of contamination. In this thesis, it is hypothesised that cobalt will be trapped near the inlet of the test cell by applying a voltage gradient to the test cell mixture. As well, it is hypothesised that under an applied voltage, the cobalt concentration past the electrokinetic barrier will be significantly less than the effluent cobalt concentration in the absence the electrokinetic barrier.

2.0 Literature Review

Groundwater is the source of drinking water for a quarter of all Canadians. Although approximately nine million Canadians rely on groundwater for potable use, the quality of groundwater has become a national concern due to contamination (Environment Canada, 2007). Groundwater can be contaminated via various anthropogenic and natural sources including agricultural runoff of pesticides and herbicides, industrial spills and pipe leakages, and leaching of mine tailings (Statistics Canada, 2012). Depending on the source of pollution, the contaminants may be organic such as naphthenic acids and asphaltenes or inorganic such as heavy metals and arsenic. Since groundwater is mobile and is not confided to one place, any pollution occurring in one region has the potential of spreading to other regions (Canadian Ground Water Association, 1999). In 2008, 1.33 billion tonnes of solid waste were generated and approximately 36% of this total came from mine waste which includes both the tailings and the mine waste rock (Statistics Canada, 2012) as reported in Figure 1.

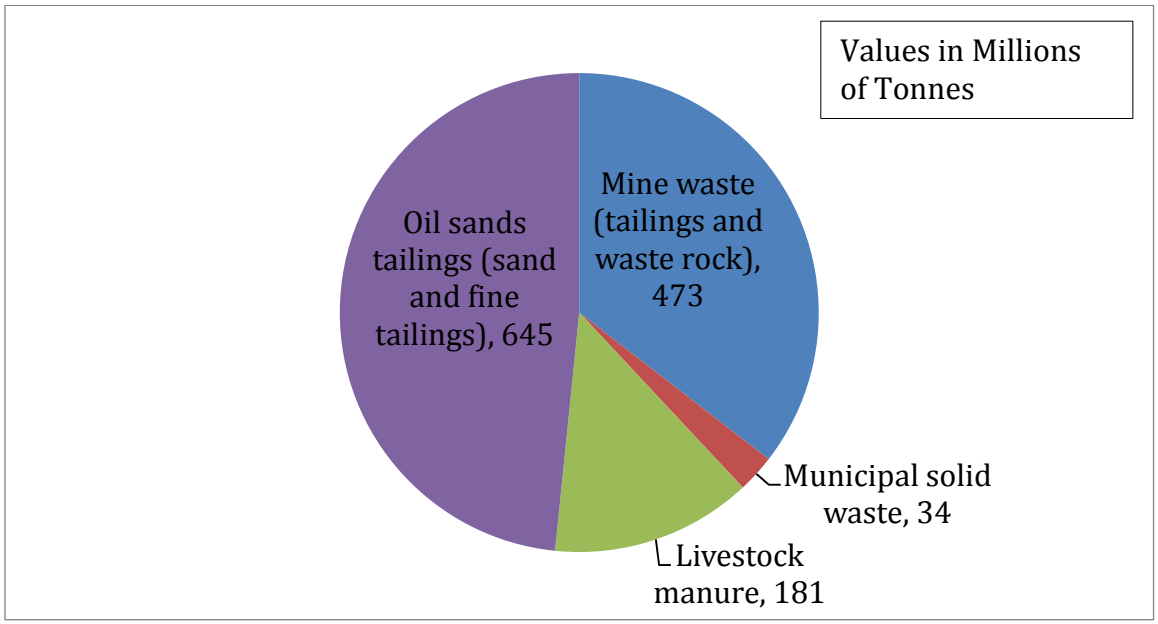

Figure 1 – Solid waste generation in Canada for 2006 and 2008 (Statistics Canada, 2012)**All data are from 2008 except those for Livestock Manure, which are for 2006.*

The mining process, waste disposal, and ore management are the main sources causing groundwater contamination near mining sites (Sparks, 2003). Ore processing generates

waste containing the waste rock which includes the below cut–off grade rock that was mined but was not economically valuable. Waste rock is stored in stockpiles or dumps (Morin & Hutt, 1997). The liquids and fine grained solids from the extraction process of the valuable products are in the size range of silt and clay particles and are often stored in surface impoundment known as tailing ponds (Jennings, et al., 2008) as shown in Figure 2. Tailings ponds have the largest surface area in mine sites due to the large volume of tailings produced in the extraction of valuable products. For example, a typical Canadian gold mine produces one tonne of tailings to extract 5 to 10 grams of gold. Furthermore, tailings impoundments have the greatest contamination generation potential in the mine sites. This is mainly due to tailings oxidation which then leads to acid mine drainage (AMD) generation (Morin & Hutt, 1997). AMD is a concern where sulfur minerals are deposited in the tailings pond. Sulfur minerals are commonly found in most Canadian mines. The most common sulfide mineral is iron sulfide (FeS_2) or pyrite which is also known as fool's gold (Sparks, 2003). In the presence of a strong oxidant (i.e. O_2) and water, FeS_2 reacts to form dissolved ferrous (Fe^{2+}) and sulfate ions (Johnson & Hallberg, 2005); and some acidity is produced (H^+) by the following reaction:

$$\boldsymbol{2FeS_2(s) + 7O_2(g) + 2H_2O(l) \rightarrow 2Fe^{2+}(aq) + 4SO_4{}^{2-}(aq) + 4H^+(aq)} \qquad \text{Re. (2.1)}$$

In the next step, the acidity is consumed and Fe^{2+} is reduced to Fe^{3+} by reaction (2.2). Reaction (2.2) is the rate limiting step (Sparks, 2003).

$$\boldsymbol{4Fe^{2+}(aq) + O_2(g) + 4H^+(aq) \rightarrow 4Fe^{3+}(aq) + 2H_2O\ (l)} \qquad \text{Re. (2.2)}$$

At low pH values, specifically less than 4.5 and in the absence of oxygen, Fe^{3+} behaves as an oxidant, as shown in reaction (2.3). This step is oxygen independent and can occur in subsurface anoxic environments (Johnson & Hallberg, 2005). The pyrite is oxidized to produce more Fe^{2+} and acidity.

$$\boldsymbol{FeS_2(s) + 14Fe^{3+}(aq) + 8H_2O(l) \rightarrow 15Fe^{2+}(aq) + 2SO_4{}^{2-}(aq) + 16H^+(s)} \qquad \text{Re. (2.3)}$$

Reactions (2.2) and (2.3) occur in a cycle where reaction (2.2) produces Fe^{3+} which oxidizes more pyrite to produce Fe^{2+} and lowers the system's pH (Jennings, et al., 2008). Eventually, the pH will drop and at pH values greater than 3.0, AMD becomes evident; Fe^{3+}

reacts with water and produces precipitates of $Fe(OH)_3$ which stain the tailings with a rusty color as shown by reaction (2.4) below.

$$\boldsymbol{Fe^{3+}(aq) + 3H_2O(l) \rightarrow Fe(OH)_3(s) + 3H^+(aq)} \quad \text{Re. (2.4)}$$

MD is characterized by low pH environments where most metal oxides dissolve. Thus, the heavy metal ions become mobile and transferable with the site hydrology (Sparks, 2003).

Figure 2 – Tailings pond at a mine site

Depending on the mine activity, several contaminants may seep from the tailings pond to the soil and reach the groundwater table where the contaminants will be carried downstream by the groundwater flow reaching nearby surface water. These contaminants may include manganese (Mn), iron (Fe), arsenic (As), sulphur (S), chromium (Cr), cadmium (Cd), zinc (Zn), copper (Cu), and cobalt (Co) (Evangelou, 1998). With increased industrial emissions to the water and soil due to mining activities, soil and groundwater contamination continue to persist as a problem and remedial actions must take place.

2.1 Groundwater Remediation Techniques

Many heavy metals such as Cr and As are human carcinogens. They may also cause birth defects in unborn babies, and liver and kidney failures when ingested (EPA, 2007). There are several techniques and methods used to remediate groundwater contamination due to heavy metals. However, the best remedy is prevention of heavy metal contamination in groundwater due to the difficulty of the processes involved in removing heavy metals from groundwater (Wuana & Okieime, 2011). Groundwater and soil remediation techniques can be categorized according to their processes–biological, chemical, and physical treatment processes, as well as the emerging electrokinetic remediation (Yao, et al., 2012).

2.1.1 Physical Remediation

The oldest physical groundwater contamination remediation technique is the pump–and–treat method. The groundwater is pumped to the surface using extraction wells where treatment takes place (Reddy, 2008). Any of the techniques later discussed may be used to treat the extracted groundwater as appropriate. The treated water is then either discharged to the nearest surface water or is sent back to the aquifer. This process is illustrated in Figure 3.

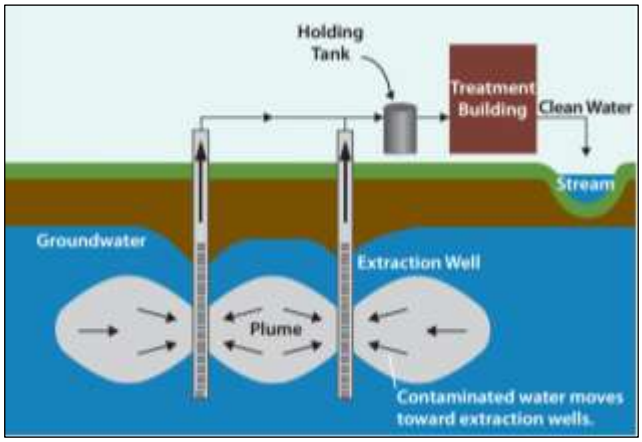

Figure 3 – Groundwater pump and treat system (U.S. EPA, 2012)

Although the technique is easy to use, the treatment of large volumes of water can be very costly and time consuming (EPA, 1966). As well, it had been reported that even though this conventional method works at the initial stages of the operation, large amounts of contaminants remain untreated in the groundwater aquifer (Caliman, et al., 2011). The pumping well is only effective over a certain volume of the aquifer.

2.1.2 Biological Remediation

Biological remediation involves the use of bacteria and biological organisms to breakdown inorganic contaminants (Brar, et al., 2006). Some bacteria are able to use heavy metals such as Cr as a source of energy for their growth and multiplication by transforming toxic metals and contaminants to other nontoxic forms, thus alleviating the contamination in soil and groundwater. Bacteria such as Thiobacillus ferrooxidans can metabolize metal oxides and can also survive extreme conditions of high temperatures and low pH environments (Evangelou, 1998; Sparks, 2003).

One biological remediation technique uses special deep rooted plants, such as hybrid poplar trees, to uptake contaminants from groundwater and soil. This process is called phytoremediation (Brar, et al., 2006; Hong, et al., 2001). It is useful to stabilize–in–place and to immobilize contaminants such as arsenic, cadmium and zinc (Wuana & Okieime, 2011). Heavy metals are trapped within the plants by two mechanisms: phytoextraction in which the contaminants are transported from the subsurface tissues, the roots, to the above ground tissues, the shoots; and by rhizofiltration where the absorption and concentrations of the contaminants by the plant roots occurs (Antiochia, et al., 2007). The plants' ability to halt the migration of the contaminated groundwater plume past the area subjected to remediation zone can be limited by the flow rate of the contaminated groundwater as well as by the rate at which the plants uptake the contaminants from the polluted groundwater (Brar, et al., 2006). For instance, if the groundwater flow rate is much greater than the plants' contaminant uptake rate, the contaminated groundwater plume will continue to spread past the phytoremediation zone. Furthermore, the efficiency of metal transport from the roots to the shoots of the plant plays a role in the overall success of phytoremediation. Hyper–accumulators, as the name suggests, are plants that can uptake and store elevated concentrations of heavy metals while bearing no effects on their growth (Baker & Brooks, 1989). Between 1990 and 2000, several American states successfully applied bioremediation techniques to land treatment (Pivetz, 2001).

The combination of bacteria with plants in phytoremediation has been subject of previous experiments. In particular, Raikumar et al. (2009) examined the potential of using endophytic bacteria with plants to enhance heavy metal uptake. It was found that

endophytic bacteria reduced the toxicity effects in plant tissues caused by the absorption of high heavy metals. Endophytic bacteria enhanced plants growth and supported their survival.

Passive bioreactors, well known as sulphate–reducing passive bioreactors, have gained grounds in soil remediation and groundwater decontamination due to acid mine drainage over the past two decades. In such reactors, acid mine drainage solutions are fed through a reactive solid mixture containing a source of carbon, bacteria, nitrogen, a neutralizing agent, and a porous solid medium (Zagury, et al., 2007). Compost material from agricultural and food wastes was successfully used to uptake toxic heavy metals such as Cd, Cr and Cu (Farrell & Jones, 2010). The heavy metals are removed in two steps. Initially the contaminants are adsorbed onto the living biomass by interactions with the functional groups present on the surface of the cells. This is known as biosorption. Once adsorbed, the metal ions penetrate the cell wall and access the cell membrane and its internal sub–structure (Das, et al., 2008). Accordingly, biosorption relies on the ability of the biomass to act as a sorbent for the heavy metals. Bioremediation is associated with several advantages including low operating cost, low energy requirements, and applicability to heavy metals removal in low pH environments (Zagury, et al., 2007). However, saturation of the metals interactive sites poses a concern for regeneration and necessitates metal ions desorption before further application (Das, et al., 2008). For long term remediation operations, this can be unattractive from an operational point of view.

2.1.3 Chemical Remediation

As the name suggests, chemical remediation involves the use of chemical(s) to transform contaminants in groundwater or soil via chemical reactions to less harmful and less toxic forms (Caliman, et al., 2011). There are several chemical treatment processes that aim at precipitating out or altering contaminants in oxidizing, reducing and/or neutralizing environments (Evanko & Dzombak, 1997). They include chemical oxidation, passive neutralization using hydrated lime, preamble reactive barriers, soil agglomeration, and soil washing and flushing.

Chemical oxidation is the change of oxidation state of elements by electron transfer (Huling & Pivetz, 2006). There are several oxidants in the literature; however, the most common are peroxide (H_2O_2), ozone (O_3), persulfate ($S_2O_8^{2-}$), and permanganate (MnO_4^-) (TOSC, 2004). For instance, As(III), a toxic contaminant known to cause dermal changes, pulmonary, respiratory, cardiovascular and carcinogenic effects (Das, et al., 1996); can be oxidized by permanganate to As(V) which is less toxic (Sparks, 2003).

Chemical oxidation is mostly applied to soluble ions in contaminated groundwater plumes where elevated toxic heavy metals concentration is a concern. In in–situ remediation, the oxidant is pumped to the groundwater or aquifer via injection wells as shown in Figure 4 (Caliman, et al., 2011). On the other hand, ex–situ chemical oxidation is achieved by pumping out the contaminated groundwater to above ground facilities where remediation takes place. The treated groundwater may be returned to the aquifer (Huling & Pivetz, 2006).

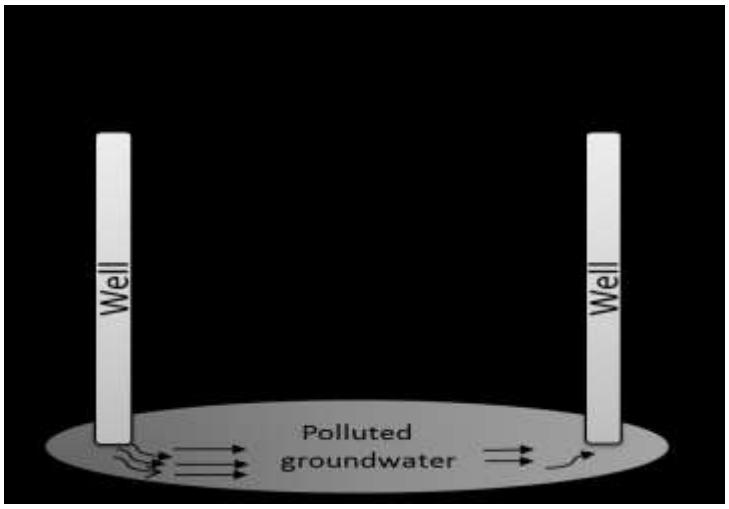

Figure 4 – Schematic of an in–situ chemical oxidation system after (EPA, 1966)

The success of chemical oxidation relies on the environmental persistence of the oxidant such that it continues to meet the oxidation demand and persists long enough in the medium in order to reach the target zones of contamination. Permanganate for example persists for very long periods, which makes it an excellent oxidant (Huling & Pivetz, 2006). However, the environmental fate of such persisting oxidants is not yet fully understood. Thus, care must be taken in order to avoid producing further contamination and toxicity (Evanko & Dzombak, 1997). Moreover, chemical oxidation is non–discriminatory and if not carefully applied increased toxicity may result. Beside the oxidation of target contaminants, the oxidation of other available metal ions to their toxic and more mobile forms may well occur (Huling & Pivetz, 2006). For example, Cr(III), which is nontoxic, can be oxidized to Cr(VI), which is a carcinogen, in a system where in–situ chemical oxidation is employed to reduce arsenic toxicity (EPA, 2007). The possibility of permeability reduction in porous media due to oxidant precipitation, high costs associated with high natural oxidant demand, and limited application in sites with elevated contamination are some of the drawbacks of chemical oxidation (Huling & Pivetz, 2006).

An alternative to chemical oxidation is passive neutralization. It is the most commonly used heavy metal removal and immobilization mechanism for acid mine drainage using a neutralizing agent such as hydrated lime, $Ca(OH)_2$, or calcium carbonate, $CaCO_3$. Neutralization relies on the principles of raising the pH of AMD to promote the

precipitation of soluble metal ions in the form of insoluble metal hydroxides and metal carbonates (Johnson & Hallberg, 2005). As well, adsorption on minerals can be favored for some metal ions at high pH values. When the neutralizing agent, hydrated lime for example, decomposes, it liberates hydroxyl ions which raise the medium's pH, and the available metal ions bind with OH^- and form insoluble metal hydroxides by several reactions (Aube, 2004).

Most metal hydroxides precipitate in a pH range of 6 to 9 with notable exceptions being cadmium, lead, copper and nickel which precipitate at more alkaline pH ranges, as demonstrated in Figure 5. Full scale experiments showed the ability of lime to raise the pH of AMD and to reduce the mobility of some heavy metals (Faulkner, et al., 2005). In the past, hydrated lime has been successfully used for its effectiveness, low cost, ease, and simplicity of application (Martin, et al., 2013). Removal efficiencies over 90% of As, Zn, and Ni were reported in previous studies (Lee, et al., 2007; Aziz, et al., 2008).

Another alternative neutralizing agent is calcium carbonate commonly known as limestone. It can be applied under anoxic conditions (known as anoxic limestone drainage, ALD) to prevent the oxidation of ferrous iron to ferric iron which then combines with OH^- to form ferric hydroxides (U.S. EPA, 1983). Similarly, the formation of aluminum hydroxides may well occur. These insoluble mineral precipitates may form on the limestone surface and hinder limestone dissolution (Bernier, et al., 2002). This process is known as metal armoring and it reduces the effectiveness of $CaCO_3$ (Evanko & Dzombak, 1997). In anoxic limestone drainage, $CaCO_3$ must be present in sufficient quantities in order to consume the already available acidity as well as to produce enough alkalinity to precipitate the metal hydroxides (Bernier, et al., 2002). As the partial pressure of carbon dioxide increases, the solubility of the calcium carbonate will increase leading to the production of more alkalinity (Johnson & Hallberg, 2005).

Even though limestone can effectively immobilize heavy metals in AMD, long term applicability remains an issue due to metal armoring (Bernier, et al., 2002). Additionally, ADL is not applicable for all types of acid mine drainage (Johnson & Hallberg, 2005).

An emerging substitute is permeable reactive barriers (PRB). PRBs are subsurface barriers that are placed in the flow path of the contaminated groundwater plume as illustrated in

Figure 6. The barrier contains reactive material. As the contaminated plume flows through the barrier, heavy metal ions are removed by adsorption, precipitation or oxidation. Some barriers can remove heavy metals by biological activity. The choice of the reactive material heavily depends on the type of contaminants to be immobilized, removed or transformed. For example, zero valent iron (Fe^0) has been used to treat groundwater contaminated with inorganic contaminants such as Chromium (Blowes, et al., 1997).

The disadvantage of using permeable reactive barriers is the lack of quality control. The installation of the barrier must extend to the bed rock or at least cover the entire area where the contaminated groundwater flows. The durability and long term applicability of PRBs is still under study. There is a variety of information on the longevity of PRBs in the literature. However, build of precipitates or biomass is inevitable which reduces the porosity of the material and reactivity (U.S EPA, 1998; The Interstate Technology & Regulatory Council–PRB: Technology Update Team, 2011). Other chemical remediation techniques that are not discussed here include ion exchange, soil washing, and soil agglomeration.

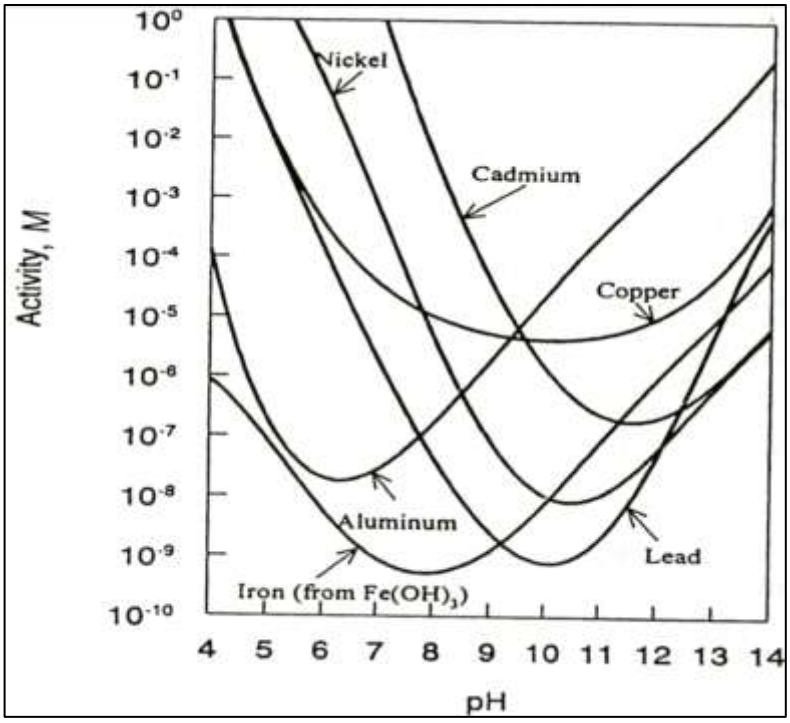

Figure 5 – Solubility of some metal hydroxides (Evangelou, 1998)

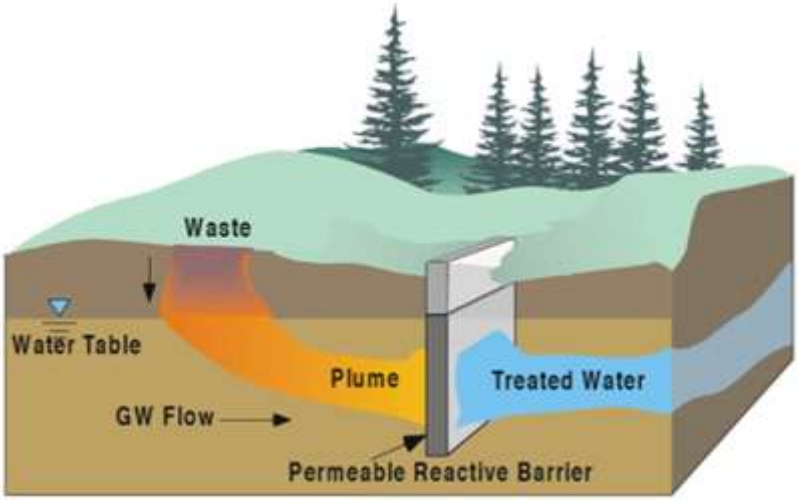

Figure 6 – Permeable reactive barriers (U.S EPA, 1998)

2.2 Electrokinetic Remediation

Electrokinetic remediation is the application of a direct current (DC) to transport contaminants in porous media such as wet soils (Alcántara, et al., 2012). It is used to remediate soil and groundwater from heavy metal contamination that spread by a hydraulic gradient and/or diffusion (Lynch, et al., 2007). Applying a potential gradient across a wet soil mass results in several electrokinetic phenomena (Yeung, 1994), shown in Figure 7. Water reduction occurs at the cathode while water oxidation occurs at the anode. These electrode reactions lead to the development of a sharp pH gradient across the soil and have direct implications on the outcome of contamination remediation and prevention (Acar, et al., 1995). The movement of the water molecules towards the cathode is termed electro–osmosis. Furthermore, under the applied voltage gradient, the ions move towards the electrode opposite to their charge by electro–migration. Electrophoresis is the movement of clay particles towards the anode owing to their negative charges.

In–situ remediation occurs by the insertion of electrodes of opposite polarity in a contaminated soil and running an electric current through them. This remediation technology is used to clean contaminated soils as well as possibly preventing the spread of contamination by groundwater (Yeung, 1994).

Abramson (1934) classified the electrokinetic phenomena in charged porous media based on the driving forces and flows; the first group described the relative movement of a solid or a liquid phase under the influence of an externally applied electrical potential which includes electro–osmosis and electrophoresis. The second group described the two phases' relative movement under a hydraulic gradient or force of gravity and includes streaming potential and migration or sedimentation potential (Abramson, 1934). Water splitting also occurs as a result of an externally applied electric field (Acar, et al., 1993). Each phenomenon is explained in detail in the following subsections.

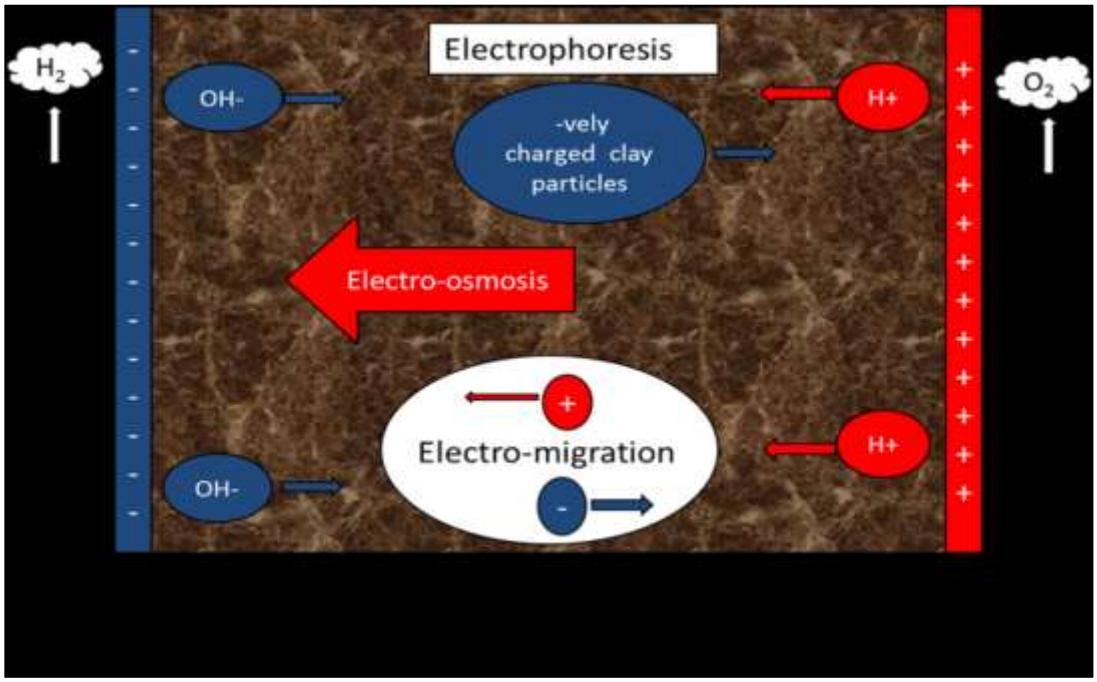

Figure 7 – Observed electrokinetic phenomena in soils

2.2.1 Water Electrolysis

Subjecting a wet medium to an electric potential creates a pH gradient due to the electrolysis of water by the following reactions:

$$2H_2O \rightarrow O_2 \uparrow + 4H^+ + 4e^- \quad \text{(Anode)} \quad \text{Re. (2.5)}$$

$$2H_2O + 2e^- \rightarrow H_2 \uparrow + 2OH^- \quad \text{(Cathode)} \quad \text{Re. (2.6)}$$

Reaction (2.5) occurs at the anode by water oxidation where oxygen gas and hydrogen ions are released. Near the anode zone, pH ranges of 2 to 5 have been reported (Vane & Zang, 1997). On the other hand, reaction (2.6) occurs at the cathode as a result of water reduction where hydrogen gas and hydroxyl ions are released. The hydroxyl ions serve to increase the pH of the cathode region. pH values as high as 12 have been reported near the cathode zone (Acar, et al., 1995). Because of the electrokinetic phenomena as well as diffusion due to a concentration gradient, the hydrogen ions travel towards the cathode while the hydroxyl ions move towards the anode (Narasimhan & Sri Ranjan, 2000). At some distance between the electrodes, the acid front meets the basic front where water is produced as a result (Ugaz, et al., 1994). Water electrolysis plays an important role in heavy metal contaminant removal as later discussed.

2.2.2 Electro–osmosis

The movement of the pore fluid in a porous media (wet soil) under the influence of an electrical field is referred to as electro–osmosis. It describes the movement of water, for example, from the anode to the cathode under an applied electric field (Paillat, et al., 2000). In other words, it is the movement of a liquid phase through a porous solid phase when an electric field is maintained (Yeung, 1994). This movement is due to the viscous drag from the mobile counterions in the double electric layer (Acar, et al., 1990). This can be explained by the Stern layer theory which combines the earlier works of both Helmholtz and Gouy–Chapman (Butt, et al., 2006). For a charged surface, the first layer is created by counter–ions held to the surface by chemical interactions. This layer is assumed to be fixed: the ions are immobile (Paillat, et al., 2000). The second layer is created by mobile ions at some distance in the bulk fluid such that they are attracted to the charged surface by weak electrostatic forces; it is also known as the mobile or diffuse layer as shown in Figure 8. The electric potential at the interface between the first fixed layer and the second mobile layer is termed the zeta potential (ζ) (Butt, et al., 2006). Applying an external electric potential causes cations and anions in the diffuse layer to move in opposite directions while the fixed layer ions remain stationary. This results in viscous drag near the charged surface and the movement of pore fluid. This phenomenon is central to the application of electrokinetics to contaminated soils.

The surfaces of clayey soil minerals are negatively charged due to the presence of organic matter such as humic acids, broken bonds, and isomorphous substitutions (Das, 2008; Acar, et al., 1995). Isomorphous substitutions result from the exchange of one ion in a mineral crystal with ions of the same or different valence number. For example, silica is often substituted with iron, magnesium, or aluminum. Although the crystal structure is maintained, the mineral surface becomes negatively charged as a result (Mitchell & Soga, 2005).

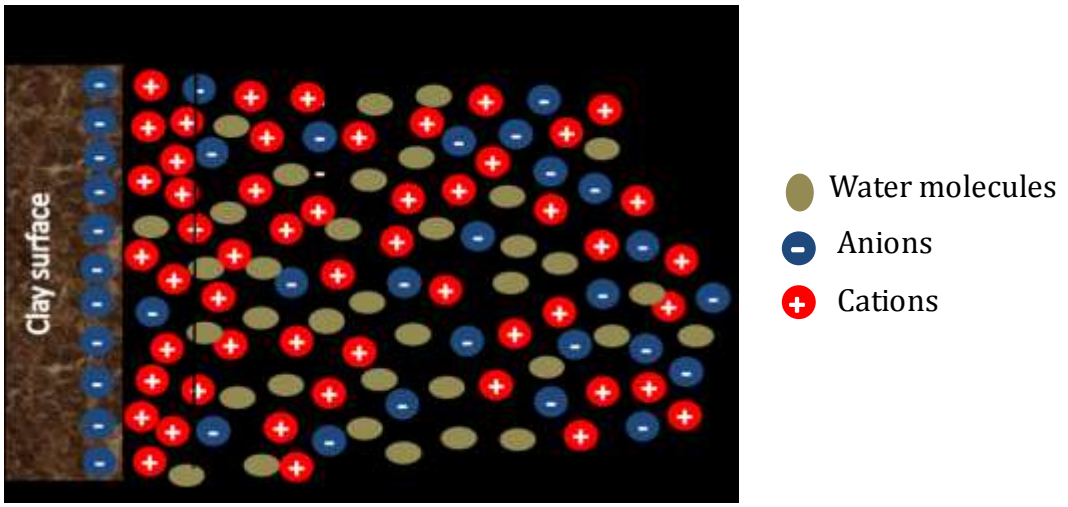

Figure 8 – Stern double layer on a negatively charged clay particle after (Hunter, 1982)

The direction of electro–osmosis flow depends on the sign of the charges in the liquid phase (Yeung, 1994). The negatively charged soil surface amasses a cluster of positively charged ions i.e., cations, at the interface with the liquid phase. When an electric potential gradient is applied across the soil, in the mobile layer the cations move to the cathode and the anions move to the anode, while the negative charges remain attached to the clay surface, as shown in Figure 9. As a result, the water molecules are dragged by the surrounding ions in the mobile layer. Since there is an excess of positively charged ions near the clay surface, the water molecules are dragged towards the cathode by the cations movement towards the cathode (Narasimhan & Sri Ranjan, 2000). Thus, the electro–osmotic flow in the soil will be towards the cathode (Figure 10).

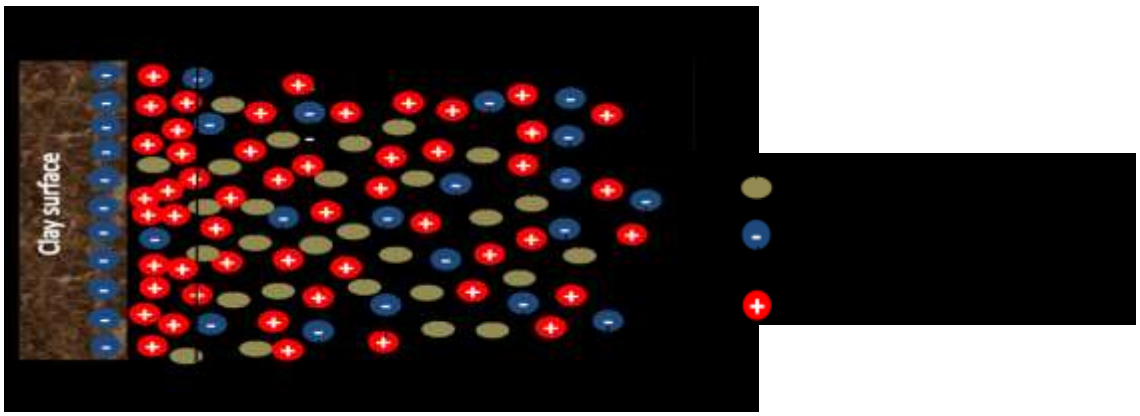

Figure 9 – Schematic of electro–osmosis at the particle surface level (the vertical line indicates the fixed layer)

Figure 10 – Schematic of electro–osmosis in soil after (Acar, et al., 1993)

For reclamation and remediation purposes, the volumetric flow rate of the electro–osmotic flow is of great importance to evaluate the efficiency and effectiveness of electrokinetic remediation (Paillat, et al., 2000), since the pore fluid transports the soluble contaminants under a voltage difference, as previously explained. A number of theories were developed to quantify the volume flow rate of in porous media in terms of electro–osmosis phenomenon. Some of the theories or models are as follows:

1. Helmholtz–Smoluchowski model
2. Schmid theory
3. Spiegler friction model
4. Ion hydration theory
5. Gray–Mitchell approach

The development and limitations of each one of the theories mentioned above are adequately explained by Yeung (1994). Osmotic flow can be described by an equation that is comparable to Darcy's law for flow in porous media as follows:

$$\boldsymbol{Q_e = K_e i_e A} \qquad \text{Eq. (2.1)}$$

where, Q_e is the electro–osmotic flow rate (m^3/s),

i_e is the electrical gradient $\Delta E/\Delta L$ (V/m), where ΔE is the difference in the applied voltage and ΔL is the distance between the electrodes

K_e is the electro–osmotic conductivity coefficient ($m^2/V{\cdot}s$), and

A is cross sectional area perpendicular to the flow (m^2)

An equation for K_e was derived by Casagrande (1949) based on the Helmholtz–Smoluchowski model for electro–osmotic flow:

$$\boldsymbol{K_e = -\frac{\epsilon \zeta n}{\eta}} \qquad \text{Eq. (2.2)}$$

where, ϵ is the permittivity of pore water (F/m),

ζ is the zeta potential (V),

n is the porosity of the medium, and

η is the dynamic viscosity of the pore water ($N{\cdot}s/m^2$)

2.2.3 Electro–migration

Under an externally applied electrical potential, ions move towards the electrode of the opposite charge: the anions move towards the anode and the cations move towards the cathode (Lynch, et al., 2007). This phenomenon is known as electro–migration, depicted in Figure 11. The movement of the soluble and desorbed ions to the oppositely charged electrode is described by the effective ionic mobility which is defined as the ion velocity in the soil under a unit of electrical potential and it is given by (Paillat, et al., 2000):

$$\boldsymbol{u_j = D_j \frac{z_j F}{RT} \tau n} \qquad \text{Eq. (2.3)}$$

where, u_j is the effective ionic mobility ($m^2/V\ s$),

D_j is the diffusion coefficient of ion species j in dilute solution (m^2/s),

z_j is the valence of ion species j,

F is Faraday's constant (96,487 C/mol),

R is the universal gas constant (8.314 J/mol K),

T is the temperature (K),

n is the porosity of soil, and

τ is the tortuosity factor

Tortuosity, τ, is an empirical coefficient that represents the ratio of the straight–through path in the direction of the net flow to the actual distance travelled by a particle, be it an ion (Ashawabkeh & Acar, 1992; Vane & Zang, 1997). τ was introduced in the above equation to account for the complexity of the movement of a particle in a soil mass under an electric potential. The tortuosity factor has values that range between 0.01 and 0.84 in the literature (Acar, et al., 1993; Ashawabkeh & Acar, 1992). A species flux can be expressed in units of mol/m^2s by multiplying equation (2.3) by the concentration of the species (mol/m^3) and the applied voltage gradient (V/m). Equation (2.3) applies to both anion and cation contaminants.

Moreover, the contaminant ions move downstream of the contamination source by diffusion as a result of the presence of a chemical concentration gradient (Acar, et al., 1995). Even though in the absence of an electric field, diffusion plays an important role in ion transport in soils, it is insignificant when compared to electro–migration and electro–osmosis (Paillat, et al., 2000). This follows from the fact that "the ionic mobility of a charged species is at least 1 order of magnitude higher than the diffusion coefficient of the same species" (Acar & Alshawabkeh, 1993). Furthermore, "the ratio of the effective ionic mobility of the charged species under a unit electrical gradient to the effective diffusion coefficient of the same species is about 40 times the charge of the species; therefore, (ion) migration becomes a major contributing component to the total flux" (Acar & Alshawabkeh, 1993).

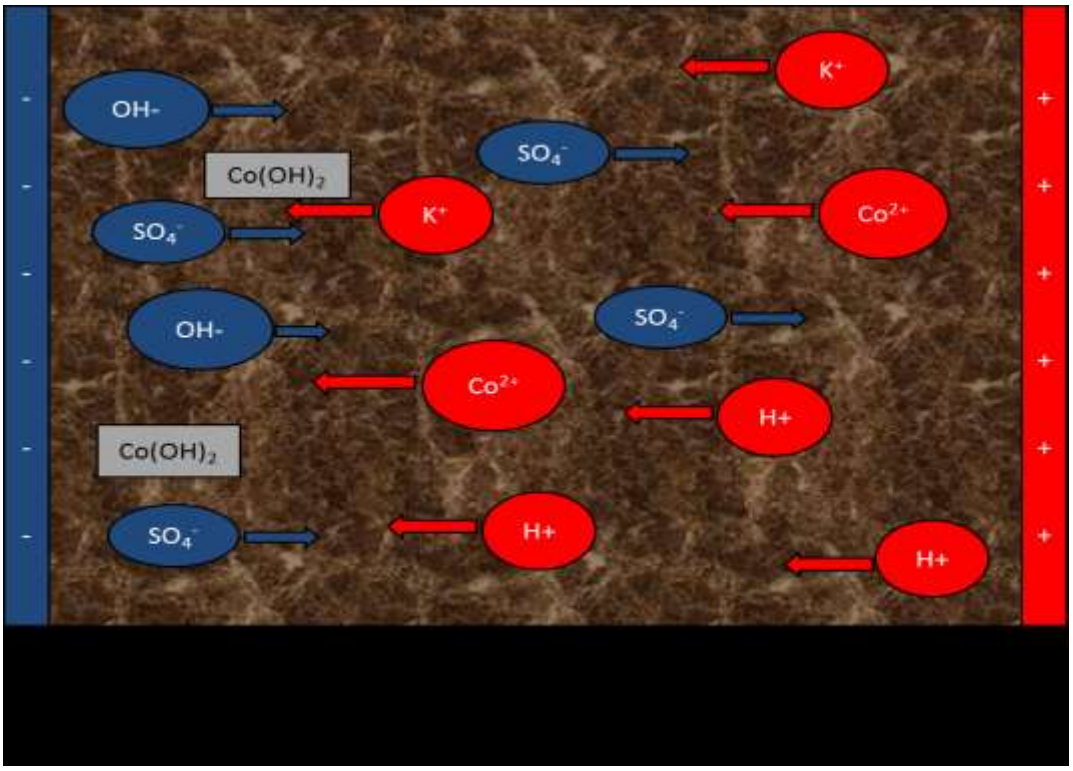

Figure 11 – Representation of electro–migration in soil

2.2.4 Electrophoresis

Under an externally applied electrical gradient, charged soil particles move towards the electrode of the opposite sign. As previously discussed, the surface of clay soil minerals is generally negatively charged leading to their drift towards the anode where they densify (Yeung, 1994), as shown by Figure 12. Electrophoresis plays a larger role in the transportation of clay particles in slurry mixtures where the water content is high and the solid particles can freely move (Lyklema, 2003). Therefore, it is not applicable in the remediation of a compacted or semi compacted soil mass.

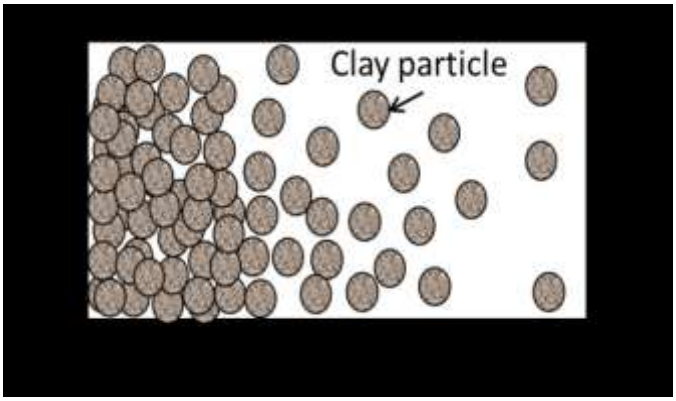

Figure 12 – Illustration of electrophoresis in slurries containing clay particles

2.2.5 Total Contaminants Flux

Theoretical descriptions of each electrokinetic phenomenon were presented in the previous sections. When an electric field is applied to a wet soil mass, these phenomena will all be observed, at least initially (Acar & Alshawabkeh, 1993). The total mass flux, the movement of ions and of the pore fluid with respect to the vertical cross sectional area perpendicular to the direction of flow with respect to the stationary soil particles where the electric field is applied, can be described by the following equation (Acar, et al., 1993):

$$\boldsymbol{J_j = -D_j \frac{\partial c_j}{\partial x} - c_j \left(D_j \frac{z_j F}{RT} \tau n + \frac{\epsilon \zeta n}{\eta} \right) \frac{\partial E}{\partial x} - c_j k_h \frac{\partial h}{\partial x}} \qquad \text{Eq. (2.4)}$$

where, J_j is the total flux of species j (mol/m^2 s),

x is the distance between the electrodes (m),

k_h is the hydraulic gradient due to a head difference (m/s),

h is the hydraulic head (m), and

c_j is the concentration of species j (mol/m^3).

The total contaminant flux is a function of all the gradients acting on species j, the electric field across the length of the soil, the zeta potential of the soil and the diffusion coefficient of species j. The first term in the right hand side of equation (2.4) is the chemical diffusion molar flux of species j due to a concentration gradient across the soil. The left hand side of the second term represents the electro–migration molar flux of species j due to ion–migration. The right hand side of the second term represents the molar electro–osmotic flux due to the electro–osmotic flow. Overall, the second term presents the combined electrokinetic fluxes that would be observed in the soil under an applied potential gradient ($\frac{\partial E}{\partial x}$). The last term in the equation is the molar flux of species j caused by the hydraulic gradient.

2.3 Applications of Electrokinetic Phenomena

There are several uses for electrokinetic processes in environmental engineering and geotechnical engineering beside soil and groundwater remediation. Some of these uses are discussed in the sections below.

2.3.1 Concentration, Consolidation, and Dewatering

Electrokinetic processes, namely electro–osmosis and electrophoresis, are used to accelerate the settling of slurries from wastewater, mine tailings and dredged materials (Yeung, 1994). Slurries are made up of high water content and fine solid particles and, due to their fine nature, particulates require long periods of time to settle by gravity alone. The installation of an electrode of an opposite polarity to the solid particles at the bottom of a dewatering or a sedimentation tank can decrease particle settling time and increase the efficiency of consolidation (Addai–Mensah & Ralston, 2005)

2.3.2 Leakage Repair of In–service Geomembrane Liner

Geomembranes (GM) used as landfill covers can have holes that compromise the primary function of the GM, which is to control infiltration (Rowe, 2004). These holes may be a result of manufacturing defects, or crack propagation under tensile stress or damages during placement (Rowe, et al., 2009). When an electric potential is applied across a defective geomembrane, an electric field is created where the cracks occur due to the fact that GM are insulating materials (Darilek, et al., 1996). If a clay suspension is placed in the impoundment, the clay particles will move towards the electric field by electrophoresis. Eventually, the clays accumulate and clog the leaks (Corapcioglu, et al., 1998). Various laboratory and field studies successfully demonstrate the viability of this in–situ leakage repair method.

Other applications include in–situ characterization of contaminants in soil pore fluid, prevention of moisture rise in capillary systems, and improvement of the carrying capacity of soils (Micic, et al., 2003).

2.3.3 Soil Remediation

Heavy metals such as Cd, Cr, Zn, Fe, and Cu have been the subject of many electrokinetic remediation studies (Shen, et al., 2007; Alcántara, et al., 2012; Darmawan & Wada, 2002; Yuan, et al., 2009; Kim, et al., 2010; Hassan & Mohamedelhassan, 2012). The literature describes several successful soil remediation laboratory scale experiments using electrokinetic barriers (Lageman, et al., 2005). Contaminants migration due to a hydraulic gradient in a porous medium (wet soil) is halted by the presence of a potential difference between two electrodes. Electrokinetic barriers take advantage of electro–osmosis and ion migration under the influence of an applied electric field.

The electro–osmotic flow is dragged towards the cathode by the migrating cations. It slows down the net flow of the contaminated water towards the anode due to a pressure difference (Lynch, et al., 2007). Furthermore, in an uncontrolled electrolyte, the water oxidation by the electrolysis reaction generates a low pH zone closer to the anode which is a suitable environment for desorption and increased metal oxides dissolution as previously demonstrated in Figure 5 (Darmawan & Wada, 2002). In an uncontrolled electrolyte, the pH of the soil near the cathode and/or the anode is not externally influenced by the addition of solutions that lower or raise the pH. The hydrogen ion will be in competition with the metal ions for the ion exchange sites on the clay fraction of the soil. Although the metal ions may be adsorbed or complexed on newly available ion exchange sites, there will be a net cations migration towards the cathode (Lageman, et al., 2005). On the other hand, closer to the cathode compartment, the pH levels rise and the system favors metal ions adsorption and precipitation (Evangelou, 1998). The anions such as sulphate and chromate will be in competition with the hydroxyl ions such that they will be displaced and carried towards the anode by electro–migration (Lageman, et al., 2005).

In other words, near the anode, the low pH promotes dissolution of metal hydroxides and enhances electro–migration of the soluble ions. As the cations migrate to the cathode they meet the high pH front generated by the pore water reduction at the cathode, equation (2.5a). Cations form insoluble precipitates in elevated pH environments. Precipitation and adsorption reduce cation contaminants availability for transport by the pore fluid. In remediation efforts contaminants precipitation is unfavourable since the goal is to extract

the contaminants and to restore the soil. Extraction, which is generally achieved in the field by extraction wells (Figure 13), aims at increasing heavy metals mobility to enhance their removal. In Figure 13, lead (Pb), is used as an example contaminant to demonstrate the various electrokinetic phenomena observed in the soil in remediation work. Near the anode, the precipitated lead (II) oxide is solubilised in the low pH environment and Pb^{+2} is moved towards the cathode by electro–migration. The water molecules are dragged by the surrounding lead ions towards the cathode. Near the cathode, where the extraction well is located, the pH rises due to water reduction and the production of hydroxyl ions. The high pH offers a suitable environment for lead (II) hydroxide to precipitate. As a result the remediation system becomes ineffective in removing lead.

Furthermore, when the anode is placed downstream of the contaminated groundwater flow path, the pore fluid travels upstream towards the cathode by electro–osmosis, as previously discussed, shown in Figure 13. This would reduce the net volumetric flow of the contaminated groundwater towards the anode. Therefore, the combination of all these phenomena and reactions form a barrier to cations (lead), including heavy metal ions spread and transport downstream. This phenomenon is only applicable to cation contaminants.

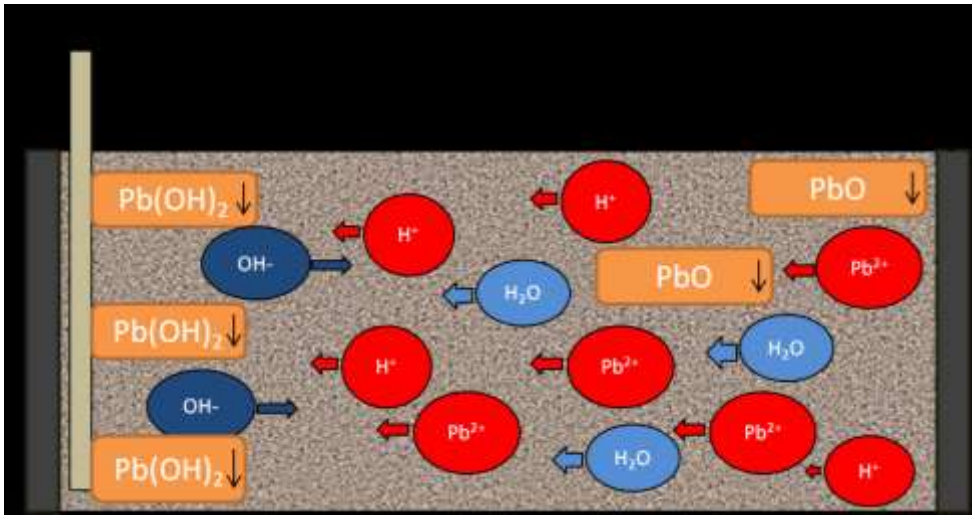

Figure 13 – Electrokinetic remediation in the field

The experimental setup for such tests mainly consists of a compacted and contaminated soil in a cell, two electrode compartments and a power supply as shown in Figure 14. The

dimensions of the cell vary throughout literature; however, in general, a ratio of 2:1 of the width to the height of the cell is observed. However, the cell length is not consistent in the literature. Different materials have been used for the electrodes; however, graphite is most commonly used (Yuan, et al., 2009; Darmawan & Wada, 2002; Li, et al., 2011; Hassan & Mohamedelhassan, 2012).

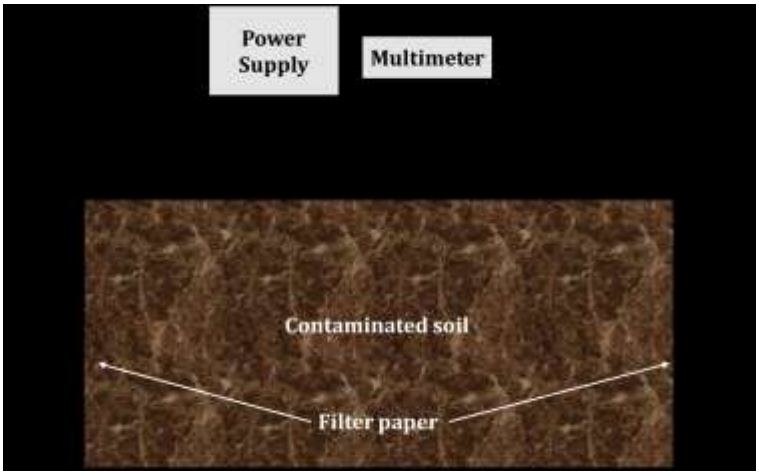

Figure 14 – Schematic of main components of an EK soil remediation cell

Several factors affect the success and efficiency of the electrokinetic barrier to halt pollutants migration. Increasing the applied voltage increases the solubilisation of metal ions at the anode and it increases the volumetric flow rate of osmotic flow towards the cathode as shown by equation (2.1). However, many experiments demonstrated that increasing the energy consumption by increasing the voltage does not result in a proportional improvement in the performance of the electrokinetic remediation cell (Kim, et al., 2010; Wei & Hui, 2011). For an electrokinetic barrier system, the optimum voltage is the voltage at which the ions that are carried by the hydraulic flux are prevented from reaching the uncontaminated soil by the electro–osmotic fluid flux (Acar, et al., 1995; Paillat, et al., 2000). Although the fluid flow ceases when the hydraulic flux equals the electro–osmotic flux, the remediation process continues to effectively immobilize the ions by electro–migration (Acar, et al., 1995). Many studies showed that ion migration is the major contributing factor of ion transport (Acar & Alshawabkeh, 1993; Paillat, et al., 2000). In turn, the current and the voltage drop across a soil mass are influenced by the fashion in

which the current is applied; either continuous or intermittent, as well as the material of the electrodes (Mohamedelhassan & Shang, 2001).

In electrokinetic configuration with intermittent current the electric field is provided with on and off periods rather than continuously. Experiments conducted by Mohamedelhassan and Shang (2001) concluded that interrupted current with two minutes on and one minute off improved electro–osmotic flow and yielded the highest electro–osmotic permeability. Reddy and Saicheck (2004) reported experimental results that confirm the advantages of current intermittence over continuous current. In another study, the use of solar cells to remove Cd from a contaminated soil gave similar results to those obtained using a conventional direct current supply (Yuan, et al., 2009). Current intermittence was established by the day and night cycles. Additionally, Sun and Ottosen (2012) evaluated the effects of current intermittence on energy consumption and the removal of cadmium and copper from a polluted soil. Even though their experiments were conducted using an ion exchange membrane (electrodialytic) to separate the soil from the solution in the electrode compartments, the principle of electrodialytic and electrokinetic remediation remains the same. They concluded that heavy metal removal was increased and power expenditure was lowered by using a pulsed current (Sun & Ottosen, 2012). Thus, there is enough evidence in the literature to confirm the superiority of discretely applying an electric field in electrokinetic remediation to its continuous application.

The electrode materials play an important role in the voltage drop at the solid–electrode interface and electrode reactions. This in turn influences the electro–osmotic flow and electrode corrosion. Therefore, the selection of a suitable electrode material is important for the success of electrokinetic processes. The electrode materials should be selected such that the voltage drop at the interface between the electrode and the soil is minimized, the electro–osmotic flow is maximized and the material has high resistance to corrosion (Mohamedelhassan & Shang, 2001; Casagrande, 1949). Both metallic and non–metallic conductors such as Fe, Cu, and graphite may be used for fabricating the electrodes (Lockhart, 1983). In one study, the flow rate generated by an iron electrode was twice as much as that generated by a graphite electrode for the same power consumption (Segall & Bruell, 1992). Mohamedelhassan and Shang (2001) conducted tests to evaluate the

influence of electrode materials on electro–osmosis by comparing different electrode pairs. The results showed that steel resulted in the least voltage loss at the soil–electrode interface. On the other hand, the largest voltage loss occurred at the carbon anode regardless of the cathode electrode material whereas copper and steel anodes resulted in comparable voltage losses (Mohamedelhassan & Shang, 2001). Even though some materials perform better than others, factors such as cost, duration of the remediation process and any environmental impacts associated with the electrodes, should be evaluated when choosing the electrode material.

Moreover, several laboratory studies in the literature examined the influence of soil type on the efficiency of electrokinetic remediation. The soil's mineralogical composition and its carbonate content (buffering capacity) (Lynch, et al., 2007) play an important role in electrokinetic remediation (Casagrande, 1949). For instance, the rates of Cr(VI) removal by glacial till, kaolin and Na–montmorillonite were compared in one study (Reddy, et al., 1997). The results showed that glacial till achieved the highest rate of removal due to its high carbonate content which served to increase the buffering capacity of glacial till. The buffering capacity prevented the development of a sharp pH gradient and minimized the adsorption of Cr(VI) thus increasing its transport and removal (Reddy, et al., 1997). In electrokinetic remediation studies, removal of heavy metals is achieved by desorbing and solubilising contaminants from a polluted specimen in order to mobilize the contaminants and allow their transport by electro–osmosis and/or electro–migration.

Additionally, it was found that while the presence of iron oxides had little to no effect on the removal efficiency of Cr(VI) in kaolin and Na–montmorillonite. However, in glacial till, the migration of chromium was hindered by the creation of complex geochemistry with hematite (Reddy, et al., 1997). A subsequent study that built on the previous work introduced a more complex contaminant environment by studying the removal of chromium, cadmium and nickel on kaolin and glacial till (Reddy & Parupudi, 1997). The results showed that migration of Ni(II) and Cd(II) was significant in the kaolin soil but the high pH near the cathode resulted in their precipitation. However, due to the buffering capacity of glacial till, the migration of these two contaminants was insignificant (Reddy & Parupudi, 1997).

Likewise, Darmawan and Wada (2002) investigated the influence of clay mineralogy on the electrokinetic remediation of different soils. The results were in agreement with other works in the field; soils with high carbonate content and iron oxides were less effective in the transport of heavy metals under an applied electric field due to heavy metal precipitation as hydroxides and/or carbonates (Darmawan & Wada, 2002; Ouhadi, et al., 2010). Evidently, the soil mineralogy and composition have great influences on the efficiency of electrokinetic decontamination of soils from heavy metals.

Precipitation and adsorption hinder the remediation process of transporting the cationic contaminants from the anode to the cathode by electrokinetics. Thus, it is important to look into the factors influencing these two phenomena. Precipitation of heavy metals is mainly controlled by the medium's pH, as previously demonstrated in Figure 5 (Evangelou, 1998). However, the influences of pH, ionic strength and zeta potential of the pore fluid on the adsorption of cations on soil particles were the subject of many laboratory works (Criscenti & Sverjensky, 1999; Vane & Zang, 1997; Mattigod, et al., 1979). The ionic strength is, itself, dependent on the electrolyte solution (Mitchell & Soga, 2005). For example, in NaCl solutions, divalent metal ions adsorption strongly decreases with increasing the ionic strength (Criscenti & Sverjensky, 1999). On the other hand, transition and heavy metal adsorption in $NaNO_3$ solutions exhibited little to no dependence on the ionic strength of the solution (Criscenti & Sverjensky, 1999). The magnitude of the zeta potential, ζ, (Butt, et al., 2006), depends on the ionic strength, the pH of the solution, and the soil minerals (Vane & Zang, 1997). Vane and Zang (1997) investigated the effect of pH, ionic strength and soil type on zeta potential and found that the zeta potential of kaolinite exhibited strong pH dependence. In fact, the zeta potentials varied from +0.7 mV to –54 mV at pH 2 and 10, respectively (Vane & Zang, 1997). On the contrary, the zeta potential of bentonite did not show the same pH dependency and was found to vary between–31mV and –36 mV in a pH between 2 and 10 (Vane & Zang, 1997). Therefore, zeta potential is, itself, a function of pH (Acar, et al., 1993) and decreases linearly with the logarithm of the pH of the soil medium (Hunter, 1982). The sign change of ζ may reverse the direction of osmotic flow (Acar, et al., 1993); Vane & Zang, 1997; West & Stewart, 2000). Furthermore, the sensitivity of the zeta potential to the ionic strength of the solution was similar to the pH dependence. The ζ of

kaolinite decreased as the electrolyte concentration increased and that of bentonite remained insensitive to the change in the electrolyte concentration (Vane & Zang, 1997). Zeta potential directly influences the electro–osmotic permeability coefficient as given by equation (1.13) (Ashawabkeh & Acar, 1992). In summary, the more negative the value of zeta potential is, the larger the osmotic flow towards the cathode will be (Acar, et al., 1993).

To improve the performance of electrokinetic remediation of soils, several solutions such as weak acids and complexing and chelating agents were tested to mobilize the heavy metals (Fansheng, et al., 2013; Kim, et al., 2005; Lee & Yang, 2000). Heavy metals are either adsorbed and/or precipitated due to the high pH of the cathode environment developed during the electrokinetic remediation process (Gidarakos & Giannis, 2006). The accumulation of heavy metals at the electrodes clogs up the soil pores, lowers electro–osmotic flow, and increases the power requirement (Acar, et al., 1995; Acar, et al., 1993).

There are several solutions, commonly known as purging solutions, such as acetic acid, citric acid, and pyridine–2–6–dicarboxylic acid (PDA), ethylenediaminetetraacetic acid (EDTA), and hydrochloric acids that are used to control the cathode pH of the contaminated soil (Gidarakos & Giannis, 2006). As previously discussed, at low pH values desorption of metal ions and dissolution of metal hydroxides/carbonates is encouraged (Darmawan & Wada, 2002; Acar, et al., 1995). A number of electrokinetic tests were performed by Fansheng et al. (2013) to compare the efficiency of distilled water, acetic acid and HCl to remove chromium from a polluted soil. The results showed that even though acetic acid did improve the removal of Cr, the greatest removal efficiency was obtained from conditioning the cathode with hydrochloric acid (Fansheng, et al., 2013). However, the use of hydrochloric acid as a purging solution adds secondary pollution to the system (Acar, et al., 1995). The released chlorine ion, Cl^-, can be oxidized to chlorine gas, as it migrates to the anode. Moreover, the formation of insoluble chlorine salts is possible which has environmental and health consequences (Acar, et al., 1995; Fansheng, et al., 2013). By contrast, acetic acid is a biodegradable, organic acid that poses no health risks when used for conditioning and forms soluble metal acetates (Gidarakos & Giannis, 2006). Gidarakos and Giannis (2006) compared the influence of acetic acid, citric acid and PDA as washing and purging solutions on the removal of Cd^{2+} from a contaminated soil. The cathode pH was

controlled such that the tests were conducted under acidic conditions (Gidarakos & Giannis, 2006). They reported that the use of acetic acid as a purging solution achieved 90% removal of Cd but it did not accelerate the desorption of Cd from the soil. PDA as a purging solution yielded the highest cadmium removal in a short duration of time (Gidarakos & Giannis, 2006). In addition, zinc removal by EDTA and metabisulfite ($Na_2S_2O_5$) was evaluated. The results showed that Zn formed a negative complex with EDTA: Zn–$HEDTA^-$, in the experiment where EDTA was used as purging solution and acetic acid as washing solution. The Zn–$HEDTA^-$ complex moved towards the anode where it was accumulated (Gidarakos & Giannis, 2006). Zn removal greater than 96% was achieved by $Na_2S_2O_5$ when used as washing solution.

Lee and Yang (2000) proposed an alternative method using a purging or washing solution to control the cathode pH. Their method relied on the circulation, by pumping, of the hydroxyl ions generated at the cathode to the anode. The pH of the cathode decreased due to H^+ migrating from the anode (Lee & Yang, 2000). Direct comparison between the removal efficiencies of their control experiment without circulation and the one with circulation could not be made due to the difference in the remediation period. However, higher removal efficiency was observed in the slices of soil exposed to circulation of the OH^- ions (Lee & Yang, 2000). The obvious advantage of this method is the elimination of introducing secondary pollution which could occur when a chelating agent or a solubilisation solution is used. Also, the circulated volume was sufficient to control the pH at the cathode. This diminished the effluent from the cathode compartment (Lee & Yang, 2000). Nonetheless, circulating to the anode some of the contaminants present at the cathode is possible.

In summary, controlling the pH in the cathode compartment is necessary for electrokinetic remediation to work in order to achieve better contaminant transport and removal from a soil medium.

To conclude, electrokinetic cells are an inexpensive in–situ technique to remediate soils and groundwater and potentially prevent groundwater contamination. Solar energy can be used to provide low voltage direct current.

3.0 Motivation for the Project

Cobalt is a concern at the Musselwhite mine because its concentration in the groundwater had steadily increased between 1997 and 2013. Unlike other contaminants such as Fe, cobalt contamination is not produced in the ore extraction process but rather it is introduced in the milling process. As part of the mining operation, the mined ore is grinded and crushed using grinding rods and balls which are completely consumed in the process, as previously mentioned. These rods and balls are the source of cobalt. Although the mine is not looking to change its operation, it is however investigating ways to lessen cobalt concentration in groundwater and to prevent adverse future cobalt contamination.

Some guidelines for cobalt were developed and adopted based on animal studies, even though the literature lacks data on the effects of cobalt on humans (US EPA, 2000). Some oral studies showed slow growth and increased death rates in pups. Additionally, it has been reported that oral intake of cobalt causes vomiting, diarrhea, liver injury, and skin inflammations in humans (US EPA, 2000). While the Canadian government does not have any guidelines for cobalt in groundwater or drinking water, the World Health Organization (WHO) recommends that a maximum total cobalt concentration of 0.110 ppm should not be exceeded to protect aquatic life from acute toxicity in fresh water. A maximum concentration of 0.004 ppm should not be exceeded to protect against chronic toxicity (Nagpa, 2004). Also, the government of Ontario developed a freshwater quality objective of 0.0009 ppm of cobalt based on the Lowest Observed Effect Concentration (LOEC) of 0.0093 ppm (Nagpa, 2004).

The current mine discharge of cobalt into the TMA is higher than the recommended chronic toxicity limits. This is inferred from the monitoring data which show that even though the groundwater flows through the aquifer where cobalt adsorption onto the soil may possibly occur, the cobalt concentration is still detectable in the sampled groundwater. The adsorption of cobalt onto the soil is explained later in more detail. It was demonstrated from the groundwater monitoring data that the cobalt concentration profile steadily increased over the past 16 years of mining operations, as shown in Figure 15.

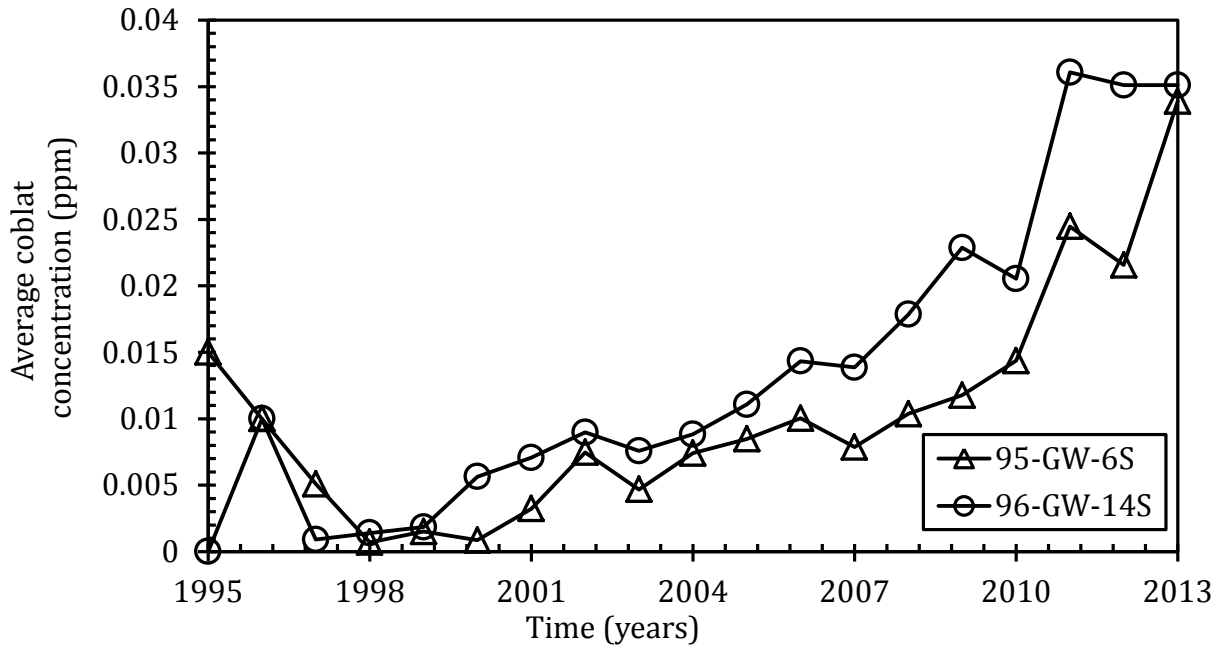

Figure 15 – Cobalt concentration trend over the past 18 years (Musselwhite Mine, 2013)

The well historical data was obtained from the Musselwhite mine and utilized by the candidate. The locations of these monitoring wells, as well as other significant locations, are indicated in Figure 16. In the light of all the facts, an electrokinetic barrier study was proposed to determine the feasibility of the technique to prevent groundwater contamination downstream of the TMA. Given that the tailings are partially saturated, initially, the cobalt present in the tailings impoundment is dissolved by oxidation due to acid mine drainage. During rainfall the dissolved cobalt and other contaminants are transported to the groundwater which is below the tailings impoundment. As the groundwater migrates due to a gradient, it contaminates the aquifer. This study focuses on hindering cobalt transport in the groundwater. It is well understood that presently the cobalt concentrations in the groundwater at the mine site are not very high. However, because the cobalt concentration continues to increase with the mine's operations, it is predicted that the cobalt concentration will become a greater concern in the future. In the light of this, the intent of this research project is to provide results that are relevant and valid in the future when the cobalt concentrations are much higher than they are today at the mine site.

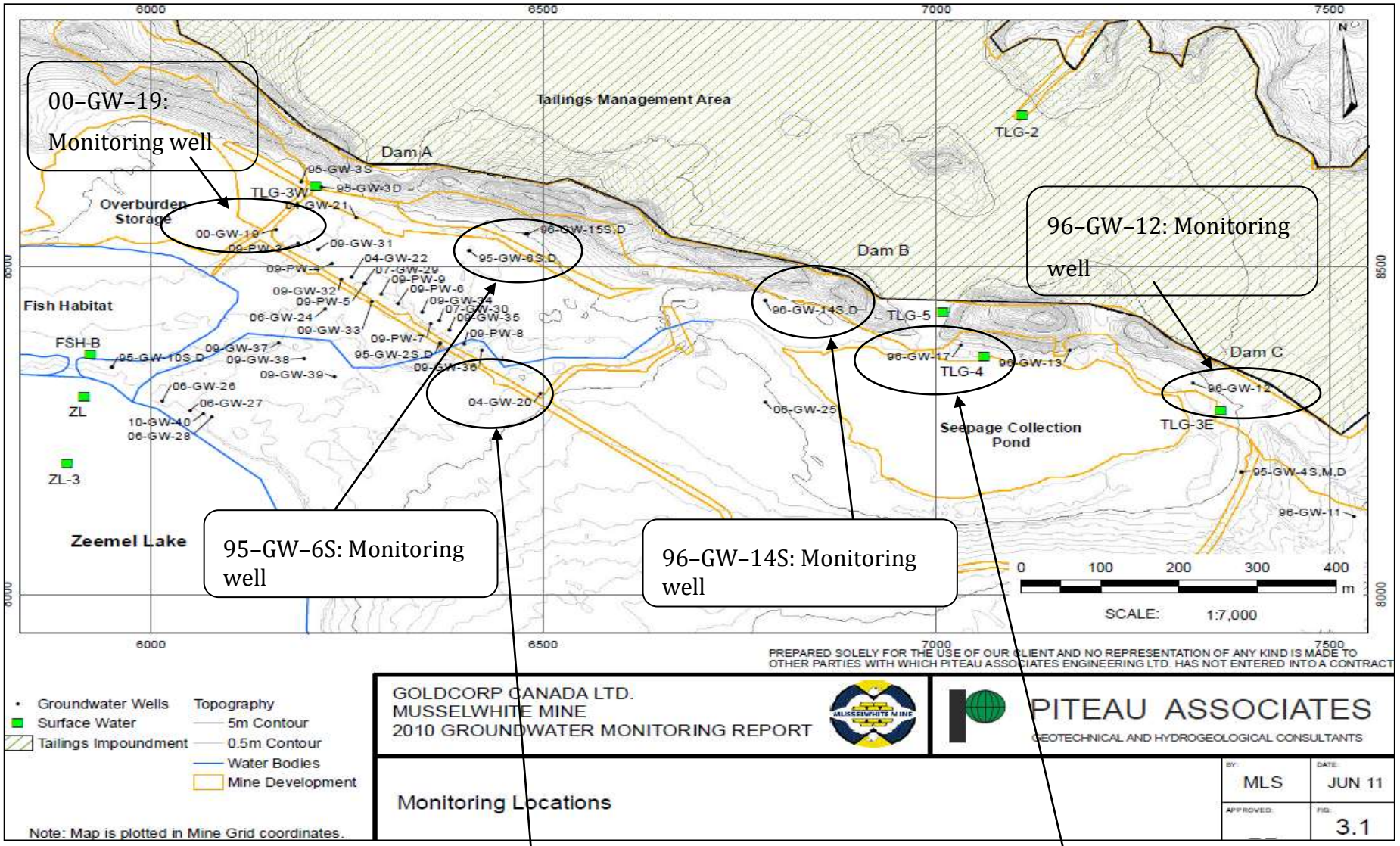

Figure 16 – Locations of several monitoring wells (Piteau Associates, 2011)

4.0 Background Information

Musselwhite mine is owned and operated by Goldcorp Canada Ltd. for gold mining. The mine is located approximately 480 km northwest of Thunder Bay, Ontario. It is an underground mine with two open pits constructed between 1996 and 2004 at Opapimiskan lake (Goldcorp, 2013). As of 2013, the mine has a milling/processing capacity of 4500 tonnes per day. The mining operation consists of crushing, grinding, leaching by cyanide, carbon in pulp recovery, and electrowinning (Goldcorp, 2013).

The coarse ore piles are fed to a surface crusher plant and then separated by size using screens with 16 mm openings. At this point, the fine ore is sent to the mill grinding where the rod mill breaks down the ore from 1.59 cm or less to approximately 80% passing 100 μm. Liquid cyanide in the form of sodium cyanide (NaCN) is added to leach the gold from the ore slurry to a solution form for further separation. Lime is also added in the process to prevent the formation of hydrogen cyanide (HCN). The leachate of cyanide and gold is then sent to the carbon in pulp recovery. The gold adsorbs onto the carbon as carbon has a large porous surface area. Then the gold loaded carbon is washed with hydrochloric acid and sent to an autoclave for stripping. The gold is stripped from the carbon under high pressure. The gold rich solution is pumped to the electrowinning cells where the gold forms a sludge that is electroplated on the cathode. The sludge is then dewatered and smelted into gold bars. In order to reduce the cyanide concentrations to less than 10 parts per million (ppm), INCO SO_2 CN destruction method is used. During this treatment, weakly bonded metal cyanides are decomposed to release free cyanide (CN^-) and metal ions (Koksal, et al., 2003). Afterwards, the tailings are thickened by decanting the slurry water in a tailings thickener. The decanted slurry water is pumped back for use as process water and the tailings are distributed in a tailings management area.

The Tailings Management Area (TMA) is located 1.5 km south of the mine site. The tailings pond, the Seepage Collection Pond (SCP), Zeemel Lake, and a few small un–named ponds are the collection of ponds in and around the TMA that influence the groundwater flow

(Piteau Associates , 2011) as shown in Figure 17. Lines A–A' and B–B' in Figure 17 represent cross sections that are not relevant to the present study.

Additionally, the net neutralization potential of the tailings at Musselwhite indicates that the tailings are potential acid mine drainage generators by the mechanisms previously discussed. The net neutralization potential (NNP) describes the tailings natural ability to balance the acidity generated in the tailings management area or as a result of low pH input to the tailings (Morin & Hutt, 1997). It is defined as the balance between the acid generation potential (AP) and the neutralization potential (NP). It is mathematically presented as: NNP= NP–AP. A negative NNP value indicates that the buffering capacity of the tailings and the soil in the tailings impoundment buffering capacity, which is mostly brought by carbonate minerals such as calcite, is not sufficient to neutralize the acidity produced by the tailings (Yalcin, et al., 2004). This means that AMD will be generated by the tailings once the buffering capacity is depleted.

Pipelines transport the tailings from the mill to the TMA. Prior to May 2010, tailings were directly discharged to the TMA at an average rate of 4,000 tonnes per day. After the aforementioned date, the tailings are first thickened and then stored in the TMA. Data on the aquifer and groundwater quality is collected from 42 groundwater monitoring wells and seven pumping wells. It is generally observed that the contaminated groundwater plume advances towards and underneath Zeemel Lake. Only iron and cobalt exceeded the trigger limits in groundwater (Piteau Associates , 2011). Furthermore, the monitoring data show increasing cobalt concentrations which pose some risks if it reaches the Zeemel Lake or the surrounding water bodies.

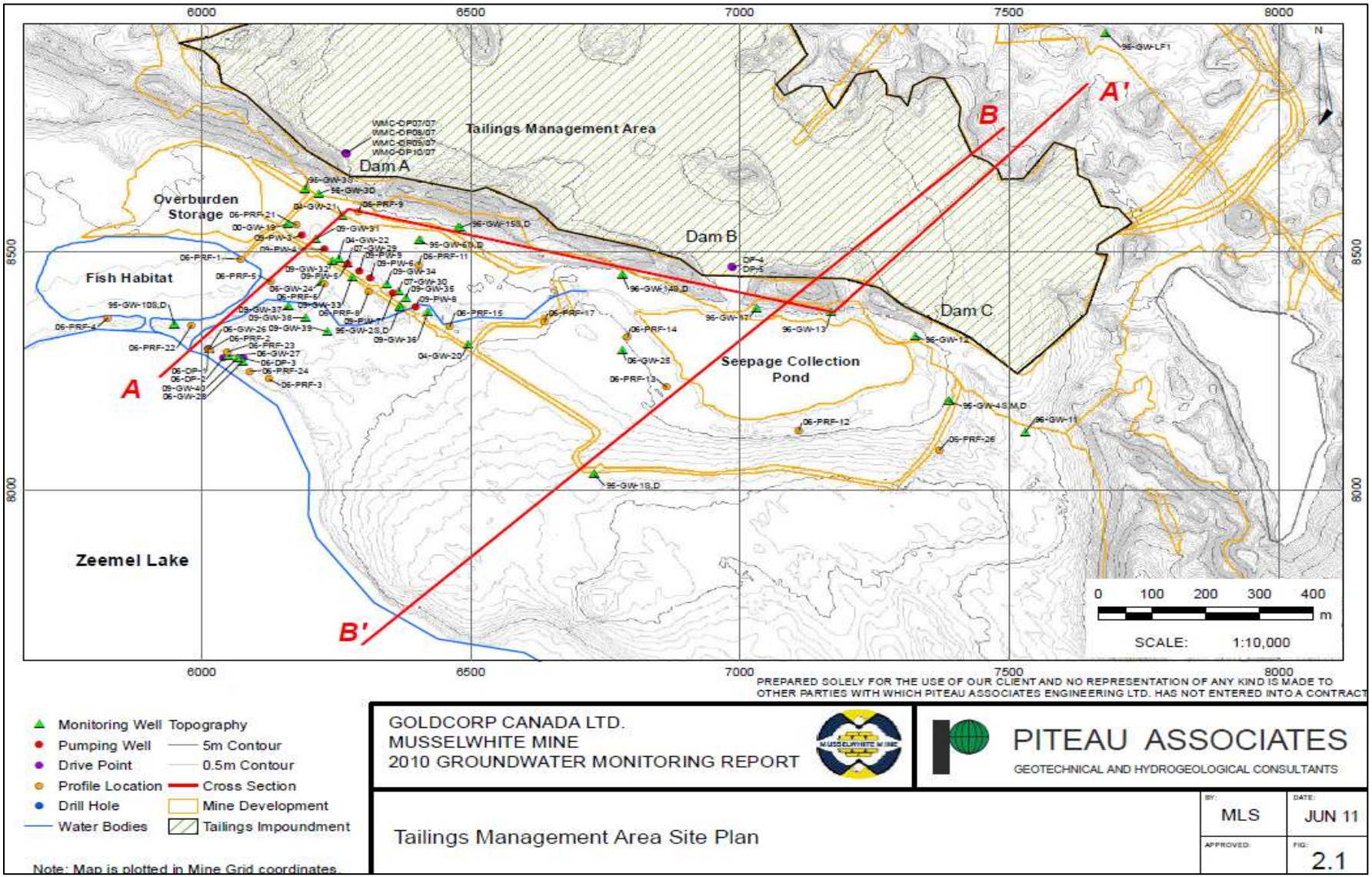

Figure 17 – Tailings management area site plan (Piteau Associates, 2011)

The background constituents of the tailings water and the solid phase, the constituents of the mine soil in the vicinity of the TMA and of the groundwater were determined by the candidate. The results are presented and discussed in the following sections. To note, the different tests and analyses (ex. dilution tests) in the following sections were carried out by the candidate.

4.1. Fresh Tailings Water

Fresh tailings water samples were obtained directly from the mill before their discharge to the tailings pond in sealed containers. In the milling operations, cyanide at high concentrations is used for separating the gold from the ore slurry. However, before the tailings are distributed to TMA, cyanide destruction takes place to ensure that the allowable discharge limits are met, as previously mentioned. Therefore, tailings water before and after cyanide destruction contains slightly different concentrations of elements as summarized in Table 1. Each of the reported concentrations is the average of three samples. The standard deviation was also reported. The pHs of the tailings water before and after CN destruction are, on average, 10.2 and 9.1 respectively. Samples from before and after cyanide destruction contain large amounts of calcium, sodium, potassium and sulfur as bolded in Table 1. It should be noted that the concentration of cobalt drops after CN destruction. This is likely due to the formation of insoluble cobalt–ferrocyanide complexes by reaction (4.1) (Koksal, et al., 2003):

$$\boldsymbol{2Co^{2+}(aq) + Fe(CN)_6^{4-}(aq) + 7H_2O(l) \rightarrow Co_2Fe(CN)_6 \cdot 7H_2O\ (s)} \qquad \text{Re. (4.1)}$$

Similarly, lower concentrations of soluble calcium are noticed in samples after CN destruction. Sulfuric acid forms as free cyanide is oxidized to the unstable cyanate ion (CNO^-). H_2SO_4 reacts with lime to form gypsum. These two reactions are shown below (Koksal, et al., 2003).

$$\boldsymbol{CN^- + SO_2 + H_2O + O_2 \rightarrow OCN^- + H_2SO_4} \qquad \text{Re. (4.2)}$$

$$\boldsymbol{H_2SO_4 + Ca(OH)_2 \rightarrow CaSO_4 \cdot 2H_2O} \qquad \text{Re. (4.3)}$$

On the other hand, the concentration of copper (Cu) in the effluent of CN destruction is noticeably higher. This increase is due to the addition of copper sulfate used as a catalyst in the CN destruction tank.

Table 1 – Detectable constituents of fresh tailings water before and after CN^- destruction

Element	Before CN^- Destruction (ppm)	After CN^- Destruction (ppm)	ICP detection limits (ppm)
Al	0.540±0.003	0.073±0.002	0.04
As	0.132±0.008	BDL	0.05
B	0.285±0.002	0.309±0.003	0.04
Ba	0.032±0.001	0.051±000	0.005
Ca	**125±1.71**	**113±0.300**	**0.1**
Co	**0.387±0.003**	**0.145±0.001**	**0.005**
Cu	6.12±0.056	**22.16±0.316**	0.003
Fe	4.81±0.021	5.04±0.056	0.008
K	**114±1.47**	**82±0.297**	**0.1**
Mg	0.589±0.082	7.37±0.034	0.01
Mn	0.005±0.000	0.006±0.000	0.002
Mo	0.064±0.003	0.038±0.001	0.02
Na	**346±4.97**	**257±0.889**	**0.1**
Ni	0.114±0.004	0.250±0.003	0.04
S	**353±2.94**	**249±0.458**	**0.1**
Si	2.32±0.043	2.29±0.001	0.03
Sr	0.7950.009±	0.738±0.003	0.004
Zn	0.008±0.001	0.041±0.000	0.005

Major ions are indicated by bolding

**BDL= Below Detection Limit*

4.2 Oxidized Tailings

Three samples of oxidized tailings were collected by the Musselwhite mine personnel from Dam A, Dam B, and Dam C along the TMA which are indicated in Figure 16. The samples were simply excavated, packed in airtight plastic bags and sent to the candidate. First, the samples were sent by the candidate to the Forest Resources & Soil Testing (FoReST) Laboratory at Lakehead University to be digested using nitric/hydrochloric acid, then analyzed with ICP–AES at the Lakehead University Instrumentation Laboratory. The test results show high concentrations of Fe, Cu, Pb and As near Dam A and high concentrations of Al, Mg, and K near Dam B. Oxidized tailings from Dams A & B are at higher pH values than Dam C (Table 3). The average pH of the oxidized tailings from Dam A, Dam B and Dam C are 6.8, 7.2 and 5.4, respectively. The pH range of the oxidized tailings around Dam A and Dam B produces favourable conditions for immobilization of heavy metals by adsorption and precipitation. Generally, this resulted in more mass of metals per mass of oxidized tailings near Dam A & Dam B.

Due to ICP–AES limitations, cobalt concentrations could not be detected as a result of strong interference with iron. However, the rinse concentrations of each oxidized tailings sample were also determined. The rinse tests were carried out by the candidate in triplicates where oxidized tailings of known mass were placed in polypropylene tubes and a known volume of distilled water was added. The mixtures were then shaken overnight in a rotary shaker. Next, the samples were centrifuged at 4000rpm for 10 minutes. The supernatant was drawn and sent to ICP for analysis. These tests were conducted at three water to tailings ratios of 2, 10, and 20 to investigate whether the cobalt concentration was a function of dilution, or pH or both. Additionally, the same rinse test analysis was performed on the fresh tailings (non–oxidized) while keeping the same ratio between the solid and the liquid phase. The results of the rinse tests are tabulated in Table 3.

Table 2 – Elemental concentrations in oxidized tailings

Concentration (mg/kg dry tailings)			
Element	**Dam A**	**Dam B**	**Dam C**
Al	11813	14307	12151
As	445.1	132.5	180.5
B	15.2	14.2	13.7
Ba	87.7	123.7	122.6
Cd	15.3	14.2	13.7
Cr	57.9	64.8	50.5
Cu	120.1	109.0	94.0
Fe	89140	80691	78296
K	4324	5023	4052
Mg	4236	5214	4306
Mn	373	352	307
Mo	0.67	0.17	1.20
Na	412	332	303
Ni	77.3	57.6	37.1
P	467	425	527
Pb	116	109	115
Sb	2.971	BDL	BDL
Si	175	215	163
Ti	657	766	692
V	56.4	57.7	51.9
Zn	46.5	45.1	38.1

**BDL=Below Detection Limit*

Table 3 – Co concentration and pH in rinsates from fresh and oxidized tailings

Source	Water/ Tailings	Average pH	Co conct. (ppm)
Dam A	2	6.86	0.099
	10	6.86	0.044
	20	6.66	0.034
Dam B	2	7.22	0.014
	10	7.22	0.006
	20	7.11	0.005
Dam C	2	5.31	0.302
	10	5.45	0.108
	20	4.84	0.088
Fresh tailings before CN destruction	2	9.59	0.0712
	10	9.58	0.0150
	20	9.40	0.0086
Fresh tailings after CN destruction	2	8.42	0.0125
	10	8.62	0.0133
	20	8.73	0.0013

The results in Table 3 suggest that the dilution of the oxidized tailings has an effect on the concentration of cobalt. As the dilution ratio increased, cobalt's concentration in the rinsate decreased, Figure 18. However, the mass of cobalt released from the tailings increased with the dilution ratio, as shown in Figure 21. This suggests that as the groundwater goes through the oxidized tailings, more cobalt will be leached out and released to the environment. As well, the masses of cobalt released from the fresh tailings are plotted against the dilution ratios in Figure 22. Dilution brings the pH down which will eventually mobilize more cobalt, since the overall trend is that more cobalt is released at lower pH values. This trend is graphically represented in Figure 20. This trend further supports the conclusion that more cobalt is released at higher dilution ratios. The cobalt concentration in the rinsate from fresh tailings prior to cyanide destruction is much higher compared to its concentration in the fresh tailings rinsate after cyanide destruction as demonstrated in Figure 19. This is due to the formation of insoluble cobalt–ferrocyanide complexes.

The degree of dilution has a more pronounced influence on the cobalt concentration and mass released than it has on the change of the rinsate pH as given in Table 3. Furthermore, it can be inferred that the tailings near Dam C are the most oxidized: they have the lowest pH values, as shown in Figure 20, and release the highest cobalt concentrations, as shown in Figure 18, at all dilution ratios.

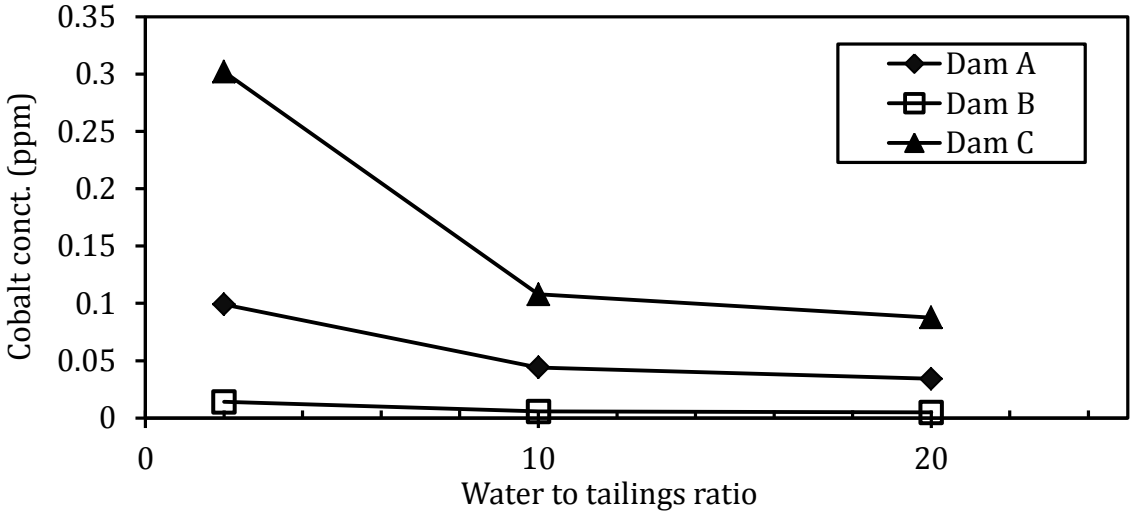

Figure 18 – Cobalt concentration in the oxidized tailings vs. dilution ratio

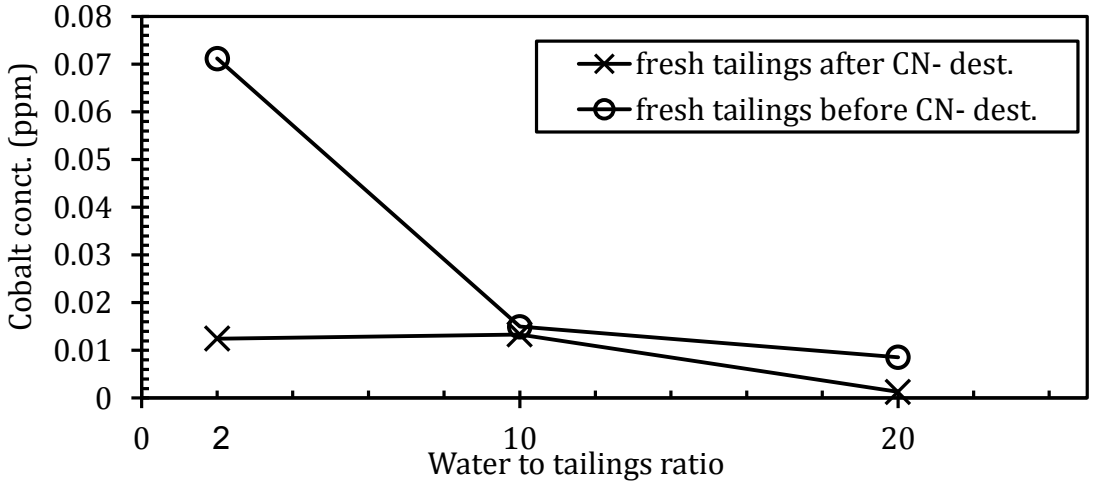

Figure 19 – Cobalt concentration in the fresh tailings before and after CN destruction vs. dilution ratio

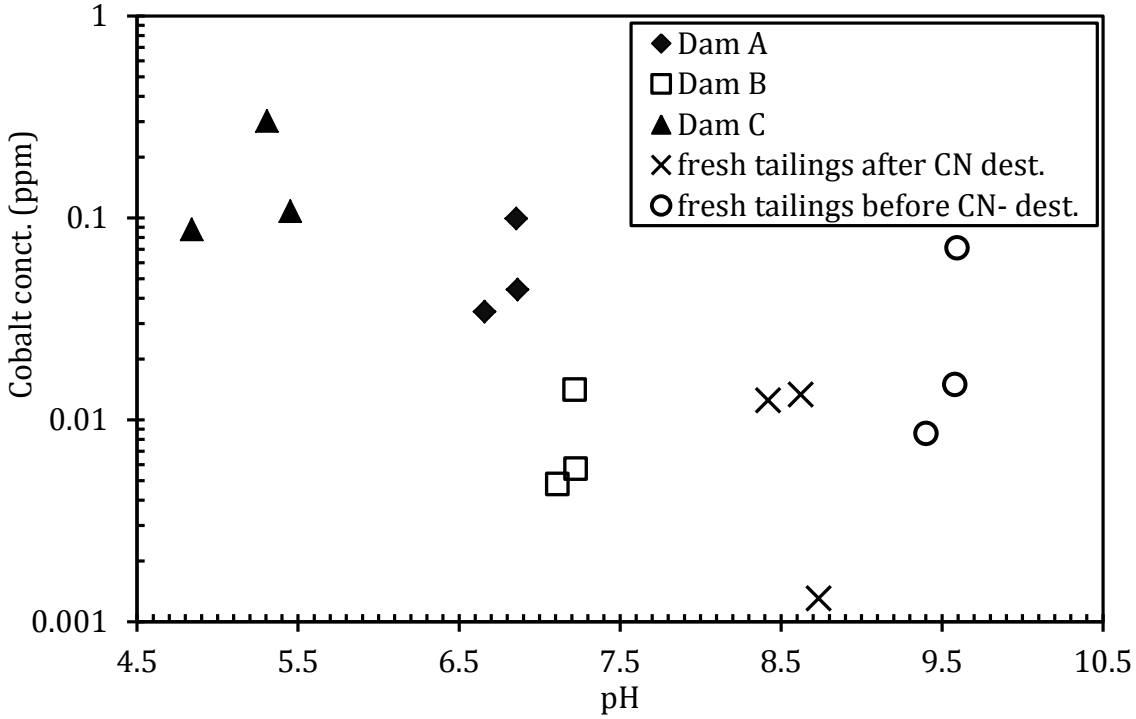

Figure 20 – Cobalt concentration vs. rinsate pH

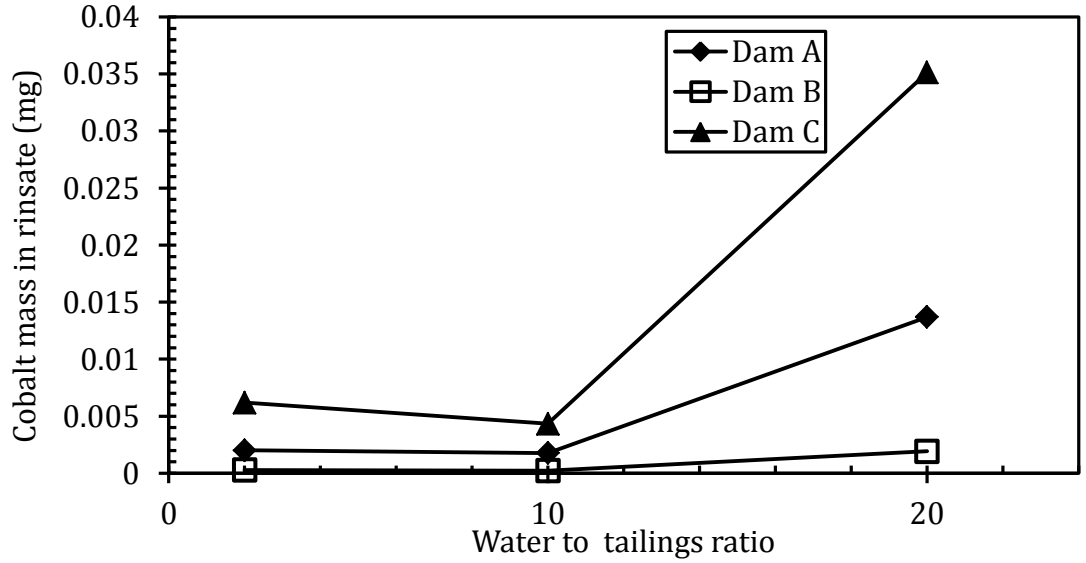

Figure 21 – Cobalt mass in oxidized tailings rinsate vs. dilution ratio

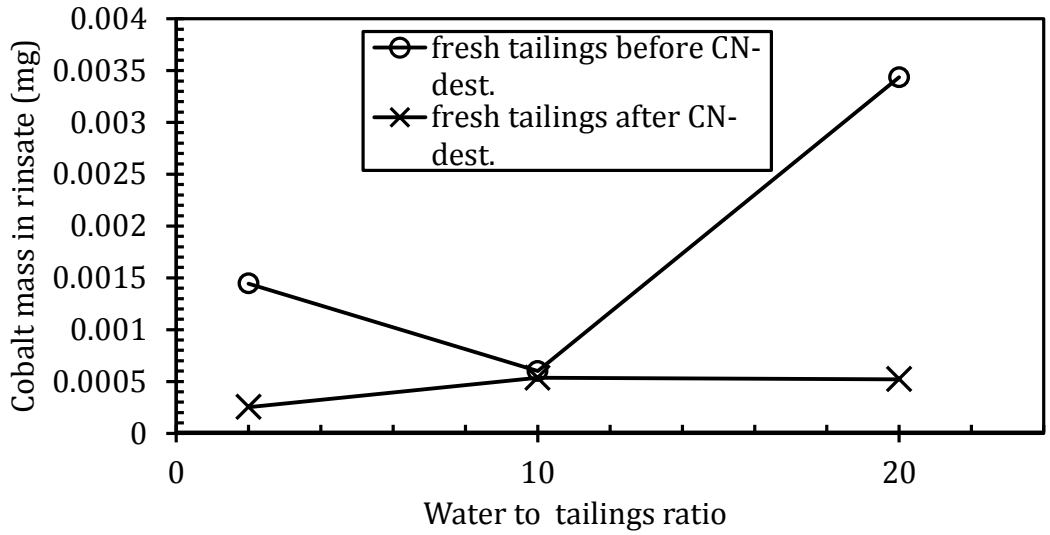

Figure 22 – Cobalt mass in fresh tailings rinsate vs. dilution ratio

4.3 Groundwater

Groundwater samples from monitoring well 96–GW–14S (Figure 16) were obtained from Musselwhite mine and analyzed by the candidate (Table 4). The groundwater contains relatively high concentrations of calcium, sodium, potassium and sulfur, similar to the fresh tailings water. The cobalt concentration in the groundwater is 10 times less than that in the fresh tailings water after CN destruction due to the soil's capacity to adsorb cobalt, as will be discussed in the following sections in more detail. However, in or order to better understand cobalt's profile in the groundwater, its concentrations for 2009 and 2010 are plotted in Figure 23 and Figure 24, respectively. The well data was provided by Musselwhite mine and the candidate analyzed it. As shown in these figures, the pH of the groundwater varies between 7 and 8, and in general the lower Co concentrations were observed at the higher pH values. In other words, increasing the pH immobilizes cobalt. This will prove beneficial for the electrokinetic barrier, as will be discussed in later sections. As well, it is worth noting that the average cobalt concentration is approximately 0.01 ppm which is in agreement with the values obtained from the rinse tests at pH 7 with water to solid ratio of 2.

Table 4 – Detectable constituents in groundwater from monitoring well 96– GW– 14S

Element	Concentration (ppm)	ICP detection limits (ppm)
Al	BDL	0.04
B	0.14	0.04
Ba	0.13	0.005
Ca	**313**	**0.01**
Co	**0.012**	**0.005**
Fe	0.025	0.008
K	**46**	**0.1**
Mg	27	0.01
Mn	2.31	0.002
Na	**124**	**0.1**
S	**416**	**0.1**
Si	8.33	0.03
Sr	0.84	0.004

Major ions are indicated in bold

**BDL= Below Detection Limit*

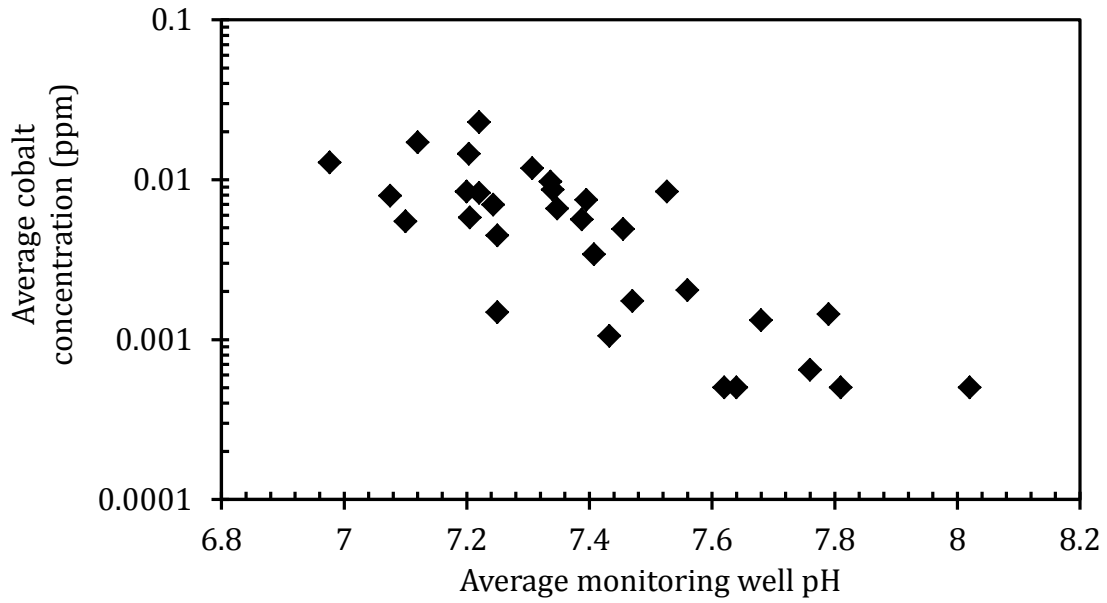

Figure 23 – Average cobalt concentration vs. average monitoring well pH–2009 (Musselwhite Mine, 2013)

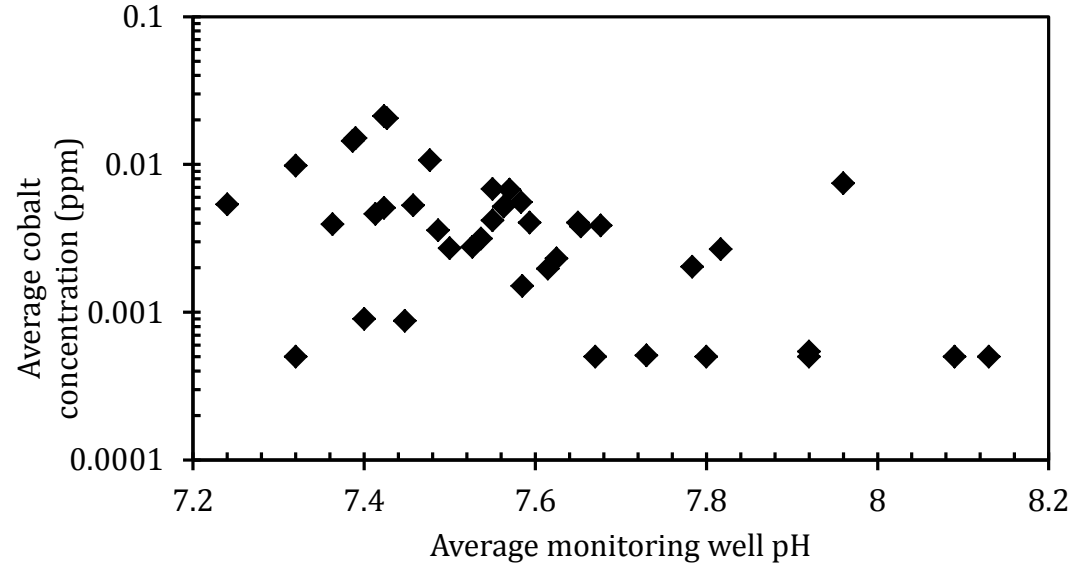

Figure 24 – Average cobalt concentration vs. average monitoring well pH–2010 (Musselwhite Mine, 2013)

4.4 Mine Soil in the Vicinity of the Proposed Electrokinetic Barrier

The mine soil samples used in the experimental study were obtained from the zone between the Tailings Management Area and Zeemel Lake. They were collected from the location proposed for the installation of the electrokinetic barrier to prevent further spread of contaminants to groundwater and surface water. The location was chosen such that the movement of cobalt and other contaminants is halted before the polluted groundwater plume can reach the surface water at Zeemel Lake and surrounding ponds. The soil was collected from a depth of 1.5 meters about 20 meters west of groundwater monitoring well 04–GW–20, as shown in Figure 16. The topsoil is highly organic due to the presence of vegetation; hence, it is not representative of the entire site's soil makeup. However, the collected soil is believed to be representative of the site's geological and physicochemical characteristics. The mine soil was digested using nitric/hydrochloric acid digestion (by FoReST Laboratory) to determine the background concentration of cobalt and other elements in the proposed area. The results are shown in Table 5. It can be noted that the mine soil contains a high cobalt concentration relative to the groundwater.

Contaminants, such as cobalt, which are deposited into the tailings management area seep through the soil by advection and diffusion. Some of the heavy metal contaminants are immobilized in the soil via various chemical mechanisms including adsorption, and precipitation. Precipitates formation can clog the soil's pores and create a physical barrier to contaminants transport out of the soil. However, as the mine continues to generate acid mine drainage, the pH of the tailings impoundment will drop such that additional cobalt may become solubilised in the pore fluid of the tailings. Eventually, the pore fluid which contains soluble cobalt will reach the groundwater table.

Table 5 – Detectable elements in the soil

Element	Concentration (mg/kg dry wt)
Ag	0.21
Al	**19116**
As	8.16
B	9.39
Ba	76.39
Be	0.99
Total Ca	**45881**
Cd	5.46
Co	4.04
Cr	45.59
Cu	22
Fe	**23405**
K	2755
Mg	**16087**
Mn	465
Mo	0.41
Na	214
Ni	30.24
P	584
Pb	13.67
Si	112
Ti	996
V	39.61
Zn	61.42
Zn	61.42

Major ions are bolded

5.0 Knowledge Gaps

Remediation normally takes place after contamination had occurred. In the electrokinetic remediation studies previously reviewed, heavy metals removal was the main objective. In order to extract the pollutants, heavy metals had to exist in a soluble form and hence the addition of a purging solution and pH control at the cathode is often necessary to avoid the heavy metal precipitation in the soil. However, prevention systems take advantage of the immobilization mechanisms occurring due to the nature of the soil (for example, buffering capacity and cation exchange capacity) and those induced by applying an electric field to a soil mass, such as the high pH zones where precipitation of metal carbonates/hydroxides is promoted. In this project, an electrokinetic barrier is proposed to prevent groundwater contamination and to trap cobalt near its source of contamination.

Although the decontamination of soils polluted with heavy metals such as Cd, As, Cr and Zn was the subject of several electrokinetic studies, cobalt was the focus of only two electrokinetic remediation investigations until now (Kim, et al., 2008; Kim, et al., 2010). As a result, much remains unknown about the behaviour of cobalt under an externally applied electric field in soils with different properties. The findings of Kim et al. (2008) were for a specific soil type and cannot be generalized or applied for the site under this investigation. Furthermore, little information is available in the literature on the fate of contaminants, specifically cobalt, after the application of electrokinetic phenomena to polluted soils.

Accordingly, the research objectives of this project are defined in the following section.

6.0 Research Objectives

The following are the objectives of this thesis project:

1. Characterize the physicochemical properties of the mean surface of the soil near the mine; namely:
    a. Identify and classify the mine soil
    b. Determine the mine soil's geotechnical properties
    c. Characterize the cobalt's adsorption/solubility behaviour on the mine soil
    d. Determine the mine soil's acid neutralization potential
2. Assess the feasibility of groundwater contamination prevention using an electrokinetic barrier for the Musselwhite mine.
3. Qualitatively distinguish the influences of each electrokinetic phenomenon on the trapping of cobalt ions; namely:
    a. Electro–osmosis; and
    b. Electro–migration
4. Examine the possibility of using intermittent power as energy source for the electrokinetic barrier
5. Determine the fate of the contaminated plume in the long term after the application of the electrokinetic barrier

7.0 Hypotheses

In order to address the above objectives, the following hypotheses were made:

1. The volumetric flow rate of water through the barrier will be significantly decreased by the application of a voltage gradient across the electrodes.
2. Cobalt will be trapped near the cathode by adsorption and precipitation.
3. The dissolved cobalt concentration will be reduced downstream of the barrier by a combination of electro–migration, adsorption and precipitation.
4. The cobalt mass flow rate through the barrier will be reduced by electro–osmosis, electro–migration, adsorption and precipitation.
5. Intermittent power can be as effective as continuous power in corroborating hypotheses 1 through 4.
6. In the long run, after the source of contamination has been exhausted and the electrokinetic barrier has been terminated, the cobalt concentration downstream of the barrier will not rise significantly.
7. The precipitated/adsorbed cobalt within the barrier will not be solubilised and removed out of the trap zone after removing the voltage gradient.
8. The pH gradient developed during the application of the electrokinetic barrier will persist after removing the voltage gradient.

8.0 Materials

The following materials and methods are employed to achieve the objectives of the research project and test the aforementioned hypotheses.

8.1 Materials

8.1.1 Mine Soil

As previously mentioned, the mine soil was obtained from Musselwhite mine 400 meters away from Zeemel Lake (Figure 16). The mine soil was stored in airtight bags to prevent moisture loss by evaporation. Figure 25 depicts the soil in–situ at the location of sampling and in the storage bags. The soil was air dried; a mortar and pestle were used to break any clumps within the soil. Lastly, the mine soil was sieved through sieve No. 200 where the mine soil passing the 0.75 mm was retained for use in the various tests conducted. This fraction of the mine soil was chosen because the depth where the electrokinetic barrier is proposed to be installed is composed of mainly medium to fine sand. Moreover, it was reasoned that adsorption and precipitation will occur on the finer fraction of the mine soil.

Figure 25 – Mine soil sampling pit (left) and stored mine soil sample (right)

8.1.2 Sand

Sand was obtained locally from a concrete supplier: Lafarge Cement Company. This sand was previously characterized as fine aggregate with 48% of the particles passing sieve No. 35 (0.5 mm diameter). The sand was sieved through sieve No. 40 (0.425 mm) where the sand passing the sieve opening was retained for mixing with the soil obtained from the mine. This was done to accurately represent the soil makeup in the region of the proposed location of the electrokinetic barrier on the mine site. The material of the aquifer at the mine site is made up of sand with fines.

8.1.3 Groundwater

The groundwater samples were stored in airtight pails. The groundwater was collected from groundwater monitoring wells 00–GW–19, 96–GW–17, 96–GW–14S, and 96–GW–12 located near Dam A, near Dam B, between Dam B and Dam C, and near Dam C, respectively, as shown in Figure 16. Sampling between the TMA and Zeemel Lake was necessary to gauge the mobility of contaminants downstream. Furthermore, as the groundwater flows underneath the oxidized tailings, cobalt and other contaminants seep through the soil and become available for transport with the groundwater. Therefore, monitoring wells close to the oxidized tailings provide valuable information regarding the release of contaminants from the TMA prior to the installation of the electrokinetic barrier. The constituents in the groundwater are listed in Table 4.

8.1.4 Mixing Water

The water used for some of the tests conducted was dispensed by a Barnstead D11911 NANOpure water purification system which produced 18.2 megaohm–cm water. Distilled water provided through the Lakehead University distilled water distribution system was used in several tests as pointed out when applicable.

8.1.5 Chemicals

- *Cobalt (II) Nitrate Hexahydrate*

$Co(NO_3)_2 \cdot 6H_2O$ was purchased from Fisher Scientific as the source of cobalt with 99% purity.

- *Sodium Nitrate*

Sodium nitrate solutions were prepared using $NaNO_3$ with purity ≥ 99% purchased from Fisher Scientific.

- *Nitric Acid and Sodium Hydroxide*

Solid sodium hydroxide with a purity of 98.8% and liquid nitric acid with a specific gravity of 1.42 and an assay between 68–70% were purchased from Fisher Scientific. Diluted solutions of each chemical were prepared for use in pH adjustments.

As well, the following compounds were purchased from Fisher Scientific with minimum purity of 98%:

- *Calcium sulfate dihydrate*
- *Potassium sulfate*
- *Sodium sulfate*
- *Magnesium sulfate heptahydrate*

8.1.6 Simulated Groundwater

The feed water used in the various laboratory tests carried out in this thesis was prepared to simulate the groundwater in the mine site. The major ions present in the mine's groundwater, Table 4, were mixed to prepare the simulated groundwater. The mixing was done with respect to the concentration of each major ion in the groundwater. Each chemical was mixed in such a way that its concentration in the feed water was the same as that in the groundwater. The major anions and cations in the mine's groundwater are listed in Table 6 as well as the chemical compounds used for each ion. It should be noted that the sulfate ion (SO_4^{-2}) is the major anion in the mine's groundwater and its total concentration was contributed by each compound.

Table 6 – Simulated groundwater constituents

Ion	Concentration in groundwater(mg/L)	Compound
Ca^{+2}	313	$CaSO_4.2H_2O$
Mg^{+2}	27	$MgSO_4.7H_2O$
Na^{+}	124	Na_2SO_4
K^{+}	46	K_2SO_4
SO_4^{-2}	416	–

9.0 Methods

9.1 Mine Soil and Sand Preparation

The mine soil samples in the bags were emptied on a large plastic tarp where the mine soil was well mixed to ensure homogeneity. The mine soil was divided into four equal piles that were mixed individually. Then, the piles were mixed together as shown in Figure 26. This was repeated several times. For all of the tests carried out except when otherwise noted, the mine soil was allowed to air dry by spreading thin layers of soil in plastic trays for 36 to 72 hours. The mine soil was then pulverized and sieved through sieve No. 200 (0.75 mm) where the mine soil passing sieve No. 200 (see Figure 27) 0.75 mm was retained for use in the various tests conducted.

Figure 26 – Homogenized mine soil

Figure 27 – Air dried and sieved mine soil

Similarly, the sand was allowed to air dry, and was then sieved through sieve No. 200 where the passed soil was retained (Figure 28).

Figure 28 – Air dried and sieved sand

9.2 Mine Soil Characterization

9.2.1 Mine Soil Natural Water Content

The natural water content, w_p, of the soil, also known as the soil's moisture content, informs about the state of the soil in the field. Knowledge of the water content is essential for determining other important geotechnical properties of the soil, such as the hydraulic conductivity and the shear strength. The water content of the mine soil was determined according to the ASTM D2216–90 procedure. The weight of a clean and dry tin tray was recorded. The tray was filled with a representative sample of the mine soil and the weight of the mine soil plus the tray was noted. Then the sample was placed in an oven overnight at 105°C, after which the weight of the dry sample was obtained and the mine soil's moisture content was determined by equation (9.1) (Bowles, 1992).

$$\boldsymbol{w_p = \frac{M_w}{M_s} x 100} \qquad \text{Eq. (9.1)}$$

where, M_w is mass of water present in the soil sample (g), and
M_s is mass of dry soil sample (g)

9.2.2 Atterberg Limits of Mine Soil

The liquid and plastic limits of soil are referred to as the Atterberg limits. The liquid limit is the moisture content at which the soil flows under its own weight. The plastic limit is the moisture content at which the soil behaves as a plastic material, i.e. unrecoverable deformation with cracking or crumbling. These tests are important for soil classification and were carried out in accordance with ASTM D 4318–10.

A sample of mine soil of 260 g passing the No. 40 sieve was pulverized and well mixed with a small amount of distilled water in an evaporating dish. A sample of 40 g of mine soil was set aside for use in the plastic limit determination test. The height of fall of the liquid limit device was adjusted to exactly 10 mm using the block on the end of the grooving tool.

A small amount of mine soil was placed in the centre of the liquid limit device and smoothed. A groove was cut using a grooving tool. Then, the cup was placed into the liquid limit tool and securely hinged. The test was carried out by rotating the crank at around 120 rpm to deliver consistent blows. With each drop the groove closed up gradually. The

number of drops that produced approximately 12.7 mm grove was recorded. This step required visual observation of the size of the groove. A moisture content sample was taken. The cup was emptied, washed, and dried. Next, more distilled water was added to produce 40 to 50 blows, 30 to 40 blows, 20 to 30 blows, 15 to 20 blows and 10 to 15 blows, respectively. The equation of the best fit line of the data points was obtained; the moisture content that produced 25 blows was interpolated and reported.

The plastic limit or the water content at which the soil exhibited plastic behaviour was determined by using the mine soil sample previously set aside. This sample was divided into ten smaller samples. Each sample was rolled on a ceramic plate to form a uniform thread diameter using approximately 90 rolling strokes per minute such that each stroke is completed by a forward and a background roll. When the diameter of the thread was 3 mm and it did not crumble, the thread was broken, reformed into a ball and the rolling process was repeated. This continued until the thread was rolled down to 3 mm diameter and was just about to crumble. At this point, the mine soil was placed into a weighed can and its moisture content was determined by oven drying overnight. This test was carried out in triplicate.

9.2.3 Mine Soil Particle Size Analysis

The particle–size analysis allows soil classification and prediction of soil–water movement under various conditions even though the permeability test, later discussed, is often generally used. The particle–size distribution analysis provides information about the relative proportions of the different grain sizes of a given soil mass (Das, 2008). The sieve analysis allows the approximation of the grain size range between two sieves though individual grain sizes cannot be known. There are standard mesh sizes and procedures that are used to categorize the particle sizes. Sieve No. 200 (0.075 mm) is used by all classification systems to separate the fines from the coarser particles. It is also the smallest sieve size that permits the passage of water but not the soil particles. For particulates that are finer than the No. 200 sieve, the hydrometer test should be carried out for gradation (Bowles, 1992). The ASTM D 421 for sample preparation and ASTM D 422 for test procedure were followed to carry out a mechanical particle–size analysis of the soil.

By visual inspection, the mine soil contained a large portion of lumps, so in order to break the lumps, a representative sample of the oven dried mine soil was crushed with a mortar and pestle. In order to separate the coarse grains, the sieves No. 10, No. 20, No. 40, No. 80, No. 100, and No. 200, were stacked as per ASTM recommendation. A pan was used at the very bottom to catch any material that was finer than sieve No. 200. The stacked sieves were placed in a mechanical sieve shaker for 10 minutes, after which the sieves and the retained soil were weighed. The percent passing a sieve was then calculated using the formulas below:

- First the quantity passing the sieve was calculated as the difference between the total mass of soil and the mass retained on the sieve
- Second the percent passing was calculated as the quantity passing divided by the total mass of soil times 100.

A semi–logarithmic plot of the particle size versus percent passing was constructed and combined with the data obtained from the hydrometer test in order to yield a cumulative grain size distribution curve.

Since approximately 88% of the mine soil is fines, it was necessary to carry out the hydrometer analysis in order to estimate the mine soil particles in the size range of 0.075 mm to 0.001 mm. A mass of 50 g of air dried mine soil was mixed with 125 mL of 4% sodium hexametaphosphate ($NaPO_3$) solution in an evaporating dish and was covered. The $NaPO_3$ is a dispersing agent used to increase soil particle repulsion and enhance suspension. The sample was left to stand overnight. The mixture was transferred to a dispersion cup that was filled with tap water until it was two thirds full. The mixture was well mixed for about 60 seconds. Meanwhile a control jar was prepared using the same dilution as the mine soil sodium hexametaphosphate mixture. A water bath was used to keep the temperatures of both the sedimentation and the control jars at 22°C and 21°C respectively. The content of the dispersion cup was carefully transferred to a 1000 mL cylinder and agitated for about a minute. The first hydrometer reading, in grams of solids per liter, was taken after 60 seconds from the instant the cylinder was set down; a 152H hydrometer and a thermometer were inserted into the cylinders. The subsequent readings were taken at elapsed times of 2, 5, 15, 30 and 60 minutes and then 2, 4, 12, and 20 hours.

Tabulated data for the viscosity of water and correction factors were used where necessary to calculate the percent clay, silt and sand. A semilogarithmic plot of the percent finer versus the soil particle diameter was constructed and combined with the previously obtained data from the mechanical sieve analysis test.

9.2.4 Mine Soil Specific Gravity

Another important geotechnical property is the specific gravity, G_S, of the soil. It is used in computations of void ratios, soil density, and in calculations of the hydrometer analysis. The specific gravity is defined as the ratio of the density of any material to that of water at 4 °C, which is approximately 1000 kg/m^3. The test was carried out at 20°C. Mathematically, this can be represented by:

$$\boldsymbol{G_S = \frac{\rho_{soilds}}{\rho_{water\ at\ 4°C}}} \qquad \text{Eq. (9.2)}$$

The determination of the specific gravity then requires obtaining the volume of a known mass of a soil sample and dividing it by the mass of water of equal volume. Hence, the specific gravity test can be carried out in a volumetric flask.

The ASTM D 854 procedure was used to determine the specific gravity of the mine soil (Bowles, 1992). A mass of 120 g of air dried mine soil was placed in a 500 mL volumetric flask and water was added until the flask was about two–thirds full. In order to reduce computational errors to the specific gravity by overestimating the mass of the water, the water–mine soil mixture was deaerated using a vacuum to remove the dissolved air from the water and any air contained within the mine soil mass. After this, water was added up to the 500 mL volume mark. The weight of the flask, the water–mine soil mixture, and the temperature were recorded. The flask was then emptied and the water–mine soil mixture was decanted and oven dried overnight. Similarly, in order to obtain the mass of the same volume of water, the flask was filled up to two–thirds with water, deaerated and then filled up to the 500 mL volume mark. The weight of the flask and the deaerated water were taken. The water temperature and that of the water–mine soil mixture were kept at 20 °C. The temperature correction coefficient for the density is one. Finally, the average specific density of the mine soil particles was obtained.

9.2.5 Mine Soil Classification

Keeping in consideration the previously conducted tests and obtained results, the mine soil was classified according to ASTM D2487–11 (Unified Soil Classification System (USCS)). The USCS classifies soil as coarse grained if more than 50% is retained on sieve No. 200 (0.075 mm). If more than 50% of the coarse fraction is retained on the sieve No. 4, the soil is classified as gravel. Whereas if more than 50% of the coarse fraction passes the sieve No. 4, the soil is classified as sand. Sieve No. 200 (0.075 mm) is used to the separate sand (coarse grained) from fines (silt and clay). If more than 50% of the soil passes sieve No. 200, then the soil is typically classified as fines. The USCS uses the Atterberg limits to further classify the fines.

9.2.6 Hydraulic Conductivity of Mine soil

The hydraulic conductivity of soil describes the movement or flow of water through the pores and cracks of a porous medium such as a soil mass. The water flows from a high pressure, created by the water head, to a lower pressure at the outlet of a given control volume and the rate of flow is quantified by Darcy's law. The determination of the hydraulic conductivity is important for predicting infiltration, groundwater flow in aquifers, and other geotechnical applications. There are two agreed upon methods to determine the hydraulic conductivity of soil in the laboratory, namely, the constant head method and the falling head method. As the name suggests, the constant head method requires the maintenance of a constant water head by means of an overflow weir (Bowles, 1992). Even though this method is preferred by many, it wastes large volumes of water especially when it is used for cohesive soils. The falling head method was decided on as the more suitable method for the soil on hand because of its cohesiveness; large amounts of water would be wasted had the constant head method was used (Bowles, 1992).

A dry mine soil sample was compacted into a cylindrical mould of known dimensions; a porous stone was placed at each end of the mould to ensure uniform water flow and distribution through the mine soil column. A graduated standpipe was clamped to a ring stand and was connected with rubber tubing to the inlet of the column, as shown in Figure 29. A graduated cylinder was placed at the outlet of the mine soil column to collect the

effluent water volume. Then, the column and tubing were subjected to vacuum to remove any air bubbles trapped within the mine soil or standpipe. The mine soil sample was then saturated. When water droplets started to exit the column and visually it appeared that the soil was moist, the soil sample was presumed saturated. Then the standpipe was filled with water to a predetermined level h_0. Then, tap water was allowed to flow through the mine soil column until level h_1. The time elapsed during the head drop was noted. The dry mass at the start of the test and the water content of the mine soil column after the test were recorded in order to calculate the void ratio of the mine soil column for each test. The hydraulic conductivity was calculated using equation (9.3).

$$\boldsymbol{k_h = \frac{a.L}{A.t}\ ln\left(\frac{h_0}{h_1}\right)} \qquad \text{Eq. (9.3)}$$

where, k_h is the hydraulic conductivity (m/sec.),

a is the cross sectional area of the burette (m^2),

L is the length of the soil column (m),

A is the area of the mine soil column perpendicular to the flow (m^2),

t is the time required to achieve a head change Δh (seconds),

Δh is the change in water head, $h_0 – h_1$ (m), and

h_0 and h_1 are the initial and final water heights relative to the table, respectively.

The hydraulic conductivity was determined for three void ratios, which were achieved by soil compaction with 2 layers at 30 blows per layer, 3 layers at 30 blows per layer, and 5 layers at 30 blows per layer respectively, all at 100% saturation.

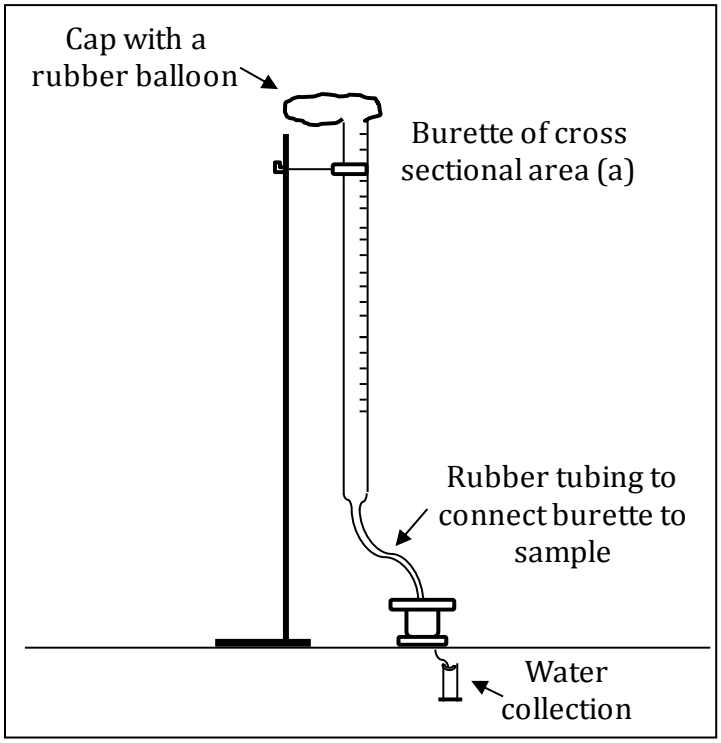

Figure 29 – Schematic of hydraulic conductivity experimental setup

9.2.7 Cation Exchange Capacity of Mine Soil

The cation exchange capacity of soil, CEC, is the capacity of a soil to hold cations such that they can readily be exchanged with competing ions in a solution (Sparks, 2003). In agricultural practice the CEC is used as a measure for soil fertility, since it relates to its capacity to hold nutrients. As well, the cation exchange capacity of soils is important for determining the capacity of soil to protect groundwater against cation pollution as it also plays a role in understanding the adsorption/desorption behaviour of ions in soil (West & Stewart, 2000). Normally, clay minerals and organic matter such as humus are responsible for the soil's CEC. The CEC of the mine soil was determined by using the ammonium replacement method by ammonium acetate extraction, ICP–AES and Sikora buffer pH. This test was outsourced to the Forest Resources & Soil Testing Laboratory at Lakehead University.

9.2.8 Organic Content of Mine Soil

The measure of the amount of carbon in organic matter is determined from the organic content test. Organic matter such as vegetation, bacteria, and humic acids plays an important part in the soil's holding capacity of contaminants, as previously discussed. The organic content of the mine soil was determined by the loss–on–ignition method. The organic matter in the mine soil is oxidized by heating a mine soil sample at 360°C for 2 hours. The percent organic matter is estimated by the weight loss of the volatile compounds after ignition. The test was carried out in triplicate. This test was also outsourced to the Forest Resources & Soil Testing Laboratory at Lakehead University.

9.2.9 Total Carbon, Nitrogen and Sulfur in Mine Soil

The total carbon (TC), nitrogen and sulfur contents of the mine soil were determined by the Lakehead University Instrumentation Laboratory (LUIL) using Elementar's Vario EL Cube. It is a purge and trap combustion analyzer. First, the samples are combusted and then the components are trapped and sequentially released and measured by a thermal conductivity detector (TCD) (Elementar, 2014). The total carbon consists of both organic carbon (OC) and inorganic carbon (IC). Inorganic carbon is mostly associated with carbonic acid salts

such as calcium carbonate. These salts have implications for the soil's buffering capacity, adsorption, and precipitation. The inorganic carbon can be calculated by difference:

$$\boldsymbol{Inorganic\ carbon = Total\ carbon - Organic\ carbon} \quad \text{Eq. (9.4)}$$

The nitrogen and sulfur content in the soil are normally used as indicators of the soil's fertility. Sulfur, more importantly, can undergo oxidation and reduction reactions in the soil (Stevenson & Cole, 1999) such that sulfates and sulfides may be released. Sulfides, as previously discussed, are essential in the formation of acid mine drainage. These three elements are normally reported in terms of percent of dry mass of soil.

9.2.10 Mine Soil pH

The pH of soil controls several chemical processes in the soil such as adsorption and precipitation of heavy metals, the solubility of minerals and the mobility of ions in the soil. It affects groundwater quality and the availability of nutrients. In order to fully define the pH of a soil, the degree of alkalinity or acidity of soil particles suspended in deionized water and a 0.01 M calcium chloride ($CaCl_2$) solution should be determined, which is necessary because calcium can replace some of the exchangeable aluminum on the soil minerals. Thus, one should expect to obtain lower pH values in the calcium chloride solution than in deionized water due to the hydrolysis of the released aluminum ions.

Before the pH measurement, the pH meter electrode was calibrated according to the manufacturer instructions using standard buffer solutions at pH 4.00 and pH 7.01. A mass of approximately 10 g of air dried mine soil was well mixed with about 10 mL of deionized water and was left to stand for an hour. Prior to taking the measurement, the mine soil–water mixture was gently agitated. Then, the pH electrode was inserted into the partially settling mixture and a reading was recorded. The pH of the mine soil in the $CaCl_2$ solution was measured in this exact manner. Both measurements were taken at room temperature.

9.2.11 Zeta Potential of Mine Soil

Zeta potential, ζ, is the electrical potential between the fixed and the mobile regions of the electrical double layer. It is important in the magnitude of the electro–osmotic permeability, k_e (Lynch, et al., 2007) given by equation (2.2) as previously discussed. The direction and amount of electro–osmotic flow depend on the value and sign of the zeta potential of the soil. A negative zeta potential value means that the electro–osmotic flow is from the anode to the cathode whereas a positive value means the opposite. The zeta potential of the soil was measured using a Zeta analyser.

The solution of deionized containing the mine soil particles is placed in a small quartz cell bounded at either end by two electrodes. To measure the zeta potential of the particles in solution, the instrument uses electrophoresis, which entails applying an electric field to the particle solution through the electrodes, first in one direction, then the other, and examining the resulting movement of the particles. This step is repeated 10 times by the instrument. This is done at a location in the cell called the 'stationary layer'. When an electric field is applied to the cell, a circulation occurs within the cell, in which the charged particles nearest the cell wall will flow towards one electrode, while the particles further within the cell circulate in the opposite direction. The Zeta analyser measures the velocity of particles at the 'stationary layer' which is at the boundary between these two flows, and where the movement of particles is due solely to the charge on the particles, and not due to the induced circulation. A video microscope then allows the visualization of the particles; and their velocity may be calculated automatically by the computer's imaging software.

In order to make a measurement of zeta potential, the instrument was calibrated by determining the location of the 'stationary layer' mentioned earlier. This involved moving the quartz cell to adjust the micrometer such that the laser illuminated the cell wall beneath the video microscope and it was visible on the computer screen. Then by clicking on the appropriate icon, the computer indicated the computed location of the stationary layer, which was placed under the laser/video microscope. Next, the pH and conductivity measurement were calibrated. Lastly, the results were recorded in an output file, along with values for pH, conductivity, temperature, and mobility. A bar graph of the percent of total number of particles versus zeta potential was then constructed.

9.2.12 Specific Surface Area of Mine Soil

The specific surface area, reported as the total surface area of the soil per unit mass, was determined for the soil obtained from the mine. The surface area of the soil is where adsorption, precipitation, and reactions occur. The specific surface area of soils can be determined from Brunauer–Emmette–Teller (BET) analysis or it can be approximated from the particle size distribution data. However, the latter does not take into account the particles' shape. The mine soil particles were assumed to be spherical. The average particle diameter bracketed between two sieves was determined as follows:

$$\boldsymbol{d_i = \frac{d_{(-)} + d_{(+)}}{2}} \qquad \text{Eq. (9.5)}$$

where, d_i is the average particle diameter bracketed between two sieves (cm)

$d_{(-)}$ is the average diameter of the higher sieve (cm), and

$d_{(+)}$ is the average diameter of the lower sieve (cm).

The mass of these particles was determined from the difference between the percent mass passing a sieve and the percent mass that was retained on the sieve below. A mass of 100 grams was taken as a basis for calculations.

Then, using volume—density relations, the total volume of the particles in a certain bracket was determined.

$$\boldsymbol{V_i = \frac{m_i}{\rho_{soil}}} \qquad \text{Eq. (9.6)}$$

where, V_i is the volume of particles in a given bracket (i) (cm^3),

m_i is the mass of the particles in a given bracket (i), and

ρ_{soil} is the density of the soil (g/cm^3)

Next, the number of particles within that bracket was calculated, keeping in mind particles were assumed to be spherical.

$$\boldsymbol{n_i = \frac{V_i}{V_{d_i}}} \qquad \text{Eq. (9.7)}$$

where, n_i is the number of particles in a given bracket (i), and

V_{di}.is the volume of a particle with diameter d_i (cm^3) and it is defined as:

$$\boldsymbol{V_{d_i} = \frac{\pi d_i^{\,3}}{6}}$$ Eq. (9.8)

where, d_i is the average particle diameter in a given bracket (i), (cm)

The surface area of particles in a given bracket was then calculated using equation (9.9), and the sum of the surface areas in each bracket, equation (9.10), yielded the specific surface area of particles in one gram of soil.

$$\boldsymbol{A_i = n_i \cdot \pi \cdot d_i}$$ Eq. (9.9)

where, A_i is the area of particles with d_i in a given bracket (i) (cm^2), and

$$\boldsymbol{A_{tot.} = \sum_{i=1}^{n} A_i}$$ Eq. (9.10)

where $A_{tot.}$ is the specific area per one gram of soil (cm^2/g), and

n is the number of brackets.

9.2.13 Cobalt Adsorption on Mine Soil

In order to achieve the objectives of the project and to determine the effectiveness of an electrokinetic barrier for the mine, the mine soil's adsorption capacity was first determined. Adsorption is a surface phenomenon: ions in a fluid are attracted to the surface of a solid, the adsorbent (Mitchell & Soga, 2005). Properties of the solution such as solution's pH and ionic strength affect heavy metal ions adsorption onto soil. As previously explained, the adsorption of heavy metal cations is enhanced with increasing the pH (Acar, et al., 1993). Another factor is the ionic strength of the solution. The work by Criscenti and Svrjensky (1999) showed that the type of electrolyte plays an important role in the ionic strength dependence of metal adsorption. Their study showed that while increasing the ionic strength of $NaNO_3$ solutions has little or no effect on transition and heavy metal's adsorption, their adsorption strongly decreased with increasing the ionic strength of NaCl solutions (Criscenti & Sverjensky, 1999). Their work studied the adsorption behavior of cobalt on metal oxides and hydroxides and its dependence on the soil's ionic strength. Adsorption can be experimentally determined by batch adsorption tests and empirical models such as Langmuir and Freundlich isotherms (Sparks, 2003).

To determine cobalt's adsorption onto the mine soil, batch adsorption tests over a wide range of initial concentrations were conducted. The initial concentration of cobalt in solution ranged from 2000 mg/L to 31.25 mg/L. To prepare these solutions, 0.99 g $Co(NO_3)_2 \cdot 6H_2O$ (291.035 g/mol) was dissolved in 100 mL of 0.01 M $NaNO_3$ solution to make a stock solution containing 2000 mg/L of cobalt. Concentrations of Co of 1000, 500, 250, 125, 62.5, 31.25 mg/L were prepared by serial dilutions. A mass of 0.85 g of $NaNO_3$ was dissolved in one liter of deionized water to prepare an electrolyte solution of 0.01 M $NaNO_3$. Seven oven dried mine soil samples of 1 g were added to 14 mL of the above cobalt solutions and placed in polypropylene centrifuge tubes. The pH of the solution was fixed at the desired pH with nitric acid solution having a concentration of approximately 9.6×10^{-3}M and sodium hydroxide solution having a concentration of 0.1 M. Then the samples were agitated in a rotary shaker (Figure 30) overnight at room temperature to allow equilibrium to be reached. After 24 hours, the pH of the equilibrated samples was measured using a digital pH meter. Then, the tubes were centrifuged for ten minutes at 4000 rpm and the

supernatant solution was drawn and diluted to ensure concentrations of less than 100 ppm for all analytes to prevent interference during the analysis. Before the samples were sent for analysis by inductive coupled plasma atomic emission spectroscopy (ICP–AES), drops of nitric acid were added to each test tube to stabilize the metal ions. Each of the concentrations was carried out in triplicates and a blank sample (non–cobalt containing) was also included for each test run. Adsorption tests at a controlled pH of 6.00 and at an uncontrolled pH were carried out.

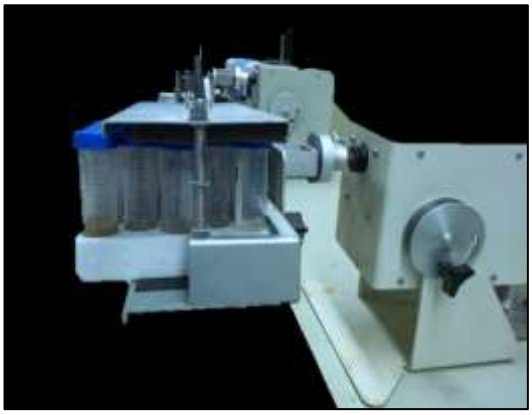

Figure 30 – Adsorption test vessels in rotary shaker

9.2.13.1 Adsorption at pH= 6.00±0.25

A total of 24 samples were prepared, 3 samples per concentration, as per the previous procedure. To fix the pH at 6.00±0.25, the pH of the mine soil solution was monitored and adjusted every couple of hours by adding drops of acid or base as was required. The equilibrium pH was recorded using a digital pH meter.

9.2.13.2 Adsorption at Uncontrolled pH

The samples were prepared similarly to the adsorption tests conducted at pH = 6.00±0.25, but the pH was not controlled. The equilibrium pH was measured for each run.

9.2.13.3 Adsorption Isotherm

The adsorption isotherms describe the amount of adsorbate (cobalt) per mass of the adsorbent (mine soil) as a function of equilibrium concentration (Evangelou, 1998). Adsorption isotherms allow for comparing the mine soil's capacity to adsorb cobalt at different pH values. Furthermore, adsorption data are important for electrokinetic barriers since ion migration is only possible when cobalt is in its soluble form (desorbed). As well, adsorption data aid in evaluating the cobalt trapping potential by the electrokinetic barrier.

9.2.14 Precipitation/Dissolution of Cobalt

The pH gradient developed by the application of an externally applied voltage provides an environment where cobalt and other heavy metals can precipitate by the formation of metal oxides/carbonates (Acar, et al., 1993). Precipitation is an important mechanism for trapping and confining the cobalt ion near its contamination zone.

Cobalt oxides are soluble over a large pH range (Alrehaily, et al., 2013). Figure 31 shows that overall cobalt is least soluble in the pH range of 10–12. This is of particular interest for this project. At the cathode region, pH values can reach up to 12 (Acar, et al., 1995; Wei & Hui, 2011). Additionally, the solubility of the positively charged cobalt species decreases with increasing pH. This has two implications: at the anode, due to the low pH, the species will exist as soluble ions, which means that they can be transported by ion migration towards the cathode. As the ions approach the cathode zone where the pH increases, their solubility will be reduced leading to their immobilization by precipitation and adsorption.

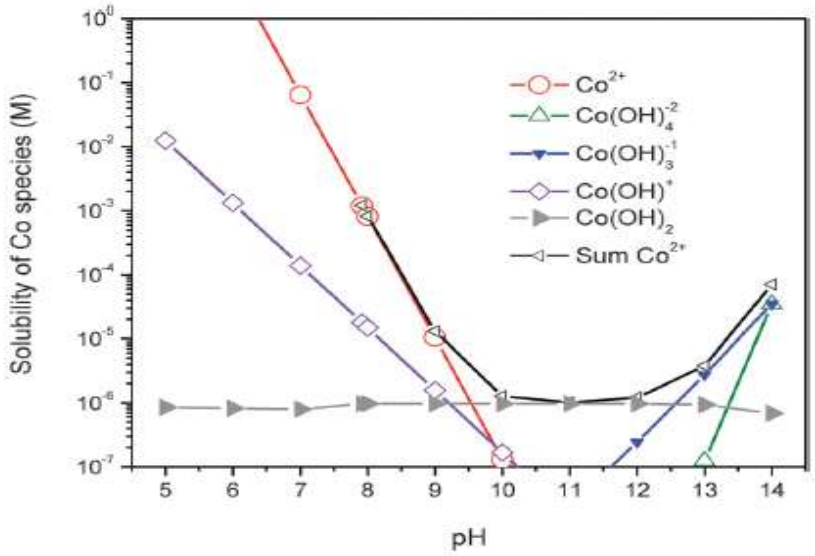

Figure 31 – Solubility of cobalt species against. pH (Alrehaily, et al., 2013)

9.2.15 Neutralization Potential of Mine Soil

The soil's ability to resist pH changes is termed buffering capacity. In other words, it is the soil's ability to absorb more acid/base without significant changes to its pH (Darmawan & Wada, 2002). This capacity is important at sites where acid mine drainage formation is of concern. Metal oxide hydrolysis and mobilization of heavy metal ions generally occur in low pH environments (Evangelou, 1998). Therefore, the soil's ability to keep the pH to levels where acid mine drainage formation is slowed down is advantageous. This neutralization potential or buffering capacity of soil can be defined as the amount of strong acid or base added in order for a predetermined pH to be observed. It is the equivalent number of moles of hydrogen ions added per kilogram of soil (Isenburg & Moore, 1992).

The neutralization tests were carried out to determine the mine soil buffering capacity at pH 4.5. Samples of 1 g of air dried mine soil were added to polypropylene centrifuge tubes containing 14 mL solutions with concentrations ranging from 0 to 0.35 M of HNO_3 prepared by serial dilution of a 2 M stock solution of HNO_3. Some gas bubble formation was observed; the bubbles were allowed to escape before the mixtures were shaken. The gaseous bubbles were believed to be carbon dioxide (CO_2) produced as a result of reacting calcium carbonate (calcite) with nitric acid. The mixtures were then left overnight in a rotary shaker to reach equilibrium. The following day, the mine soil mixture was centrifuged for 10 minutes at 4000 rpm and the pH of the liquid phase was measured. Each test was carried out in triplicate.

9.3 Electrokinetic Barrier Tests

It has been proposed to install an electrokinetic barrier between the TMA and Zeemel Lake to prevent the migration of cobalt to the lake. A schematic of the barrier is presented in Figure 32. The dashed black rectangle represents the zone of influenced of the anode and cathode of the electrokinetic barrier; this area is referred to as the treatment zone. The cathode is depicted as a grey vertical line. As previously explained, the pore water electrolysis at the cathode results in a high pH zone, and it is portrayed as a blue ellipse. Similarly, the anode, further downstream from the reactive mine tailings, is indicated by a grey vertical line. The low pH zone near the anode is depicted as the red ellipse. The pH gradient across the electrodes is represented in elliptical shapes to capture the fact that due to chemical diffusion both the OH^- and H^+ ions will migrate in the area surrounding the electrodes. Because the ion mobility of the hydrogen ion is 1.75 times that of the hydroxyl ion (Narasimhan & Sri Ranjan, 2000), the low pH zone (red ellipse) is larger. As hypothesized, the groundwater will contain less cobalt as it flows past the barrier.

To carry out electrokinetic tests in the laboratory, four electrokinetic cells were used. Each electrokinetic cell was 40 cm long, 11.5 cm wide and 24 cm high (Figure 33). However, the soil specimen cell, for each and every test, was 20 cm long, 11.5 cm wide and 12.5 cm high. The electric field is parallel to the length of the soil specimen cell (20cm). As previously discussed, graphite was the material of choice for the electrodes to avoid metallic electrode corrosion. A 200HM graphite sheet measuring 1 m x 1 m in area and 3.2 mm in thickness was purchased from Wajax Industrial Components, Toronto, Ontario. For use in each test, two rectangular electrodes, 11.5 cm wide and at least 16 cm high, were cut out and perforated such that the openings matched those on the Plexiglas, as shown in Figure 33. The electrodes were inserted at approximately 8.6 cm from either side of the cell and reached the bottom of the cell, as shown in Figure 33.

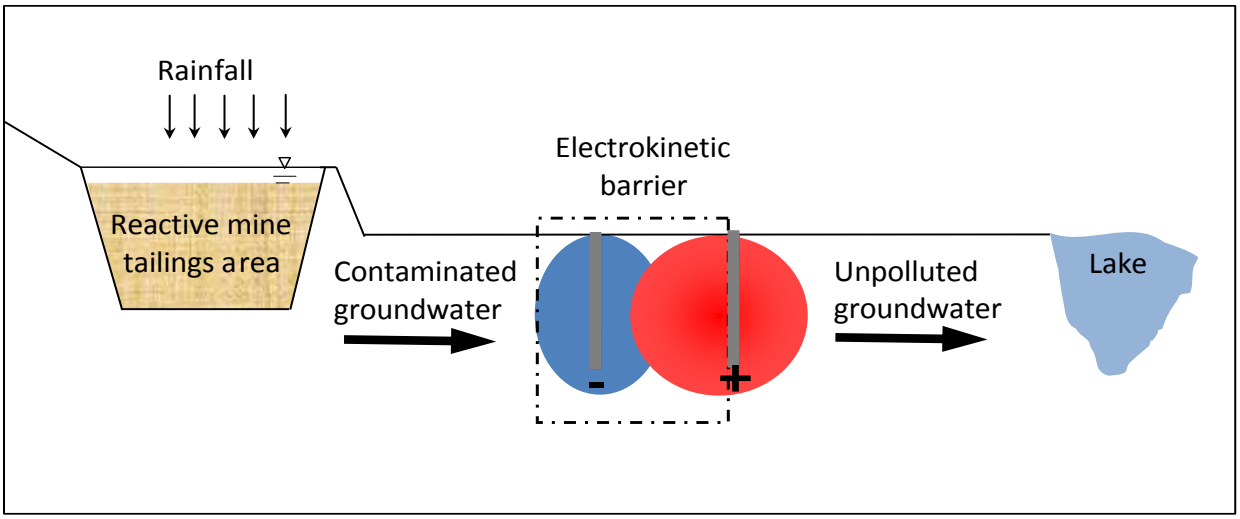

Figure 32 – Schematic of the EK barrier in the field

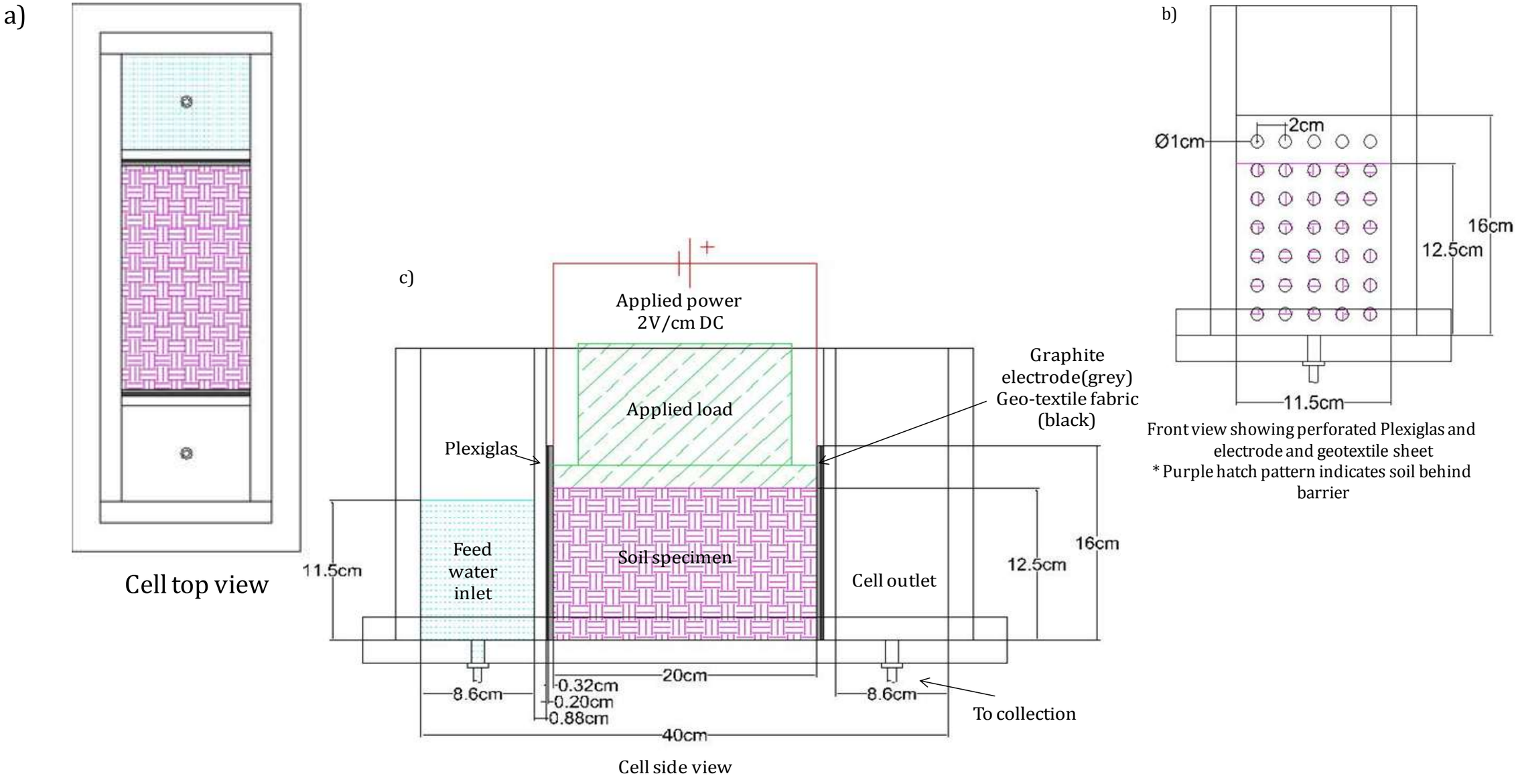

Figure 33 – Top, front and side view schematics of EK barrier cell setup in the lab

Upstream in the cathode compartment, a feed solution containing 1000 mg/L of cobalt served as the contamination source, as shown in

Figure 34. This concentration was chosen for two reasons. First, based on the adsorption tests previously discussed, the goal was to provide enough Co ions for adsorption/precipitation and to allow for analytically detectable effluent concentrations. Second, the electrokinetic barrier was proposed as a preventive measure in the future for when the cobalt concentration is much higher than it is currently at the mine site. Therefore, in order to ensure that the results obtained from this work are valid in the future, 1000 ppm of cobalt was used in the tests.

The hydraulic pressure exerted by the water head was kept constant throughout each experiment. The hydraulic head was maintained by keeping the flow control valve slightly open such that the flow rate of the water entering the feed compartment was equal to flow rate exiting the test cell in the anode compartment. The contaminated feed water was allowed to seep through the mine soil–sand mixture due to a hydraulic gradient. The water flowed through the boundary of the electrokinetic cell which consisted of a perforated Plexiglas sheet, a filter made of geotextile fabric to prevent the back wash of the soil particles into the feed compartment, and a perforated graphite electrode, as shown in Figure 33. The water exited the cell through a tube connected to the bottom of the anode compartment and flowed to a sealed graduated cylinder, where the effluent water was collected, as shown in

Figure 34.

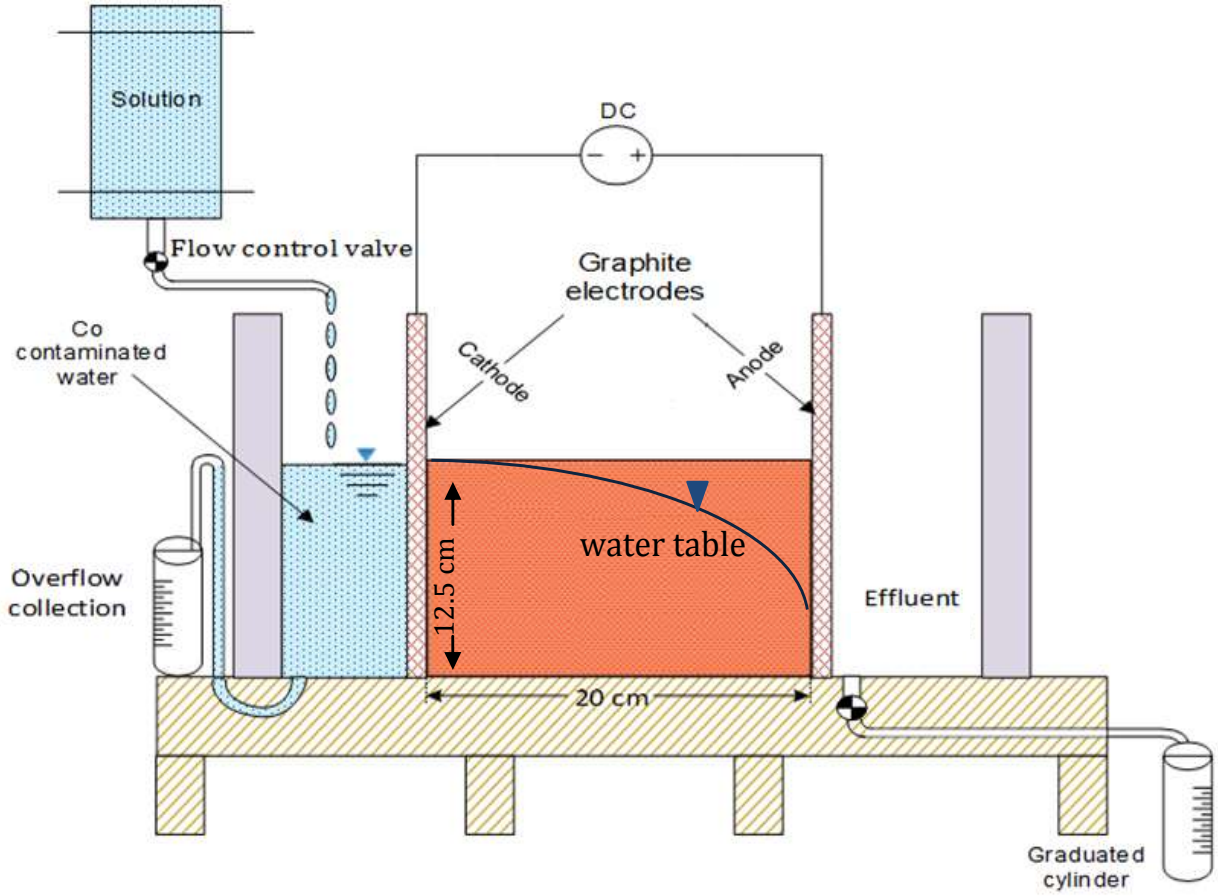

Figure 34 – Schematic of EK barrier setup in the lab

9.3.1 Experimental Program

Various tests were conducted in order to address the objectives of this study and investigate the previously made hypotheses. The control variables which were kept constant throughout the experiments for all experiments are listed in Table 7. Several experiments were conducted by manipulating the independent variables listed in Table 8, and several dependent variables, listed in Table 9, we measured.

Table 7 – Electrokinetic cell tests controlled variables

Parameter	Value
Cell dimensions (cm)	20 x 11.5 x 12.5
Inlet hydraulic head (cm)	11.5
Spacing between electrodes (cm)	20
Dry mass of sand & mine soil mixture in cell (g)	5288
Electrodes material	Graphite
Surcharge pressure on soil specimen (kN/m^2)	7

Table 8 – Electrokinetic cell tests independent variables

Variable	Range/ value
Cobalt concentration in feed water (mg/L)	0 or 1000
Fines in cell (%)	10 or 20
Cell voltage (V)	0 or 40
Nominal pore volumes collected	0–12

Table 9 – Electrokinetic cell tests dependent variables

Variable
Effluent cobalt concentration (mg/L)
Effluent volume (mL)
Pore fluid pH

9.3.2 Cell Tests

To assess the feasibility of an electrokinetic barrier for groundwater contamination prevention at the Musselwhite mine, several electrokinetic barrier studies were performed.

Initially, 100% of the mine soil was intended to be used in all the electrokinetic barrier experiments (hence the extensive characterization of the mine soil), but as later discussed, the hydraulic conductivity of the mine soil was very low and the experiments would not work. Therefore, it was decided to mix the fines of the mine soil with sand. This decision was justified by the composition of the aquifer material through which the groundwater flows at the mine site, as shown in the cross section in Figure 35. The cross section represents the section directly north of the mine which outlines the edge of the tailings management area.

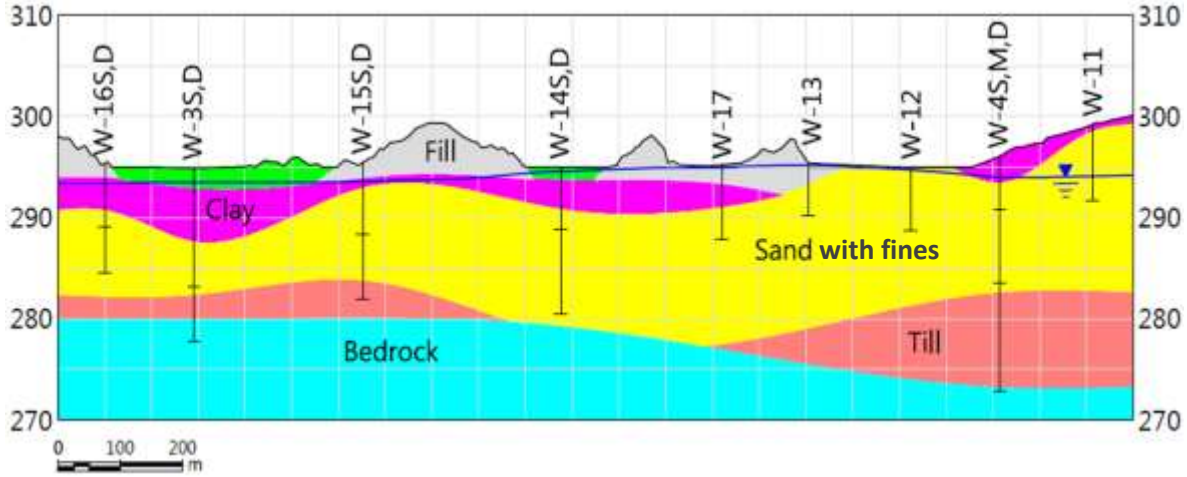

Figure 35 – Cross section of the groundwater aquifer

A cross section near the proposed site of the pilot scale barrier could not be constructed due to lack of borehole data. However, from Figure 35, it can be concluded that the mine site is mostly made up of sand with fines and some clay. Therefore, conducting tests with 10% fines and 20% fines would capture the composition of the aquifer material from a geotechnical point of view. The mine soil fines and sand mixtures used were intended to simulate the zone between groundwater monitoring wells W–14SD and W–17. The monitoring well locations are indicated in Figure 16 and Figure 17.

The electrokinetic barrier tests were completed by filling the cell with 5288 g of an air dry mixture made of 80% (by mass) sand and 20% fines or 90% sand and 10% fines. The percent fines were obtained from the mine soil in the vicinity of the proposed barrier. In this thesis, the clay size particles (less than 2μm) and silt fraction (between 2μm and 75μm) of the mine soil were combined. The combined silt and clay fractions are termed fines throughout this work. By performing the grain size distribution analysis on the mine soil, the fines and sand contents by mass were determined. In order to achieve the desired fines percentage in the cell, the following calculation was performed.

$$\%\,\boldsymbol{fines} = \frac{\boldsymbol{M_{ms}} \times \%\,\boldsymbol{fines_{ms}}}{\boldsymbol{M_{sand}} + \boldsymbol{M_{ms}}} \qquad \text{Eq. (9.11)}$$

where, % fines is the percentage of fines in the cell mixture (%)

M_{ms} is the mass of the mine soil (g)

% $fines_{ms}$ is the percentage of fines in the mine soil (%)

M_{sand} is the mass of the sand from Lafarge (g)

The appropriate masses of sand and the mine soil fines were separately prepared and then mixed for 10 minutes in a dough mixer, shown in Figure 36. Once the mixture was homogenous, it was poured into the cell. Then, a surcharge load of 10.4 kg (corresponding to a pressure of 7 kN/m^2) was applied to the surface of the fines–sand mixture in the test cell, as shown in Figure 33. The cathode compartment was filled with simulated groundwater up to 11.5 cm and the cell was sealed with plastic wrap, as shown in Figure 37. At this point, the saturation of the test cell mixture was started. The hydraulic head was kept constant by slowly dripping the simulated groundwater in the feed compartment, and the overflow was collected in a plastic pail. The overflow was not recycled back to the feed tank; it was discarded. Once the soil was saturated, the volumetric flow rate at steady state was determined. Saturation was assessed by observing the cell mixture and the volumetric flow rate. Volumetric flow rate data were collected over at least 90 minutes. When the plot of cumulative volume versus time produced a straight line, the volumetric flow rate was assumed to have reached steady state. Correlation coefficient (R^2) values greater than 0.99 of the best fit line were used to confirm the linearity of the data points.

Figure 36 – Dough mixer for sand–fines mixtures

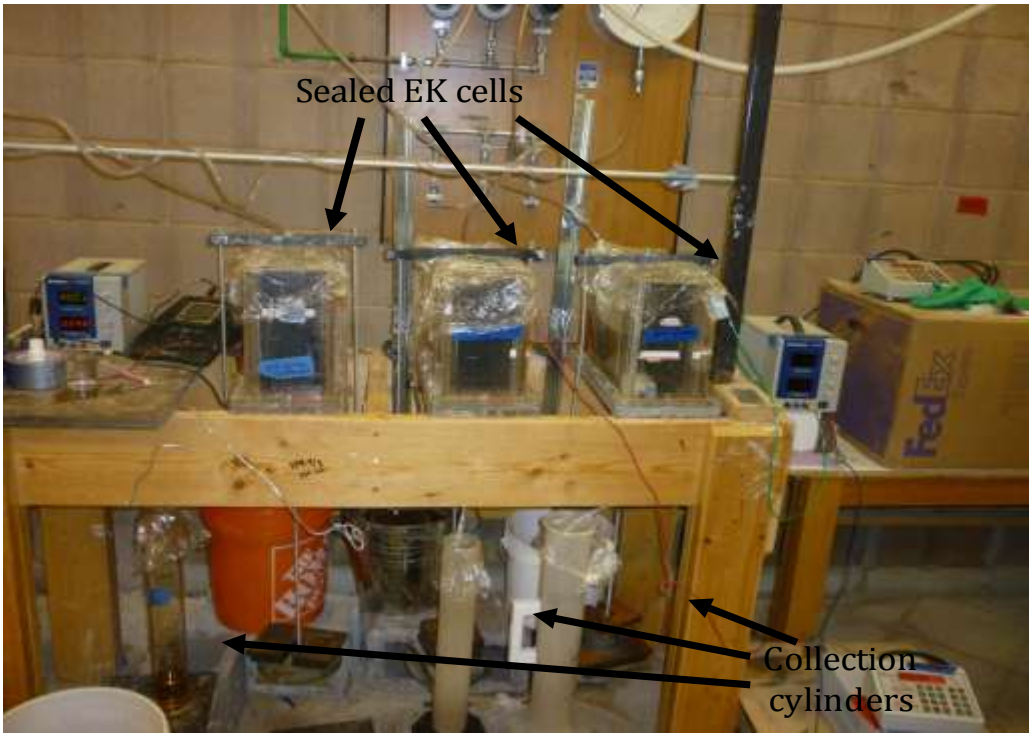

Figure 37 – Sealed EK cells in the laboratory

Since information regarding the seepage of groundwater through the test cell mixture was gathered in the laboratory, it was important to understand the cobalt ion mobility under the influence of a hydraulic gradient alone. Diffusion due to a concentration gradient would also be present, as previously discussed (Acar, et al., 1993; Acar & Alshawabkeh, 1993; Probstein & Hicks, 1993). Therefore, the simulated groundwater was then drained from the inlet compartment at the cathode. This was done by simply opening the overflow tubing. Then, the water in the feed tank was replaced with a solution containing 1000 ppm cobalt. Depending on the test being conducted, once the feed compartment was filled with the cobalt solution, the power supply would be turned on. The effluent water flow rate was measured by placing a graduated cylinder at the exit of the cell as previously described. The graduated cylinder was sealed with a plastic wrap such that water would not be lost by evaporation. Samples of effluent water were taken initially every half nominal pore volume (470 mL) for the first two nominal pore volumes and every one nominal pore volume (940 mL) afterwards for up to 12 nominal pore volumes in total. The nominal pore volume is defined, in this work, as the pore volume calculated with the assumption that the cell mixture of sand and fines is fully saturated and that the whole volume of the cell mixture is under the phreatic line. More details and calculations of the nominal pore volume are found in Appendix A. Upon collection of water samples, the pH of each sample was measured and the sample was sent to LUIL to be analyzed by ICP–AES. At the end of each test, typically after 12 nominal pore volumes had been collected, the test was terminated by shutting off the power supply (if applicable) and the supply of feed water followed by draining the feed tank. In order to examine the effects of adsorption and precipitation, the soil sample was vertically sliced into 5 rectangular pieces, which were 11.5 cm long, 12.5 cm high and 4 cm thick, using a knife. Each slice was well mixed in a clean and dry bowl, as shown Figure 38, and samples were sent to the Lakehead University Environmental Laboratory (LUEL) for soil digestion analysis. As well, water content of each slice was determined according to the ASTM D2216–90 procedure previously explained.

It is worth noting that the graphite electrodes were connected to electrical leads which were connected to a direct current (DC) power supply. This was true for all experiments to minimize variability between tests; however, the power supply was switched on or off in

accordance with the requirements of each experiment. The power supply was switched off during saturation and steady state determination of all tests. It was also always switched off for all control tests.

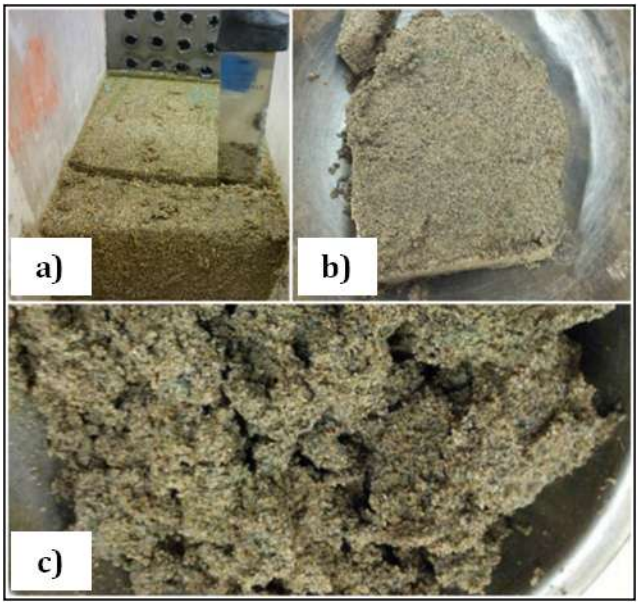

a) Soil slicing
b) One of five (5) soil slices
c) A homogenized soil slice

Figure 38 – Post experiment slicing and mixing of soil

For the electrokinetic barrier tests conducted under an external continuously applied voltage of (40.00±0.01) V, the power supply was switched on for the duration of the tests. As for the electrokinetic barrier intermittent current tests, the DC power supply was alternated for 24 hours on and 24 hours off. This was done to mimic the availability of solar power during day and night and to test hypothesis 5. It is well understood that solar radiation does not occur over 24 hour periods; however, the 24 hours on/off cycle was chosen such that enough data might be obtained. As well, taking three readings per on or off cycle was chosen to be practical for a single person to carry out the experiments and to take measurements. These tests were run for eight days involving four on and four off cycles.

Unlike the control and the continuous current tests, effluent volumes, ICP–AES samples, and pH readings were taken every eight hours for the intermittent current tests instead of at the predetermined nominal pore volumes. However, to allow for comparison between the intermittent current tests, the continuous current tests, and the control tests with

respect to the pore volume, the number of nominal pore volumes collected, from the intermittent current tests, during each eight (8) hour reading was back calculated as follows:

$$PV_{nominal} = \frac{V_{collected}}{940} \quad \text{Eq. (9.12)}$$

where, $PV_{nominal}$ is the number of nominal pore volumes collected at the end of eight hours,

$V_{collected}$ is the total effluent volume collected at the end of eight hours (mL),

940 is the value of one nominal pore volume (mL).

9.3.2.1 Post Electrokinetic Barrier Application

Even though the electrokinetic barrier was initially proposed as a long term, walk away prevention plan, at some point in time, the electrokinetic barrier might be terminated. In the literature, there are very few data on the fate of the contaminant plume past the barrier after the end of the prevention period, even at the laboratory scale.

Wash out tests were carried out to determine the fate of the cobalt precipitated/adsorbed during the application of the electrokinetic barrier. As well, a better understanding of what happens to the pH of the soil post prevention (after the electrokinetic barrier is terminated) was gained.

The wash out tests were conducted in two steps. First, the tests were carried out similar to the electrokinetic barrier tests with continuous current using the 10% fines–90% sand mixtures until approximately 7.5 nominal pore volumes were collected (power on). Second, the power supply was switched off, and the feed water containing cobalt was replaced with the simulated groundwater which contained the same concentrations of all the major ions present in the groundwater in the Musselwhite mine. The test continued until another 7.5 nominal pore volumes were collected.

The first part of the tests represented the period during which the electrokinetic barrier would be in effect. In the field, after the stop of the voltage gradient, the groundwater would continue to flow through the aquifer. However, it was unknown whether the cobalt accumulated in the soil would be remobilized and if the quality of the effluent would change. These questions were investigated in the second part of the experiments. This study aimed at answering the question: will cobalt be washed out of the electrokinetic barrier zone in the absence of a potential gradient?

The wash out tests were conducted after all the other electrokinetic tests were completed. This influenced the decision of collecting only 7.5 pore volumes (before and after the application of the voltage gradient) instead of 12 pore volumes similar to the other tests. This decision was made based on the fact that the flow rate was greatly reduced during the application of the electrokinetic barrier due to reduction of the specimen permeability.

Therefore, to avoid lengthy run times for the wash out tests, only 7.5 pore volumes were collected.

10.0 Results

10.1 Mine Soil Characterization

The geotechnical and physicochemical properties of the mine soil were determined according to the methods discussed earlier. The results of these tests are summarized in Table 10 and 11.

Table 10 – Mine soil's geotechnical properties

Parameter	Value	Method
Water content (%)	15	ASTM D2216–90
Liquid limit	24	ASTM D4318–10
Plastic limit	13	ASTM D4318–10
Specific gravity	2.73	ASTM D 854
USCS group symbol	CL	USCS (ASTM D 2487–11)
USCS group name	Sandy lean clay	USCS (ASTM D 2487–11)
Optimum moisture content	16.7	ASTM D 7380–08
Maximum dry unit weight (kN/m^3)	17.1	ASTM D 7380–08

Table 11 – Mine soil's physicochemical properties

Parameter	Value	Method
CEC (meq/100g)	22.0±0.2	NH^{4+} replacement
Organic content (%)	1.20±0.01	Loss–on–ignition
CNS (% mass)	1.9,0.05, 0.006	CHNS Analyzer
pH in H_2O	7.20±0.02	ASTM D4972–01
pH in NaCl	6.87±0.01	ASTM D4972–01
Mean ζ (mV) @ pH=4.96	–43.6±9.4	Zeta potential Analyzer
Specific surface area (m^2/g)	19	Particle size dist.
Soil's minerals	Silica, albite, calcite, nontronite	XRD
Acid buffering capacity @ pH 4.5 (mol H+/kg of soil)	2.63	Neutralization tests

10.1.2 Atterberg Limits of Mine Soil

Six liquid limit tests were performed. A plot of the water content versus the number of blows was constructed, Figure 39. The liquid limit, at 25 drops was determined by using the equation of the best fit line. The liquid limit was determined to be 24. This means that the soil will flow under its own weight when its water content is approximately 24% of dry mass (Mitchell & Soga, 2005).

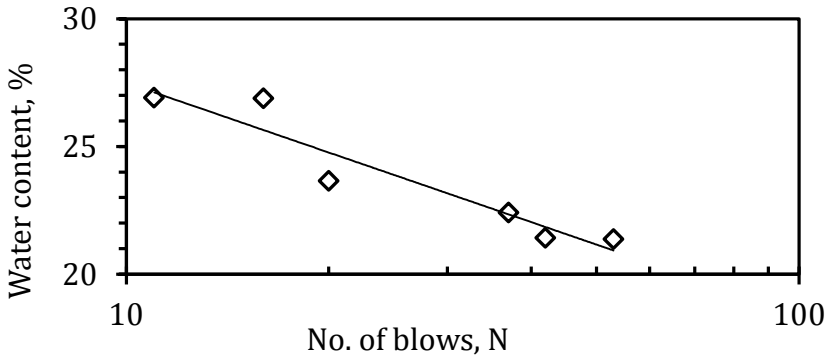

Figure 39 – Liquid limit determination curve

The plastic limit was determined to be 13. Subsequently, the Plasticity Index of the soil defined as the range of water content where the soil exhibits plastic properties is 11 (the liquid limit minus the plastic limit).

10.1.3 Particle Size Analysis of Mine Soil

The data obtained from the sieve analysis and that from the hydrometer test were combined in a semi–logarithmic plot of the percent weight passing versus the average particle diameter, Figure 40. Approximately 88% of the soil passed the sieve No. 200 (0.075mm diameter) which means that 88% of the soil is fines particles (i.e. silt and clay). Table 12 and Figure 40 summarize the results of these two tests.

Table 12 – Grain size distribution

Grain size	Particle size range (μm)	% mass
Medium sand	425–2000	0.2
Fine sand	75–425	12
Silt	2–75	80
Clay	< 2	8

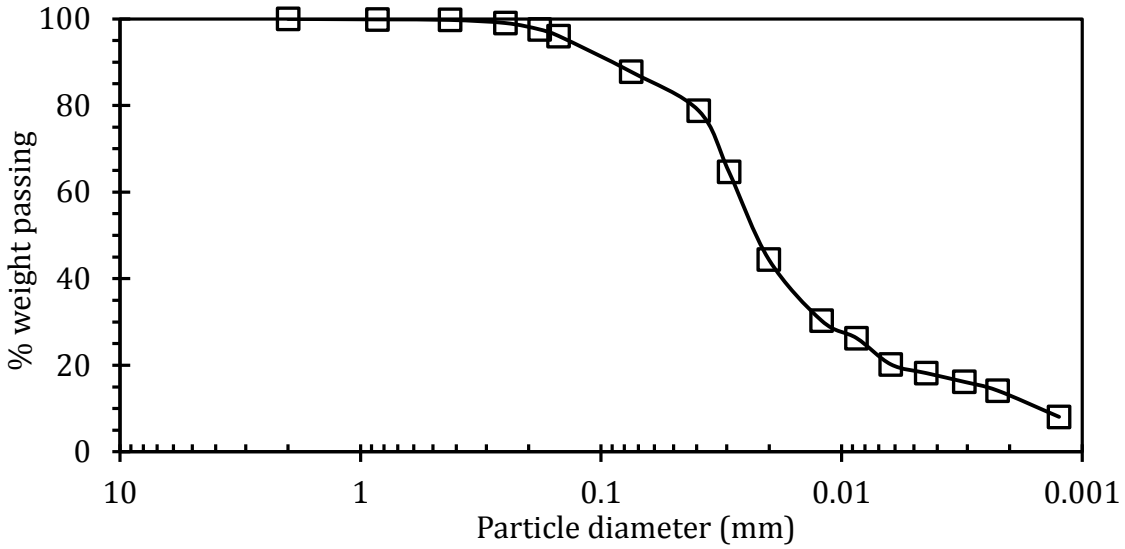

Figure 40 – Cumulative grain size distribution

The finding that the soil contains mainly fines, about 88% by mass, correlates well with the value obtained for the specific gravity of 2.73. It falls within the bracket for clayey and silty soils which have specific gravity that varies between 2.6 to 2.9 (Das, 2008).

10.1.4 Mine Soil Classification

The soil samples obtained from the Musselwhite mine have a light greyish brown color. The soil can be visually described as fine sandy and silty clay. Since more than 50% of the mine soil passes sieve No. 200, it is classified as fine grained soil. The Unified Soil Classification System group symbol is CL (C refers to "clay" and "L" to the liquid limit of less than 50) and the group name is sandy lean clay. From visual observations, it is believed that the mine soil contains low quantities of organic matter.

10.1.5 Hydraulic Conductivity of Mine Soil

Using the falling head method previously discussed, the hydraulic conductivity of the mine soil at three different void ratios was determined. The results are summarized in Table 13. By plotting the hydraulic conductivity against the void ratio, the equation for the best fit line can be obtained which enables the determination of the hydraulic conductivity of the mine soil at other void ratios, as shown in Figure 41. As the data below shows, increasing the void ratio increases the hydraulic conductivity. Due to the cohesiveness of the mine soil, the mine soil has low hydraulic conductivity.

Table 13 – Hydraulic conductivity of soil at various void ratios

Void ratio	Hydraulic conductivity, k_h, (cm/hr.)
0.94	2.6×10^{-6}
0.92	1.6×10^{-6}
0.85	1.2×10^{-6}

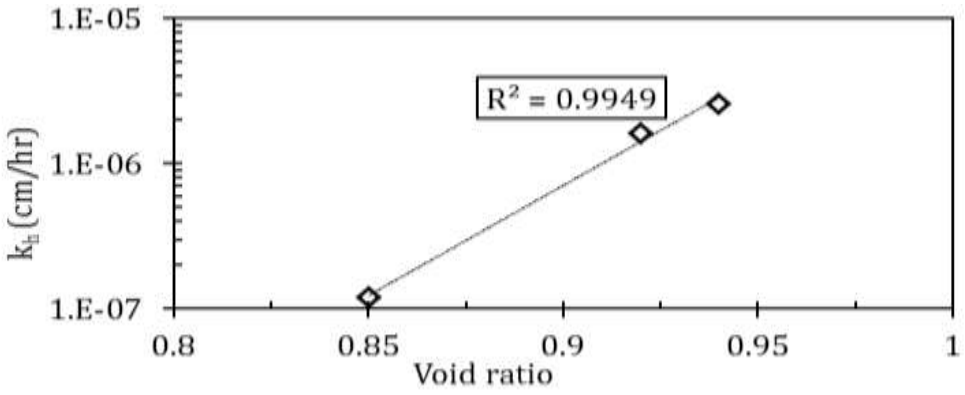

Figure 41 – Hydraulic conductivity versus the void ratio

10.1.6 Zeta Potential (ζ)

The mean of the zeta potential of the mine soil was measured to be –43.6± 9.4 mV at a pH of 4.96 using a zeta potential analyzer. The zeta potential distribution is shown in Figure 42.

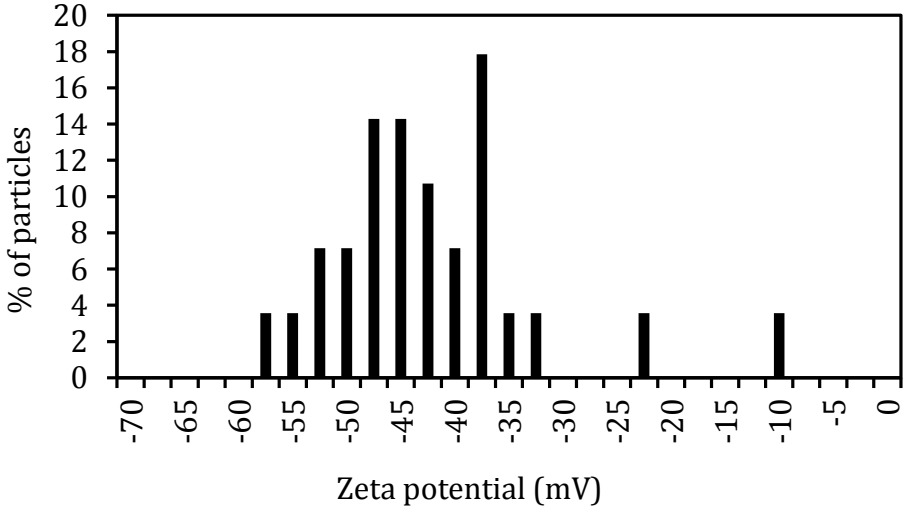

Figure 42 – Soil's zeta potential distribution

10.1.7 Cobalt Adsorption Tests

For the controlled pH adsorption tests, the average equilibrium pH was 6.05 with a standard deviation of 0.16. For the uncontrolled pH adsorption tests, the pH of the samples varied from 6.74 to 8.16 (Figure 43) with an average value of 7.42 and a standard deviation of 0.50. Vertical and horizontal error bars were constructed from uncertainties of the average equilibrium pH and the average equilibrium concentration (C_e), respectively. However, due to very small uncertainties in the equilibrium pH, the vertical error bars are relatively small in comparison with the horizontal bars. This was also true for some of the C_e values. The equilibrium cobalt concentration decreased as pH increased. Thus, it was presumed that more cobalt precipitated/adsorbed at the higher pH values.

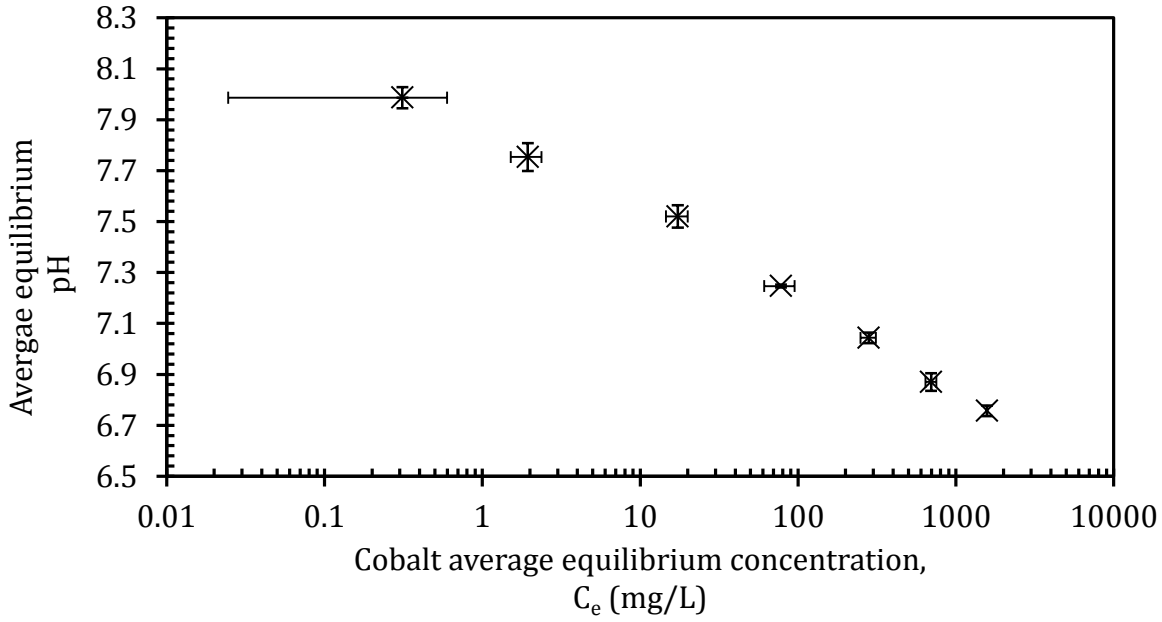

Figure 43 – Uncontrolled pH versus equilibrium concentration of cobalt

10.1.7.1 Adsorption Isotherms

In order to determine the adsorption isotherm that best represented the cobalt adsorption onto the mine soil, some plots were constructed. The amount of cobalt adsorbed per gram of soil, q (mg/g), was plotted against the average equilibrium concentration of cobalt (C_e) at pH 6.05 in Figure 44. The vertical error bars represent the standard deviation on the amount adsorbed calculated from the three trials at each concentration. Again, initially the

uncertainties were very small compared to the plotted values. At pH 6.05, the adsorption isotherm is a C–curve which is best represented by a linear isotherm (Evangelou, 1998).

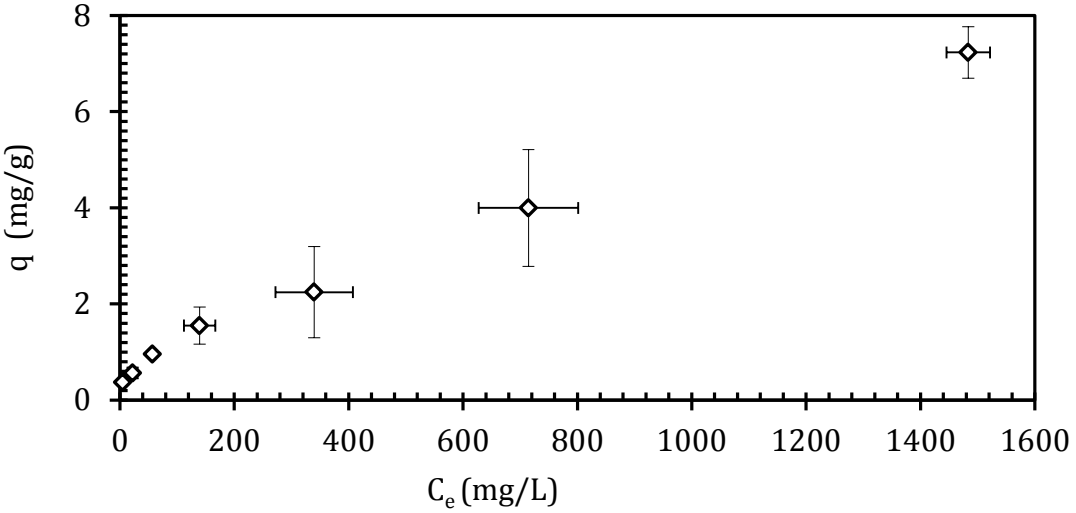

Figure 44 – Cobalt adsorption isotherm at pH=6.05±0.16

In Figure 45, the log of the amount of cobalt adsorbed per mass of soil (mg/g) was plotted against the average equilibrium concentration of cobalt remaining in solution (C_e). The plot represents a Freundlich isotherm of cobalt adsorption at a pH of 6.05±0.16.

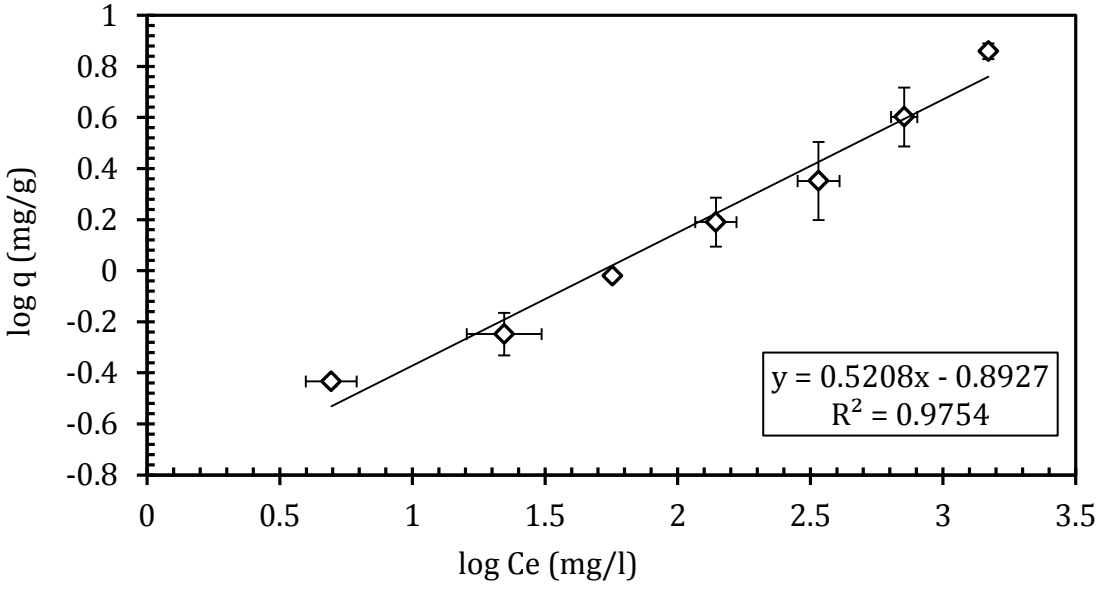

Figure 45 – Cobalt Freundlich isotherm at pH=6.05±0.16

To test Langmuir equation, the ratio of the equilibrium concentration of cobalt per adsorbed cobalt per gram of soil (C_e/q) versus the equilibrium concentration of cobalt (C_e) was plotted, Figure 46. It is clear in Figure 46 that the data points do not fit well to the Langmuir isotherm.

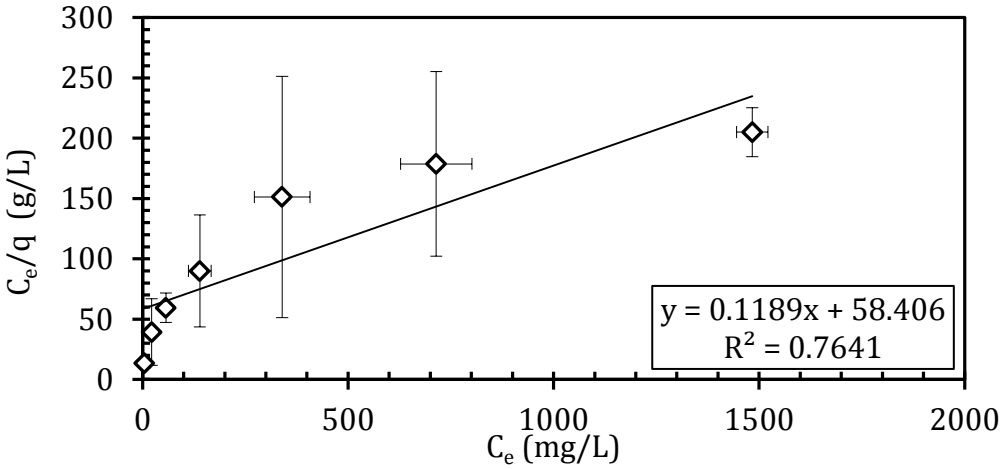

Figure 46 – Cobalt Langmuir isotherm at pH=6.05±0.16

Similarly, the amount of adsorbed of cobalt per gram of soil (mg/g) was plotted against the average equilibrium concentration of cobalt at uncontrolled pH in Figure 47. The isotherm curve produced an L–shape which is best represented by a Freundlich isotherm (Evangelou, 1998). Again, the vertical error bars represent the standard deviation on q at each concentration; however, due to the small magnitude of the error compared to the amount adsorbed some of these error bars are not visible.

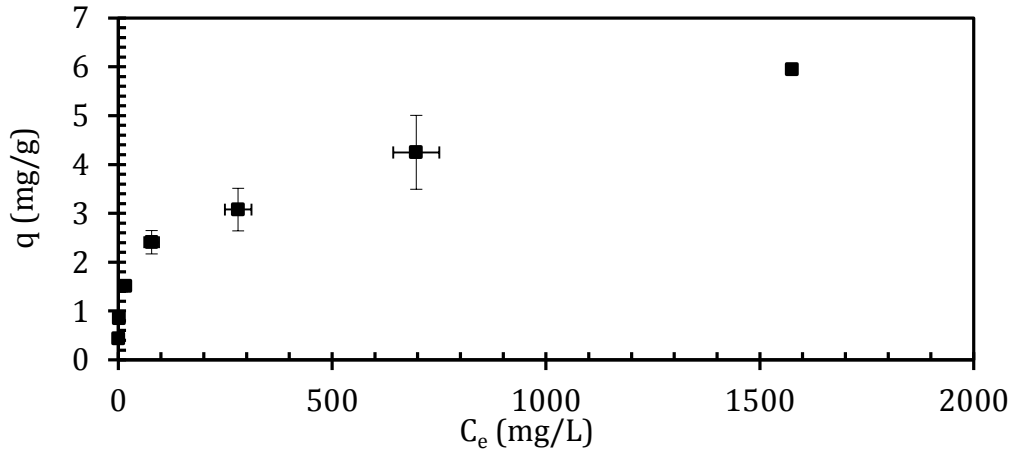

Figure 47 – Cobalt adsorption isotherm at uncontrolled pH (pH=7.42±0.50)

The Freundlich isotherm was fitted to the adsorption data, as demonstrated in Figure 48, and the fit to the Langmuir equation is shown in Figure 49. From the fit of these two curves, it is clear that cobalt adsorption may be modelled by the Freundlich isotherm.

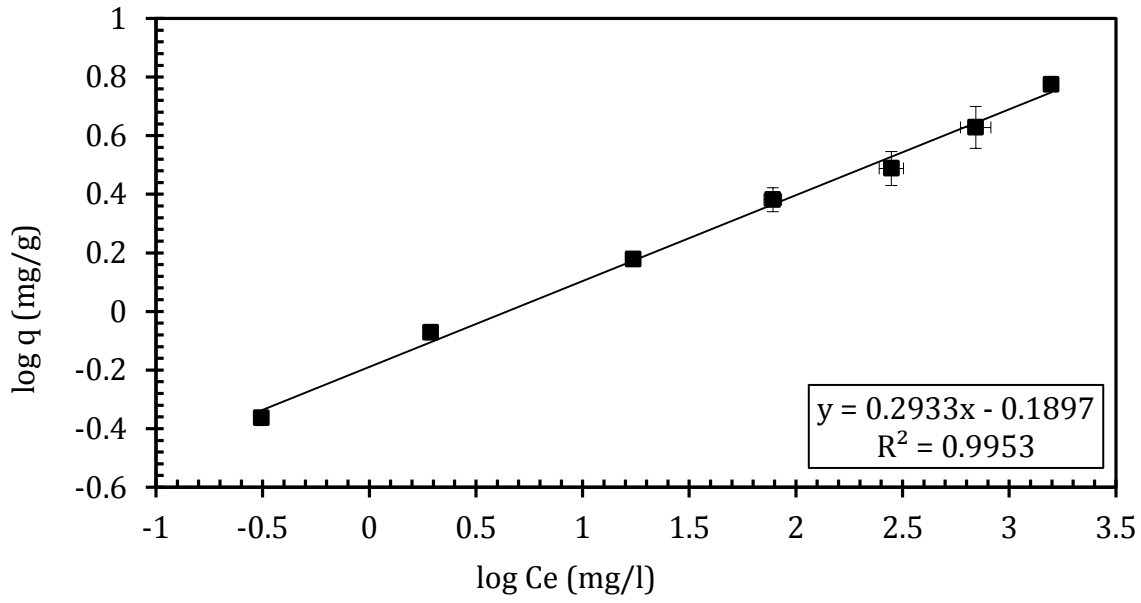

Figure 48 – Cobalt Freundlich isotherm at uncontrolled pH (pH=7.42±0.50)

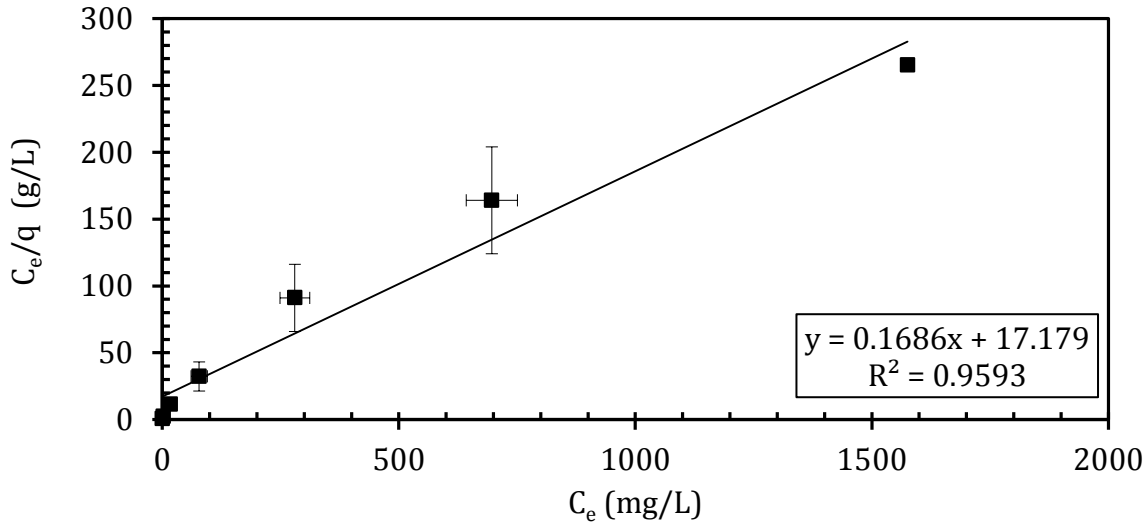

Figure 49 – Cobalt Langmuir isotherm at uncontrolled pH (pH=7.42±0.50)

As the initial concentration of cobalt present in solution increased, the amount adsorbed increased at both pH ranges, as expected. Primarily, cobalt adsorption was thought to fit

the Langmuir equation because the q vs. C_e plot resembled a C–curve (Evangelou, 1998). This curve is observed due to the linearity of the data points at concentrations greater than 250 mg/L. However, comparing the fit of the Langmuir isotherm and the Freundlich isotherm using the best fit line and the value of the correlation coefficient (R^2), it isevident that at both pH values, the cobalt adsorption on the soil is best represented by the Freundlich isotherm. Thus, the parameters of the Freundlich equation which define the adsorption behaviour of cobalt on the Musselwhite mine soil can be estimated from the best fit line equation. The Freundlich equation is given by equation (10.1) (Evangelou, 1998) and can be written to solve for the fitting parameters as shown in equation (10.2):

$$\mathbf{q} = \boldsymbol{K_f C_e^{\frac{1}{n}}} \qquad \text{Eq. (10.1)}$$

$$\mathbf{\log} \boldsymbol{q} = \mathbf{\log} \boldsymbol{K_f} + \frac{\mathbf{1}}{\boldsymbol{n}} \mathbf{\log} \boldsymbol{C_e} \qquad \text{Eq. (10.2)}$$

where, q is the amount of adsorbate (cobalt) per gram of adsorbent (soil) (mg/g),

K_f is a Freundlich model fitting parameter ($mg^{1-1/n} L^{1/n}/g$),

1/n is a Freundlich model fitting parameter (dimensionless), and

C_e is the equilibrium concentration remaining in solution (mg/L)

K_f and 1/n are constants in the Freundlich equation. At low concentrations, equation (10.1) can be simplified to a linear expression where n=1 (Watts, 1997) and becomes:

$$\mathbf{q} = \boldsymbol{K_d C_e} \qquad \text{Eq. (10.3)}$$

where, K_d is termed the distribution coefficient (L/g).

In the controlled pH batch adsorption tests (Figure 44), the data points exhibit a linear trend in the equilibrium concentrations range of 4.94 mg/L to 56.78 mg/L. These data points were used to calculate the distribution coefficient for the controlled pH batch adsorption tests. Similarly, the equilibrium concentrations from 77.96 mg/L to 696.62 mg/L produce a linear trend (Figure 47) for the uncontrolled pH batch adsorption tests, and these data points were used to calculate the K_d. The magnitude of the uncertainty associated with the distribution coefficient obtained from the uncontrolled pH batch

adsorption tests suggests that the linear assumption is incorrect for this set of data (Table 14).

The entire data sets for both batch tests were taken into account in order to determine the overall Freundlich constants at each pH. These parameters are summarized in Table 14. As the value of 1/n increases, adsorption becomes more favorable; consequently, the cobalt adsorption is more favorable at pH 6 as can be seen from Figure 45 and Figure 48.

Table 14 – Freundlich isotherm parameters

Parameters	**pH = 6.05 ±0.16**	**pH= 7.42±0.50**
	Overall Freundlich fit	
1/n	0.521±0.037	0.293±0.009
K_f	(0.128±0.043) $mg^{0.479}L^{0.521}/g$	(0.646±0.028) $mg^{0.707}L^{0.293}/g$
	Simplified linear assumption	
n	1	1
K_d (L/g)	0.0114±0.0014	0.003±0.121

10.1.8 Precipitation

A bluish green precipitate of cobalt was visually observed during the electrokinetic cell tests, Figure 50. Cobalt precipitate formation along the wall of the cell during the application of the voltage gradient (greenish–blue), on the left, and on the soil slices, on the right, were observed, Figure 50. This bluish green color is a characteristic of both cobalt II oxide (CoO) and cobalt II hydroxide ($Co(OH)_2$).

Figure 50 – Cobalt precipitation on soil

10.1.9 Neutralization Potential

The soil resisted changes to its pH, which means that it exhibited a buffering capacity. The change of pH with respect to the added moles of H^+ ions is shown in Figure 51. For an end point of pH 4.5, the soil has a buffering capacity of approximately 2.63 mol H^+/kg of soil. Calcite was believed to account for most of the soil's buffering capacity.

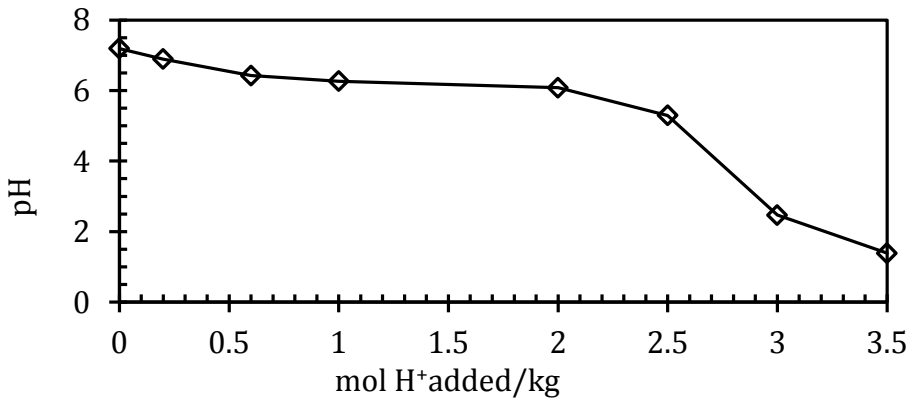

Figure 51 – Soil's buffering capacity curve

The soil's buffering capacity is likely due to the presence of carbonate minerals in the mine soil. The formation of gaseous bubbles was observed as nitric acid was added to the mine soil during the buffering capacity tests. The gaseous bubbles are believed to be carbon dioxide gas (CO_2).

10.2. Electrokinetic Barrier Tests

10.2.1 10% Fines–90% Sand Mixture

The following results are for electrokinetic barrier tests carried out using a mixture of 10% fines (by mass) and 90% sand. The percent fines was calculated according to equation (9.11).

10.2.1.1 10% Fines Control Tests

10.2.1.1.1 Steady State Volumetric Flow Rate

In order to start each test, the volumetric flow rate was ensured to have reached a steady state. This was done by introducing simulated groundwater in the feed. Each test was carried out in duplicate and the tests were labeled test (1) and test (2). The volumetric flow rates during steady state are presented in Figure 52. As seen in the figure, the flow rate for each test reached steady state almost immediately producing a straight line for the effluent cumulative volume during the test. Even though the two tests were carried out in the exact fashion previously described, the flow rate in test (1) was slightly higher than in test (2). It is hypothesized that the difference may be caused by the normal variation in the packing of soil particles in the cells. The average effluent flow rate resulting from the hydraulic gradient (natural seepage of water through the test cell mixture in the absence of a voltage gradient) was approximately 8.6mL per minute (mL/min) (Figure 52).

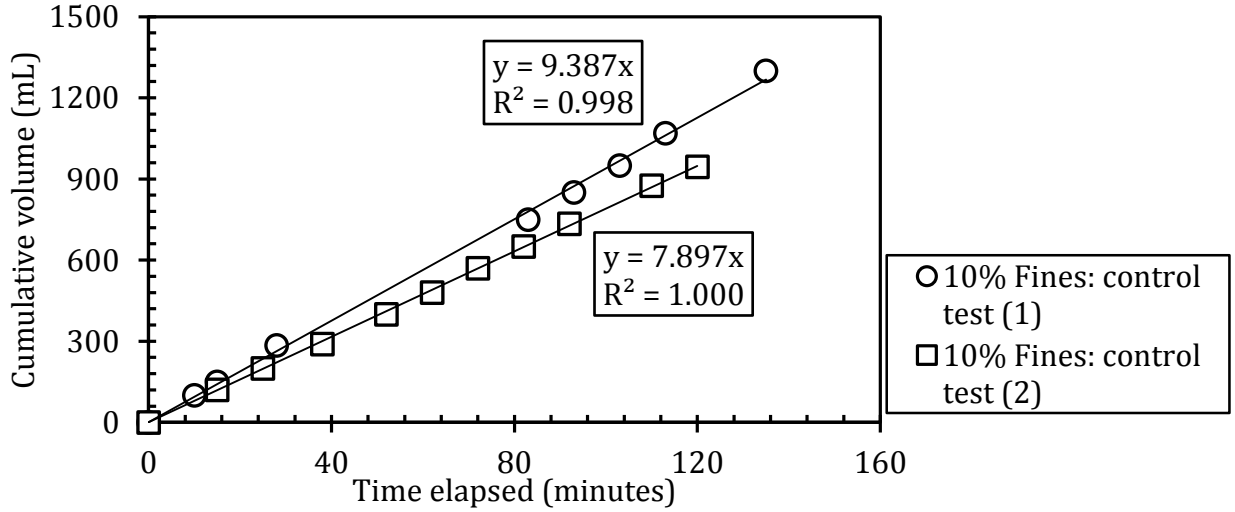

Figure 52 – 10% fines control tests: Steady state determination curves

10.2.1.1.2 Volumetric Flow Rate

After establishing steady state flow, the simulated groundwater was replaced with feed water that contained 1000 ppm of cobalt with the power supply switched off. Comparing the control tests to the electrokinetic barrier tests at the same pore volumes eliminates the influence of the soil properties, such as sorption, on the effectiveness of the electrokinetic barrier to halt the migration of cobalt. Therefore, it is useful to plot the number pore volumes collected against time. The flow rate plots of both control tests are shown in Figure 53. It is important to note that, throughout the rest of this thesis, in all the flow rate figures including Figure 53, zero minutes corresponds to the time when cobalt was introduced into the cell. When the cobalt solution was introduced to the cells (i.e. after steady state flow was achieved using the simulated groundwater), the average flow rate decreased to 6 mL/min (the flow rate was calculated from the actual effluent volumes collected over the collection period and averaged over the two tests). Equally, the flow rate can be obtained by multiplying the slope of the nominal pore volume vs. collection time by the value of the nominal pore volume (940 mL). A plausible explanation for the reduction of the hydraulic conductivity of the cell mixture is the introduction of cobalt solution containing a significantly large ion concentration (1000 ppm cobalt). One would expect that increasing the cation concentration in the pore fluid would shrink the diffuse double layer and increase the hydraulic conductivity. However, cobalt accumulation along the length of the soil may have decreased the soil's porosity and led to a flow reduction.

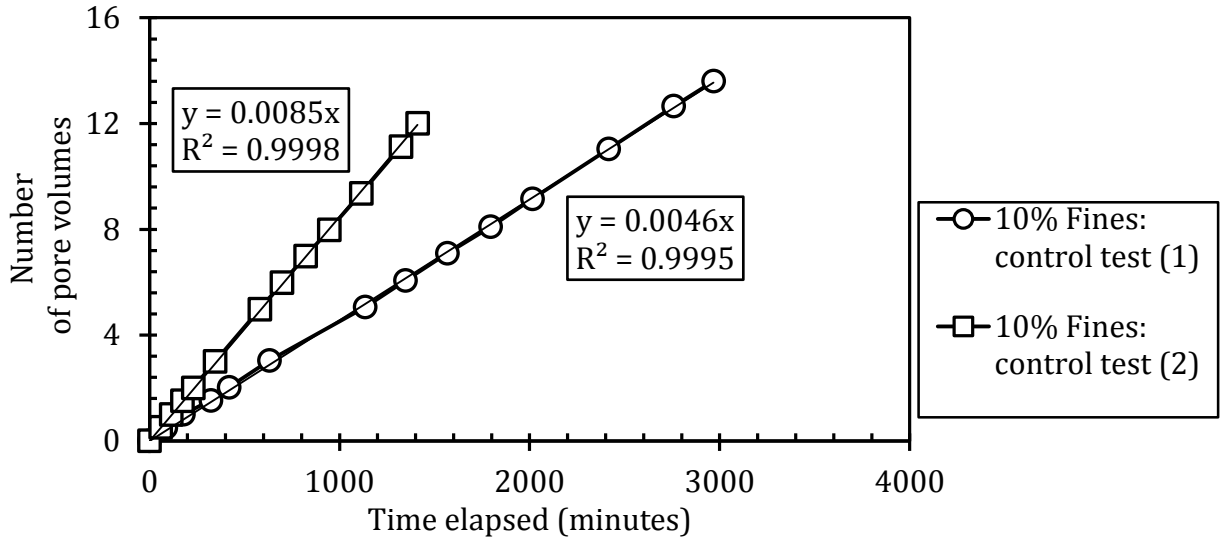

Figure 53 – 10% fines control tests: Pore volume versus collection time

10.2.1.1.3 Cobalt Effluent Concentration Profile

The concentration of cobalt exiting the test cell at the anode was determined for each pore volume collected. The concentration profiles obtained from both control tests are presented in Figure 54 where the normalized concentration is plotted against the pore volume. The normalized cobalt concentration was obtained by dividing the effluent concentration by the initial concentration.

$$[\boldsymbol{Co}]_{\boldsymbol{normalized}} = \frac{[\boldsymbol{Co}]_{\boldsymbol{effluent}}}{[\boldsymbol{Co}]_{\boldsymbol{initial}}} \qquad \text{Eq. (10.4)}$$

where, $[Co]_{normalized}$ is the normalized cobalt concentration

$[Co]_{effluent}$ is cobalt concentration in the effluent (mg/L)

$[Co]_{initial}$ is the cobalt concentration initially in the feed water (mg/L)

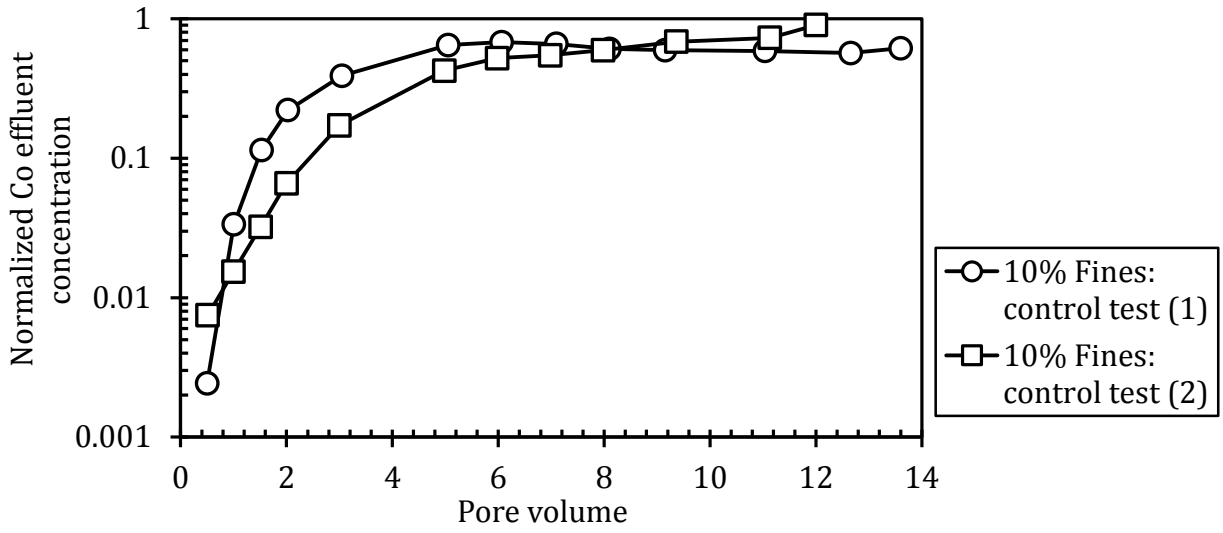

Figure 54 – 10% fines control tests: Co effluent concentration profile

When a contaminated fluid flows through a porous medium, some contaminants will be adsorbed/retained by the medium by physical and/or chemical mechanisms. Consequently, the effluent concentration will increase until the medium reaches its full adsorption/retention capacity. Upon reaching adsorption capacity, the effluent concentration will become equal to the influent concentration, and the concentration profile will plateau (Ingham, 2005). Additionally, dilution of cobalt's concentration in the pores by dispersion and the displacement of the non–contaminated groundwater play part in the overall cobalt concentration profile. As the cobalt solution flows through the soil cell, the uncontaminated feed water, initially present in the cell from the steady state determination test, will be displaced by the feed solution containing 1000 ppm of cobalt. The cobalt concentration profiles in Figure 54 exhibited a similar trend such that the cobalt concentration in the effluent increased with time and as more pore volumes were collected. In these tests, up to 90% of the influent cobalt concentration exited the cell in the absence of an electrokinetic barrier. This scenario is analogous to the flow of cobalt with groundwater in the aquifer where there are no barriers to flow.

The pH of the effluent was plotted against the pore volume in Figure 55. The average pH of the effluent solutions in test (1) was approximately 6.7 and that in test (2) was 7.4. The pH is stable and perhaps slightly decreasing in control test (2).

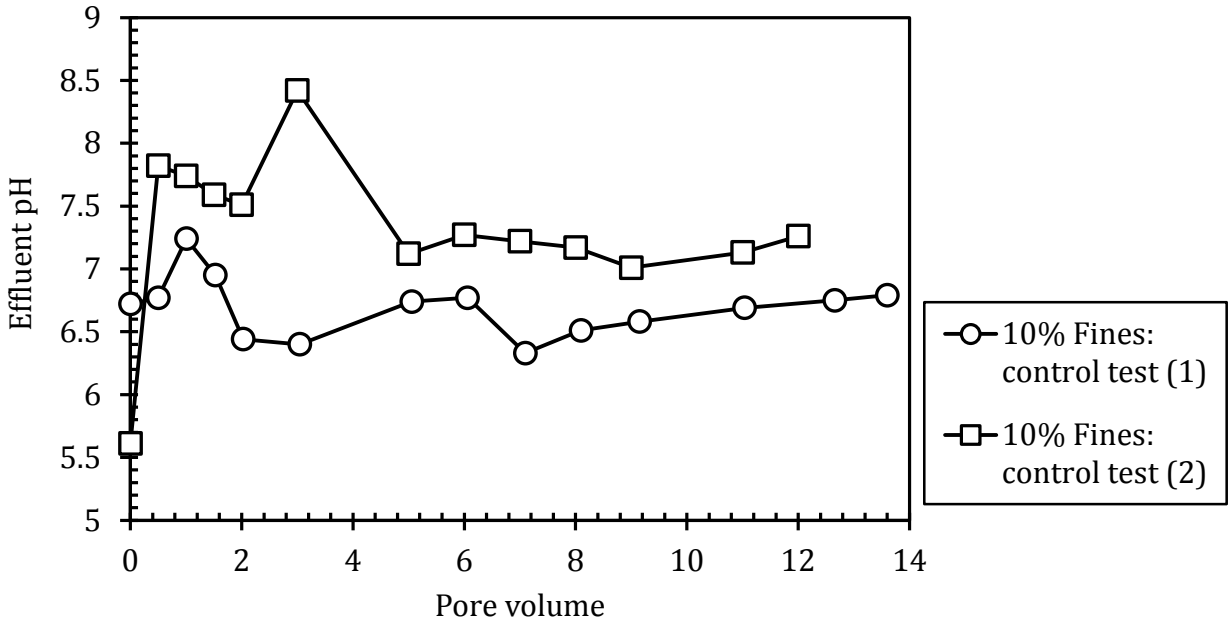

Figure 55 – 10% fines control tests: Effluent pH profile

10.2.1.1.4 Cobalt Accumulation in the Soil

The total cobalt accumulated on the soil due to adsorption and/or precipitation was determined by means of soil digestion as previously discussed. The mass of cobalt accumulated on the soil as a function of the normalized distance from the cathode at the centre of each of the five (5) slices is plotted in Figure 57 for both tests. The normalized distance was calculated as:

$$\boldsymbol{x_{normalized}} = \frac{\boldsymbol{x_{centre}}}{\boldsymbol{x_{tot.}}} \qquad \text{Eq. (10.5)}$$

where, $x_{normalized}$ is the normalized distance with the cathode as the reference

x_{centre} is the distance between the cathode and the centre of each slice (cm)

$x_{tot.}$ is the total distance from the cathode to the anode (cm)

In test (1), 5.8 mg/g of cobalt adsorbed/precipitated in the soil: 24% of the cobalt mass accumulated near the inlet of the cell (the cathode region) and only 16% accumulated near outlet of the cell (the anode region), as calculated from equation (10.5). Even though 4.9 mg/g of cobalt accumulated in test (2), the cobalt distribution in the inlet and outlet regions was very consistent. If cobalt distribution in the soil was assumed to be uniform, then 20% of cobalt would have accumulated on each slice. However, it can be seen that more cobalt accumulated near the inlet of the cell. This may be explained by the fact that

near the inlet of the cell most of the soil is under the phreatic line, as shown in

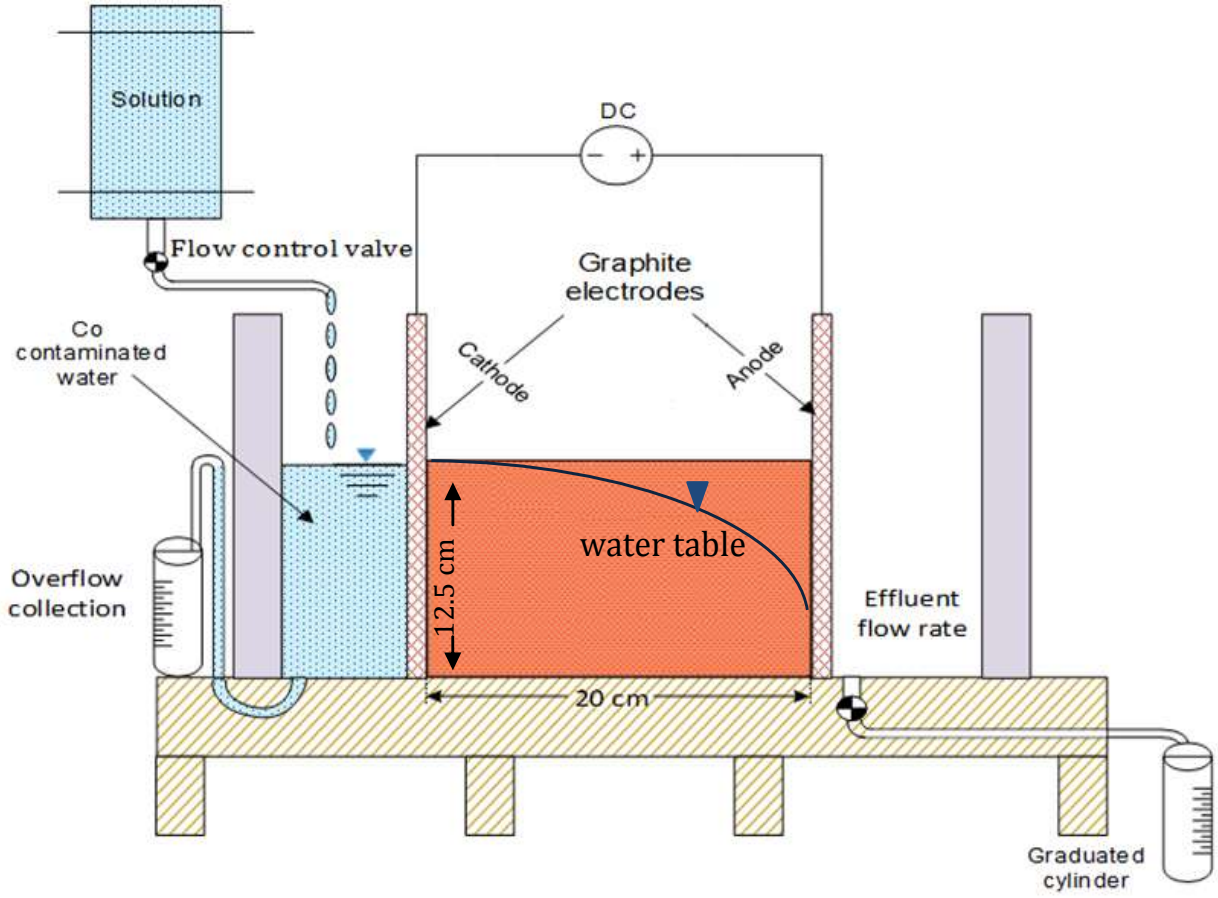

Figure 34. This means that the inlet region is saturated with the cobalt solution (1000 ppm), whereas a smaller section of the outlet region is under the phreatic line. This conclusion is supported by the moisture content, which was calculated on wet basis, at each normalized distance from the cathode, as shown in Figure 56.

$$\%\boldsymbol{Co_x} = \frac{\boldsymbol{Co_x}}{\boldsymbol{Co_{tot}}}\ \mathbf{100}\% \qquad \text{Eq. (10.6)}$$

where, $\%Co_x$ is the percentage of cobalt accumulated in any $x_{normalized}$ region on the soil.

Co_x is the mass of cobalt accumulated in region $x_{normalized}$ (g), and

Co_{tot} is the mass of cobalt accumulated in the entire cell (g)

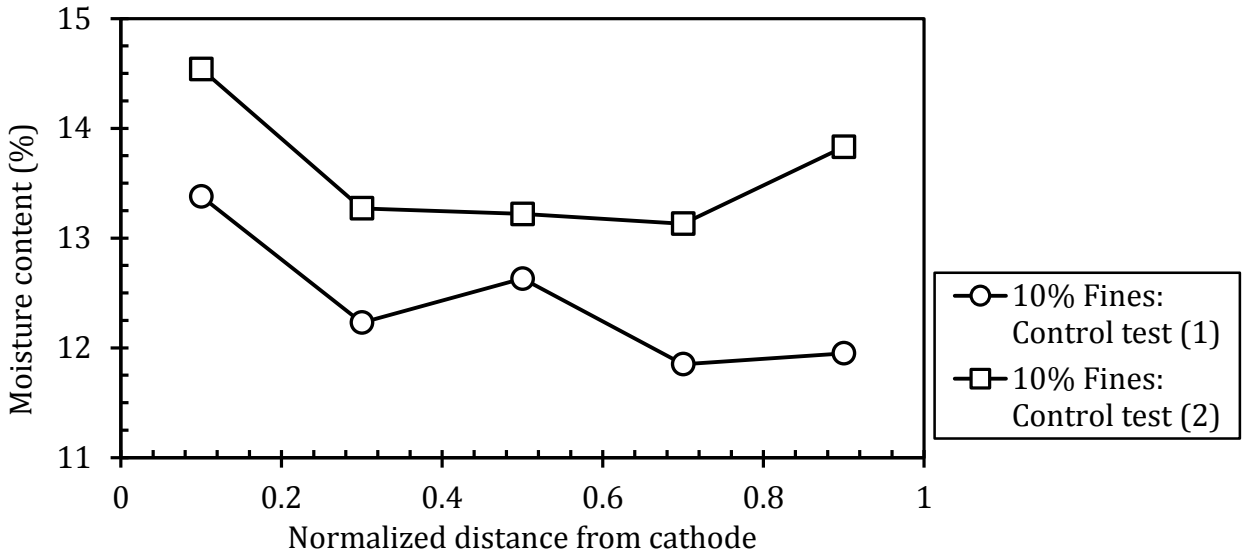

Figure 56 – 10% fines control tests: Moisture content of each

The pore fluid pH averaged around 6.9, as shown in Figure 58. The pH increased as the anode was approached. It is hypothesized that the accumulated cobalt behaved as a Lewis acid and lowered the pH in the region it accumulated via an acid–base reaction.

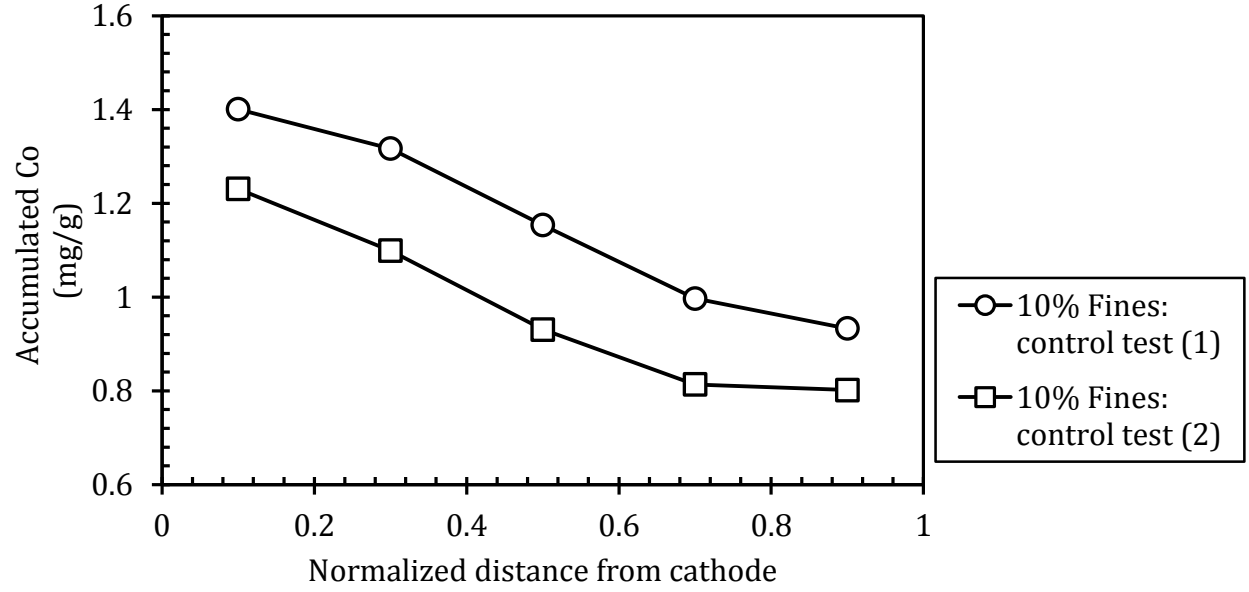

Figure 57 – 10% fines control tests: Accumulated cobalt

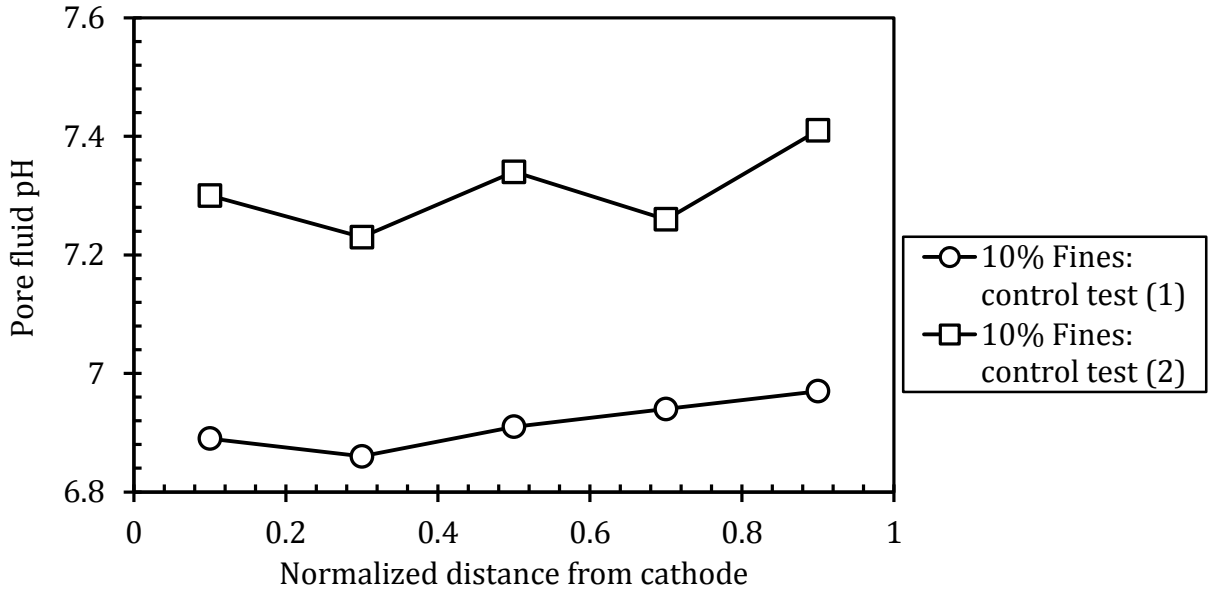

Figure 58 – 10% fines control tests: Pore fluid pH profile

10.2.1.2 10% Fines Electrokinetic Barrier Tests–Continuous Current

The electrokinetic (EK) barrier tests were conducted at an applied voltage of 40 V (i.e. voltage gradient of 2V/cm) across the length of the test cell specimen. The results of these tests are presented in the following sections.

10.2.1.2.1 Steady State Volumetric Flow Rate

Similar to the control tests, the steady state flow rate was first determined for each test, and presented in Figure 59. Each steady state determination test provides insights about the change of flow rate after subjecting the test cell mixture to the voltage gradient. Both the first test and its repeat have the same flow rates prior to application of the voltage gradient. The average flow rate was 9.4 mL/min.

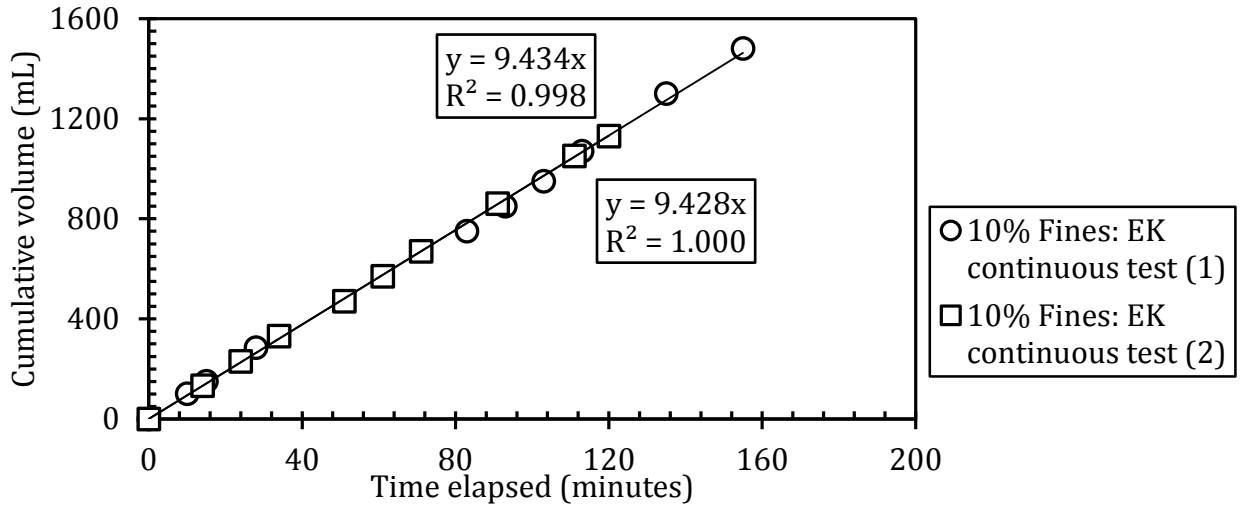

Figure 59 – 10% fines EK continuous tests: Steady state determination curves

10.2.1.2.2 Volumetric Flow Rate with Continuous Current

Once steady state flow had been achieved, the cobalt solution was added to the influent compartment and 40V were applied to the cell. The volumetric flow rates were determined for both tests and are presented in Figure 60. From these plots, it is clear that under an applied electric potential, the volumetric flow rate is much lower, on average, than that in the absence of a voltage gradient. Under the continuously applied Voltage of 40 V, the flow rate constantly decreased particularly in test (1). During the control tests, Figure 53, the volumetric flow rate remained relatively unchanged contrary to the electrokinetic barrier

tests. Under an applied voltage, the flow rate deviated from linearity. During slicing the soil specimen in the electrokinetic test and as approaching the cathode, precipitation of cobalt on the soil specimen was observed and slicing became more difficult as a result.

Cobalt accumulated in both control and electrokinetic barrier tests; however, greater amounts of cobalt accumulated in the electrokinetic barrier tests. Thus, it was hypothesised that the pores in the test cell mixture were clogged by cobalt precipitation which greatly reduced the flow. In other words, cobalt accumulation created a barrier to entry of the influent solution into the cell. The cathode region after the termination of the test is depicted in Figure 61. Furthermore, for each given test, the time required to collect a nominal pore volume of 940 mL under the applied voltage was significantly higher than in the absence of a potential gradient. The time it took to collect 12 pore volumes (11.28 L) from test (1) was approximately 9.5 days, as depicted in Figure 60. Meanwhile it took just under a day to collect 12 pore volumes from control test (2) and 2 days to collect 13.5 pore volumes from control test (1) in the absence of a potential gradient (Figure 53). It is realized that the flow rate decreased in the control test as cobalt was introduced in the cell where it accumulated near the cathode. However, the effectiveness of the electrokinetic barrier in reducing the flow rate is much greater.

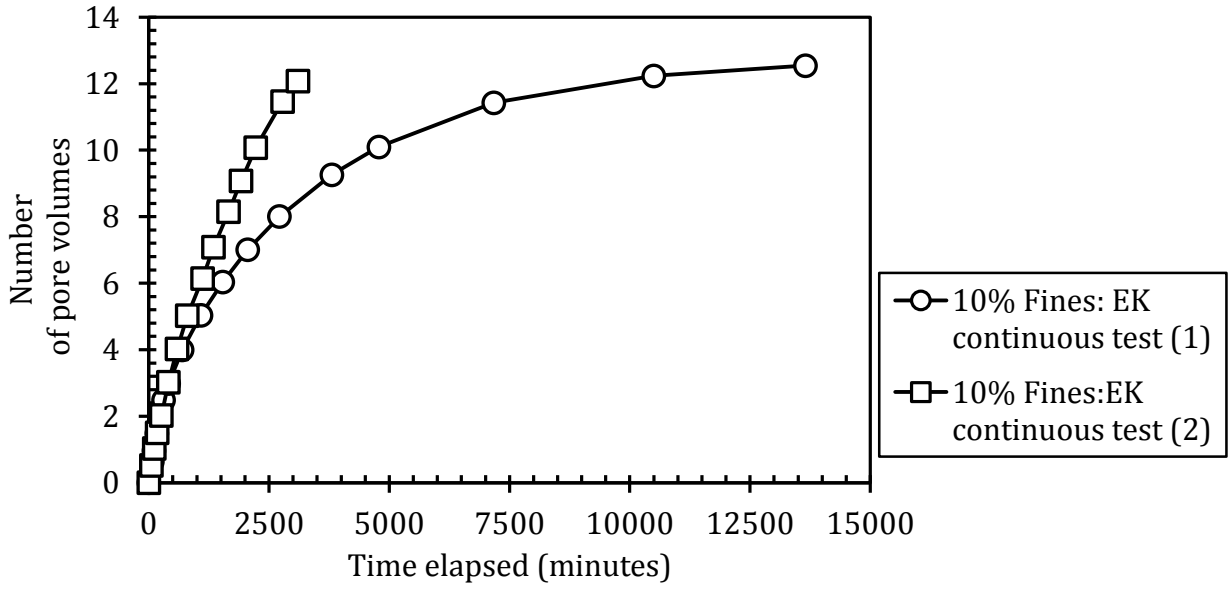

Figure 60 – 10% fines EK continuous tests: Pore volume versus collection time

Figure 61 – Cobalt precipitation at cathode region (bluish–green)

It was surprising at first that the 10% fines–90% sand mixture test (2) resulted in an overall higher volumetric flow rate than test (1) under the applied voltage (Figure 60). However, the former test (2) was conducted with a slight variation. Holes were drilled on the soil specimen near the cathode and the anode for pH measurements at each pore volume during the test, as shown in Figure 62.

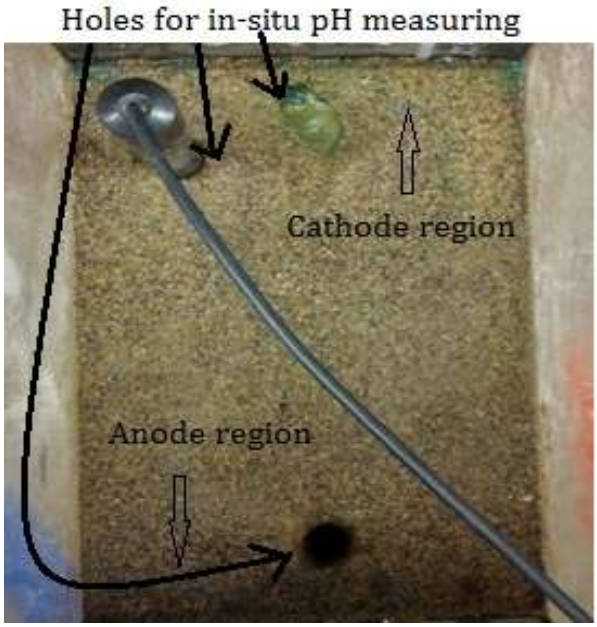

Figure 62 – In–situ pH measurement locations near cathode and anode

In light of this information, it was hypothesized that drilling holes might have created channelling in the test cell which resulted in an increased flow rate of solution through the test cell. As well, the creation of cobalt "reservoirs", such that the holes acted as impoundment of cobalt solution, resulted in overestimation of the amount of cobalt

accumulated near the cathode. In other words, an amount of cobalt solution was stored in the drilled pH hole for the duration of the experiment. Furthermore, the storage of cobalt solution near the cathode reduced its availability for transport downstream which resulted in lower cobalt concentrations in the effluent of test (2) compared to those of test (1).

10.2.1.2.3 Cobalt Effluent Concentration Profile

Similar to the control tests, the normalized cobalt concentration in the effluent water was determined and plotted against pore volumes, as shown in Figure 63. The effluent concentration in test (1) reaches a maximum value before decreasing to a very small value; however, the effluent concentrations in test (2) slowly increased to a plateau. The maximum effluent concentration was less than 40% of the inlet concentration.

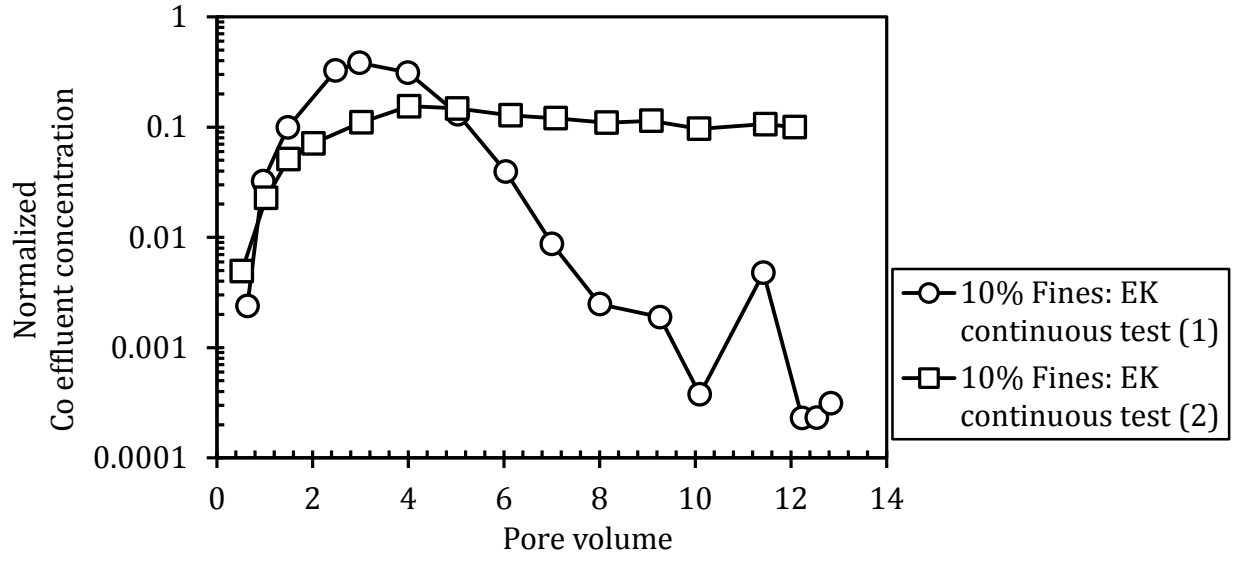

Figure 63 – 10% fines EK continuous tests: Co effluent concentration profile

The pH of the effluent decreased with each pore volume collected, as shown in Figure 64. As the anode reaction produced hydrogen ions, the effluent pH dropped. The pH ranged from 6.2 in the feed solutions to 1.9 at the end of the tests. The change of the effluent pH was expected, since a pH gradient would develop and become more pronounced with the passage of time (Acar, et al., 1990).

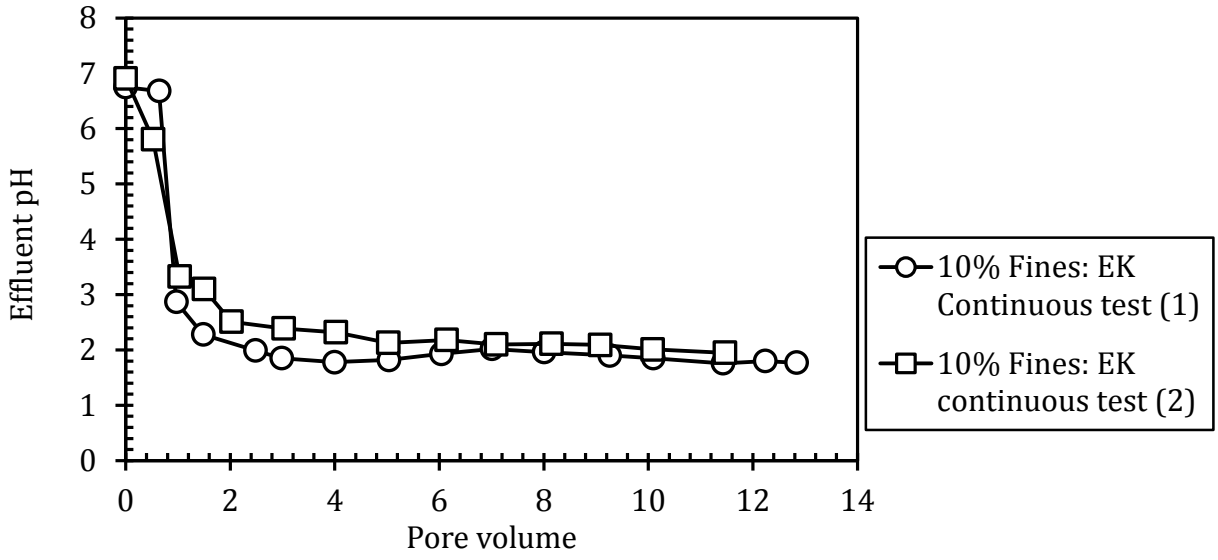

Figure 64 – 10% fines EK continuous tests: Effluent pH profile

10.2.1.2.4 Cobalt Accumulation in the Soil

The distribution of cobalt on the test cell from the cathode to the anode differed from that in the control tests (see Figure 65). The concentration of the cobalt accumulated was 6.8 mg/g in test (1) and 9.5 mg/g in test (2) of the electrokinetic barrier with continuous current, which is 40 to 94 % higher than the cobalt accumulated in the control tests, with most of the accumulation near the cathode. Approximately 61% of the cobalt accumulated near the cathode in test (1) and only 3% accumulated near the anode, i.e. the cobalt accumulated in the cathode region was 22 times higher than that accumulated closer to the anode. The 10% fines test (2) resulted in similar distribution of cobalt at the cathode and the anode. By contrast, the cobalt accumulation near the inlet of the cell was approximately 1.5 times higher than near the outlet in the 10% fines control tests, as demonstrated in Figure 57. This difference can be explained by the pore fluid pH profile in the electrokinetic barrier test shown in Figure 67. A sharp pH gradient developed between the cathode and anode. On average, the cathode region reached a pH of 12.2 and it gradually decreased to a pH of 7.2 near the anode. The high pH at the cathode promoted the precipitation/adsorption of cobalt. The cobalt accumulation near the cathode was visually observed, shown in Figure 66. Using VMINTEQ (Gustafsson, 2000), it was determined that at high alkaline conditions, cobalt would precipitate as $Co(OH)_2$ and CoO. This finding was

consistent with the observation of the precipitate color in the cells. Both cobalt hydroxide, $Co(OH)_2$, and cobalt (II) oxide, CoO, are characterized with bluish–greenish color (Winter, 2014).

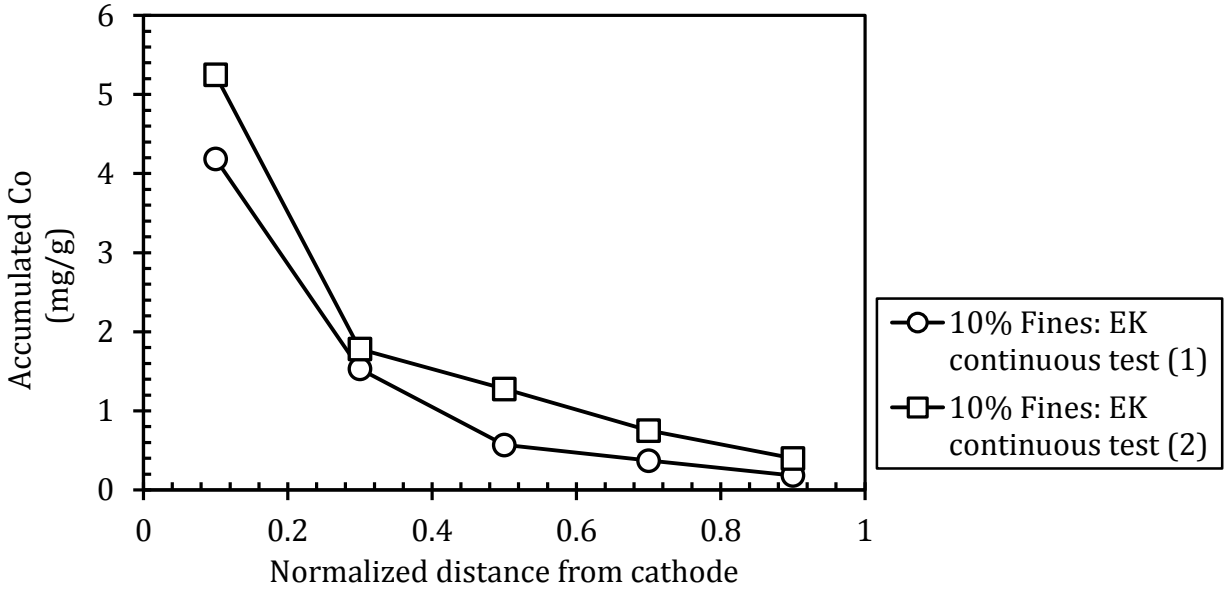

Figure 65 – 10% fines EK continuous tests: Accumulated cobalt

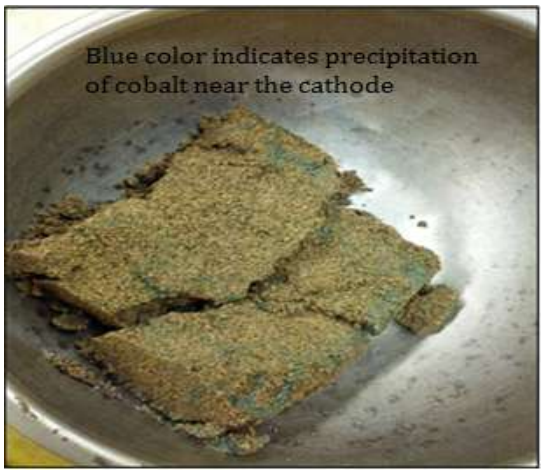

Figure 66 – 10% fines EK continuous tests: Visual observation of cobalt precipitation near the cathode (bluish–green)

It must be acknowledged that the pH near the anode might be erroneous (Figure 67). After the voltage gradient was terminated and the soil was cut into five (5) equal slices, each slice was well mixed, squeezed, and the pH of the pore fluid was determined. For all of the tests

carried out, the pH readings were taken 24 to 30 hours after the termination of the test. It is believed that the minerals present in the soil, like calcite, reacted with the acidity generated by the anode and neutralized the pore fluid pH. In Figure 68 the moisture content of each slice is plotted against the normalized distance from the cathode. Initially, it was predicted that the cell mixture near the cathode (inlet of the cell) would be fully under the phreatic line, i.e. fully saturated, whereas only a small portion of the anode region would under the phreatic line, i.e partially saturated. However, this was not observed (Figure 68). The complexity of the hydraulic flow under a voltage gradient makes it difficult to explain the moisture content profile across the soil specimen.

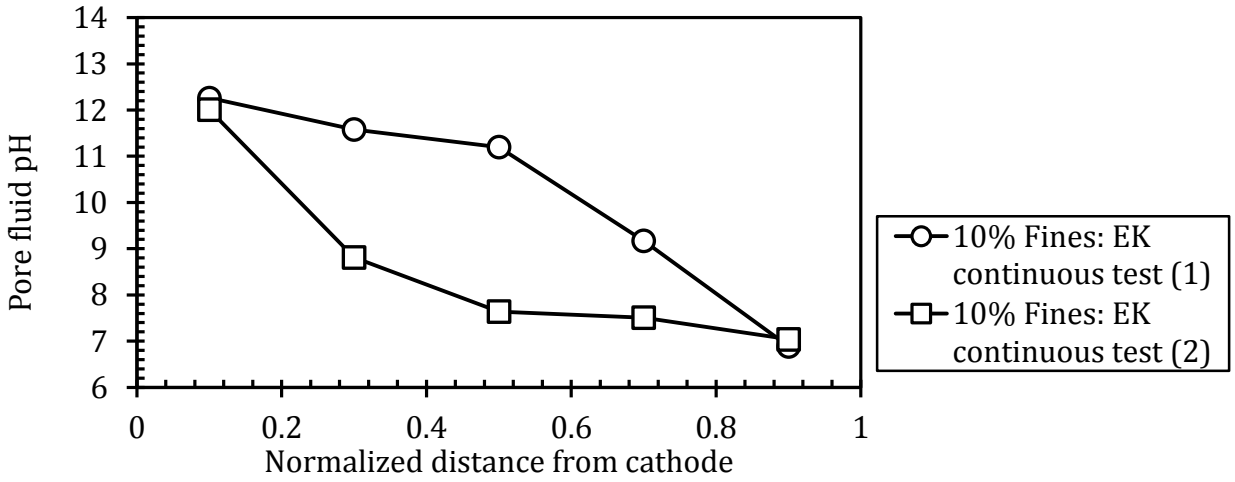

Figure 67 – 10% fines EK continuous tests: Pore fluid pH profile

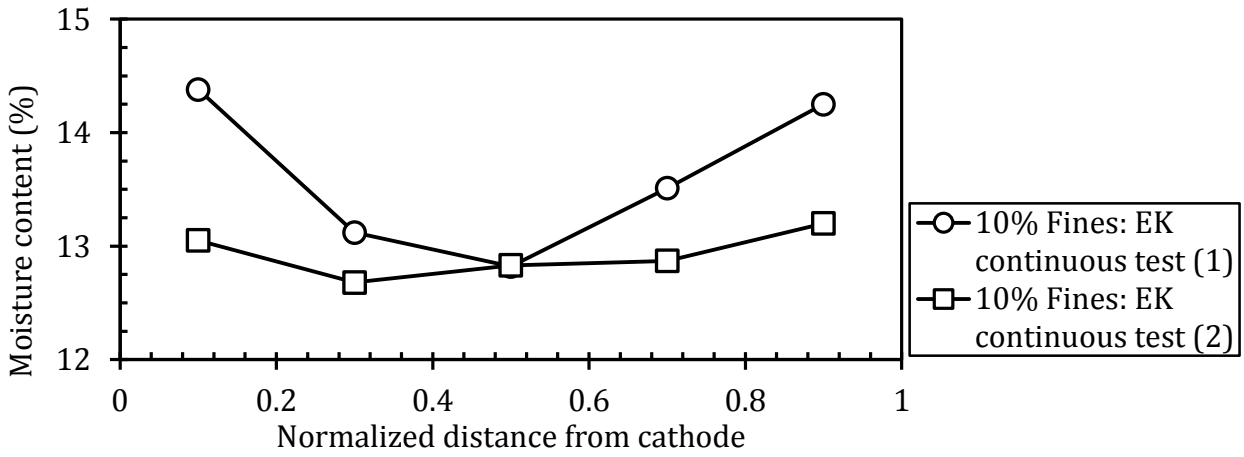

Figure 68 – 10% fines EK continuous tests: Moisture content of each slice

10.2.1.3 10% Fines Electrokinetic Barrier Tests–Intermittent Current

In the following sections, the results obtained by conducting experiments that investigated the use of intermittent current for the electrokinetic barrier are presented. As well, the results are discussed to examine the viability of using solar cells to power the electrokinetic barrier in future work. The power supply operated on on–off cycles of 24 hours. Readings of the effluent's volume, concentration and pH were taken every eight (8) hours for a period of eight (8) days.

10.2.1.3.1 Steady State Volumetric Flow Rate

The volumetric flow rates for test (1) and test (2) were allowed to reach steady state with respect to time, as shown in Figure 69, prior to starting the electrokinetic barrier intermittent current experiments. The cell produced an average volumetric flow rate of 8.5 mL/min.

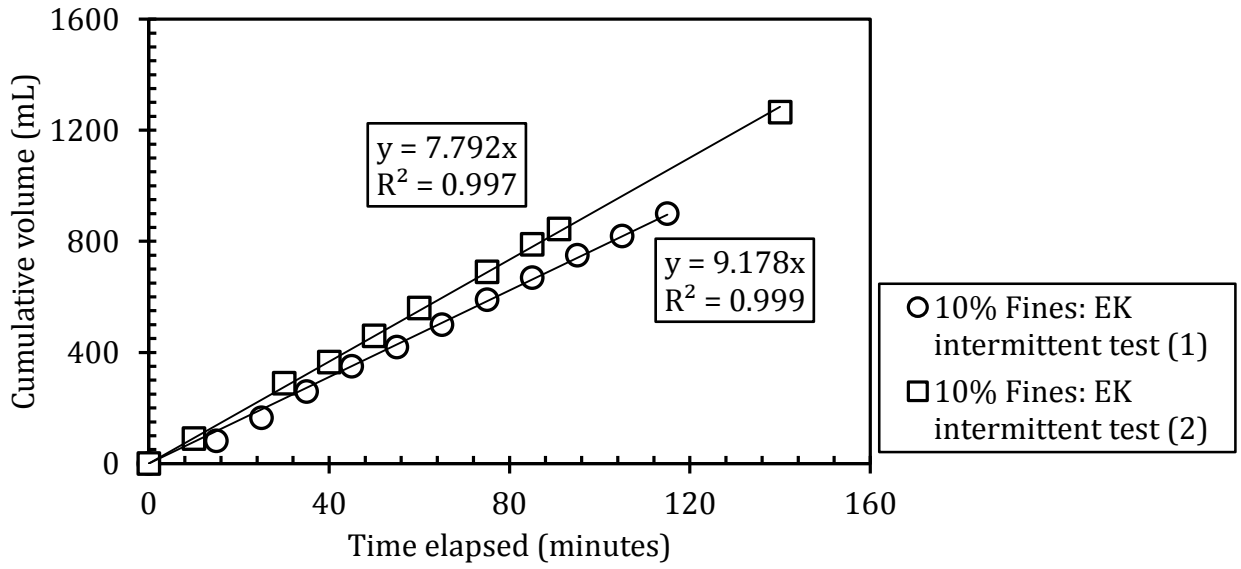

Figure 69 – 10% fines EK intermittent current tests: Steady state determination curves

10.2.1.3.2 Volumetric Flow Rate with Intermittent Current

Figure 70 shows the number of pore volumes collected versus the elapsed time of the test. It was clear that both tests followed a similar trend. It was found that the flow rate increased during the power off periods and decreased during the power on periods. Even though electro–osmosis did not stop the advancement of the contaminated plume

downstream during the on cycles, it did reduce the net flow rate. This was true for all the intermittent current experiments. Over the duration of the tests, an average of 16.2 pore volumes was collected from the 10% fines–90% sand mixture cells.

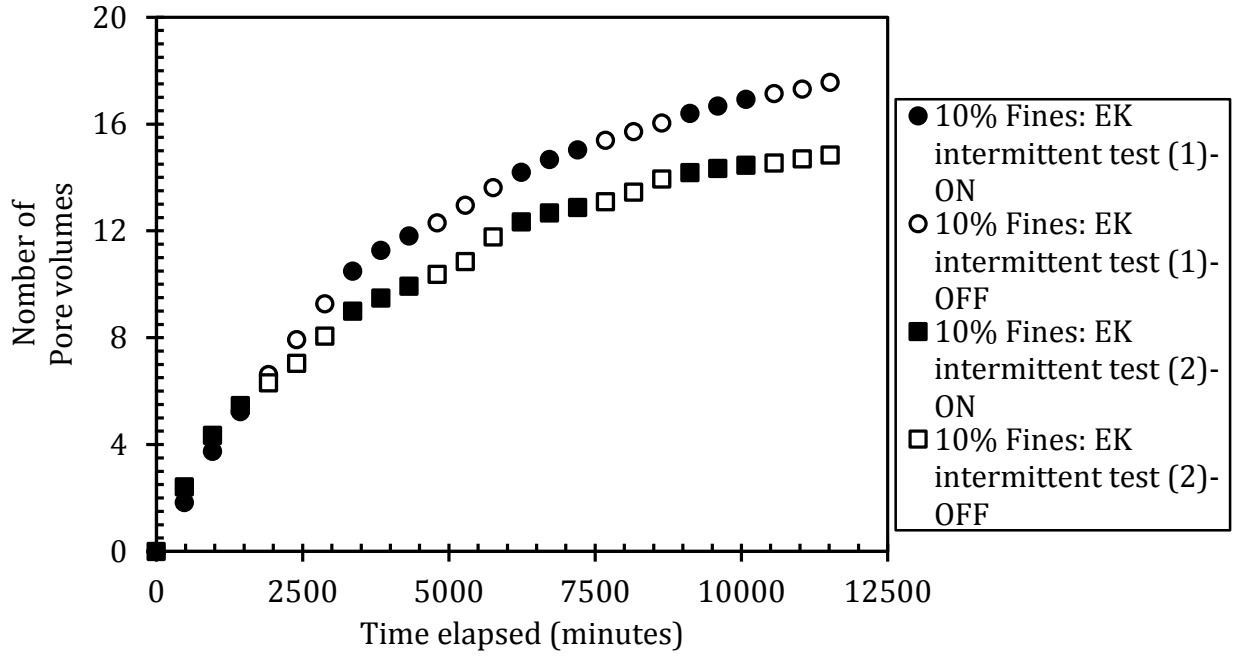

Figure 70 – 10% fines EK intermittent current tests: Pore volume versus collection time

10.2.1.3.3 Cobalt Effluent Concentration Profile

The effluent concentration of cobalt fluctuated between the 24 hours on and off cycles. This was observed in both tests as shown in Figure 71. The data points in Figure 71 were all recorded eight hours apart. The symbols alternate in groups of three to indicate when the electrokinetic barrier was turned on and off respectively. At the time when each third data point was recorded, the switch from on or off was made such that each first data point was recorded after eight hours of run time.

The highest effluent cobalt concentration was reached after two days at the end of the first off cycle. The highest effluent cobalt concentration ranged from 20% to 43% of the inlet cobalt concentration. The effects of electro–migration and electro–osmosis, though coupled with the reduction of the soil's porosity due to cobalt's accumulation in the cell, were observed during the intermittent cell tests. It was hypothesized that during the on cycles, the high pH environment near the cathode promoted cobalt's precipitation and adsorption.

As well, electro–migration would push cobalt towards the cathode. However, during the off cycles and due to the absence of ion migration, cobalt would travel towards the anode without hindrance. As a result, the cobalt effluent concentration increased and so did the flow rate. This may explain the fluctuation of cobalt concentration in the effluent during the test as shown in Figure 71. At the end of the eight (8) days, the effluent concentration was significantly reduced.

A similar fluctuation was observed in the effluent pH during the tests, as shown in Figure 72. The effluent pH decreased when the power was switched on (H^+ generation at the anode) and increased when the power was off. This is contrary to the tests with a continuous electric current where the effluent pH decreased steadily during the test.

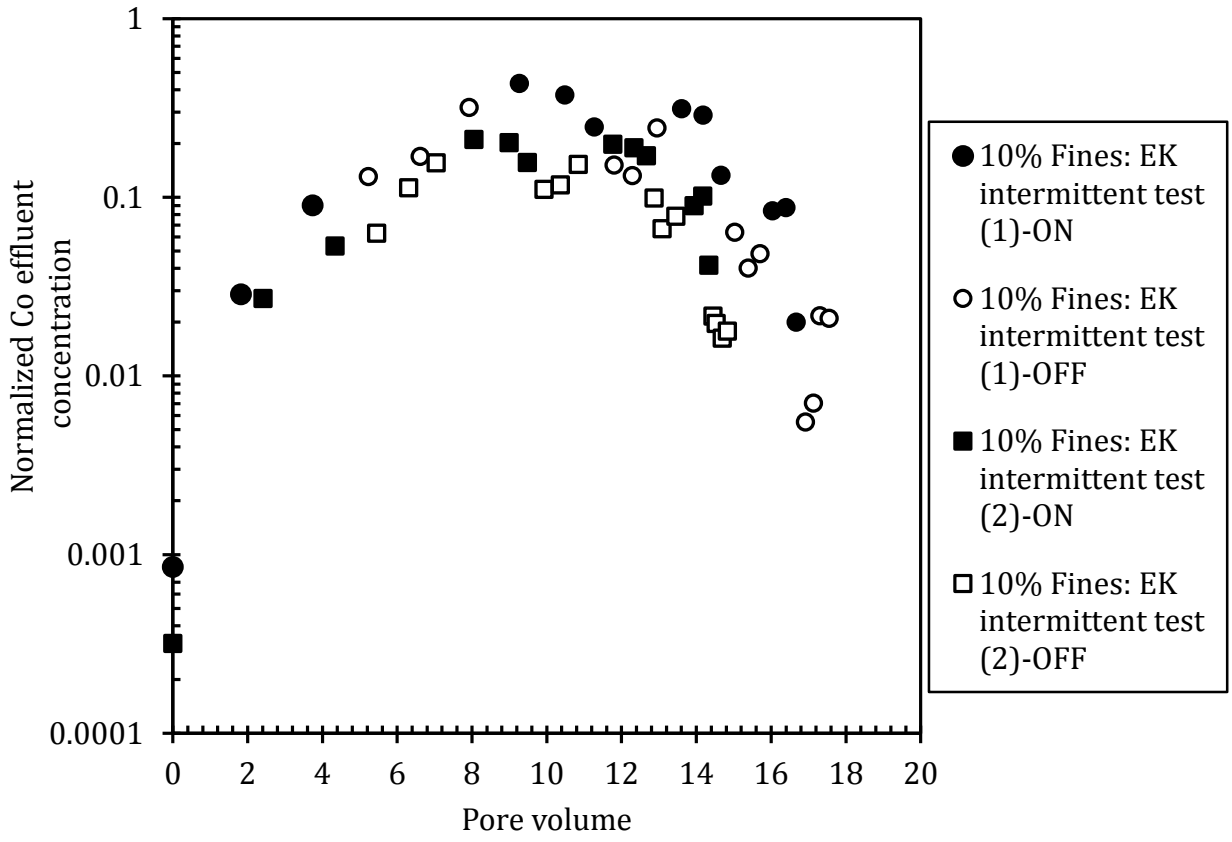

Figure 71 – 10% fines EK intermittent current tests: Co effluent concentration profile

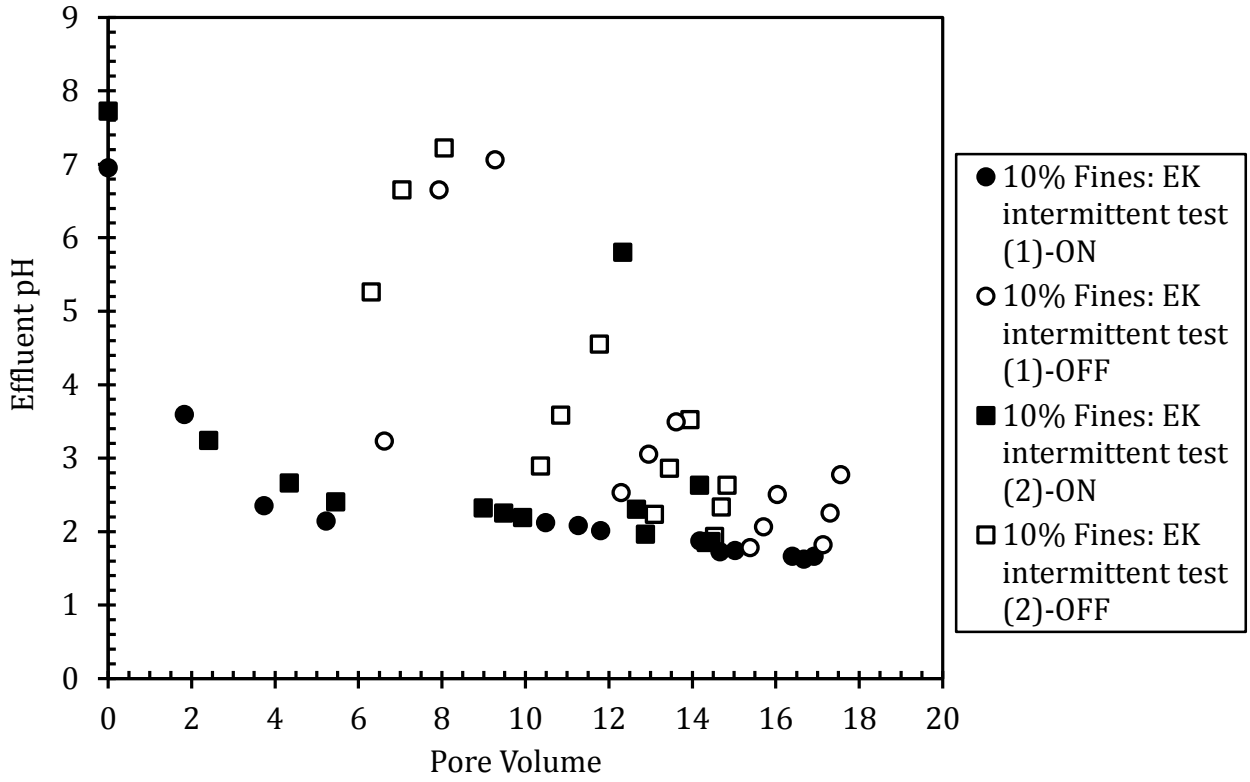

Figure 72 – 10% fines EK intermittent current tests: Effluent pH profile

10.2.1.3.4 Cobalt Accumulation in the Soil

The results from the s digestion tests revealed similar distribution of cobalt across the electrokinetic barrier for both tests as made evident by Figure 73. During the intermittent current test (1) 10.7 mg/g of cobalt precipitated/adsorbed in the cell. Approximately, 61% of the cobalt accumulated in the cathode region, by contrast, only 1% of cobalt accumulated near the anode. Test (2) showed similar results. Again, more cobalt accumulation near the cathode can be explained by the sharp pH gradient, Figure 74, produced by pore water electrolysis near the cathode and the anode, and the saturation of the cathode region with cobalt solution. Overall, more cobalt accumulated during the intermittent tests than in the continuous current tests. This may be due to the fact that more pore volumes were collected (more cobalt passed through the cell) in the intermittent tests.

The pH of pore water at the anode was measured to be 7.2 and that at the cathode was 12.4. Heavy metal ion precipitation and adsorption are enhanced in high pH environments such as the cathode region in the electrokinetic barrier tests.

Again, the resulting moisture content profile of soil specimen (Figure 75) was unpredicted. In the absence of the electrokinetic barrier, the opposite profile would be expected such that the inlet region (cathode) would be fully saturated and the outlet (anode) region would be less saturated. However, due to the complexity of the flow under an applied potential difference, the moisture content presented in Figure 75 cannot be explained.

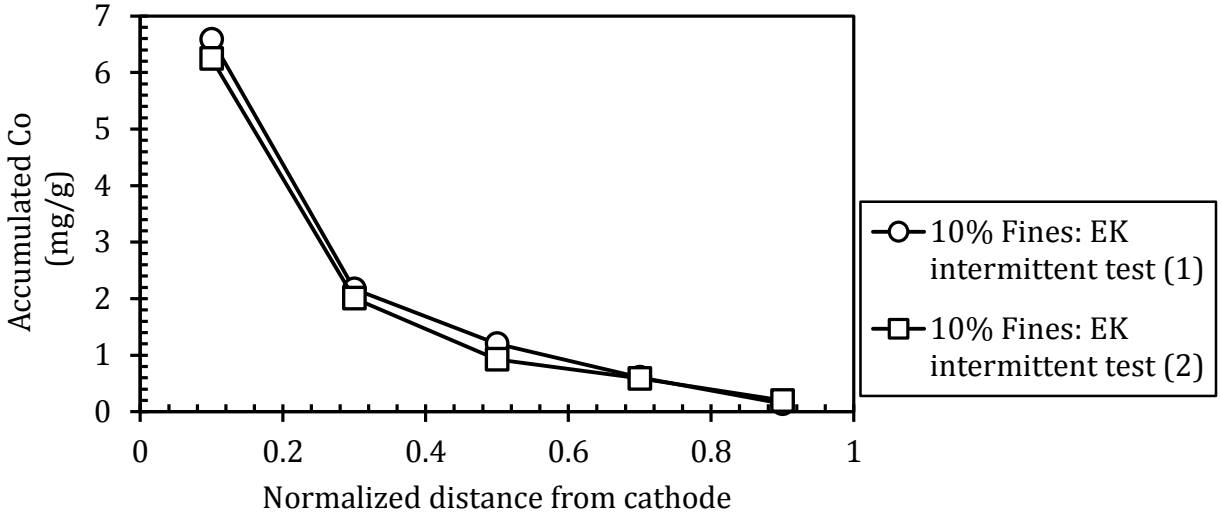

Figure 73 – 10% fines EK intermittent current tests: Accumulated cobalt

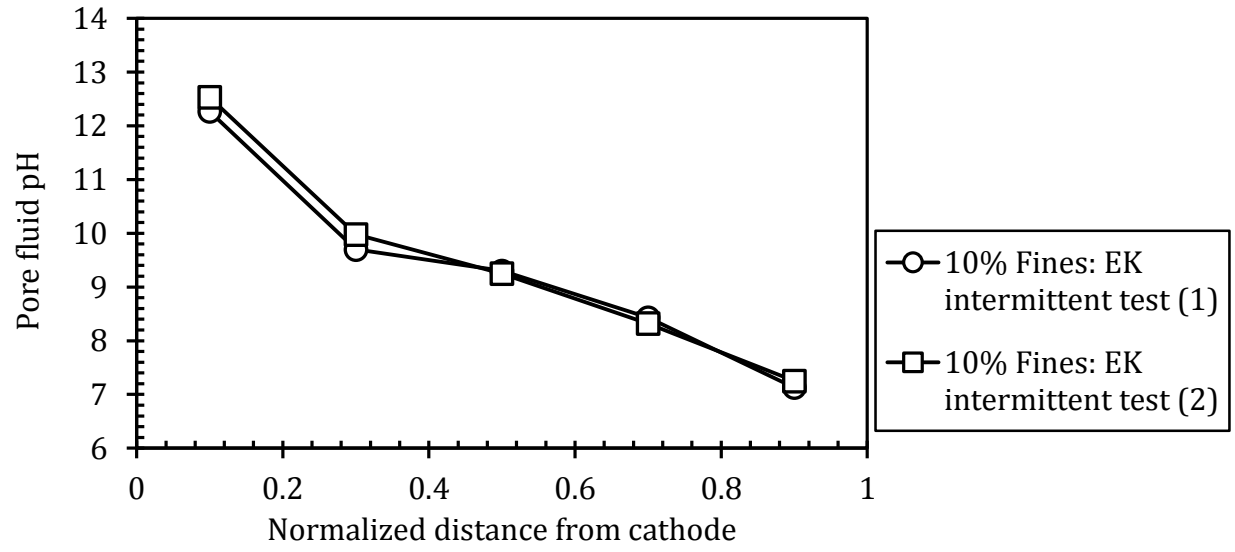

Figure 74 – 10% fines EK intermittent current tests: Pore fluid pH profile

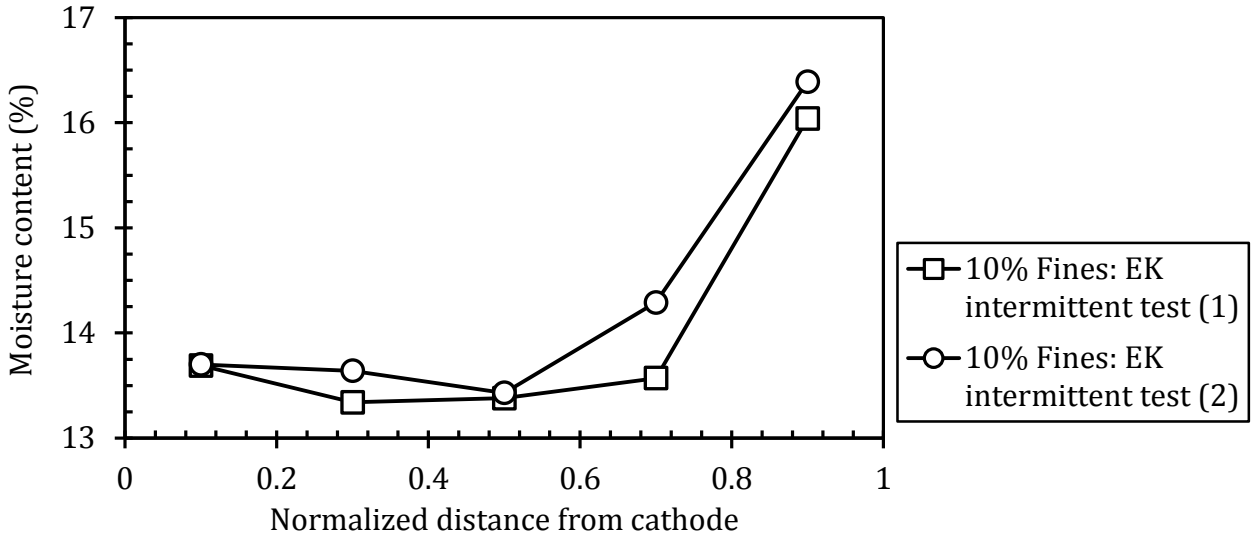

Figure 75 – 10% fines EK intermittent current tests: Moisture content of each slice

10.2.2 20% Fines–80% Sand Mixture

10.2.2.1 20% Fines Control Tests

Similar to the 10% fines–90% sand mixture, control tests with 20% fines–80% sand mixtures were conducted.

10.2.2.1.1 Steady State Volumetric Flow Rate

The plot of the cumulative volume collected against the time elapsed from the start of the tests was constructed to confirm that the flow rate had reached steady state, as shown in Figure 76. Increasing the percent of clay to 20% decreased the average effluent flow rate to 4.5mL/min from an average flow rate of 8.6 mL/min in the 10% fines cells (Figure 52). The flow rate decreased due to the reduction of the cell's permeability resulting from a more cohesive mixture (Kasenow, 2002).

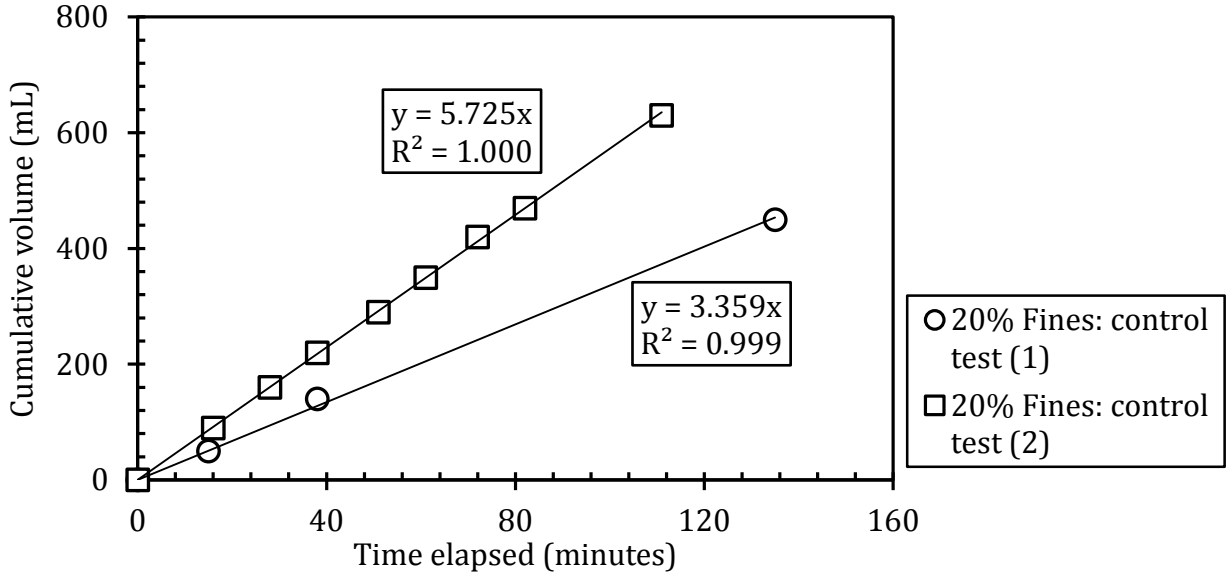

Figure 76 – 20% fines control tests: Steady state determination curves

10.2.2.1.2 Volumetric Flow Rate

The volumetric flow rate was obtained by plotting the number of pore volumes versus time elapsed (Figure 77). The flow rate decreased to 3.8 mL/min on average after switching from the simulated groundwater to the 1000 ppm cobalt solution. Similar to the 10% control test, the reduction could be explained by cobalt accumulation in the cell. Precipitation and adsorption could reduce the availability of flow paths by clogging the pores (Mackenzie, et al., 1999).

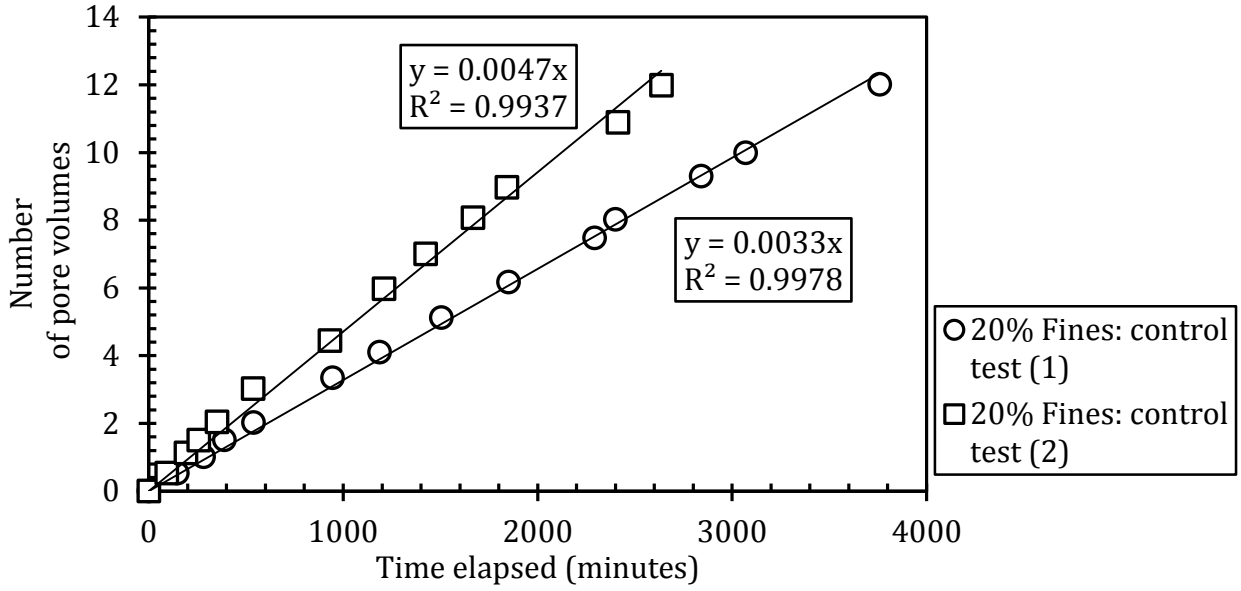

Figure 77 – 20% fines control tests: Volumetric flow rate

10.2.2.1.3 Cobalt Effluent Concentration Profile

Similar to the previous tests, the normalized cobalt concentration in the effluent is given in Figure 78. The overall trend is that the cobalt concentration exiting the cells increased with the pore volumes collected. Even though all the test conditions were kept the same, test (2) exhibited a slightly different trend than test (1). The concentration peaked at approximately 40% of the inlet concentration, decreased and then increased again. It was hypothesized that this behaviour may be due to cross contamination or oversaturation of the ICP–AES sensor as a result of previously analysing samples of high concentrations. Overall, the trends were comparable, the concentration increased with time. Overall, both test (1) and test (2) yielded expected trends of the effluent concentration of a contaminant

solution passing through a porous medium when accounting for dilution of cobalt's concentration in the pores by dispersion and the displacement of the non–contaminated feed water. The effluent concentration would increase until a break through point where the cobalt effluent concentration would equal the cobalt influent concentration, and the plot would plateau. In these tests, the break through point would have been observed if the tests were run for a longer period. The pH of the effluent at each pore volume is presented in Figure 79. On average, test (1) produced lower effluent pH values than test (2). Given that the effluent concentration in test (1) was higher than in test (2), the lower pH values in test (1) are consistent. The average pH of the samples obtained was 7.3.

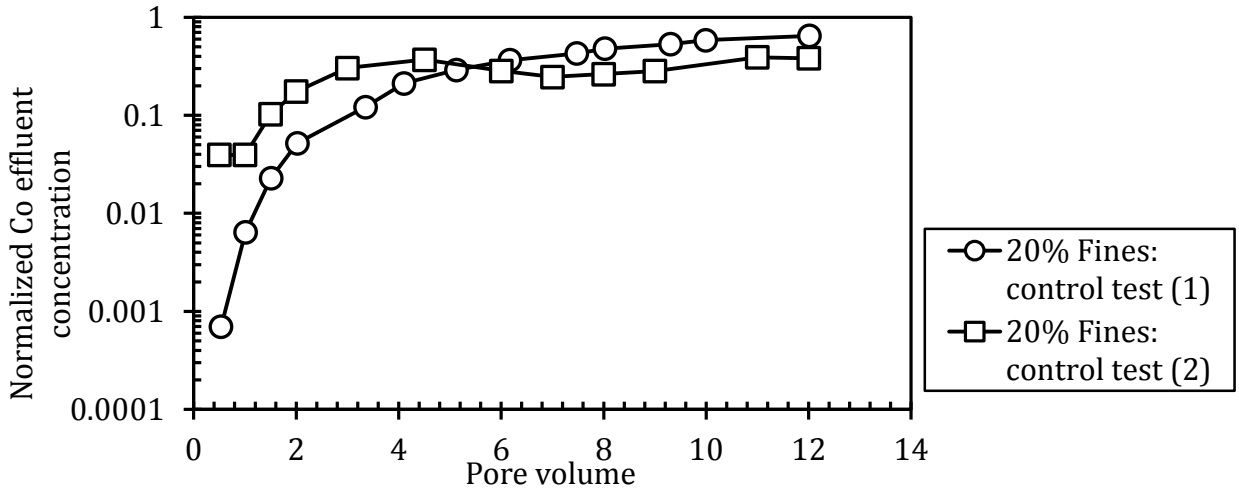

Figure 78 – 20% fines control tests: Co effluent concentration profile

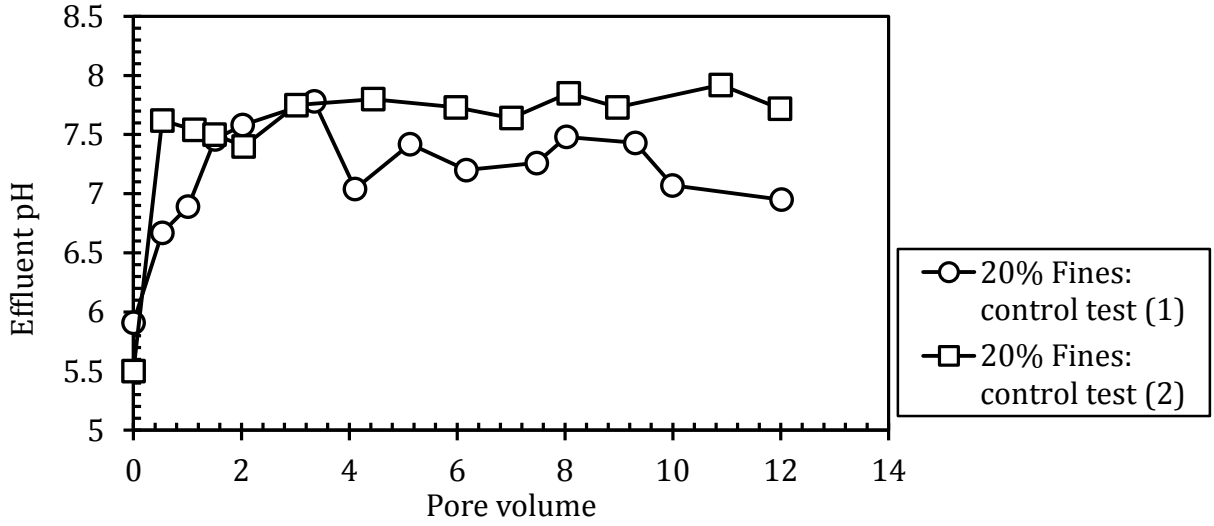

Figure 79 – 20% fines control tests: Effluent pH profile

10.2.2.1.4 Cobalt Accumulation in the Soil

The concentrations of cobalt accumulated in the test cell (mg/g) during the control tests using 20% fines and 80% sand mixtures are given in Figure 80. Overall, the average amount of cobalt accumulated in the cell was slightly higher in the cells containing 20% fines than in those containing 10% fines during the control tests. A cobalt mass of 6.2 mg/g precipitated/adsorbed in the 20% fines control test (1) which represented an increase of 8 to 23% from the tests conducted with 10% fines, Figure 57. This increase may be attributed to the increase of CEC, availability of bonding sites, and the carbonate content of the cell due to increasing the clay content in the cells (Acar, et al., 1995; Darmawan & Wada, 2002; Ouhadi, et al., 2010). 29% of the cobalt accumulated near the inlet of test (1) containing 20% fines and only 12% accumulated near the outlet of the cell. Test (2) showed similar results. The pH of the pore fluid was around 6.86, Figure 81, which is close to the average pore fluid pH of 6.9 obtained in the 10% fines cells, shown in Figure 58.

The moisture content (on wet basis) of each slice is presented in Figure 82. The moisture content from both test (1) and test (2) decreased from the cathode to the anode. This profile is typical of hydraulic flow in the absence of a voltage gradient. The cathode region was presumed to be fully saturated whereas the anode region was presumed to be less saturated, as demonstrated by Figure 82.

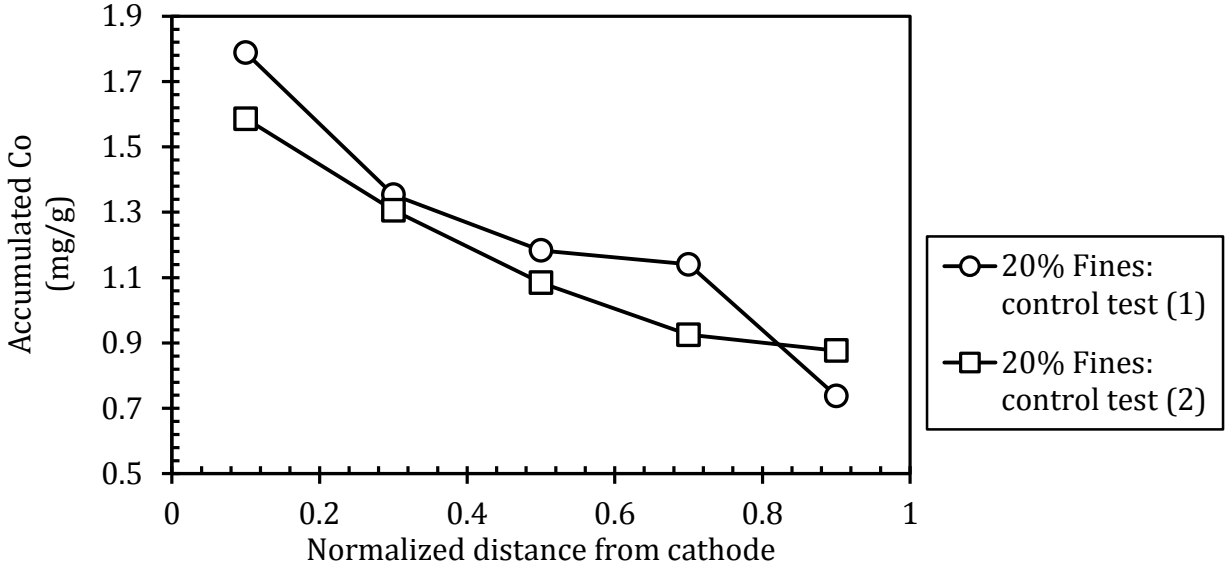

Figure 80 – 2 0% clay control tests: Accumulated cobalt

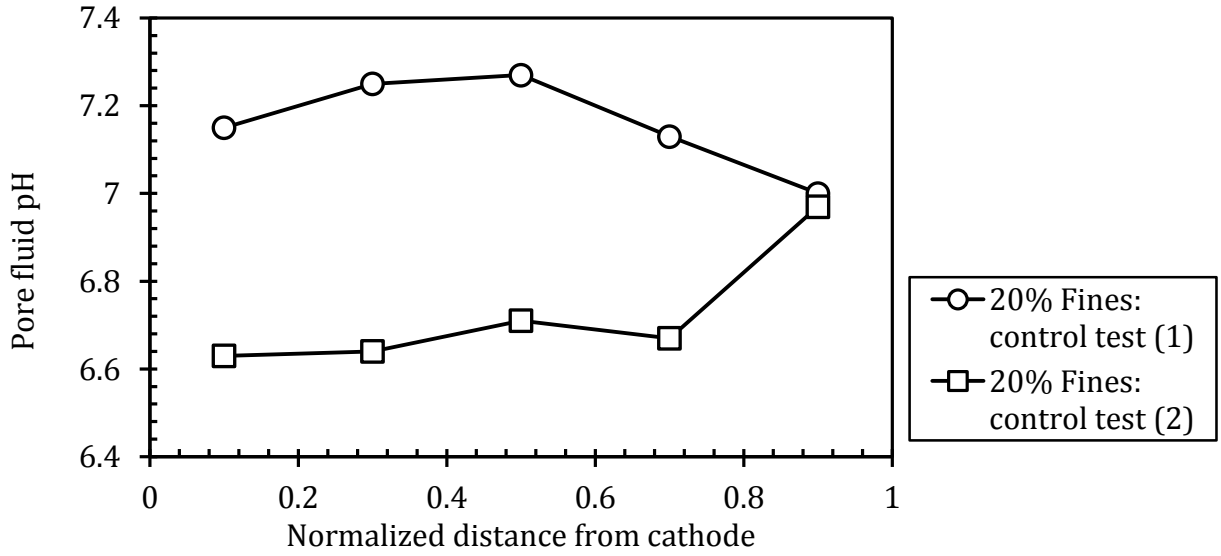

Figure 81 – 20% fines control tests: Pore fluid pH profile

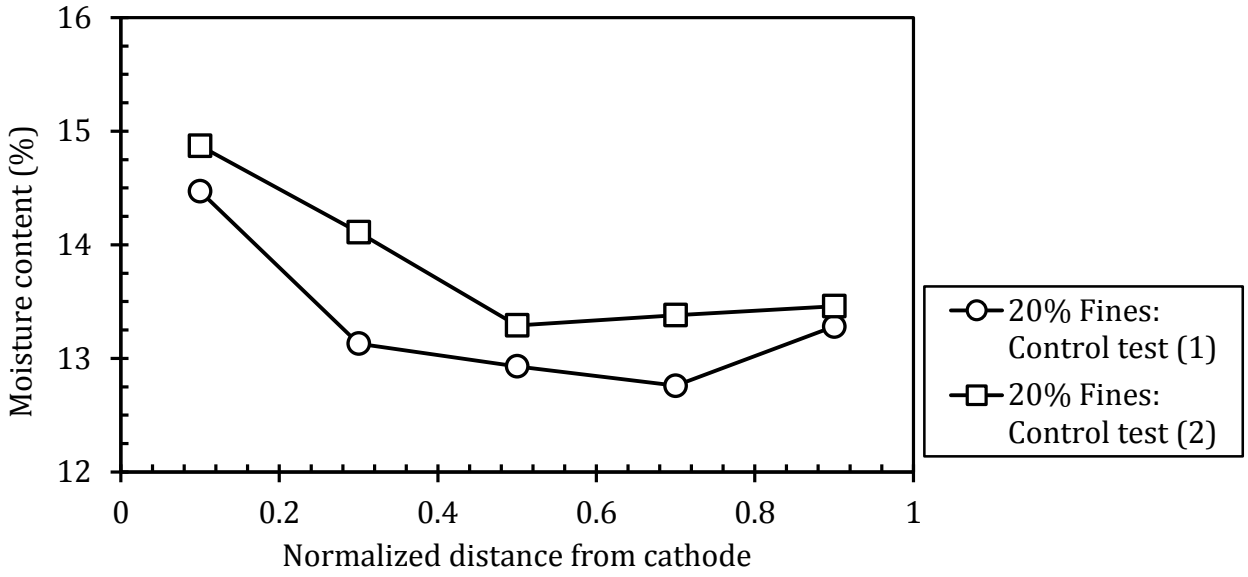

Figure 82 – 20% fines control tests: Moisture content of each slice

10.2.2.2 20% Fines Electrokinetic Barrier Tests–Continuous Current

Similarly, the barrier tests were conducted by applying 40V (2V/cm) across the length of the test cell. The results of these tests are presented in the following sections.

10.2.2.2.1 Steady State Volumetric Flow Rate

At steady state the volumetric flow rate for the control tests for the 20% fines–80% sand mixture was approximately 2.9 mL per minute prior to applying a continuous potential difference of 40 Volts, Figure 83. This flow rate is 30% of the rate in the 10% fines–90% sand mixtures, Figure 59. Again, this is due to doubling the fines content.

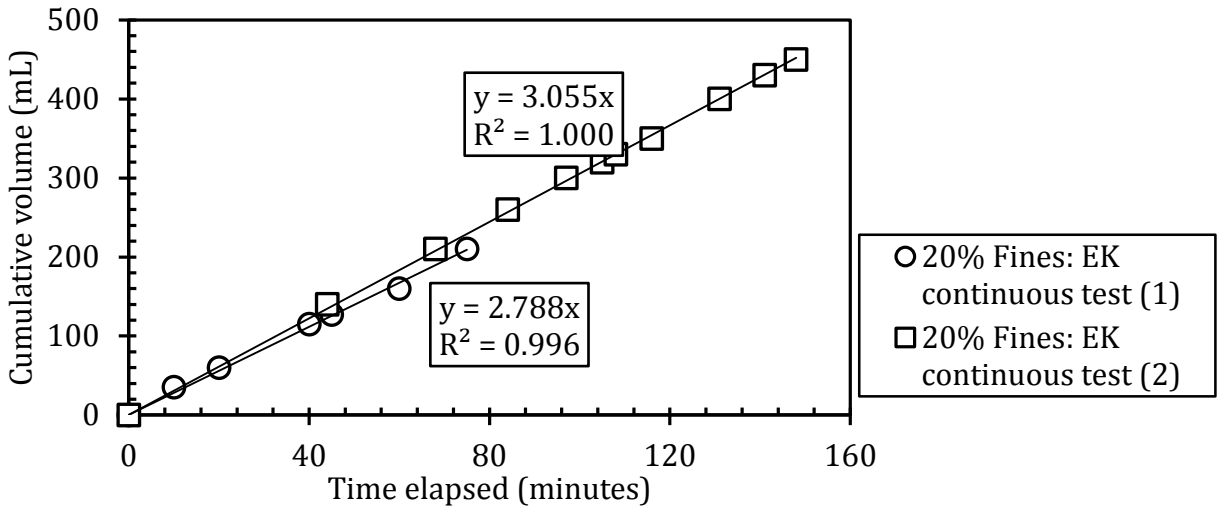

Figure 83 – 20% fines EK continuous tests: Steady state determination curves

10.2.2.2.2 Volumetric Flow Rate with Continuous Current

Plotted in Figure 84 is the number of pore volumes collected against time under a continuous voltage gradient of 2V/cm. Under the continuous voltage, longer periods were required to collect a nominal pore volume as compared with the control test. This trend was observed during both tests. In fact, 26 days were required to collect 12 pore volumes from test (1) and almost 34 days were required to collect 11 pore volumes from test (2). Meanwhile, 12 pore volumes were collected in less than three (3) days from the control tests, Figure 77. Again, applying a continuous voltage of 40V significantly reduced the flow rate. The continuous voltage created a barrier for cobalt solution to enter the cell tests. The sharp pH gradient in the soil, Figure 88, allowed for cobalt accumulation near the cathode, Figure 87, which clogged the soil pores and slowed down the contaminated plume movement towards the anode. As a result long periods of time were required to collect one pore volume. On average, it took to 18 hours to collect one pore volume from the cell containing 10% fines (test (1)) under continuous current. By contrast, to collect one pore volume from test (1) and test (2) using 20% fines cells under continuous current it took 52 hours and 76 hours, respectively.

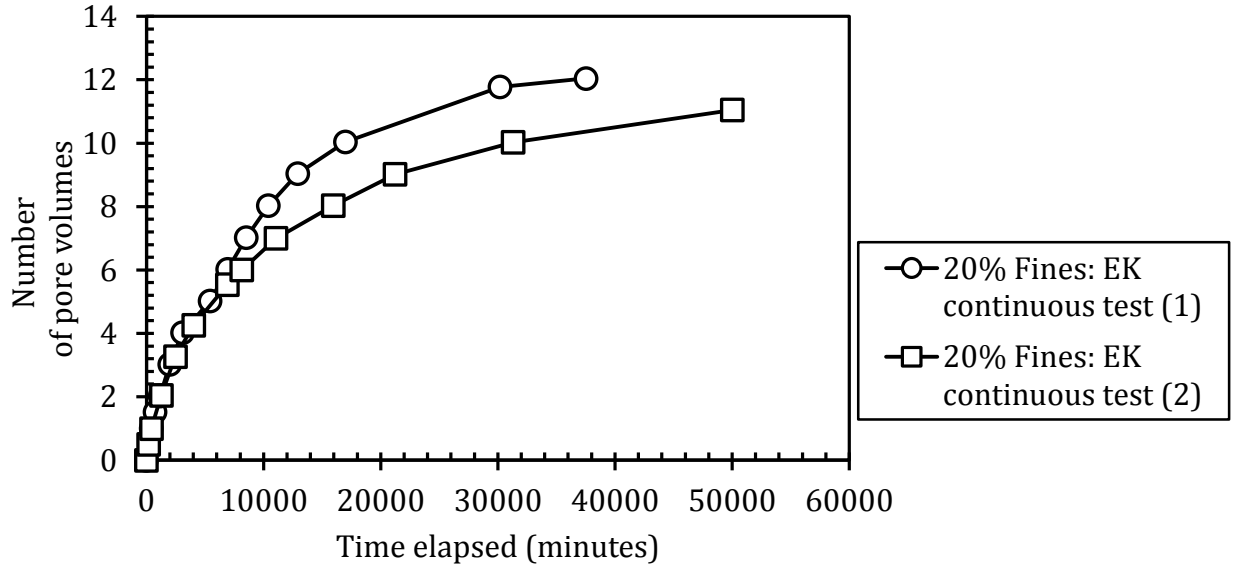

Figure 84 – 20% fines EK continuous tests: Pore volumes versus collection time

10.2.2.2.3 Cobalt Effluent Concentration Profile

Initially, the cobalt concentration in the effluent increased up to a maximum before it decreased to very low concentrations. The maximum effluent concentration was less than 10% of the inlet concentration, Figure 85. The effluent concentrations at the end of the tests decreased to 0.9 mg/L in test (1) and to 0.17 mg/L in test (2). Both tests showed a similar trend qualitatively. Even though the effluent concentrations exceeded the recommend chronic and acute toxicity limits of 0.004 mg/L and 0.11 mg/L, respectively, it should be acknowledged that initially a cobalt solution of 1000 mg/L was used to run the tests. However, this concentration will not be encountered in the field.

The pH of the effluent decreased to less than 2 as shown in Figure 86. Similarly, as the anode reaction produced hydrogen ions, the effluent pH dropped. The pH ranged from 5.82 in the feed solutions to 1.24 at the end of the tests. The change of the effluent pH was expected, since a pH gradient would develop and become more pronounced with the passage of time (Acar, et al., 1990).

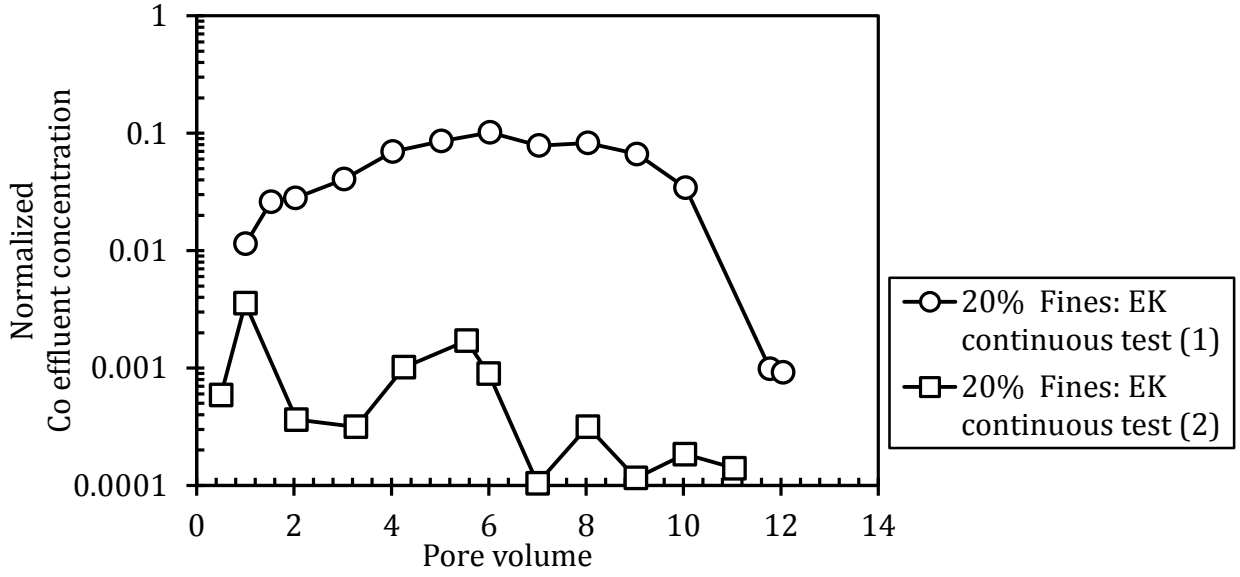

Figure 85 – 20% fines EK continuous tests: Co effluent concentration profile

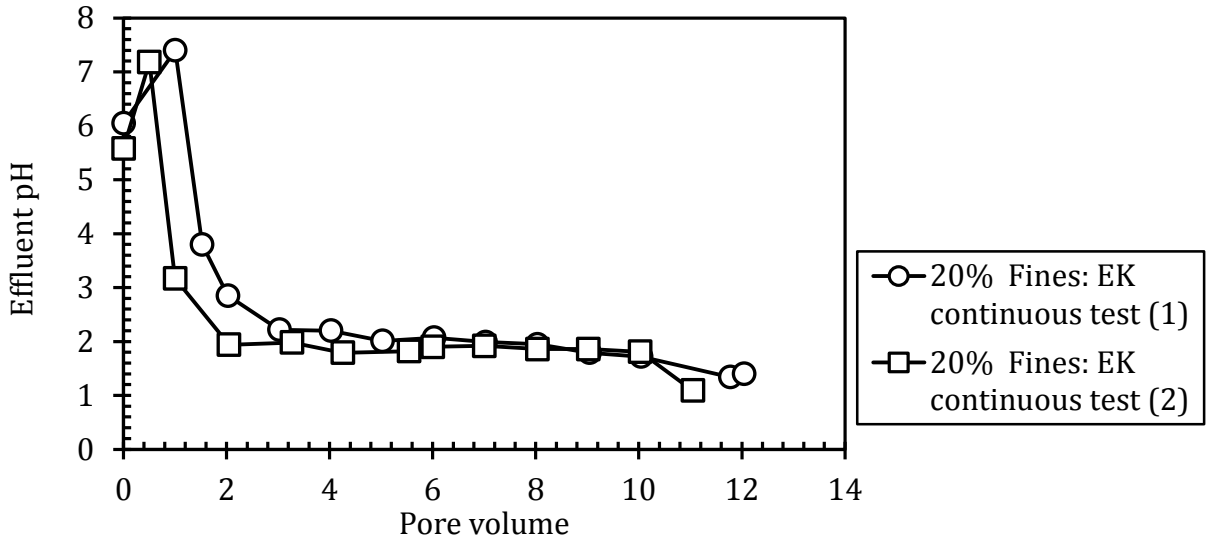

Figure 86 – 20% fines EK continuous tests: Effluent pH profile

10.2.2.2.4 Cobalt Accumulation in the Soil

A plot of the mass of cobalt per gram of soil (mg/g) versus the normalized distance from the cathode showed that more and more cobalt accumulated as the cathode was approached, Figure 87. The mass of cobalt accumulated in the cell during the application of a continuous potential difference (Figure 87) was not significantly higher than the amount of cobalt accumulated in the cell in the absence of a potential gradient, Figure 80. During the control test, 6.2 mg/g and 5.8 mg/g of cobalt accumulated in test (1) and test (2) respectively (Figure 80). Whereas, during the electrokinetic barrier test with continuous current 7 mg/g and 5.5 mg/g of cobalt accumulated in test (1) and test (2), respectively. However, the cobalt distribution in the cell was significantly different. 63% of the mass of cobalt accumulated near the cathode in test (1) (29% near the inlet of control test (1)) and less than 0.5% accumulated near the anode (12% near the outlet of control test (1)). Even more cobalt accumulated near the cathode in continuous test (2) (81% versus 0.2% at the anode). These results suggest that the electrokinetic barrier may not be effective in accumulating more cobalt; however, it is very effective in concentrating cobalt and confining it to a zone (the cathode region). The difference in distribution is due to the development of the sharp pH gradient in the pore fluid, Figure 88. In fact, the pore fluid pH ranged between an average of 7.4 at the anode and an average of 12.6 at the cathode. As well, the very low volumetric flow rates are attributed to the high accumulation of cobalt in the cathode region which resulted in blockage of pores and reduction of the cell's porosity, as previously discussed. Again, the time gap between terminating the tests and squeezing the soil slices and measuring the pH allowed the soil minerals to neutralize the pore fluid pH. As well, the low level of the pore fluid near the anode would contribute to the inaccurate pH readings. However, from these tests, it can be concluded that the application of an electrokinetic barrier on the soil prevented the spread of cobalt downstream, towards the anode, and trapped the cobalt near its contamination source.

The moisture profile obtained from the 20% fines–80% sand cells contradicts each other. The individual profiles could not be justified.

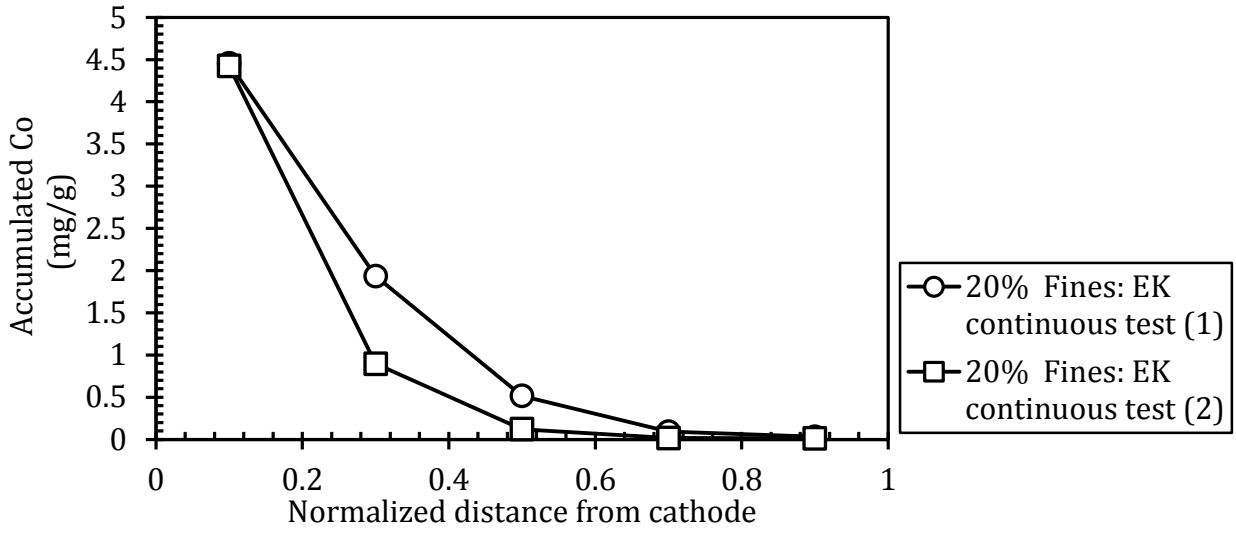

Figure 87 – 20% fines EK continuous tests: Accumulated cobalt

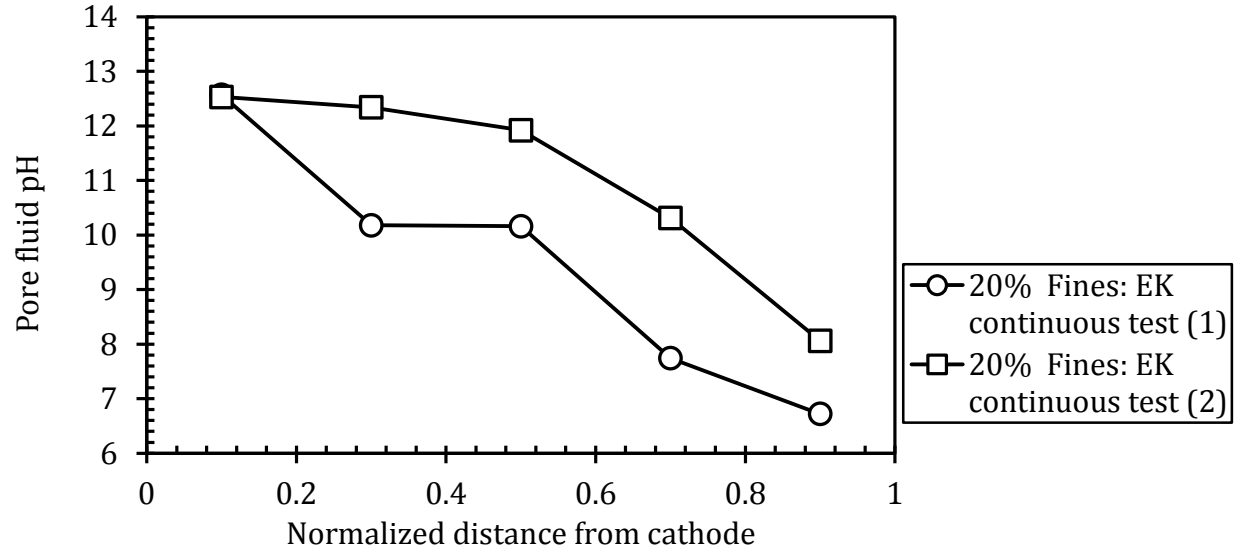

Figure 88 – 20% fines EK continuous tests: Pore fluid pH profile

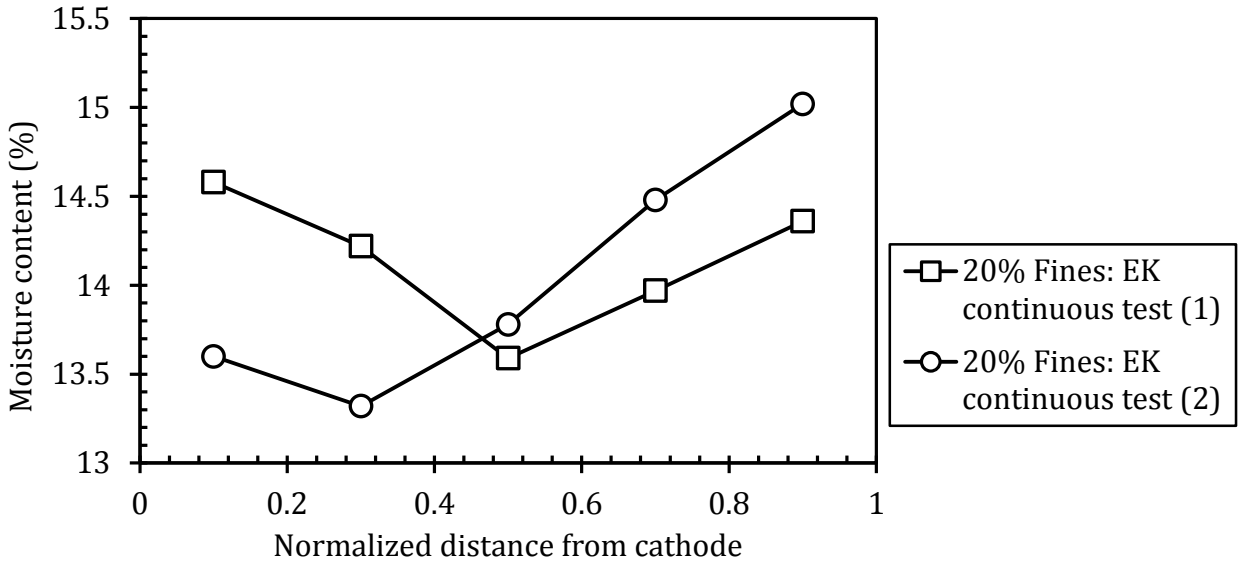

Figure 89 – 20% fines EK continuous tests: Moisture content of each slice

10.2.2.3 20% Fines Electrokinetic Barrier Tests–Intermittent Current

10.2.2.3.1 Steady State Volumetric Flow Rate

Steady state determination yielded the following two plots, shown in Figure 90. Even though the tests were prepared in the same manner, the tests containing 20% fines resulted in consistently lower volumetric flow rates compared to the tests conducted with 10% fines. This was due to increasing the cohesiveness of the cell by doubling the fines content, as previously discussed.

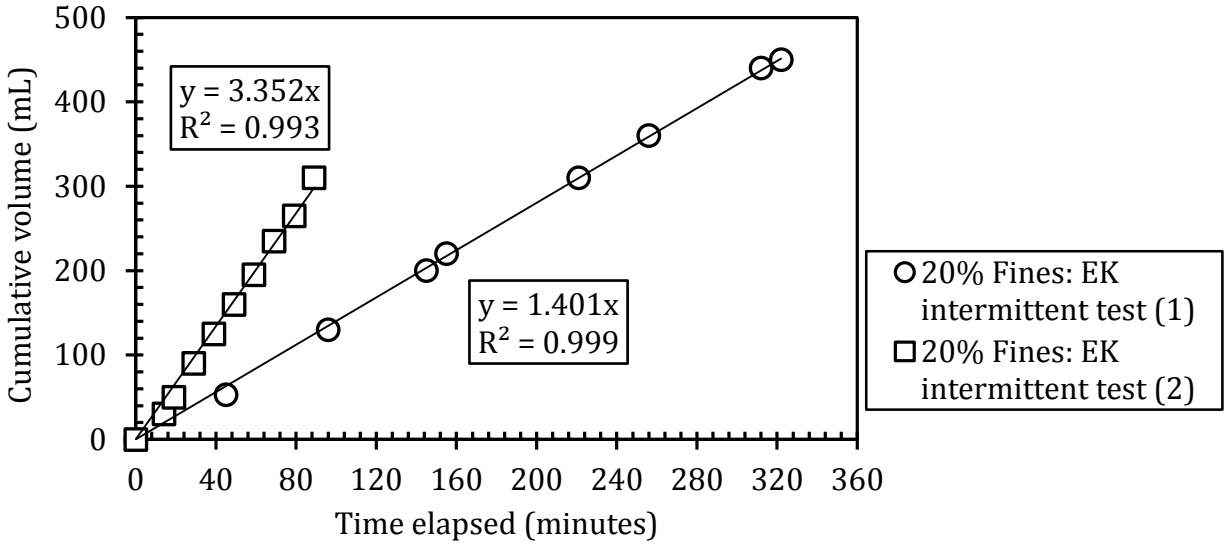

Figure 90 – 20% fines EK intermittent current tests: Steady state determination curves

10.2.2.3.2 Volumetric Flow Rate with Intermittent Current

The nominal pore volumes collected vs. time are plotted in Figure 91. Over the duration of the test of eight (8) days, an average of 7.4 pore volumes were collected from the test cells containing 20% fines, compared to 16.2 pore volumes collected from the cells containing 10% fines, Figure 70. More volume was collected in two (2) days from the control tests than the volume collected from the intermittent current tests in eight (8) days.

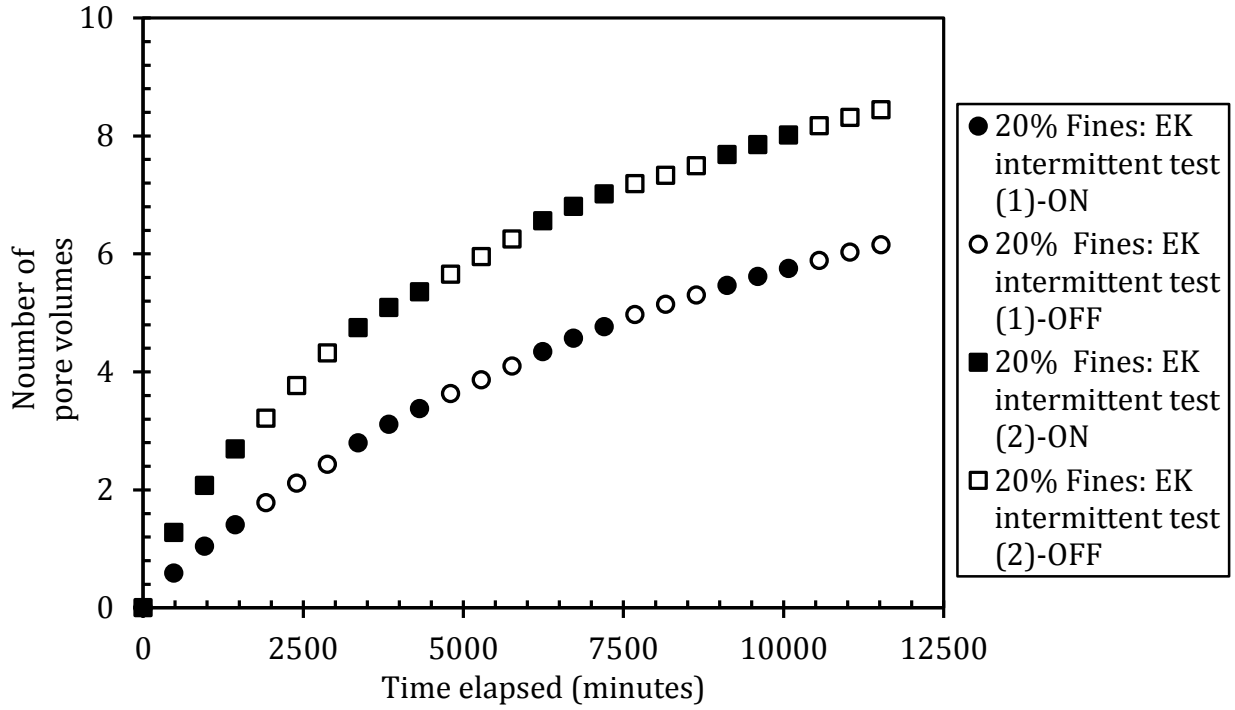

Figure 91 – 20% fines EK intermittent current tests: Pore volume versus collection time

10.2.2.3.3 Cobalt Effluent Concentration Profile

The normalized cobalt concentration in the effluent is given in Figure 92. The data points in the figure were all recorded eight hours apart. The symbols alternate in groups of three to indicate when the electrokinetic barrier was turned on and off respectively. At the time when each third data point was recorded, the switch from on or off was made such that each first data point was recorded after eight hours of run time.

Similar to the 10% fines–90% sand cell tests, the pH decreased during the power on cycles and increased during the power off cycles, Figure 93. In fact, the highest pH was recorded for the feed solution which averaged to be 7.70 and the lowest value was 1.67. The average pH of all the samples was 2.63. The highest normalized effluent cobalt concentration ranged between 1% and 3% in the 20% fines–80% sand cells. Meanwhile the highest normalized effluent cobalt concentration ranged from 20% to 43% in the 10% fines–90% sand tests, Figure 71. It is hypothesized that the lower effluent concentrations were obtained from the cells containing 20% fines due to the fact that more cobalt accumulated in the cathode region of the 20% fines cells than in the 10% fines cells. Accumulation of

cobalt in the cell prevented the advancement of the contaminated plume to the exit of the cell. Consequently, less cobalt was observed in the effluent volume. The effluent cobalt concentrations from the 20% cells with current intermittence were 4 mg/L from test (1) and 0.13 mg/L from test (2) in the last nominal pore volume sample collected.

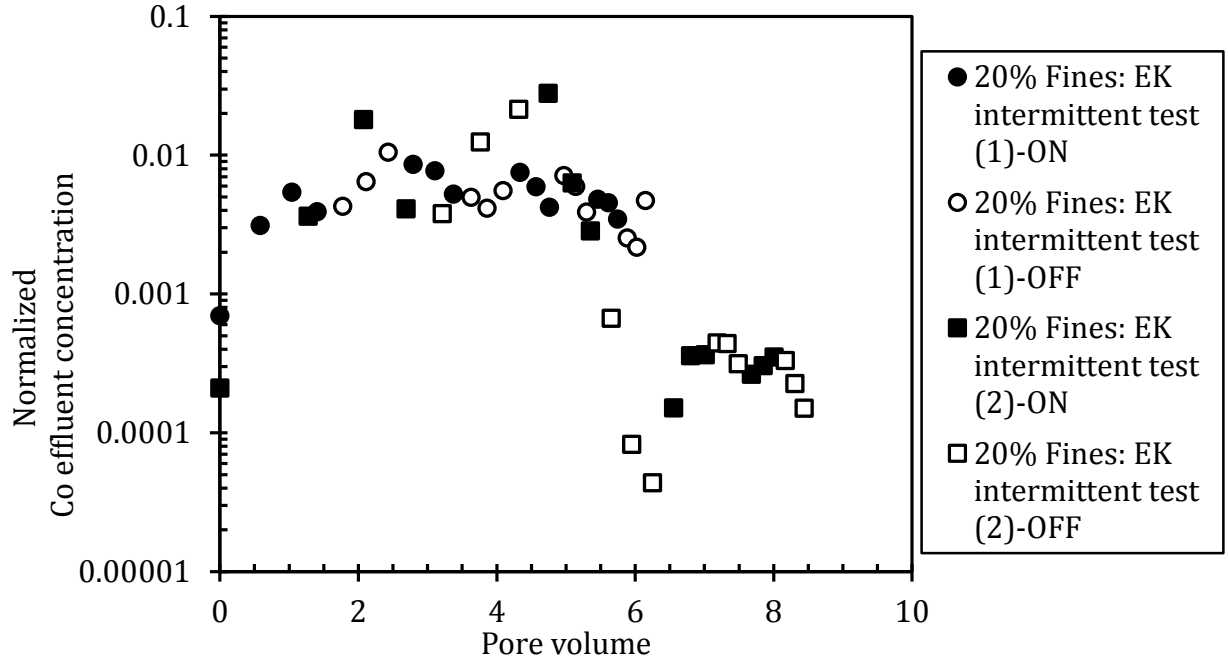

Figure 92 – 20% fines EK intermittent current tests: Co effluent concentration profile

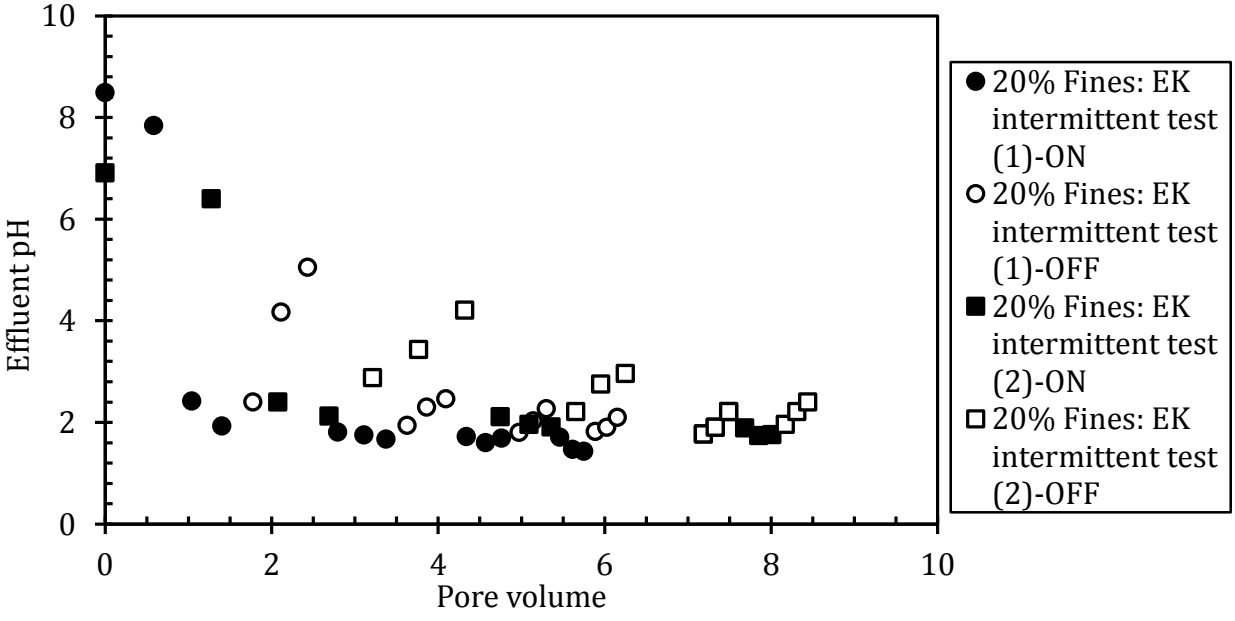

Figure 93 – 20% fines intermittent current tests: Effluent pH profile

10.2.2.3.4 Cobalt Accumulation in the Soil

The profile of the cobalt accumulated in the test cells in both cells exhibited a similar trend to the previous tests, Figure 94. Again, a pH gradient across the test cell was developed resulting in pore fluid pH that ranged from 7.3 at the anode to 12.02 at the cathode, Figure 95. The higher clay percentage would offer a larger surface area for adsorption and more cation exchange sites. Even though, less cobalt accumulated in the cells during the intermittent current tests than during the control tests, the mass of cobalt accumulated near the cathode in the intermittent tests was approximately 2 times higher than that accumulated in the control tests. Additionally, only 1% of the cobalt accumulated near the anode of the intermittent current tests versus 12% accumulated in the outlet region of the control tests. It must be noted that during the control tests, 12 nominal pore volumes were collected from each cell but only 6.2 and 8.4 nominal pore volumes were collected from test (1) and test (2), respectively from the intermittent current tests. These results further support the conclusion on the effectiveness of the electrokinetic barrier in trapping the cobalt near the cathode.

The moisture content profiles of both test (1) and test (2) in presented in Figure 96.

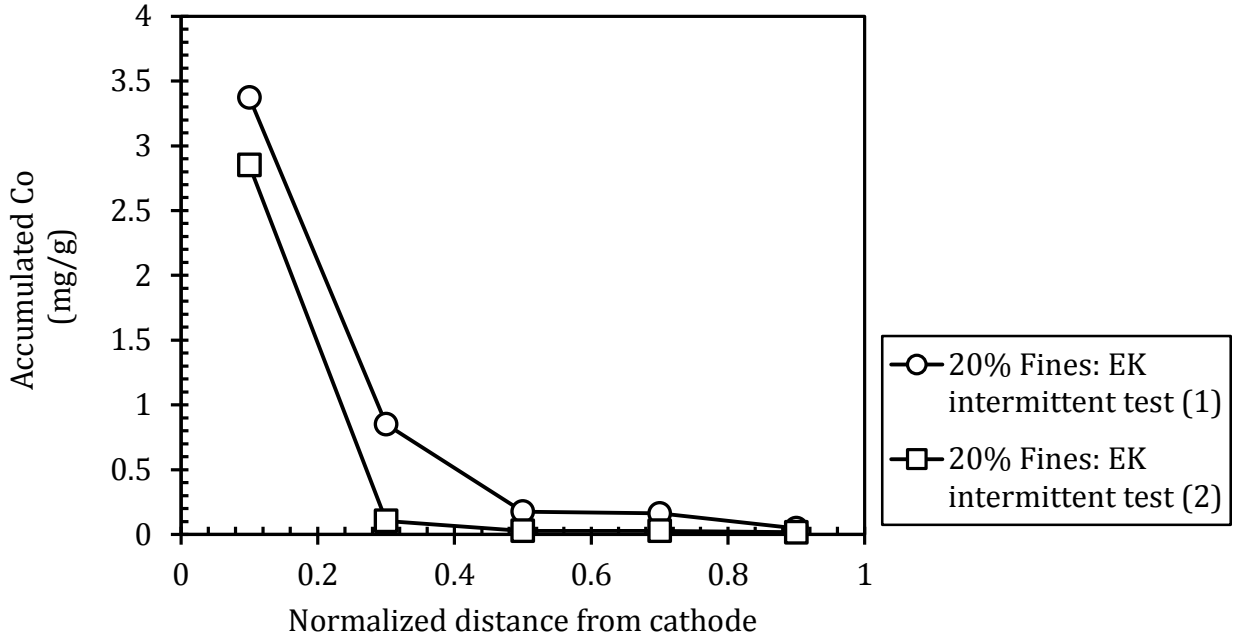

Figure 94 – 20% fines EK intermittent current tests: Accumulated cobalt

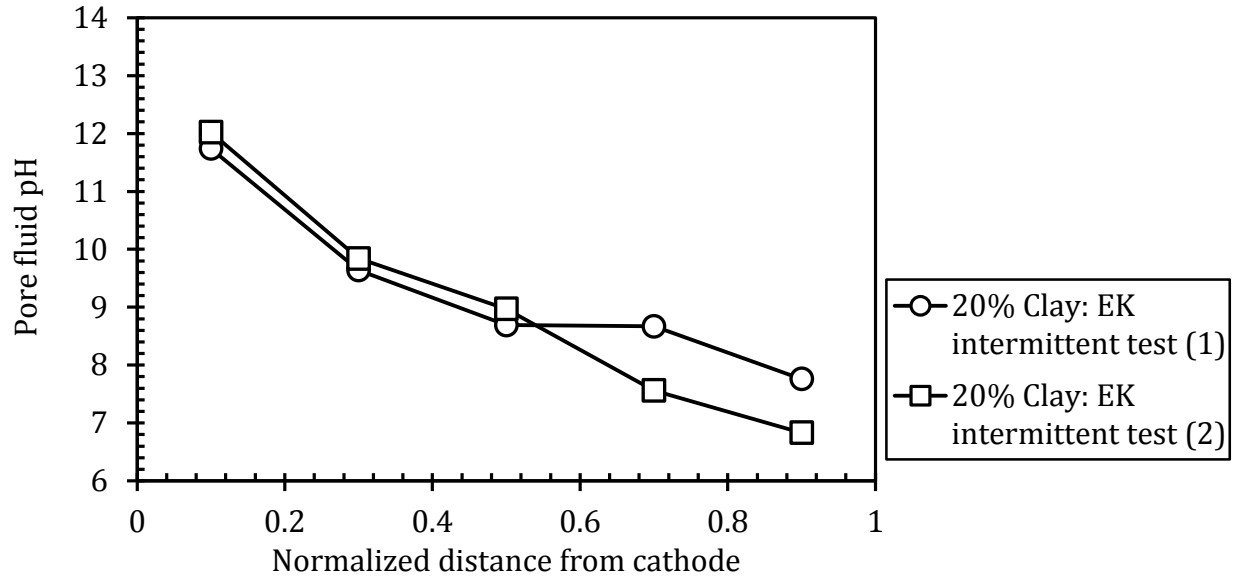

Figure 95 – 20% fines EK intermittent current tests: Pore fluid pH profile

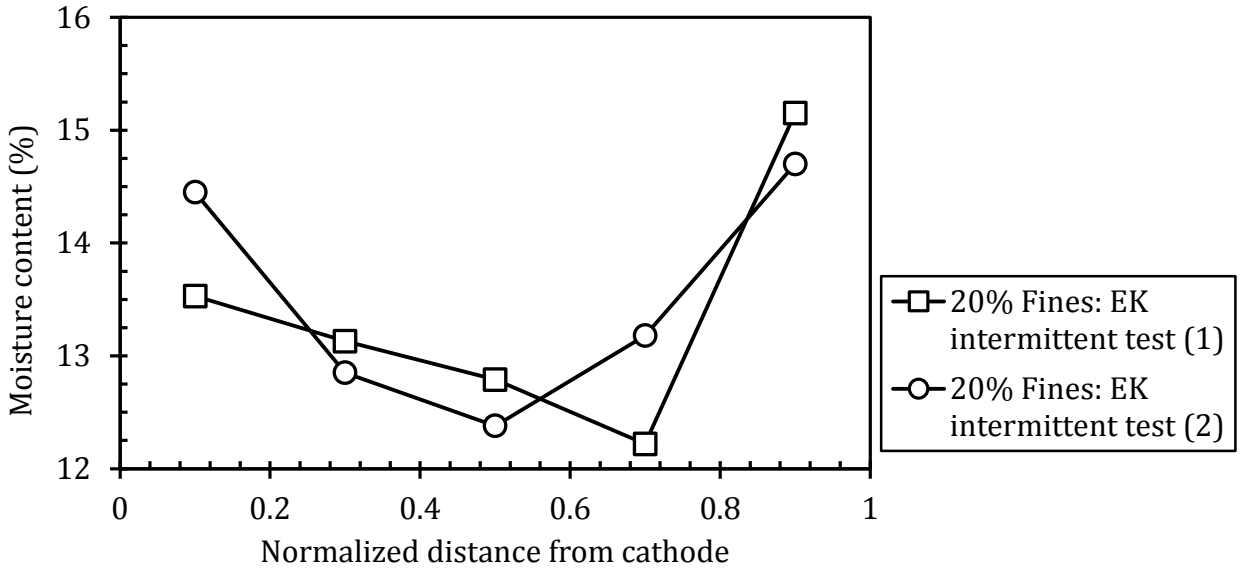

Figure 96 – 20% fines EK intermittent current tests: Moisture content of each slice

10.2.2.4 Wash out Tests

10.2.2.4.1 Steady State Volumetric Flow Rate

Similar to previous tests, the steady state was determined for the wash out cells using 10% fines–90% sand mixtures, as presented in Figure 92. The average flow rate of the wash out tests during steady state determination was 11.5 mL/min which is comparable to the flow rates obtained from 10% fines–90% sand mixtures.

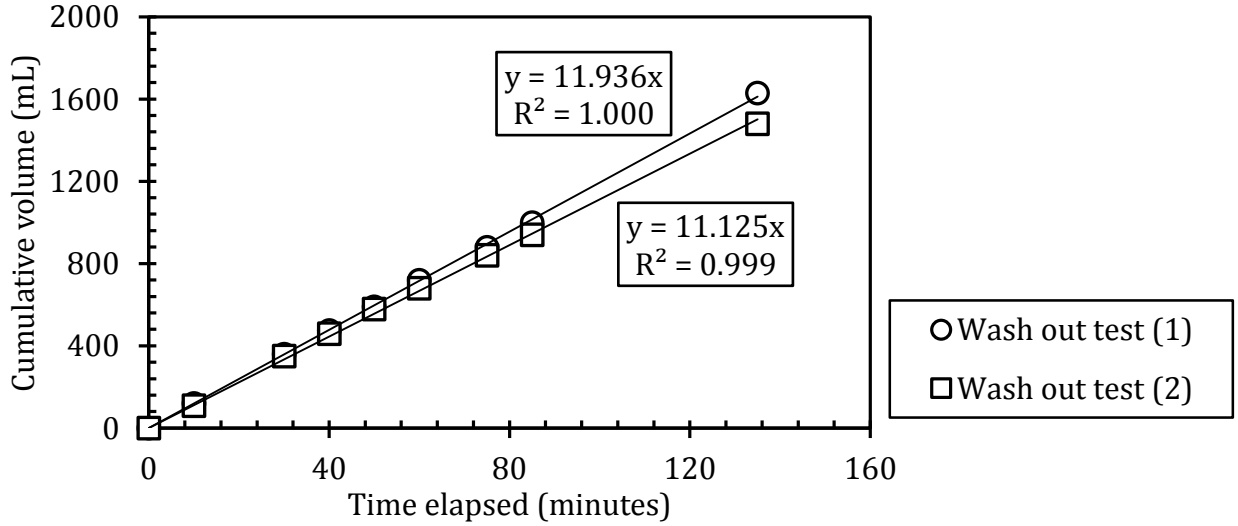

Figure 97 – Wash out tests: Steady state determination curves

10.2.2.4.2 Volumetric Flow Rate

The volumetric flow rate was determined and plotted for the two stages of the wash out tests, as shown in Figure 98. The dashed line at 7.6 pore volumes represents the point at which the potential gradient was turned off and the cobalt feed solution was replaced with simulated groundwater. As seen in the figure, the flow rate dropped with time during the first 7.6 pore volumes (power on), likely due to precipitation of cobalt in the cell. The flow rate gradually increased again when the power was switched off. This could be attributed to the ceasing of electro–osmotic flow.

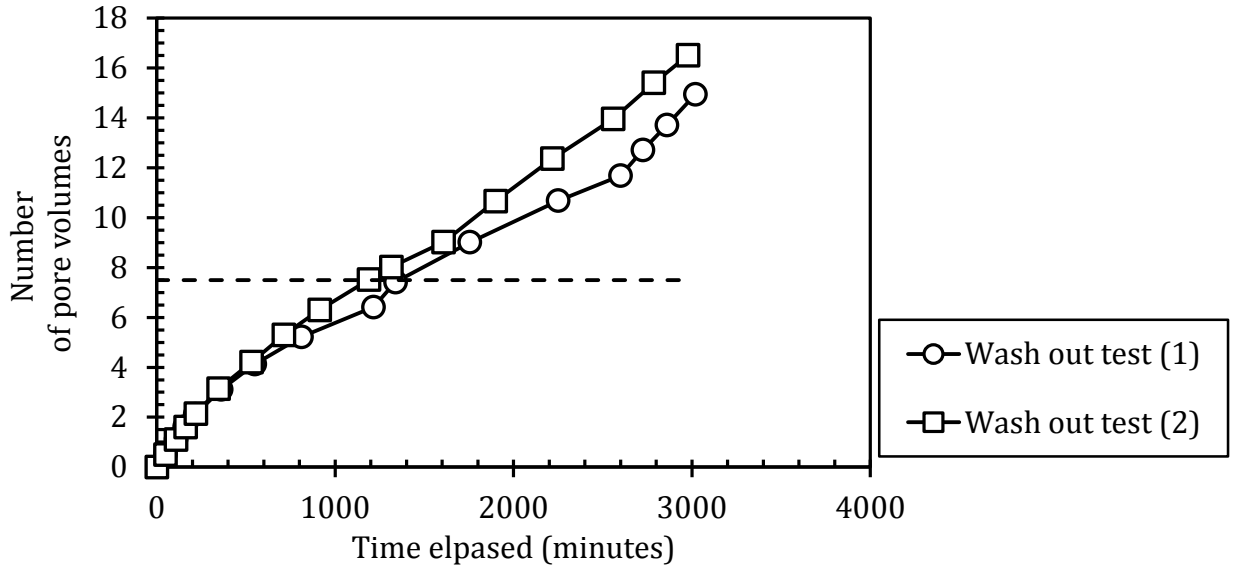

Figure 98 – Wash out tests: Pore volume versus collection time

10.2.2.4.3 Cobalt Effluent Concentration Profile

The normalized effluent concentration profiles were determined (Figure 99). Similar to the previous trends, the effluent concentration of cobalt initially increased as more and more pore volumes were collected. The observed effluent concentration trends could possibly be a result of: displacement of the non–contaminated fluid (simulated groundwater) already present in the pores from the steady state determination stage and dilution of cobalt concentration in the pores by dispersion. These mechanisms can result in the initial increase in cobalt concentration in the effluent. However, adsorption/precipitation of cobalt in the cell can explain the decrease of the cobalt concentration in the effluent as more pore volumes were collected. The maximum normalized effluent concentration ranged between 25% and 50%. After the collection of approximately 7.5 pore volumes, the simulated groundwater was allowed to seep through the test cell mixture in the absence of the voltage gradient. It was hypothesized that the simulated groundwater did not result in more dilution of the pore concentration or dissolution of the precipitated cobalt; hence, the effluent concentration continued to drop, for the duration of the test. Furthermore, this hypothesis led to presuming that the cobalt accumulated in the test specimen was not removed from the cell, for the duration of the test. Had the cobalt been solubilised and

mobilized, it would only be reasonable to expect that the dissolved cobalt concentration in the effluent would gradually increase with time.

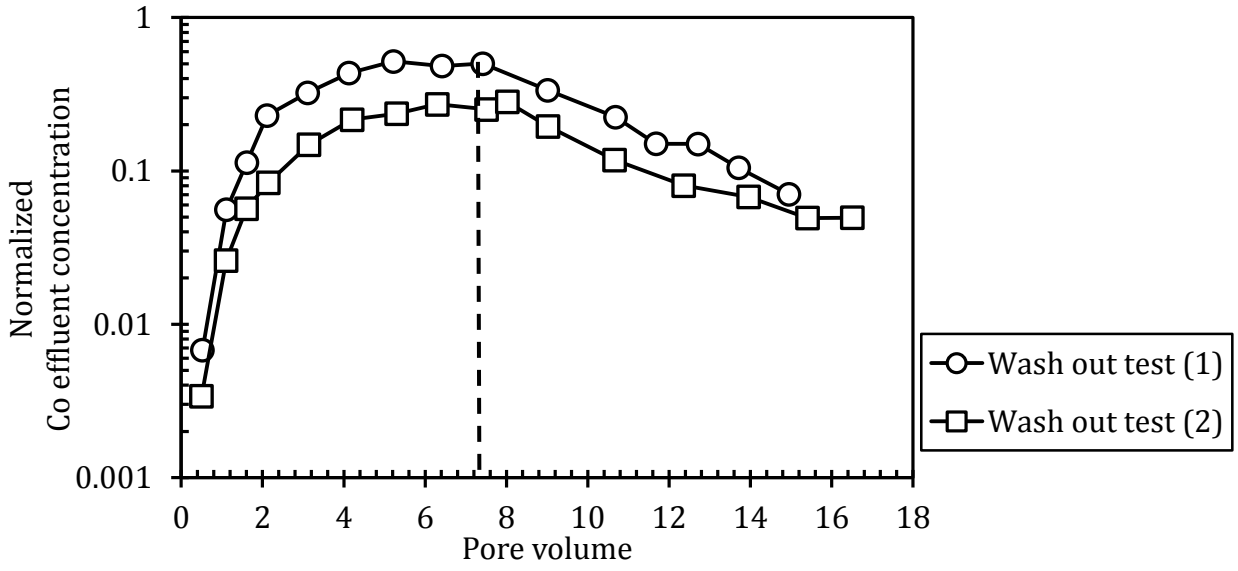

Figure 99 – Wash out tests: Co effluent concentration profile

The effluent pH profile is shown in Figure 100. The pH of the effluent started to increase immediately after the reintroduction of simulated groundwater and the elimination of the electric field. It was hypothesized that when the voltage gradient was terminated, the pore fluid pH was gradually neutralized by the soil minerals.

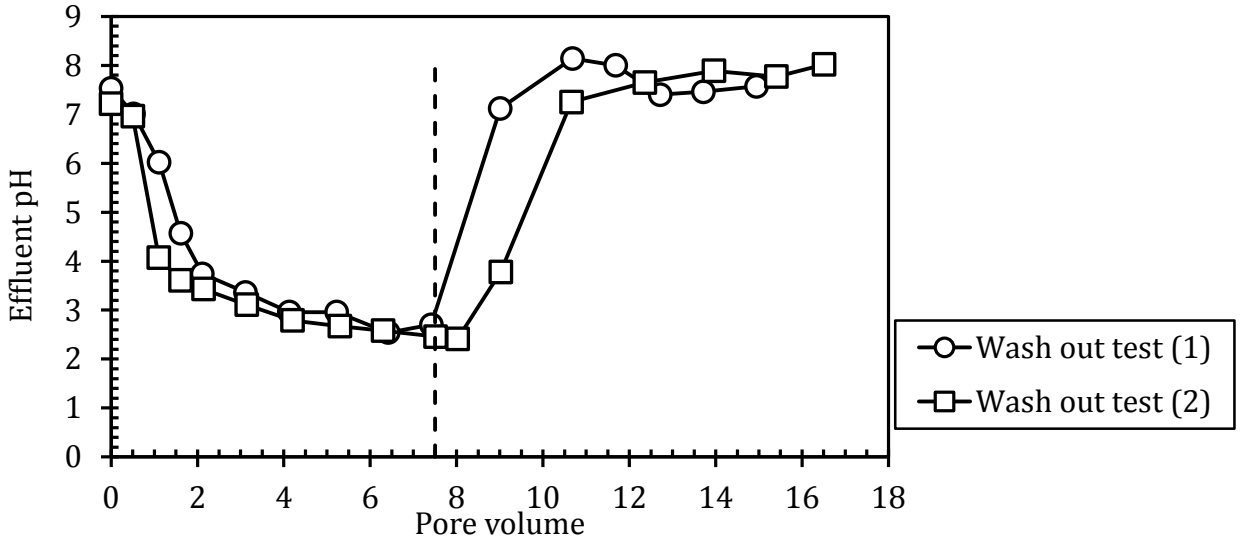

Figure 100 – Wash out tests: Effluent pH profile

10.2.2.4.4 Cobalt Accumulation in the Soil

The cobalt distribution on the soil was determined from the soil slicing and digestion tests. The results are plotted in Figure 101. In the wash out cells, 4.6 mg/g of cobalt precipitated/adsorbed in test (1). About 49% of the cobalt mass was distributed evenly over 80% of the cell. However, approximately 51% of cobalt was precipitated/adsorbed in the cathode region of test (1). Test (2) exhibited a similar distribution. Additionally, even though the accumulated cobalt was not removed out of the cell, as demonstrated by the concentration profile (Figure 99), its mass was redistributed along the length of the test cell as shown by Figure 101. This is a reasonable conclusion given cobalt's distribution in the continuous and intermittent current cells containing 10% fines, Figure 65 and Figure 73 respectively. Of all the cells containing 10% fines, the intermittent current tests were comparable to the wash out tests on the basis of the volume collected from each test. Furthermore, the termination of the electrokinetic barrier did not result in immediate wash out of the cobalt in the cell. After an equivalent number of pore volumes were collected, the cell mixture still retained the cobalt, for the duration of the tests.

Overall, a much smaller pH gradient in the pore fluid was achieved in the wash out test, as shown in Figure 102, as compared to the pH gradient developed during the continuous and intermittent current tests. A minimum pH was observed at the centre of the cell. This occurrence was not observed previously. Possibly, the pore fluid pH measurement at 0.5 (normalized distance from the cathode) is an outlier due to an error in the analysis.

The moisture content profile obtained from the wash out tests is given in Figure 103

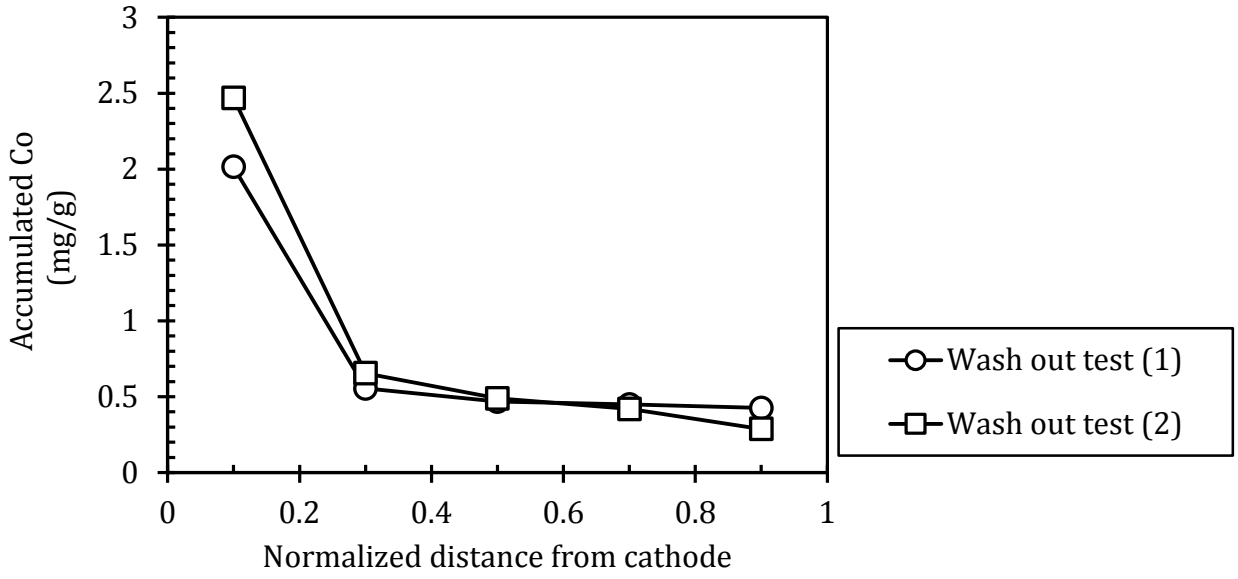

Figure 101 – Wash out tests: Accumulated cobalt

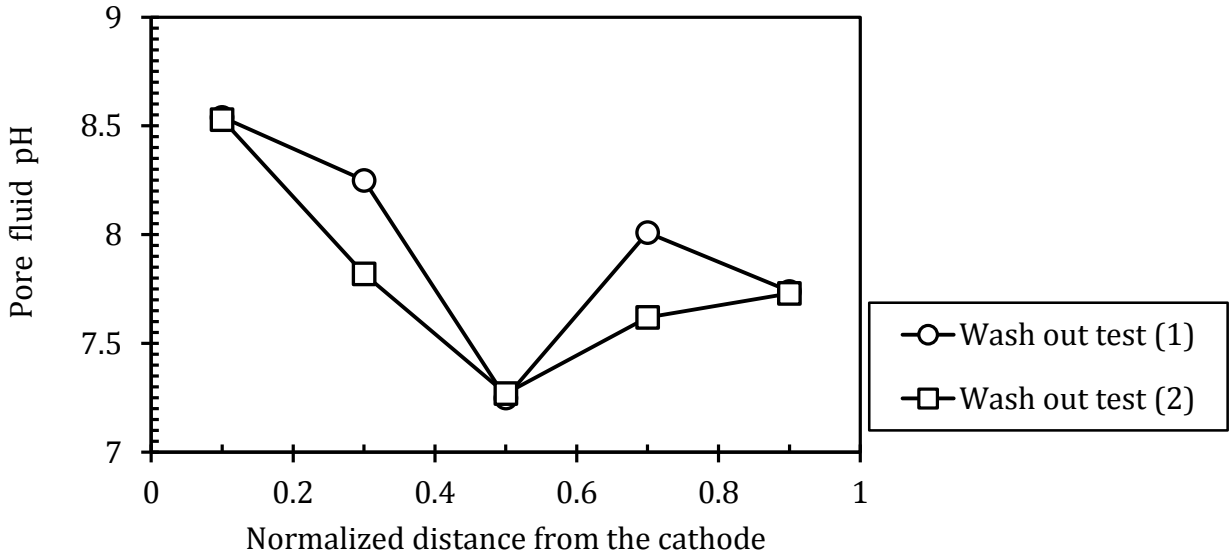

Figure 102 – Wash out tests: Pore fluid pH profile

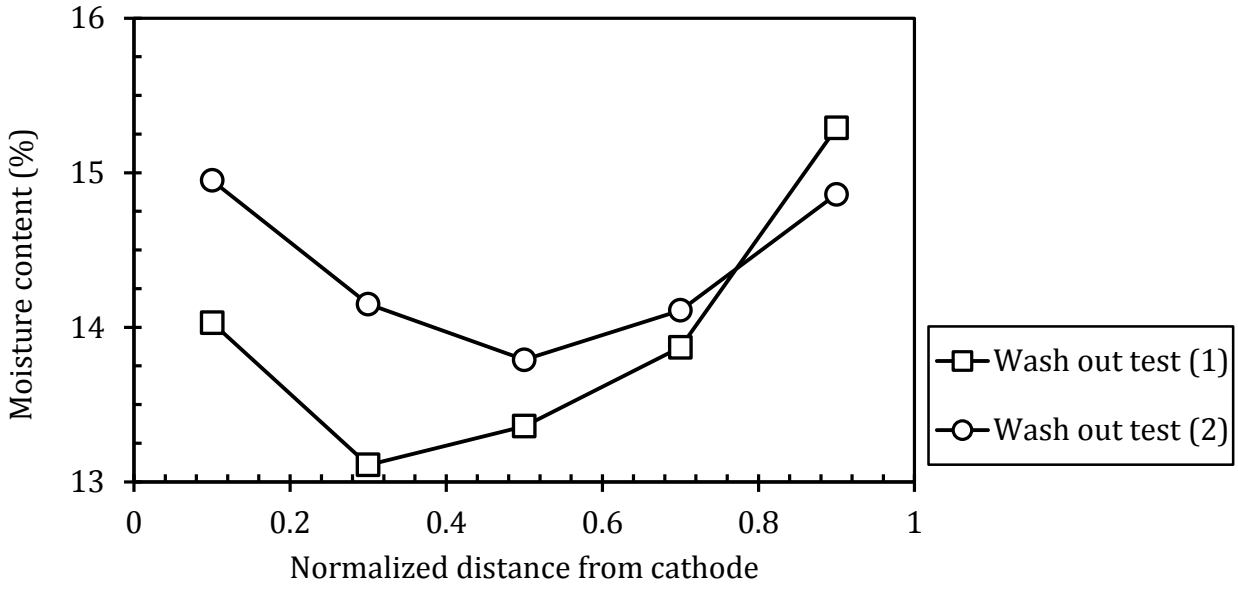

Figure 103 – Wash out tests: Moisture content profile

10.2.3 Electrokinetic Barrier Tests Summary

Table 15 and Table 16 summarize the test results carried out with cells containing 10% fines (by mass) and 90% sand and 20% fines (by mass) and 80% sand, respectively. The normalized cobalt effluent concentration in the tables indicates the cobalt concentration obtained from the last pore volume collected normalized with respect to the initial cobalt concentration in the feed solution. As well, the effluent pH pertains to the last pore volume collected which was consistently neutral for the control tests and very acidic for the electrokinetic barrier tests (as a result of water oxidation at the anode). The inlet mass of cobalt was calculated as the product of the initial cobalt concentration in the feed solution and the total volume collected from the cell (equation 10.7). It is assumed that the inflow is equal to the outflow. The effectiveness of a cell test to immobilize cobalt is reported as the % retained which was calculated by equation (10.9).

$$\boldsymbol{m_{Co-in} = [Co]_{initial} \cdot PV \cdot 940} \qquad \text{Eq. (10.7)}$$

where, m_{Co-in} is total the mass of cobalt that entered the cell (g),

$[Co]_{initial}$ is the initial cobalt concentration (g/L),

PV is the total number of pore volumes collected, and

0.940 is the value of one pore volume (L).

$$\boldsymbol{m_{Co-out} = \sum_{i=1}^{PV}([Co]_i \cdot i \cdot 940)} \qquad \text{Eq. (10.8)}$$

where, m_{Co-out} is the total mass of cobalt exited the cell (g),

$\boldsymbol{[Co]_i}$ is the concentration of cobalt in a given pore volume (g/L), and

i is an integer representing the pore volume from which the Co concentration is sampled.

$$\boldsymbol{\%\ Co\ retained = \left(1 - \frac{m_{Co-out}}{m_{Co-in}}\right) \cdot 100\%} \qquad \text{Eq. (10.9)}$$

where, % Co retained is the percentage of cobalt mass immobilized in the cell.

The % retained shows the effectiveness of the electrokinetic barrier tests (continuous and intermittent current) in enhancing the ability of the fines–sand mixture in the test cells to immobilize (retain) and remove the cobalt from the pore fluid compared to the control

tests. However, the accumulated cobalt mass obtained from the soil digestion tests, calculated by equation (10.10), did not match the mass obtained from the overall mass balance due to analytical errors. Since, the data could not be reconciled, it was deemed more suitable to discuss the results relative to the percent retained of cobalt near the cathode and the anode. In all the tests that were carried out, even though the electrokinetic barrier did not always accumulate more cobalt in the cells, it concentrated more cobalt near the cathode. For instance more cobalt accumulated in the control tests of the 20% fines–80% sand cell mixtures than that accumulated in the cells containing the 20% fines mixtures during the intermittent current tests. However, more pore volumes were collected from the control tests (12 PV) whereas only 6.2 PVs and 8.4 PVs were collected from 20% fines–80% sand intermittent current tests (1) and test (2), respectively. This implies that less cobalt was introduced into the intermittent current tests than in the control tests as indicated in Table 16.

$$\boldsymbol{m_{Co-cell}} = [\boldsymbol{Co_{cell}}] \times \boldsymbol{m_{mixture}} \qquad \text{Eq. (10.10)}$$

where, $m_{co-cell}$ is the mass of cobalt accumulated in the cell (g);

$[Co_{cell}]$. is the average cobalt concentration accumulated in the cell (g/g);

$m_{mixture}$ is the dry mass of the soil mine fines–sand mixture of 5288g (g).

Table 15 – 10% fines–90% sand tests summary

10 % fines–90% sand mixtures								
	Control		Continuous current (2V/cm)		Intermittent current (2V/cm)		Wash out	
	Test (1)	Test (2)	Test (1)	Test (2)	Test (1)	Test (2)	Test (1)	Test (2)
No. of pore volumes (PV)	13.5	12	12.8	12.1	17.6	14.8	14.9	16.5
Collection time (hour)	49.5	23.5	227.5	51.6	192	192	50.3	49.7
Effluent $[\boldsymbol{Co}]_{\boldsymbol{normalized}}$ @ final PV	0.6	0.9	0.00031	0.1	0.021	0.018	0.07	0.05
$[\boldsymbol{Co}]$ (mg/L) @ final PV	554	845	0.26	96	16	20	51	41
Effluent pH @ final PV	6.8	7.3	1.76	2	2.9	3.4	7.6	8.0
Co inlet mass (g)	15.2	10.8	11.4	10.9	12.2	15.5	10.2	12.8
Co outlet mass (g)	8.9	5.2	0.97	1.2	2.2	1.7	2.7	1.7
% Co retained	41.1	52.4	91.5	89.5	81.9	89.2	73.1	86.6
Co mass accumulated in cell (g)	6.1	5.2	7.2	10.0	11.3	10.5	4.1	4.6
% mass of Co at cathode ($x_{normalized}$=0.1)	24	25	61	55	61	63	52	57
% massof Co at anode ($x_{normalized}$ =0.9)	16	16	3	4	1	2	11	7
Pore fluid pH cathode ($x_{normalized}$ =0.1)	6.9	7.3	12.3	12.0	12.3	12.5	7.5	8.5
Pore fluid pH anode ($x_{normalized}$ =0.9)	7	7.4	6.9	7.0	7.1	7.2	7.7	7.7

Table 16 – 20% fines–80% sand tests summary

20 % fines–80% Sand mixtures						
	Control		Continuous current (2V/cm)		Intermittent current (2V/cm)	
	Test (1)	Test (2)	Test (1)	Test (2)	Test (1)	Test (2)
No. of pore volumes (PV)	12	12	12	11	6.2	8.4
Collection time (hour)	63	44	625	834	192	192
Effluent $[\boldsymbol{Co}]_{\boldsymbol{normalized}}$@ final PV	0.65	0.38	0.0009	0.0001	0.005	0.0002
$[\boldsymbol{Co}]$ (mg/L) @ final PV	574	528	0.84	0.17	4	0.13
Effluent pH @ final PV	7	7.7	1.4	1.1	2.1	2.4
Co inlet mass (g)	10	15.6	10.3	12.8	4.8	6.9
Co outlet mass (g)	3.6	4.4	0.52	0.008	0.03	0.05
% Co retained	64.7	71.7	95	99.9	99.5	99.3
Co mass accumulated in cell (g)	6.6	6.1	7.4	5.8	4.9	3.2
% mass of Co at cathode ($x_{normalized}$ =0.1)	29	27	63	81	73	94
% mass of Co at anode ($x_{normalized}$ =0.9)	12	15	0.4	0.2	1	0.5
Pore fluid pH cathode ($x_{normalized}$ =0.1)	7.2	6.6	12.6	12.5	11.7	12.0
Pore fluid pH anode ($x_{normalized}$ =0.9)	7	7	6.72	8.1	7.7	6.8

11.0 Discussion

The first objective of this study is to characterize the physicochemical properties of a mean surface soil sample collected from the vicinity of the mine site. A comprehensive characterization of the soil was completed. In order to ensure that results of this study were general yet appropriately applicable to Musselwhite mine, the mine soil was used in the tests. Furthermore, the feed water used to saturate the test cells and establish steady state flow replicated the groundwater of the mine site. Thus, the first objective was accomplished.

Hypothesis 1 states that the volumetric flow rate through the electrokinetic barrier will be significantly decreased by the application of a voltage gradient across the electrodes. In all the tests that were conducted in this thesis, the flow rate was significantly decreased under a continuously applied voltage using 10% (Figure 104) and 20% fines. Furthermore, the flow rate was significantly reduced using intermittent power in the 10% fines cells (Figure 104).and 20% fines cells (Figure 105).

Much literature justified this phenomenon as a direct proof of electro–osmotic flow towards the cathode and electro–migration (Acar, et al., 1995; Acar & Alshawabkeh, 1993; Ashawabkeh & Acar, 1992). However, it is hard to make such a direct connection in the light of the present work. It is plausible that the pH gradient brought by the voltage gradient is the cause of enhanced precipitation of cobalt near the cathode which in turn resulted in reducing the flow rate compared to the control tests.

At the start of any given test, the electrodes' reactions did not produce enough H^+/OH^- ions to impact the pore fluid pH as the soil's buffering capacity needed to be depleted first. The rate of water electrolysis was visually observed by the formation of bubbles caused by the respective gas at each electrode compartment (Hydrogen gas at cathode and Oxygen at the anode). However, as more and more pore volumes were collected, a sharp pH gradient developed across the cell which led to cobalt precipitation in the cathode region. As a result, the soil specimen’s porosity was decreased by precipitation which resulted in reduced flow rates. In summary, the data demonstrated the effectiveness of the applied

voltage in reducing the flow rate past the barrier. In the light of this information, the first hypothesis was corroborated.

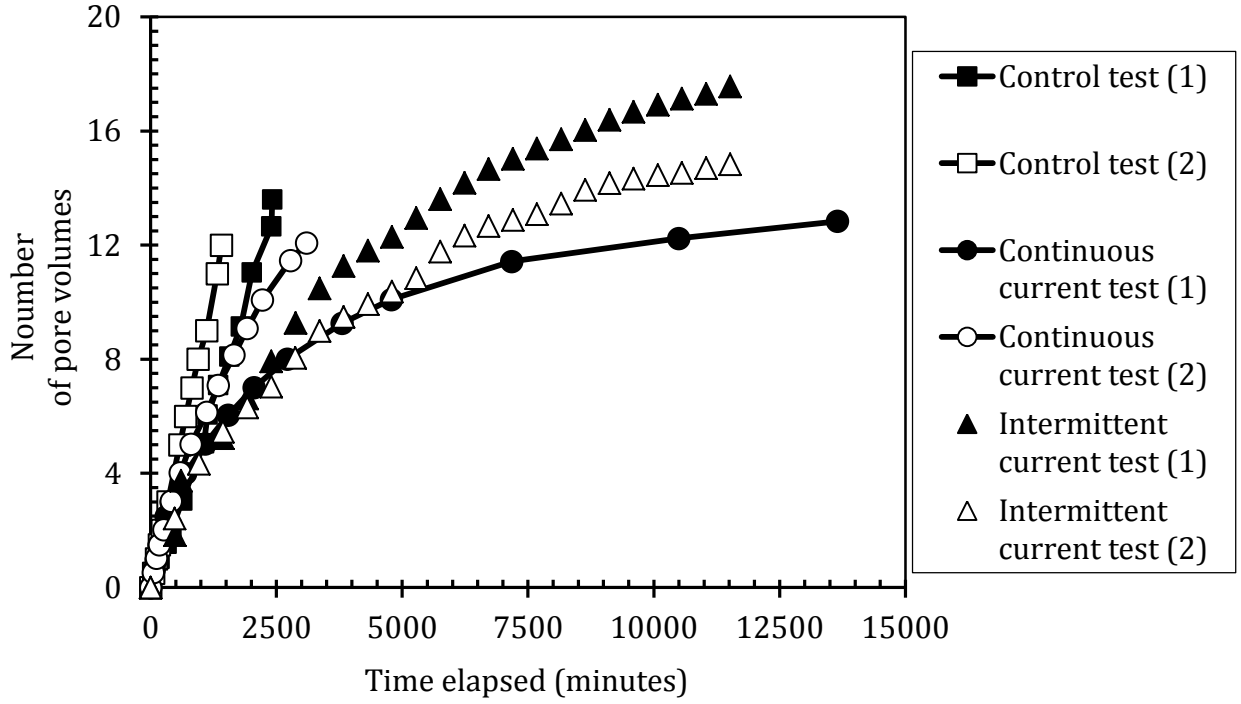

Figure 104 – 10% fines tests: Pore volume vs. collection time

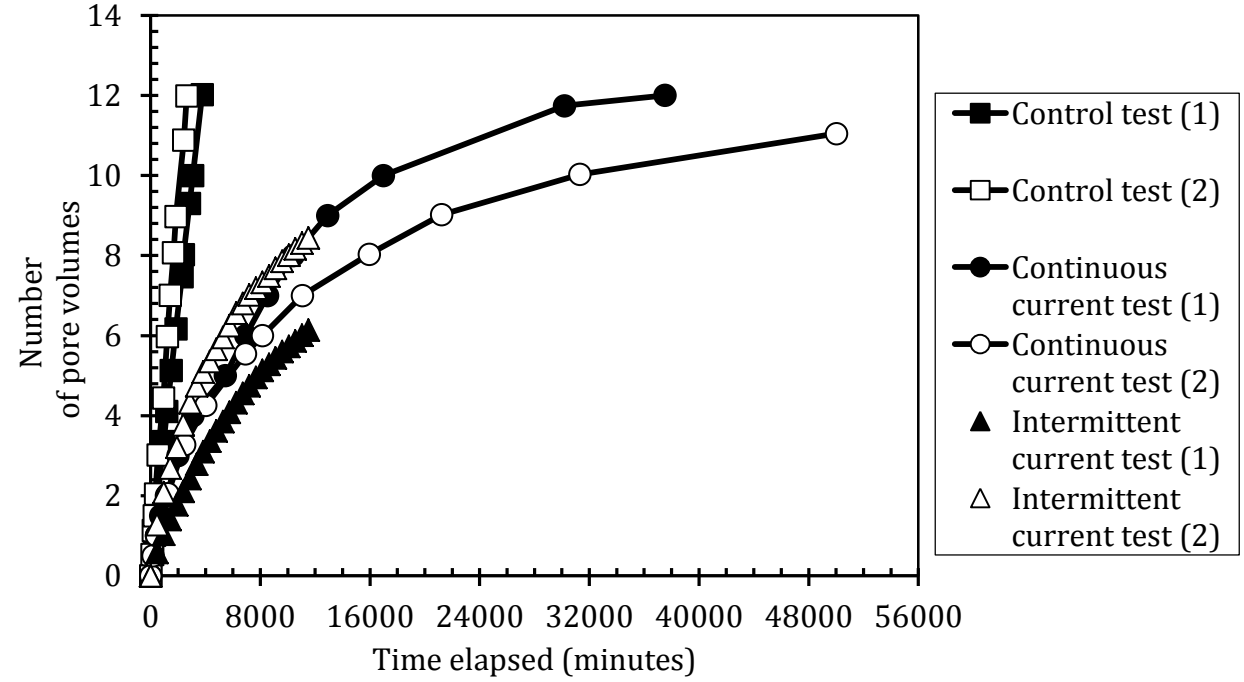

Figure 105 – 20% fines tests: Pore volume vs. collection time

Hypothesis 2 states that cobalt will be trapped near the cathode by adsorption and precipitation. The soil digestion tests revealed that in the control experiments, of the cobalt mass accumulated in the cell, less than 30% accumulated in the cathode region. Meanwhile, at least 60% of the accumulated cobalt was near the cathode in the continuous and intermittent current tests, as shown by Figure 106 and Figure 107 for the 10% fines and 20% fines tests, respectively. Consequently, the second hypothesis was corroborated.

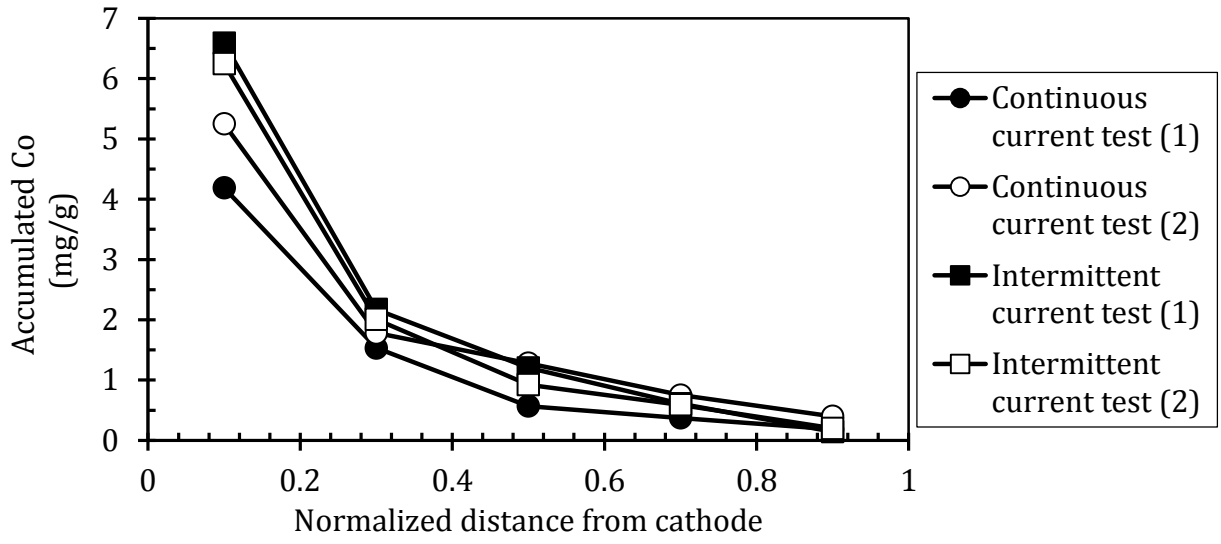

Figure 106 – 10% fines tests: Accumulated cobalt–continuous & intermittent current tests

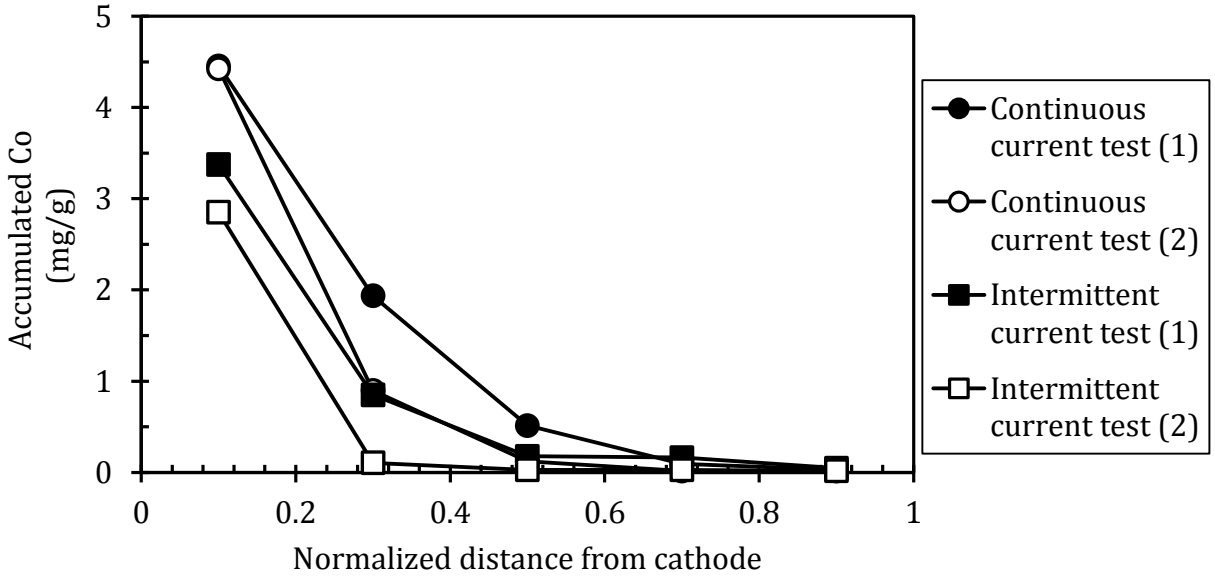

Figure 107 – 20% fines tests: Accumulated cobalt–continuous & intermittent current tests

Hypothesis 3 states that the dissolved cobalt concentration will be reduced downstream of the barrier by a combination of electro–migration, adsorption and precipitation. During the control tests, the cobalt concentration in the effluent increased with the number of pore volumes collected. It was presumed that this trend would continue until a break through point was reached when the concentration profile would plateau. However, after applying a voltage gradient cobalt's concentration increased to a maximum before it decreased (Figure 108 and Figure 109). The effluent concentrations consistently did not meet the World Health Organization's recommended limits of 0.004 ppm and 0.11 ppm to protect aquatic life against chronic and acute toxicity in fresh water, respectively. However, the tests were carried out using feed solutions that contained 1000 ppm of cobalt. This elevated concentration would not be encountered in the field. Therefore, a conclusion about the effectiveness of the electrokinetic barrier to meet the guidelines for cobalt could not be reached. The digestion tests revealed that cobalt was adsorbed and precipitated in the soil. As well, cobalt's distribution across the cell suggested that most of the cobalt was adsorbed/precipitated in the cathode region, near the inlet of the cell. Electro–migration coupled with adsorption/precipitation reduced the advancement of the dissolved cobalt downstream past the barrier. Thus, the third hypothesis was corroborated.

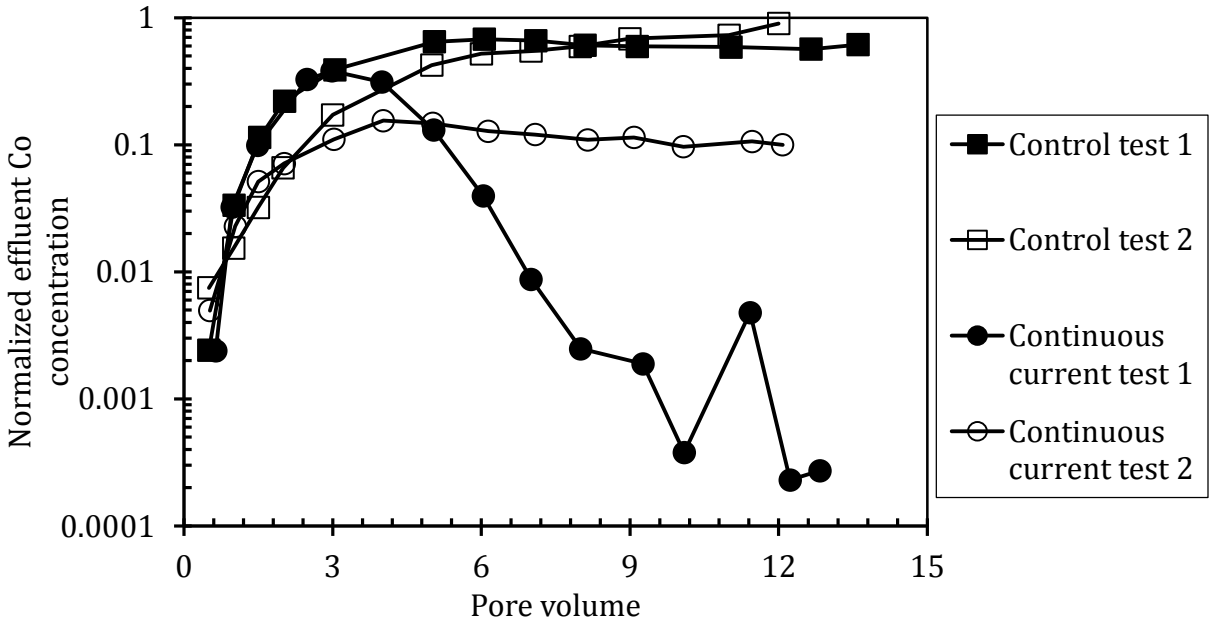

Figure 108 – 10% fines tests: Effluent cobalt concentration profiles–control & continuous tests

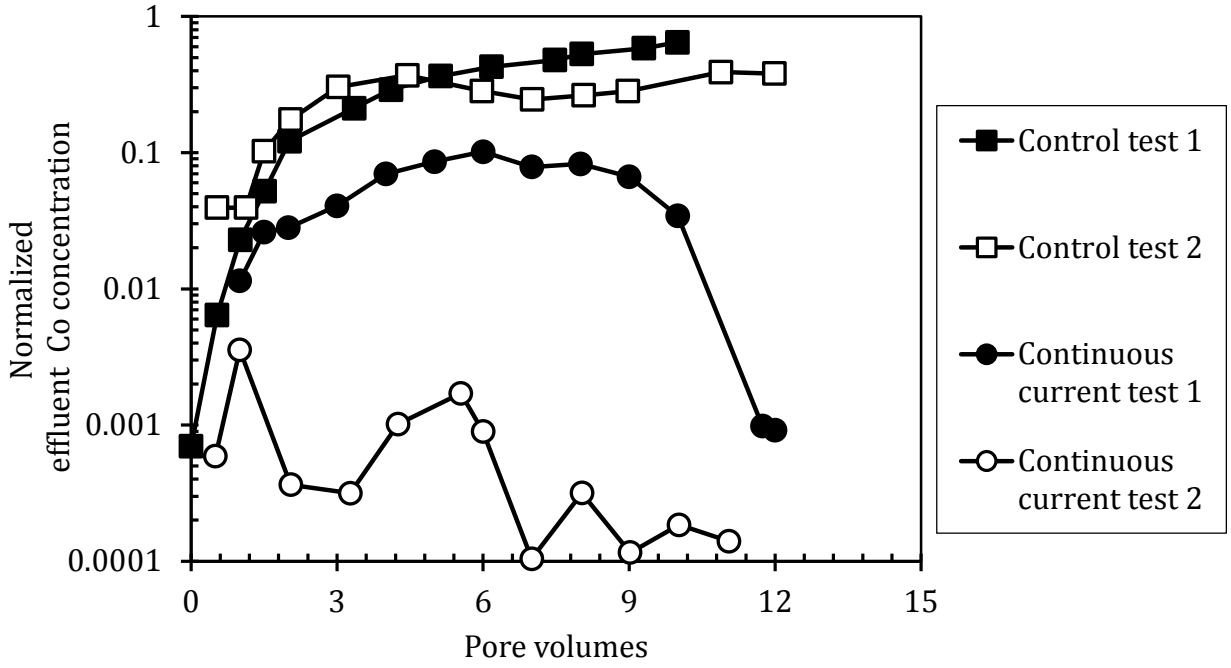

Figure 109 – 20% fines tests: Effluent cobalt concentration profiles–control & continuous tests

The fourth hypothesis states that the cobalt mass flow rate through the barrier will be reduced by electro–osmosis, electro–migration, adsorption and precipitation. The mass flow rate of cobalt is directly proportional to the product of the volumetric flow rate and the concentration of cobalt in the effluent. In all the tests conducted under an applied voltage (continuously and intermittently), the cobalt concentration and the effluent volumetric flow rate decreased past the electrokinetic barrier. Consequently, the mass flow rate also decreased past the barrier. The coupled effects of electro–osmosis, electro–migration, adsorption and precipitation reduced the net flow rate of cobalt solution past the barrier, reduced the spread of cobalt past the high pH zone, and diminished cobalt's concentration past the barrier. As a result, cobalt mass flow rates were greatly reduced when compared to the control tests. Therefore, the fourth hypothesis was corroborated.

The second objective of this work is to assess the feasibility of groundwater contamination prevention using electrokinetic barrier for the Musselwhite mine. From the third and fourth hypotheses, it can be concluded that the use of an electrokinetic barrier on the

Musselwhite mine soil to prevent groundwater contamination of cobalt was feasible. Hence, the second objective was also achieved.

The third objective of this work is to distinguish the influences of electro–osmosis and electro–migration on trapping the cobalt ions. However, the effects of electro–osmosis and electro–migration were coupled in this experiment. Therefore, it was difficult to separate the contributions of electro–osmosis as it related to the reduction of the net flow rate or contaminant transport. Thus, the third objective of this study was not met.

Hypothesis 5 states that intermittent power can be as effective as continuous power. Using continuous current to power the electrokinetic barrier generated sharp pH gradients with high pH values near the cathode which were sustained throughout the application period (Figure 67 and Figure 88). On the other hand, applying the current intermittently to the test cell led to a high pH gradient during the power on cycles only. This was demonstrated by the effluent pH which increased during the power off cycles (Figure 72 and Figure 93). The different fashions in which the power was applied yielded higher cobalt accumulation in the cells during continuous current tests than in the intermittent current tests (Figure 106). Accordingly, the continuous current cells produced lower flow rates (Figure 104). Nonetheless, the effluent concentrations from all electrokinetic barrier tests were significantly reduced (Figure 110 and Figure 111). Even though more cobalt accumulated in the cells under the application of continuous power, the amount of cobalt accumulated in the cells near the cathode was comparable for both power applications (Figure 106). More specifically, using cells containing 10% fines, approximately 61% of the cobalt accumulated near the cathode of under continuous and intermittent power applications. In addition using the cells containing 20% fines, 63% and 81% of the cobalt accumulated near the cathode in test (1) and test (2) under a continuous voltage gradient, and under an intermittent current 73% of the cobalt accumulated near the cathode of test (1) and 94% accumulated near the cathode of test (2). Hence, comparable results to the continuous current of flow rate, effluent concentration and percentage cobalt accumulation near the cathode were obtained. Therefore, hypothesis 5 was corroborated.

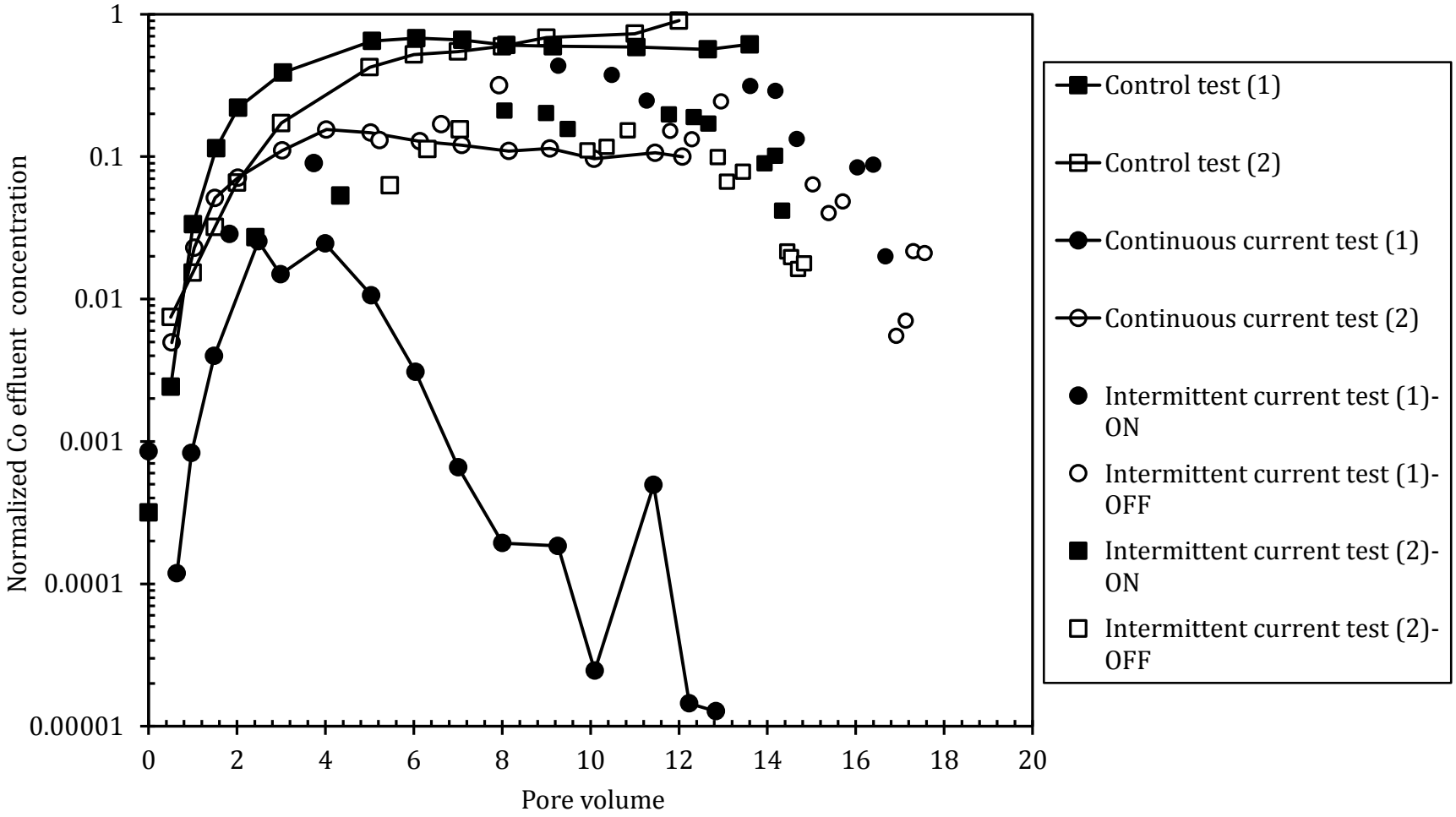

Figure 110 – 10% fines tests: Effluent cobalt concentration profiles

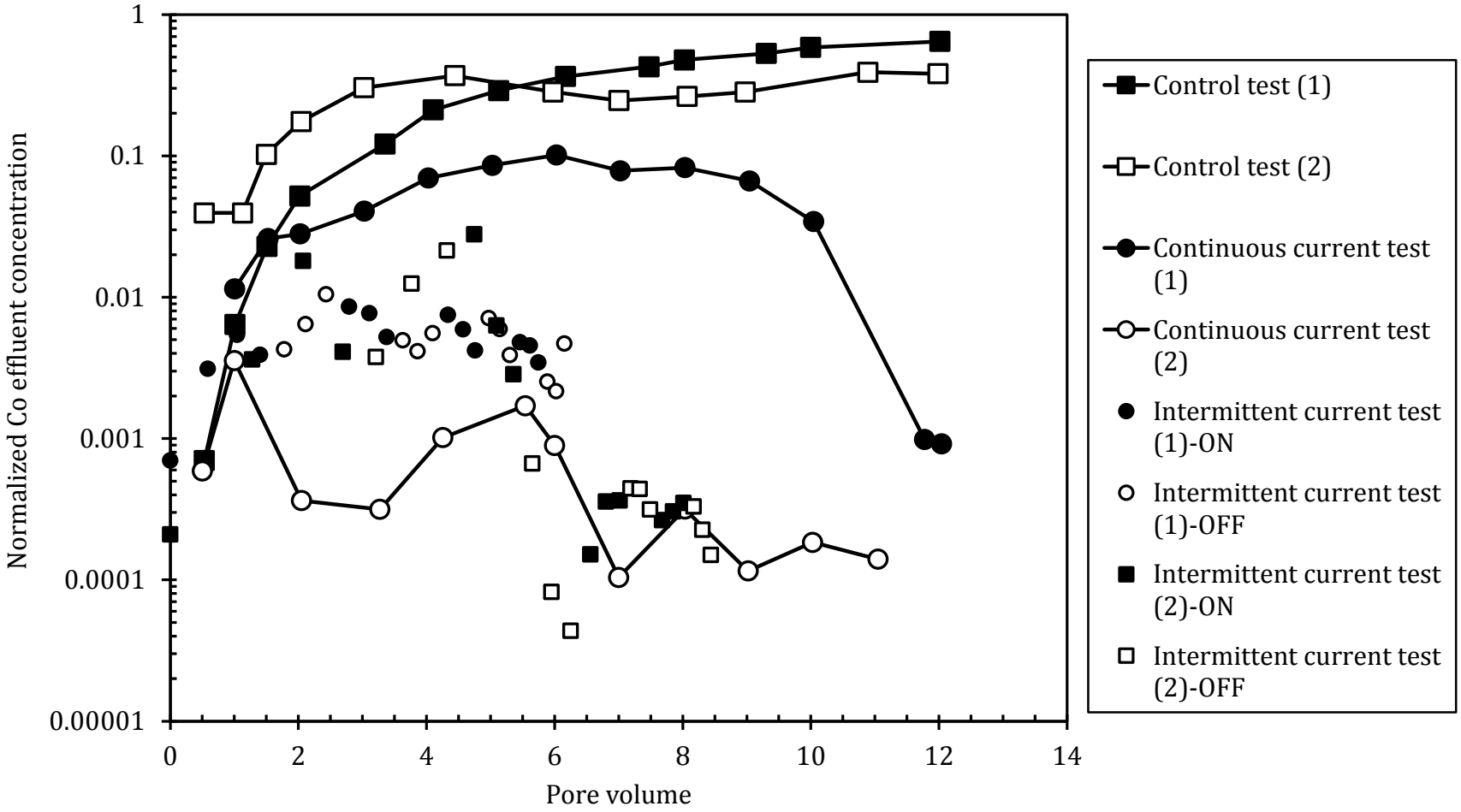

Figure 111 – 20% fines tests: Effluent cobalt concentration profiles

The fourth objective to examine the feasibility of using intermittent power as the energy source for the electrokinetic barrier was achieved.

Hypothesis 6 states that after the source of contamination has been exhausted and the electrokinetic barrier has been terminated, the cobalt concentration downstream of the barrier will not rise significantly. To test this hypothesis, the wash out tests were conducted. In these tests, the effluent cobalt concentration continued to decrease after stopping the continuous voltage of 40V and replacing the cobalt solution feed water with simulated groundwater, as shown in Figure 99. In fact, the concentrations continued to decrease for the duration of the tests. As well, the % Co retained in the wash out tests was greater than that retained in the control tests. It was concluded that the wash out tests (second stage of the tests) were not effective in mobilizing the cobalt that had been immobilized during the application of the electrokinetic barrier (first stage of the tests). Thus, the 6th hypothesis was corroborated for the duration of the tests.

Hypothesis 7 states that the precipitated/adsorbed cobalt within the barrier will not be solubilised and removed out of the trap zone after removing the voltage gradient. An increase of the cobalt concentration past the barrier after terminating the voltage gradient and the replacement of the feed water with simulated groundwater would indicate remobilization of the cobalt that accumulated during the continuous voltage application. Therefore examining Figure 99, it can be concluded that the mass flow rate of cobalt did not increase after eliminating the voltage gradient. This implied that the precipitated/adsorbed cobalt was retained by the soil and was not solubilised or removed from within the cells. Consequently, hypothesis 7 was corroborated.

Lastly, it is hypothesized that pH gradient developed during the application of the electrokinetic barrier will persist after removing the voltage gradient. Figure 102 demonstrates that the pore fluid pH was near neutral. It was concluded that due to the termination of the electrokinetic barrier and the elimination of the electrodes' reactions, the minerals present in the soil neutralized the pore fluid pH. As a result, the pore fluid pH gradient was not maintained after the termination of the voltage gradient. Accordingly, hypothesis 8 would be rejected. However, because the pore fluid was squeezed and its pH was measured 24 hours after the tests were completed, the minerals in the soil would have

neutralized the pore fluid pH. This introduced a source of error and lack of confidence in the pore fluid pH readings. Therefore, hypothesis 8 would be neither corroborated nor rejected.

Additionally, the fifth objective to determine the fate of the contaminated plume in the long term after the termination of the electrokinetic barrier was achieved. It was found that cobalt was retained within the barrier (73% in test (1) and 87% in test (2)), the effluent Co concentration and mass continued to drop, for the duration of the wash out tests.

12.0 Conclusions

In this thesis, the feasibility of preventing groundwater contamination using an electrokinetic barrier was investigated in a laboratory experimental study. Furthermore, cobalt was used as an example contaminant. Four groups of tests were conducted using fines–sand mixtures and 1000 ppm cobalt. Three of the tests, namely the control tests, continuous current and intermittent current tests were performed with cell mixtures containing 10% or 20% fines. However, the fourth test, which examined the transport and fate of cobalt after the voltage gradient was terminated and the source of contamination was exhausted, was performed only with the 10% fines–90% sand mixtures.

Applying a potential difference to the test cell resulted in a significant reduction in the volumetric flow rate past the electrokinetic barrier. Even though the data demonstrated the effectiveness of the applied voltage in reducing the flow rate past the barrier, it could not be concluded that the reduction was due to electro–osmosis alone due to the complexity of the coupling effects of adsorption/precipitation of cobalt in the cell with the electrokinetic phenomena. Furthermore, the influences of electro–migration and electro–osmosis could not be distinguished.

The soil digestion tests reveal that in the control experiments, of the mass of cobalt that accumulated in the cell, less than 30% accumulated in the cathode region. Meanwhile, at least 60% of the accumulated cobalt was near the cathode in the continuous and intermittent current tests. Thus, the effectiveness of electrokinetic barrier in trapping the cobalt near the cathode was successfully demonstrated. This has desirable long term implications.

Comparing the control tests to the continuous current tests, the effluent cobalt concentration significantly decreased under an applied potential. In fact, the highest normalized effluent cobalt concentration was less than 15% in the continuous current tests compared to a maximum normalized effluent cobalt concentration of higher than 80% in the control tests. It can be concluded that the use of an electrokinetic barrier on the Musselwhite mine soil to prevent groundwater contamination of cobalt is feasible. It is

worth noting that the highest effluent cobalt concentration did not occur at the last nominal pore volume collected.

In order to determine the effectiveness of using intermittent power, electrokinetic tests were conducted by alternating the current between on and off periods of 24 hours. Even though the rate at which water seeped through the test cell under an intermittent current was faster than under a continuous current, the effluent concentration from all tests was significantly reduced in all the intermittent tests. These tests showed that intermittently applying a voltage gradient of 2V/cm to the test cell resulted in overall comparable results to applying the same voltage gradient continuously.

The wash out tests provided a better understanding of the fate of cobalt after the termination of the voltage gradient. The tests showed that even though the distribution of the cobalt accumulated in the cells differed from that observed in the continuous and intermittent tests, the cobalt mass and concentration past the barrier did not increase, for the duration of the test. The effluent concentration was significantly decreased past the barrier.

13.0 Recommendations

The following are some recommendations for future work:

1. Determine the pore size distribution of the cell test mixture before and after the application of the electrokinetic barrier to study the long term implications, environmental and geotechnical, of an externally applied voltage gradient to soil.
2. Determine the soil's zeta potential as a function of the normalized distance from the cathode to gain a better understanding of its relation to adsorption/precipitation, electro–osmosis and changes to the volumetric flow rate by quantifying the electro–osmotic flow. This could be useful in isolating the influences of electro–osmosis. As well, determining the zeta potential of the soil will allow the quantification of electro–osmotic flow. As a result, the decision of the voltage gradient to be used could be better informed which could lead to savings in energy consumption.
3. Develop a protocol to measure the in–situ pH of the soil as a function of time in order to verify the role of pH on flow reduction, accumulation of cobalt (any contaminant of interest), and electro–migration.
4. Conduct wash out experiments for a longer duration for both the continuous and the intermittent current tests to better understand the fate of cobalt as a function of time.
5. Vary the applied voltage per centimetre to determine the optimum voltage gradient to minimize energy consumption without compromising the effectiveness of the barrier.
6. Drawing from the results obtained from the intermittent current tests, determine the feasibility of using solar power as the energy source for the electrokinetic barrier. This would result in a greener approach to contamination prevention.
7. To further investigate whether the flow rate reduction is due to electro–osmosis or due to the high pH environment near the cathode, cell tests with only sand should be conducted. Electro–osmosis will not be observed in media that do not contain uncharged soil surfaces. This is one way to uncouple the effects of electro–osmosis and those of the water electrolysis on the effluent flow rate.

14.0 References

Abramson, H. A., 1934. *Electrokinetic Phenomena and Their Application to Biology and Medicine.* New York: Chemical Catalog.

Acar, Y. B., Ashawabkheh, A. N. & Gale, R. J., 1993. Fundamentals of extracting species from soils by electrokinetics. *Waste Management,* Volume 13, pp. 141–151.

Acar, Y. B. et al., 1995. Electrokinetic remediation: Basics and technology status. *Journal of Hazardous Materials,* Volume 40, pp. 117–137.

Acar, Y. B. et al., 1990. Electrochemical processing of soils: Theory of pH gradient development by diffusion, migration, and linear convection. *Journal of Environmental Health and Science,* 25(6), pp. 687–714.

Acar, Y. D. & Alshawabkeh, A. N., 1993. Principles of Electronkinetic Remediation. *Environ. Sci. Technol,* 27(13), pp. 2638–2647.

Addai–Mensah, J. & Ralston, J., 2005. Investigation of the role of interfacial chemistry on partical interactions, sedimentation and electroosmotic dewatering of model kaolinite dispresions. *Powder Technology,* Volume 160, pp. 35–39.

Alcántara, M. T., Gómez, J., Pazos , M. & Sanromán , M. A., 2012. Electrokinetic Remediation of Lead and Phenanthrene Polluted Soils. *Geoderma,* Issue 173, pp. 128–133.

Alrehaily, L. M. et al., 2013. Gamma–radiolysis–assisted cobalt oxide nanoparticle formation. *Phys. Chem. Chem. Phys.,* Volume 15, pp. 1014–1024.

Antiochia, R., Campanella, L., Ghezzi, P. & Movassaghi, K., 2007. The use of vetiver for remediation of heavy metal soil contamination. *Anal Bioanal Chem,* 28 April, Issue 388, pp. 947–956.

Ashawabkeh, A. N. & Acar, Y. B., 1992. Removal of contaminants from soils by Electrokinetics: A theoretical treatise. *J. Environ. Sci. Health,* A27(7), pp. 1835–1861.

ASTM International, 2007. D 4972–01 Standard Test Method for pH of Soils. *ASTM International.*

ASTM Standard, n.d. *Standard Test Methods for Liquid Limit, Plastic Limit, and Plasticity Index of Soils.* s.l.:ASTM International .

Aube, B., 2004. *The Science of Treating Acid Mine Drainage and Smelter Effluents.* Ste. Anne–de– bellevue: EnvirAube.

Baker, A. & Brooks, R. R., 1989. Terrestial higher plants which hyperaccumulate metallic elements–a review of their distribution, ecology, and phytochemistry. *biorecovery,* Issue 1, pp. 81–126.

Bernier, L. R., Aubertin, M., Poirier, C. & Bussiere, B., 2002. *The use of limestone drains in the passive treatment of acid mine drainage (AMD).* Montreal , s.n.

Blowes, D. W., Ptacek, C. J. & Lambor, J. L., 1997. In–Situ Remediation of Cr(VI)–Contaminated Groundwater Using Permeable Reactive Walls: Laboratory Studies. *Environmental Science & Technology,* 31(12), pp. 3348–3357.

Bowles, J. E., 1992. *Engineering Properties of Soils and Their Measurement.* s.l.:McGraw Hill Inc..

Brar, S. K. et al., 2006. Bioremediation of Hazardous Wastes–A Review. *PRACTICE PERIODICAL OF HAZARDOUS, TOXIC, AND RADIOACTIVE WASTE MANAGEMENT*, April, pp. 59–72.

Butt, H.–J., Graf, K. & Kappl, M., 2006. *Physics and Chemistry of Interfaces.* 2nd ed. s.l.:Wiley–VCH.

Caliman, F. A. et al., 2011. Soil and groundwater cleanup: benefits and limits of emerging technologies. *Chean Techn Environ Policy,* Issue 13, pp. 241–268.

Canadian ground water association, 1999. *Fact Sheets.* [Online] Available at: http://www.cgwa.org/press/fact sheets.htm [Accessed 25 July 2013].

Casagrande, L., 1949. Electroosmosis in Soils. *Geothechnique,* 1(3), pp. 159–177.

Corapcioglu, M. T., Kambham, k. K. R. & Tuncay, K., 1998. Electrophoretic Repair of Impoudment Leaks: Analysis and Verification with Experimental Data. *Environ. Sci. Technol.,* Volume 32, pp. 3778–3784.

Criscenti, L. J. & Sverjensky, D. A., 1999. The role of electrolyte anions (ClO4–, NO30, and Cl–) in divalent metal (M+2) adsorption on oxide and hydroxide surfaces in salt solutions. *American Journal of Science,* Volume 299, pp. 828–899.

Darilek, G. T., Corapcioglu, M. Y. & Yeung, A. T., 1996. Sealing leaks in geomembrane liners using electropgrophesis. *Journal of Environmental Engineering,* Volume 122, pp. 540–544.

Darmawan & Wada, S.–I., 2002. Effect of clay mineralogy on the feasibility of electrokinetic soil decontamination technology. *Applied Clay Science,* Volume 20, pp. 283–293.

Das, B. M., 2008. *Fundamentals of Geotechnical Engineering.* 3rd ed. s.l.:Thomson.

Das, D., Samanta, G., Mandal, B. K. & Chowdhury, T., 1996. Arsenic in groundwater in six districts of West bengal, India. *Environmental Geochemistry and Health,* Issue 18, pp. 5–15.

Das, N., Vimala, R. & Karthika, P., 2008. Bisorption of heavy metals– An overview. *Indian Journal of Biotechnology,* April, Volume 7, pp. 159–169.

Doherty, R. et al., 2006. Development of modified flaysh as a permeable reactive barrier medium for a former manufactured gas plant site, Northern Ireland. *Environ Geol,* Volume 50, pp. 37–46.

Elementar, 2014. *Elementar Analysensysteme GmbHVario EL Cube.* [Online] Available at: http://www.elementar.de/en/products/elementar–products/vario–el–cube.html [Accessed 25 June 2014].

Environment Canada, 2007. *Environment Canada – Water – Groundwater.* [Online] Available at: http://www.ec.gc.ca/eau–water/default.asp?lang=En&n=300688DC–

1#sub5.
[Accessed 15 June 2013].

EPA, 1966. *Introduction to Pump & Treat Remediation.* [Online] Available at: http://www.qedenv.com/files/Introduction%20to%20Pump%20&%20Treat%20Remediation.pdf
[Accessed 25 July 2013].

EPA, 2007. *Chromium Compounds–echnology Transfer Network Air Toxics Web Site.* [Online] Available at: http://www.epa.gov/ttnatw01/hlthef/chromium.html
[Accessed 09 August 2013].

Esrig, M. I., 1968. Pore pressure, consolidation, and electrokinetics. *Journal of the Soil Mechanics Foundation Division, ASCE,* 94(4), pp. 899–921.

Evangelou, V. P., 1998. *Environmental Soil and Water Chemistry: Principles and Applications.* New York: John Wiley..

Evanko, C. R. & Dzombak, D. A., 1997. *Remediation of Metals–Contaminated Soils and Groundwater.* Pittsburgh: Ground–water Remediation Technologies Analysis Center.

Fansheng, M., Lingli, L., Juling, W. & Yeyao, W., 2013. *Effect of pH control at the cathode for the electrokinetic remediation efficiency.* s.l., IEEE, pp. 646–650.

Farrell, M. & Jones, D. L., 2010. Use of composts in the remediation of heavy metal contaminated soil. *Journal of Hazardous Materials,* Volume 175, pp. 575–582.

Faulkner, B. B., Griff Wyatt, E., Chermak, J. A. & Miller, F. K., 2005. *The largest acid mine drainage treatment plant in the world.* Virgina: s.n.

Gibb, J. P., Barcelona, M. J., Ritchey, J. D. & LeFaivre, M. H., 1984. *EFFECTIVE POROSITY OF GEOLOGIC MATERIALS FIRST ANNUAL REPORT,* Illinois: Illinois Department of Energy and Natural Resources.

Gidarakos, E. & Giannis, A., 2006. Chelate agents enhanced electrokinetic remediation for removal of cadmium and zinc by conditioning catholyte pH. *Water, Air and Soil Pollution,* Volume 172, pp. 295–312.

Goldcorp, 2013. *Goldcorp Inc. – Unrivalled Assets – Mines & Projects – Canada & US – Operations – Musselwhite – Overview & Operating Highlights.* [Online] Available at: http://www.goldcorp.com/English/Unrivalled–Assets/Mines–and–Projects/Canada–and–US/Operations/Musselwhite/Overview–and–Operating–Highlights/default.aspx
[Accessed 15 August 2013].

Hassan, I. & Mohamedelhassan, E., 2012. *Adsoprtion, desoprtion, remediation and fertility characteristics of a clay soil.* Winnipeg, s.n.

Hong, M. S., Farmayan, W. F., Dortch, I. J. & Chiang, C. Y., 2001. Phytoremediation of MTBE from a Groundwater Plume. *Environ. Sci. Technol.,* Issue 35, pp. 1231–1239.

Huling, S. G. & Pivetz, B. E., 2006. *In–Situ Chemical Oxidation.* [Online] Available at:

http://www.epa.gov/ada/gw/pdfs/insituchemicaloxidation_engineering_issue.pdf [Accessed 31 October 2013].

Humboldt Mfg. Co, 2014. *Liquid Limit Machine with Counter.* [Online] Available at: http://www.humboldtmfg.com/liquid_limit_machine_with_counter.html [Accessed 28 June 2014].

Hunter, R. J., 1982. *Zeta potential of Colloid Science.* London: Academic Press.

Ingham, D. B., 2005. *Transport Phenomena In Porous Media.* s.l.:Elsevier Science and Tech.

Isenburg, J. & Moore, M., 1992. Generalized Acid Neutralization Capacity Test. In: M. Gilliam & C. C. Viles, eds. *Stabilization and Solidification of Hazardous, Radioactive, and Mixed Wastes.* Philadelphia: s.n., pp. 361–377.

Jennings, S. R., Neuman, D. R. & Blicker, P. S., 2008. *Acid Mine Drainage and Effects on Fish Health and Ecology: A Review,* Bozeman: Reclamation Research Group Publication.

Johnson, D. B. & Hallberg, K. B., 2005. Acid mine drainage remediation options; a review. *Science of the Total Environment,* Issue 338, pp. 3–14.

Kasenow, M., 2002. *Determination of Hydraulic Conductivity from Grain Size Analysis.* s.l.:Water Resources Publications, LLC.

Kim, G.–N.et al., 2008. An analysis of a flushing effect on the electrokinetic–flushing removal of cobalt and cesium from a soil around decommissioning site. *Separation and Purification Technology,* Volume 63, pp. 116–121.

Kim, G.–N.et al., 2010. Development of pilot–scale electrokinetic remediation technology to remove Co–60 and Cs–137 from soil. *Journal of Industrial and Engineering Chemistry,* Volume 16, pp. 986–991.

Kim, W.–S., Kim, S.–O. & Kim, K.–W., 2005. Enhanced electrokinetic extraction of heavy metals from soils assisted by ion exchange membranes. *Journal of Hazardous Materials,* Volume B118, pp. 93–102.

Koksal, E., Ormanoglu, G. & Devuyst, E. A., 2003. Cyanide destruction: full–scale operation at Ovacik gold mine. *The European Journal of Mineral Processing and Environmnetal Protection,* 3(3), pp. 270–280.

Lageman, R., Clarke, R. L. & Pool, W., 2005. Electro–reclamation, a versatile soil remediation solution. *Engineering Geology,* Volume 77, pp. 191–201.

Lee, H.–H. & Yang, J.–W., 2000. A new method to control electrolytes pH by circulation system in electrokinetic soil remediation. *Journal of Hazardous Materials,* Volume B77, pp. 227–240.

Lee, M., Paik, I. S., Kang, H. & Lee, S., 2007. Remediation of heavy metal contamined groundwater originated from abandoned mine using lime and calcium carbonate. *J. of Hazardous Materials,* Issue 144, pp. 208–214.

Li, S. et al., 2011. *Application of sequential extraction analysis to electrokinetic remediation of chromium contaminted soil.* Shenyang, s.n., pp. 1–4.

Lockhart, N. C., 1983. Electro–osmostic dewatering of clays. III. Influence of clay type, exchangeable cations, and electrode materials. *Colloid and Surfaces,* Volume 6, pp. 253–259.

Lyklema, J., 2003. Electrokinetics after Smoluchowski. *Colloids and Surfaces A: Physicochem. Eng. Aspects,* Volume 222, pp. 5–14.

Lynch, R. J., Muntoni, A., Ruggeri, R. & Winfield, K. C., 2007. Preliminary tests of an electrokinetic barrier to prebent heavy metal pollution of soils. *Electrochimica Acta,* Volume 52, pp. 3432–3440.

Mackenzie, P. D., Horney, D. P. & Sivavec, T. M., 1999. Mineral Precipitation and Porosity Losses in Granular Iron Columns. *Journal of Hazardous Materials,* 68(1–2), pp. 1–17.

Martin, W. A. et al., 2013. Hydrated Lime for Metal Immoblization and Explosive Trasnformation: Field Demonstration. *J. Hazard. Toxic Radioact. Waste,* July, Issue 17, pp. 237–244.

Mattigod, S. V., Gibali, A. S. & Page, A. L., 1979. Effect of ionic strength and ion pair formation on the adsorption of nickel by kaolinite. *Clasy and Clay Minerals,* 237(6), pp. 411–416.

Micic, S., Shang, J. Q. & Lo, K. Y., 2003. Improvement of the load–carrying capacity of offshore skirted foundations by electrokinetics. *Canadian Geotech. J.,* Volume 40, pp. 949–963.

Mitchell, J. K. & Soga, K., 2005. *Fundamentals of Soil Behavior.* 3rd ed. s.l.:Wiley.

Mohamedelhassan , E. & Shang, J. Q., 2001. Effects of electrode materials and current intermittence in electro–osmosis. *Ground Improvement,* Volume 5, pp. 3–11.

Morin, K. A. & Hutt, N. M., 1997. *Environmental Geochemistry of Minesite Drainage–Practical Theory and Case Studies.* Vancouver: MDAG Publishing.

Nagpa, N. K., 2004. *TECHNICAL REPORT – WATER QUALITY GUIDELINES FOR COBALT,* s.l.: Ministry of Water, Land and Air Protection.

Narasimhan, B. & Sri Ranjan, R., 2000. Electrokinetic Barrier to prevent subsurface contaminant migration: theoretical model development and validation. *Journal of Contaminant Hydrology ,* Volume 42, pp. 1–17.

Ouhadi, V. R. et al., 2010. Impact of carbonate on the efficiency of heavy metal removal from kaolinite soil by the electrokinetic soil remediation method. *Journal of Hazardous Materials,* Volume 173, pp. 87–94.

Paillat, T., Moreau, E., Grimaud, P. O. & Touchard, G., 2000. Electrokinetic Phenomena in Porous Media Applied to Soil Decontamination. *IEEE Transactions on Dielectrics and Electrical Insulation,* October, 7(5), pp. 693–704.

Piteau Associates , 2011. *2010 Biennial Groundwater Monitoring Report,* s.l.: Goldcorp Canada Ltd.

Pivetz, B. E., 2001. *Phytoremediation of Contaminated Soil and Ground Water at Hazardous waste Sites,* s.l.: s.n.

Probstein, R. F. & Hicks, E. R., 1993. Removal of Contaminants from Soils by Electric Fields. *Science,* 23 April, Volume 260, pp. 498–502.

Rajkumar, M., Ae, N. & Freitas, H., 2009. Endophytic bacteria and their potential to enhance heavy metal phytoextraction. *Chemosphere,* Issue 77, pp. 153–160.

Reddy, K. R., 2008. Physical and Chemical Groundwater. In: C. J. G. Darnault, ed. *Overexploitation and Contamination of Shared Groundwater Resources.* Illinois: Springer , pp. 257–274.

Reddy, K. R. & Parupudi, U. S., 1997. Removal of chromium, nickel, cadmium from clays by in–situ electrokinetic remediation. *Journal of soil Contamination,* 6(4), pp. 391–407.

Reddy, K. R., Paupudi, U. S., Devulapalli, S. N. & Xu, C. Y., 1997. Effects of soil compositiobn on the removal of chromium from soils by electrokentics. *Journal of Hazardous Materials,* January, 55(1), pp. 135–158.

Reddy, K. R. & Saichek, R. E., 2004. Enhanced electrokinetic removal of phenanthrene from clay soil by periodic electric potential application. *J. Environ. Sci. Heal. A,* Volume 39, pp. 1189–1212.

Rowe, K. R., 2004. *Barrier Systems for Waste Disposal Facilities.* 2nd ed. s.l.:Spon. Press.

Rowe, R. K., Rimal, S. & Sangam, H., 2009. Ageing of HDPE geomembrane exposed to air, water and leachate at different temperatures. *Geotextiles and Geomembranes,* Volume 27, pp. 137–151.

Segall, B. A. & Bruell, C. J., 1992. Electro–osmotic contaminant removal process. *Journal of Environmental Engineering, ASCE,* Volume 118, pp. 84–100.

Shen, Z. et al., 2007. Comparison of electrokinetic soil remediation methods using one fixed anode and approaching andoes. *Environmental Pollution,* Volume 150, pp. 193–199.

Sparks, D. L., 2003. *Environmental Soil Chemistry.* 2nd ed. New York: Academic Press.

Statistics Canada, 2012. *Human Activity and the Environment.* [Online] Available at: http://www5.statcan.gc.ca/bsolc/olc–cel/olc–cel?catno=16–201–XWE&lang=eng. [Accessed 5 June 2013].

Statistics Canada, 2013. *Table 3.8 Mineral extraction waste from select mining industries, 2001 and 2008.* [Online] Available at: http://www.statcan.gc.ca/pub/16–201–x/2012000/t008–eng.htm [Accessed 30 October 2013].

Stevenson, F. J. & Cole, M. A., 1999. *Cycles of Soils: Carbon, Nitrogen, Phosphorus, Sulfur, Micronutrients.* 2nd ed. s.l.:Wiley & Sons, Inc..

Sun, T. R. & Ottosen, L. M., 2012. Effects of pulse current on energy consumption and removal of heavy metals during electrodialytic soil remediaton. *Electrochimica Acta,* Volume 86, pp. 28–35.

The Interstate Technology & Regulatory Council–PRB: Technology Update Team, 2011. *Interstate Technology & Regulatory Council (ITRC).* [Online]

Available at: http://www.itrcweb.org/GuidanceDocuments/PRB–5–1.pdf [Accessed 27 June 2014].

TOSC, 2004. *Chemical Oxidation for Groundwater Remediation.* [Online] Available at: http://www.egr.msu.edu/tosc/gelman/chemical oxidation fact sheet final .pdf [Accessed 08 October 2013].

U.S EPA, 1998. *Permeable Reactive Barrier– Technologies for Contaminants Remediation.* [Online] Available at: http://clu–in.org/download/rtdf/prb/reactbar.pdf [Accessed 27 June 2014].

U.S. EPA, 1983. Neutralization of acid mine drainage–Design Manual. January.

U.S. EPA, 2012. *National Service Center for Environmental Publications (NSCEP).* [Online] Available at: http://nepis.epa.gov/Exe/ZyNET.exe/P100F9X4.TXT?ZyActionD=ZyDocument&Client=EPA&Index=2011+Thru+2015&Docs=&Query=&Time=&EndTime=&SearchMethod=1&TocRestrict=n&Toc=&TocEntry=&QField=&QFieldYear=&QFieldMonth=&QFieldDay=&IntQFieldOp=0&ExtQFieldOp=0&XmlQuery=& [Accessed 27 June 2014].

Ugaz, A., Puppala, S., Gale, R. J. & Acar, Y. B., 1994. Electrokinetic Soil Processing Complicating Features of Electrokinetic Remediation of Soils and Slurries: Saturation Effects and the Role of the Cathode Electrolysis. *Chemical Engineering Communication,* 129(1), pp. 183–200.

US EPA, 2000. *Technology Transfer Network – Air Toxics Web Site.* [Online] Available at: http://www.epa.gov/ttnatw01/hlthef/cobalt.html [Accessed 28 November 2013].

Vane, L. M. & Zang, G. M., 1997. Effect of Aqueous Phase Properties on Clay Particle Zeta Potential and Electro–osmotic Permeability: Implications for Electro–kinetic Soil Remediation Processes. *Journal of Hazardous Materials,* August.pp. 1–22.

Wei, Y. & Hui, Z., 2011. *Experimental Study on Electrokinetic Remediation of In–situ Cd Contaminated Soil by Applied Voltage.* Shanghai, Materials for Renewable Energy & Environment (ICMREE).

West, J. L. & Stewart, D. I., 2000. Effect of Zeta Potential on Soil Electrokinesis. In: R. Naidu, E. Smith, G. Owens & P. Bhattacharya, eds. *Managing Arsenic in the Environment: From Soil to Human Health.* s.l.:Geoenviron, pp. 1535–1549.

Wuana, R. A. & Okieime, F. E., 2011. Heavy Metals in Contaminated Soils: A Review of Sources, Chemistry, Risks and Best Available Strategies for Remediation. *International Scholarly Research Network,* pp. 1–20.

Yalcin, T., Papadakis, M., Hmidi, N. & Hilscher, B., 2004. Desulphurization of Place Dome's Musselwhite Mine gold cyandation tailings. *Mineral Processing*, November/December, pp. 1–7.

Yao, Z., Li, J., Xie, H. & Yu, C., 2012. Review on Re,ediation Technologies of Soil Contaminatined By Heay Metal. *Procedia Environmental Sciences,* pp. 722–729.

Yeung, A. T., 1994. Electrokinetic flow processes in porous media and their applications. In: M. Y. Corapcioglu, ed. *Advances in Porous Media.* s.l.:E;sevier, pp. 309–395.

Yuan, S., Zheng, Z., Chen, J. & Lu, X., 2009. Use of solar cell in electrokinetic remediation of cadmium–contaminated soil. *Journal of Hazardous Materials,* Volume 162, pp. 1583–1587.

Yuan, S., Zheng, Z., Chen, J. & Lu, X., 2009. Use of solar cell in electrokinetic remediation of cadmium–contaminated soil. *Journal of Hazardous Materials,* Volume 162, pp. 1583–1587.

Zagury, G. J., Neculita, C. & Bussiere, B., 2007. passive treatment of acid mine drainage in bioreactors: short review, applications, and research needs. *OttawaGeo,* pp. 1439–1446.

Zhang, Y. F., Sheng, J. C. & Lu, Q. Y., 2004. Review on the soil remediation technologies. *Gansu Agricultural Science and Technology,* Issue 10, pp. 36–8.

15.0 Appendix A–Nominal Pore Volume Calculation

The following assumptions were made in calculating the nominal pore volume:

1. The cell mixture is fully saturated such that the entire cell volume contributed to the flow.
2. The height of the mixture in the cell is the same for both 10% fines and 20% fines mixtures.
3. The specific gravity of the mine soil is assumed to be representative of the fines–sand mixture.
4. As a result of keeping the dry mass of the mixture in the cell constant and the height being the same, the volume of the test cell mixture in both cells containing 10% fines and 20% fines is the same.
5. The applied compaction effort (load of 7 kN/m^2) eliminated volume changes due to fines–sand mixture swelling.

The pore volume was calculated by the following equations:

$$\boldsymbol{V_{cell} = L \times W \times H} \qquad \text{Eq. (A.1)}$$

where, V_{cell} is the volume of the test cell (cm^3), and

L, W, H are the dimensions of the cell length, width, height, respectively (cm).

$V_{cell} = (20 \times 11.5 \times 12.5) cm^3$

$\boldsymbol{V_{cell} = 2875\ cm^3}$

$$\boldsymbol{V_{mixture} = \frac{m_{mixture}}{\rho \cdot G_s}} \qquad \text{Eq. (A.2)}$$

where, $V_{mixture}$ is the volume of the fines and sand mixture in the test cell (cm^3),

$m_{mixture}$ is the dry mass of the fines and sand mixture in the cell (g),

ρ is the density of water (g/cm^3), and

G_s is the specific gravity of the mine soil (dimensionless).

$$V_{mixture} = \frac{5288\ g}{\left(1\frac{g}{cm^3}\right)(2.73)}$$

$$\boldsymbol{V_{mixture} = 1937\ cm^3}$$

$$\boldsymbol{V_{voids} = V_{cell} - V_{mixture}} \qquad \text{Eq. (A.3)}$$

where, Voids is the volume of voids in the cell (cm^3).

$$V_{voids} = (2875 - 1937) cm^3$$

$$\boldsymbol{V_{voids} = 938\ cm^3 \cong 940\ cm^3}$$

Since the mixture is assumed to be fully saturated, the volume of voids is equal to the nominal pore volume.